

Politecnico di Torino

Corso di Laurea Magistrale in Ingegneria Biomedica



**The design of an aortic heart valve prosthesis.  
Analysis of 100 target population patients**

Tesi di Laurea Magistrale

Candidato:

*Immacolata Ambrosino*

Tutor aziendale:

*Ing. Fausto Giacosa*

Relatore:

*Cristina Bignardi*

Livanova Saluggia (VC)

Settembre 2018

*A mia madre,  
che ha saputo gestire  
la nostra lontananza.*

*Alle mie amiche, in sede e fuori sede,  
che non hanno smesso di essermi vicine  
anche quando vicine non lo eravamo per niente.*

*A Simona,  
che mi ha accompagnato  
in avventure e disavventure.*

*A Lucio,  
che ha sopportato pianti inconsolabili  
o risate isteriche, senza battere ciglio.*

*E a te,  
se sei rimasto con me  
fin proprio alla fine.*

# Index

Introduction .....	5
1 Anatomy and physiology.....	7
1.1 Diseases of the circulatory system.....	21
1.1.1 Valvular vices .....	22
1.1.2 Aortic stenosis .....	22
2 Aortic root .....	31
2.1 Anatomy of the aortic root.....	31
2.2 Aortic root surgery .....	33
3 Aortic valve replacement.....	39
3.1 Definition and clinical consequences of aortic valve stenosis.....	39
3.2 Evolving treatment options for severe aortic valve stenosis .....	39
3.3 Definition of TAVR .....	40
3.4 Preoperative imaging of potential access routes.....	42
3.5 CT acquisition .....	46
3.6 Noninvasive imaging of the annulus: ongoing controversies and current insights .....	51
3.7 Native aortic valve: further imaging features and relationship to the coronary artery ostia.....	56
3.8 Determining the best fluoroscopic projection angle for device deployment .....	58
3.9 Other preprocedural findings.....	59
3.10 Incidental findings.....	60
3.11 Postprocedural imaging .....	60
3.12 Sutureless valves .....	60
4 Materials and methods.....	64
4.1 CT scan analysis.....	64
4.2 Procedure.....	67
5 Results .....	77
5.1 Database measured .....	77
5.1.1 Annulus plane.....	77
5.1.2 Valsalva sinus plane .....	79

5.1.3	STJ.....	81
5.2	Database calculated .....	83
5.2.1	Annulus plane .....	83
5.2.2	Valsalva sinus plane .....	85
5.2.3	STJ.....	87
5.3	Mean, standard deviation, maximum and minimum .....	89
6	Discussion.....	91
6.1	Data repeatability.....	91
6.1.1	A/B .....	91
6.1.2	A/C .....	113
6.2	Analysis of variance (ANOVA) .....	135
6.3	Normality test .....	152
6.4	Regressions.....	164
6.5	Outliers .....	196
7	Conclusion.....	199
	Index of figures.....	201
	Index of the tables .....	204
	Bibliography .....	205
	Sitography.....	205

## Introduction

The present work originates from a stage of six months internship carried out in the research and development department of Livanova company in Saluggia (VC), leader in the production of cardiac valve prostheses.

Valvular heart disease refers to any disease that affects the heart valves and is considered one of the main causes of cardiovascular problems. For this reason, many studies on the anatomy of heart valves have been carried out in recent years. The work presented focuses on the aortic valve and on the surrounding anatomical district, the aortic root.

The diseases affecting the aortic valve are commonly treated through a valve implant, either biological or mechanical, which include a valve suturing at the base of the aortic root. The final step of a valve prosthesis project involves the execution of in vitro tests, the purpose of which is to verify the structural and mechanical characteristics of the valve. Nowadays, tests are carried out using a theoretical model of aortic root that has a very regular geometry, not always representative of the actual geometry of the aortic root.

The aim of this thesis is the study of a 3D model of the aortic root representative of the real anatomy in order to carry out experimental tests able to provide results comparable with the patient's physiological conditions and useful to optimize the valve prosthesis design.

An overview of the anatomy and physiology of the heart will be presented.

The study of the anatomy of the aortic root is fundamental for the realization of the model, and for this reason the attention will be focused on it and all its aspects, evaluating which are the main geometric characteristics. An analysis on patients through the visualization of pre-operative CT scans was carried out by using a specific program, Mimics, a software processing the DICOM format images produced by medical diagnostic apparatus.

The analysis of the CT scans, from a data-base of 100 patients, allowed to extrapolate the geometrical parameters useful for defining the design of a new valve.

A statistical analysis was then performed for each parameters (perimeter, area and eccentricity of the annulus, distance of the annulus plane from the plane of the sinuses of Valsalva and from the tubular sinus junction, and other geometrical quantities) obtained from different operators, to demonstrate the procedure repeatability, and the correlation between the data, to explain which and how data correlate each other. Also, an analysis of variance (ANOVA) was performed.

For this analysis, the Minitab software was used, and it was possible to compare data groups obtained from different operators and also to understand information of interests in terms of statistical equalities or differences.

The analysis carried out identified parametric and Gaussian distributions, having the patient populations a random variability between one patient and the other, even though they are patients with an aortic pathology that could affect the data distributions.

Once the normality of the distributions was established, a parametric analysis was performed.

For the normality test, the P-value was considered, verifying a normal distribution, for the variable under examination, only for P - values above 0.05, ie corresponding to a 95% confidence level.

The corresponding boxplots were also made for each variable.

In order to understand how the parameters influence each other, regressions were also performed.

With ANOVA it was possible to compare more than two groups of data.

# 1 Anatomy and physiology

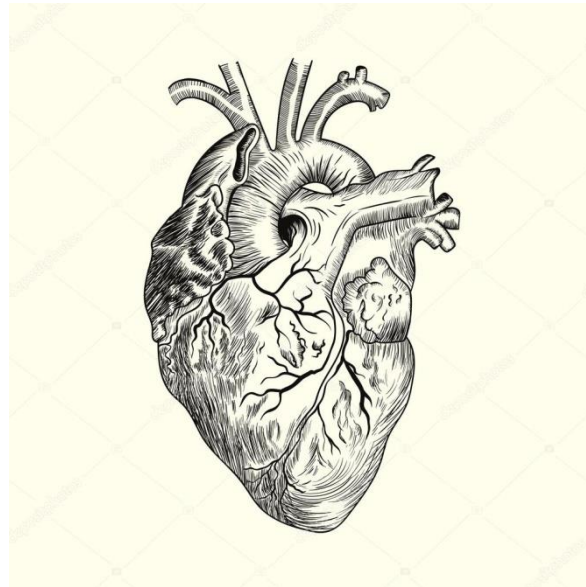


Figure 1.1 Sketch of a human heart

**The cardiovascular system** consists of a pump, a series of distribution and collection ducts and a vast network of small vessels that allow a rapid exchange of substances between signs and tissues.

The heart consists of two pumps arranged in series: the right ventricle, pushing blood through the lungs to ensure the exchange of oxygen and carbon dioxide, and the left ventricle, pushing blood into all the other tissues of the body.

The unidirectionality of the blood flow through the heart is ensured by an appropriate arrangement of effective valves. Although the cardiac output is intermittent, in periphery the flow is transformed from pulsatile to continuous, by dilatation of the aorta and its branches, which occurs during the ventricular contraction (*systole*), and the subsequent elastic return of the walls of the large arteries, pushing blood forward during ventricular relaxation (*diastole*).

The blood flows rapidly in the aorta and in its arterial branches that progressively decrease in diameter as they proceed towards the periphery. Also, the thickness and the histological structure of their walls are modified. We move from an elastic structure in the aorta to a more muscular structure in the peripheral arteries and to a predominantly muscular structure in the arterioles.

Proceeding from the aorta to the small arteries and arterioles, the frictional resistances (viscosity) to the flow are relatively small, and also the pressure drop between the root of the aorta and the beginning of these vessels is relatively small. Arterioles are the main site of resistance to blood flow in the circulatory system. The high resistance offered by arterioles causes a significant pressure drop between arterioles and capillaries. The variations in the contraction state of the circular muscles of these small vessels regulate the blood flow in the tissues and they play an important role in the regulation of the arterial pressure.

In addition to a rapid pressure drop, through the arterioles the flow is transformed from pulsatile to continuous. The pulsatile character of the arterial flow, due to the intermittence of the cardiac injection, is

dampened at the level of the capillaries by the combined action of the distension of the large arteries and the frictional resistance of the arterioles.

From each arteriole originates different capillaries, so the total area of the transverse section of the capillary bed is much wider than that of the arteriole of origin, even if the total area of the transverse section of each capillary is smaller. As a result, the blood flow through the capillary bed will slow down.

The capillaries are very short, with a single cell wall thick and with a low flow rate. The capillaries therefore possess the most suitable conditions for the exchange of substances diffusible between blood and tissues.

In its return to the heart the blood passes first from the capillaries to the venules, and then into larger veins. Progressing towards the heart, the number of veins is progressively reduced and both the thickness and the structure of their walls are modified. Also, the area of transverse section is reduced and the speed of blood flow increases. In systemic circulation a large part of the blood is contained in the venous vessels.

The blood entering the right ventricle after passing through the right atrium is pumped into the pulmonary arterial system at a mean pressure of about one-seventh of that in the systemic circulation. The oxygenated blood passes through the pulmonary veins and the left atrium and finally enters the left ventricle completing the cycle.

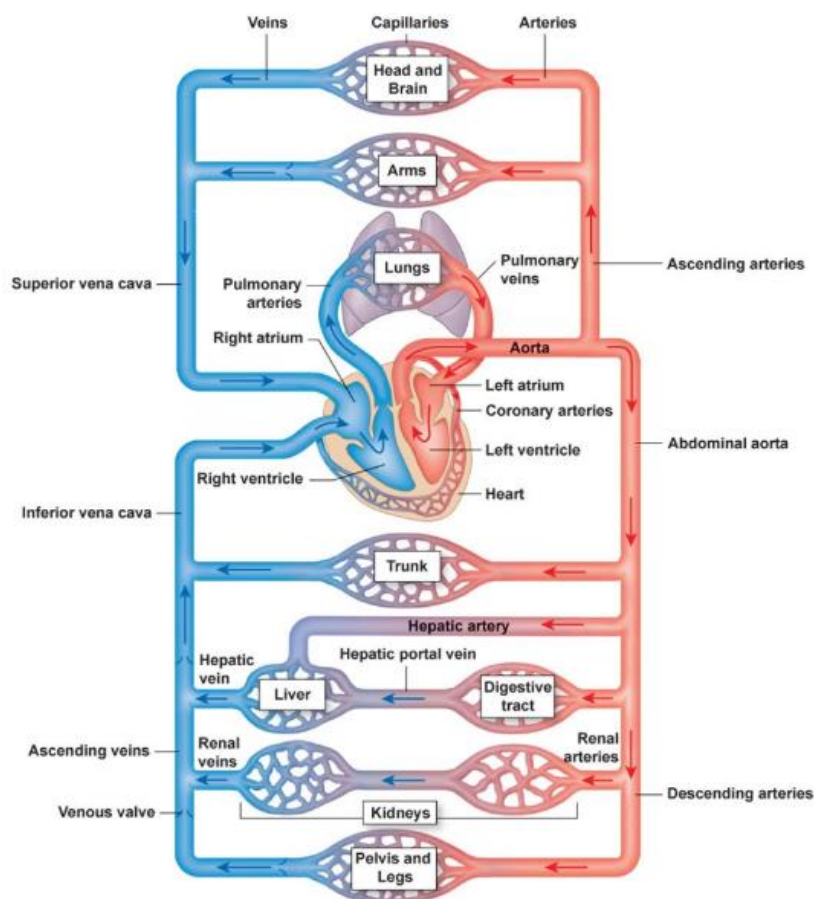


Figure 1.2 Scheme of the vessels that make up the circulatory system

**The heart** is a muscular organ which pumps blood through the blood vessels of the circulatory system. Blood provides the body with oxygen and nutrients, as well as assists in the removal of metabolic wastes.

In humans, the heart has size of a fist and it contracts in response to electrical signals produced by its electrical system. Over an average lifetime, the heart contracts more than 2.5 billion times. It pumps 5 to 6 liters of blood in one minute at rest with a frequency of about 70 beats per minute, but during a very intense physical effort its frequency can reach 200 contractions per minute by pumping almost 200 ml per beat (50 liters per minute).

It is located between the lungs, in the middle mediastinum, at the level of thoracic vertebrae T5-T8, and it is divided into four chambers: upper left and right atria; and lower left and right ventricles. Commonly the right atrium and ventricle are referred together as the right heart and their left counterparts as the left heart.

In a healthy heart blood flows one way through the heart due to heart valves, which prevent backflow.

The heart is enclosed in a protective sac, the pericardium, which also contains a small amount of fluid. The wall of the heart is made up of three layers: epicardium, myocardium, and endocardium.

The heart pumps blood with a rhythm determined by a group of pacemaking cells in sinoatrial node. These generate a current that causes contraction of the heart, traveling through the atrioventricular node and along the conduction system of the heart. The heart receives blood low in oxygen from the systemic circulation, which enters the right atrium from the superior and inferior venae cavae and passes to the right ventricle. From here it is pumped into the pulmonary circulation, through the lungs where it receives oxygen and gives off carbon dioxide. Oxygenated blood returning to the left atrium, passes through the left ventricle and is pumped out through the aorta to the systemic circulation – where the oxygen is used and metabolized to carbon dioxide. The heart beats at a resting rate close to 72 beats per minute. Exercise temporarily increases the rate, but lowers resting heart rate in the long term, and is good for heart health.

A double-membraned sac called the pericardium surrounds the heart and attaches to the mediastinum. The back surface of the heart lies near the vertebral column, and the front surface sits behind the sternum and rib cartilages. The upper part of the heart is the attachment point for several large blood vessels – the venae cavae, aorta and pulmonary trunk. The upper part of the heart is located at the level of the third costal cartilage. The lower tip of the heart, the apex, lies to the left of the sternum (8 to 9 cm from the midsternal line) between the junction of the fourth and fifth ribs near their articulation with the costal cartilages.

The largest part of the heart is usually slightly offset to the left side of the chest (though occasionally it may be offset to the right) and is felt to be on the left because the left heart is stronger and larger, since it pumps to all body parts. Because the heart is between the lungs, the left lung is smaller than the right lung and has a cardiac notch in its border to accommodate the heart. The heart is cone-shaped, with its base positioned upwards and tapering down to the apex. An adult heart has a mass of 250–350 grams (9–12 oz).

The heart is often described as the size of a fist: 12 cm (5 in) in length, 8 cm (3.5 in) wide, and 6 cm (2.5 in) in thickness, although this description is disputed, as the heart is likely to be slightly larger. Well-trained athletes can have much larger hearts because of exercise on the heart muscle, similar to the response of skeletal muscle.

The wall of the heart was taken from three layers:

- the endocardium is the thin epithelial layer that covers the internal cavities and forms the valves;
- the myocardium is the muscular layer, forms the actual structure of the wall and is internally reinforced by a thick fibrous connective layer;
- the epicardium is a thin serous membrane externally covering the heart.

Outside the epicardium there is another serous membrane that connects the heart to the sternum and the diaphragm, keeping it in position in the chest. The epicardium and the outer serous membrane together controlled the pericardium. Between these membranes there is a thin layer of liquid that functions as a lubricant.

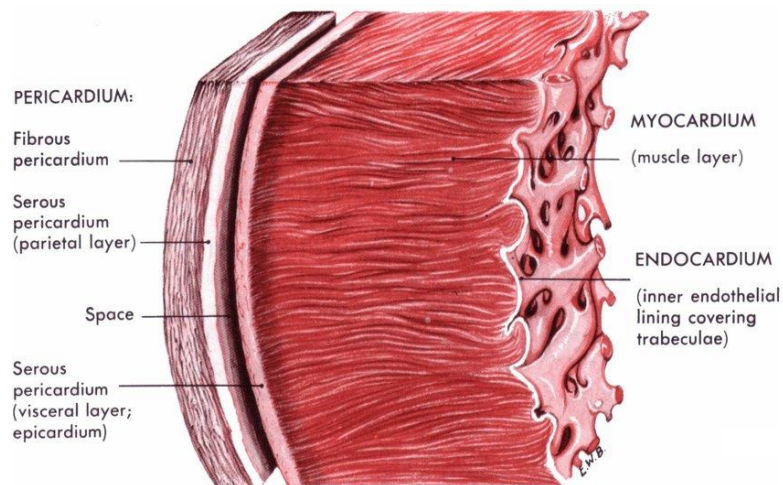


**Figure 1.3 Section of the heart wall showing the components of the outer pericardium (heart sac), muscle layer (myocardium), and inner lining (endocardium).**

The walls, although always having the same structure in every part of the heart, have different thickness: the layer of the myocardium is thinner in the atria than the ventricles, because the latter must provide the blood with the thrust to move in the arteries. In addition, the walls of the left ventricle are thicker than those of the right ventricle: the left ventricle must in fact push the blood through a path of many more kilometers of blood vessels than the right ventricle, and must therefore exert more pressure.

The myocardium receives nutriment and oxygen from the coronary arteries, which derive from a branching of the aorta. The coronaries run on the surface of the heart and give rise to a system of vessels that irradiates the walls of atria and ventricles. The blood from this system is then drained directly into the right atrium from the cardiac veins.

The right heart and the left heart work in sync, so every contraction of the heart simultaneously pushes the blood into both the pulmonary circulation and the systemic circulation. The path of the blood is presented in Figure 1.4: the right atrium receives oxygen-poor blood from the superior vena cava and inferior vena cava; these wide-caliber veins collect the blood that is returning to the heart respectively from the upper and lower parts of the body.

From the right atrium, blood passes through an atrioventricular valve called a tricuspid valve, located in the right ventricle. Most of the blood enters the ventricle while the heart is relaxed, in the interval between beats.

Immediately after the end of this period of passive filling of the ventricle, the atrium contracts and adds a small volume of blood to that already present in the ventricle.

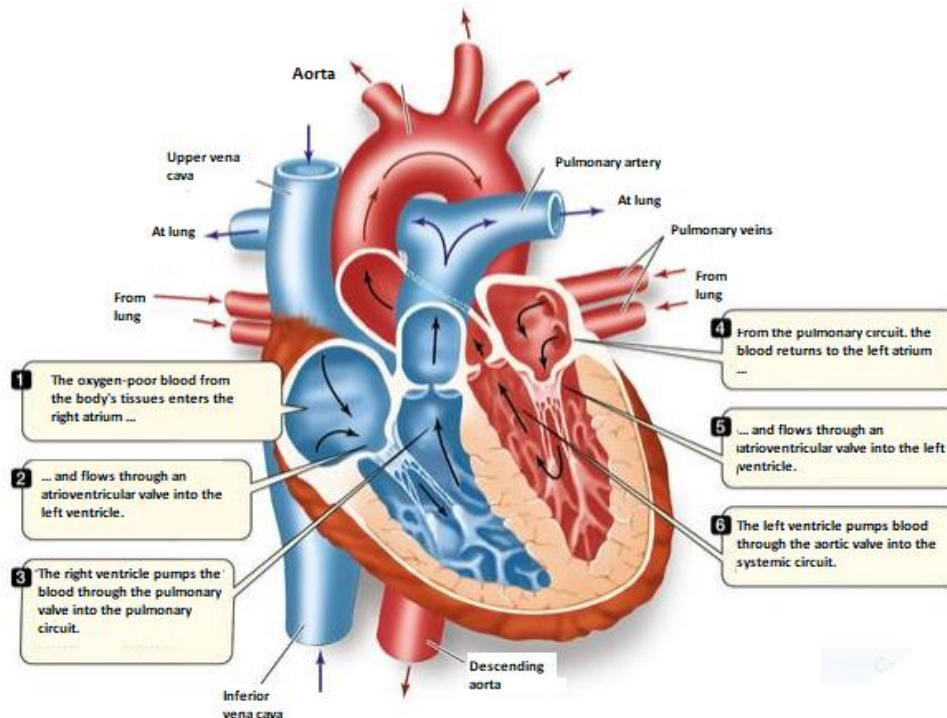


**Figure 1.4** In the human heart, blood flows from the right heart to the lungs, then to the left heart and then to the body. Atrioventricular valves prevent the reflux of blood into the atria when the ventricles contract. Pulmonary and aortic valves prevent reflux from the arteries to the ventricles when the ventricles relax.

At this point, the right ventricle contracts, leading to the closure of the atrioventricular valve and pumping the blood into a large artery that immediately divides into two pulmonary arteries, directed to the lungs.

In the lungs the arteries branch out; inside the capillaries the blood is charged with oxygen and gets rid of carbon dioxide.

The oxygenated blood passes from the capillaries to the pulmonary veins, which are directed from the lungs to the left atrium.

From the left atrium the blood enters the left ventricle through another atrioventricular valve called the bicuspid or mitral valve. As happens in the right portion of the heart, most of the filling of the left ventricle is passive, but the ventricle fills completely due to the atrial contraction that occurs immediately after the end of the passive filling period.

The walls of the left ventricle are powerful muscles that contract with a movement that originates from the basal portion. The increase in tension that is generated closes the bicuspid valve and, when the pressure in the left ventricle is quite high, opens the aortic valve, the blood pours into the aorta to resume its path through the body.

Summarizing, therefore, the pulmonary circulation starts from the right ventricle, with the pulmonary arteries, and ends in the left atrium, with the pulmonary veins; the systemic circulation starts from the left ventricle, with the aorta, and ends in the right atrium, with the hollow veins.

## Cardiac chambers

The heart has four chambers, two upper atria, the receiving chambers, and two lower ventricles, the discharging chambers.

The atria are low pressure chambers, with thin walls, and function more like large reserve ducts for the blood destined for the respective ventricles, which as load-bearing pumps for ventricular filling. The ventricles consist of a continuous lining of muscle fibers that starts from the fibrous skeleton at the base of the heart, especially around the orifice of the aorta. These fibers move towards the apex to the epicardial surface, then pass to the endocardium and undergo a partial inversion of direction of about 180 °, parallel to the epicardial fibers; they eventually form the wall of the endocardium and the papillary muscles. At the apex of the heart the fibers twine and spiral inwards to form the papillary muscles. At the base of the heart and around the valve orifices, the fibers form a thick and powerful muscular bundle that acts not only to reduce the ventricular circumference during the ejection of the blood but also to reduce the diameter of the AV hosts, thus supporting the action of closing of the valves. Ventricular ejection takes place not only by reducing the circumference but also by reducing the longitudinal axis of the heart, caused by a lowering of the base. the precocial contraction of the apical region of the heart, associated with an approach of the ventricular walls, pushes the blood through the outlet ducts.

## Heart valves

The heart valves are thin, flexible but resistant foils of endothelium-coated fibrous tissue, firmly inserted into the fibrous valvular rings. The movements of the valvular flaps are passive, and the orientation of the heart valves ensures the unidirectional flow of blood through the heart. in the heart there are two types of valves: the AV valves and the semilunar valves.

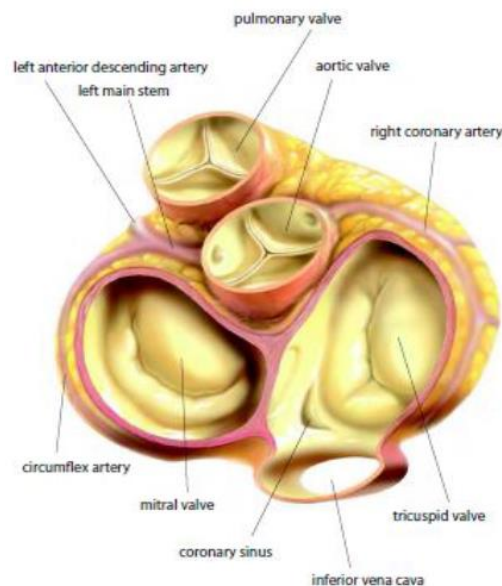


**Figure 1.5** With the atria and major vessels removed, all four valves are clearly visible.

*Atrioventricular valves:* there are two; the tricuspid valve is located between the right atrium and the right ventricle, and consists of three cusps, while the mitral valve (bicuspid valve) is located between the left

atrium and the left ventricle and consists of two cusps. The total area of the cusps of each AV valve is about twice the area of the respective AV orifice, to ensure a considerable overlap of the flaps in the closing position. At the free edges of these valves are inserted strong and thin filaments (tendon ropes) that arise from the powerful papillary muscles of the respective ventricles and serve to prevent the protrusion of the valves during systole.

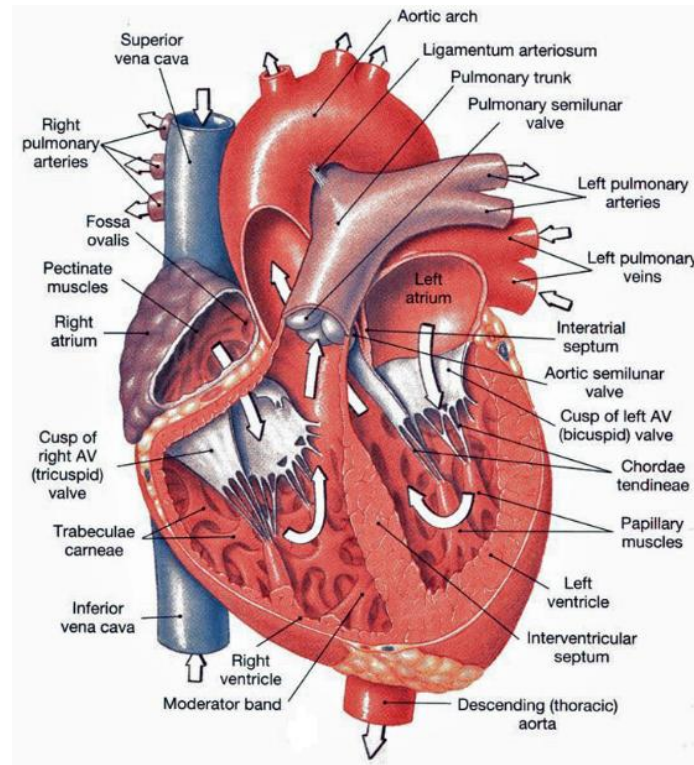


**Figure 1.6 Scheme of a sectioned heart**

In a normal heart the valvular flaps are relatively closed during ventricular filling and form a funnel for the passage of blood from the atria to the ventricles. It is believed that this partial approach of the valvular surfaces during diastole is caused mainly by the swirling currents that form behind the flaps and, in part, by the tendon cords and the papillary muscles, stretched during ventricular filling, which exert tension on the free edges of valves.

The movements of the mitral valve leaflets during a cardiac cycle are shown in the echocardiogram reproduced in Figure 1.7.

- A. The tricuspid valve, or right atrioventricular valve, is on the right dorsal side of the mammalian heart, between the right atrium and the right ventricle. The function of the valve is to prevent back flow of blood from the right ventricle into the right atrium. Normally, the tricuspid valve usually has three leaflets, named the anterior, posterior, and septal leaflets. Each leaflet is connected via chordae tendineae to the anterior, posterior, and septal papillary muscles of the right ventricle, respectively. Tricuspid valves may also occur with two or four leaflets; the number may change over a lifetime. The tricuspid valve functions as a one-way valve that closes during ventricular systole to prevent regurgitation of blood from the right ventricle back into the right atrium. It opens during ventricular diastole, allowing blood to flow from the right atrium into right ventricle. The back flow of blood is

also known as regression or tricuspid regurgitation. Tricuspid regurgitation can result in increased ventricular preload because the blood refluxed back into the atrium is added to the volume of blood that must be pumped back into the ventricle during the next cycle of ventricular diastole. Increased right ventricular preload over a prolonged period of time may lead to right ventricular enlargement (dilatation), which can progress to right heart failure if left uncorrected.

- B. The mitral valve, also known as the bicuspid valve or left atrioventricular valve, is a valve with two flaps in the heart, that lies between the left atrium and the left ventricle.

In normal conditions, blood flows through an open mitral valve during diastole with contraction of the left atrium, and the mitral valve closes during systole with contraction of the left ventricle. The valve opens and closes because of pressure differences, opening when there is greater pressure in the left atrium than ventricle, and closing when there is greater pressure in the ventricle than atrium; in abnormal conditions, blood may flow backwards through the valve (mitral regurgitation) or the mitral valve may be narrowed (mitral stenosis). Rheumatic heart disease often affects the mitral valve; the valve may also prolapse with age, and be affected by infective endocarditis. The mitral valve is named after the mitre of a bishop, which resembles its flaps.

The mitral valve is typically 4 to 6 square centimetres (0.62 to 0.93 sq in) in area, and sits in the left heart between the left atrium and the left ventricle. It has two leaflets (or 'cusps'), an anteromedial leaflet, and a posterolateral leaflet. The opening of the mitral valve is surrounded by a fibrous ring known as the mitral annulus. The anterior cusp covers approximately two-thirds of the valve (imagine a crescent moon within the circle, where the crescent represents the posterior cusp). Although the anterior leaflet takes up a larger part of the ring and rises higher, the posterior leaflet has a larger surface area.

The valve leaflets are prevented from prolapsing into the left atrium by the action of chordae tendineae. The chordae tendineae are inelastic tendons attached at one end to papillary muscles in the left ventricle, and at the other to the valve cusps. Papillary muscles are finger-like projections from the wall of the left ventricle.

When the left ventricle contracts, the pressure in the ventricle forces the valve to close, while the tendons keep the leaflets coapting together and prevent the valve from opening in the wrong direction (thus preventing blood to flow back to the left atrium). Each chord has a different thickness. The thinnest ones are attached to the free leaflet margin, whereas thickest ones (strut chords) are attached quite away from the free margin. This disposition has important effects on systolic stress distribution physiology.

During left ventricular diastole, after the pressure drops in the left ventricle due to relaxation of the ventricular myocardium, the mitral valve opens, and blood travels from the left atrium to the left ventricle. About 70 to 80% of the blood that travels across the mitral valve occurs during the early filling phase of the left ventricle. This early filling phase is due to active relaxation of the ventricular myocardium, causing a pressure gradient that allows a rapid flow of blood from the left atrium,

across the mitral valve. This early filling across the mitral valve is seen on doppler echocardiography of the mitral valve as the E wave. After the E wave, there is a period of slow filling of the ventricle. Left atrial contraction (left atrial systole) (during left ventricular diastole) causes added blood to flow across the mitral valve immediately before left ventricular systole. This late flow across the open mitral valve is seen on doppler echocardiography of the mitral valve as the A wave. The late filling of the left ventricle contributes about 20% to the volume in the left ventricle prior to ventricular systole, and is known as the atrial kick.

The mitral annulus changes in shape and size during the cardiac cycle. It is smaller at the end of atrial systole due to the contraction of the left atrium around it, like a sphincter. This reduction in annulus size at the end of atrial systole may be important for the proper coapting of the leaflets of the mitral valve when the left ventricle contracts and pumps blood. Leaking valves can be corrected by mitral valve annuloplasty, a common surgical procedure that aims at restoring proper leaflet adjustment.

*Semilunar valves:* the valve between the right ventricle and the pulmonary artery and that between the left ventricle and the aorta consist of three cup-shaped cusps attached to the fibrous valvular ring. At the end of the reduced ejection phase of the ventricular systole, the blood flow momentarily reverses to the ventricles (referred to as the negative flow in the phasic aortic flow curve of Figure 1.8). This inversion of flow causes rapid cusps of the cusps thus preventing the reflux of blood into the ventricles. During ventricular systole the cusps do not adhere to the wall of the aorta or pulmonary artery, but soar in the blood remaining about halfway between the vessel wall and their closed position, behind the semilunar valves of the pulmonary artery and of the aorta there are small pockets (sinuses of Valsalva), where vortexes are formed which prevent the valve cusps from taking on the walls of the vases. The orifices of the right and left coronary arteries are, respectively, behind the right and left cusp of the aortic valve. If it were not for the presence of the sinuses of Valsalva and of the swirling currents that develop, the hosts of the coronary arteries would be blocked by the cusps of the valvular.

- A. The aortic valve normally has three cusps – a left, right and posterior cusp, although in 1–2% of the population it is found to congenitally have two leaflets.

When the left ventricle contracts (systole), pressure rises in the left ventricle. When the pressure in the left ventricle rises above the pressure in the aorta, the aortic valve opens, allowing blood to exit the left ventricle into the aorta. When ventricular systole ends, pressure in the left ventricle rapidly drops. When the pressure in the left ventricle decreases, the aortic pressure forces the aortic valve to close.

- B. The pulmonary valve (sometimes referred to as the pulmonic valve) is the semilunar valve of the heart that lies between the right ventricle and the pulmonary artery and has three cusps. Similar to the aortic valve, the pulmonary valve opens in ventricular systole, when the pressure in the right ventricle rises above the pressure in the pulmonary artery. At the end of ventricular systole, when the

pressure in the right ventricle falls rapidly, the pressure in the pulmonary artery will close the pulmonary valve.

At the apex of the infundibulum, the pulmonary orifice is guarded by three semilunar cusps - two in front and one behind, with free edges projecting upward into the lumen of pulmonary trunk. The free edge of each cusp presents a fibrous nodule of semilunar cusp at the center with two lateral thin portions, the lunule of semilunar cusp. Each cusp forms pocket like dilatation called pulmonary sinus at initial portion of pulmonary trunk.

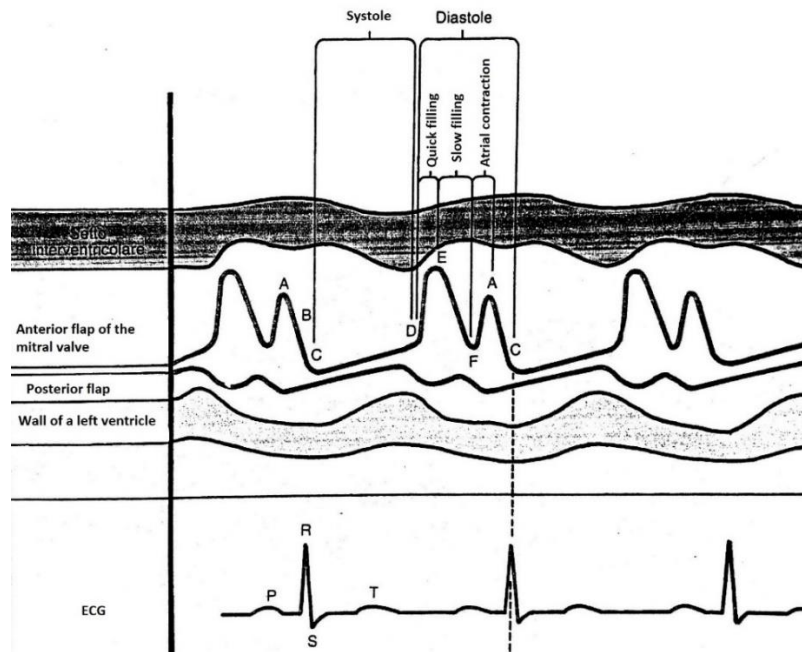


**Figure 1.7** Echocardiogram showing the movements of the valvular flaps of the mitral (in particular the anterior flap), the variation of the diameter of the left ventricular cavity and of the thickness of the left ventricular wall, during a cardiac cycle of a normal subject. From D to C, ventricular diastole; from C to D, ventricular systole; from D to E, fast filling; from E to F, slow filling (diastasis), from F to A, atrial contraction. The mitral valve closes in C and opens in D. Simultaneous recording of the ECG at the bottom.

### Heart tones

Generally four noises are generated in the heart, or tones, but only two are ordinarily perceptible through the stethoscope. With the aid of electronic amplifiers, the less intense tones can be detected and recorded graphically using a phonocardiogram.

The first cardiac tone occurs at the beginning of the ventricular systole (Figure 1.8) and consists of a series of low-frequency vibrations that are out of phase with each other (noises). It is the most intense and prolonged of cardiac tones, has a growing – decreasing quality, and is better audible at the apical region of the heart. The first cardiac tone is mainly generated by the vibrations of the blood in the ventricular chambers and by the vibrations of the ventricular walls. The vibrations are produced in part by the sudden increase in ventricular pressure which causes acceleration of blood towards the atria and, above all, for the sudden tension and rebound of the AV valves and adjacent structures, when the blood is decelerated by closing the valves AV.

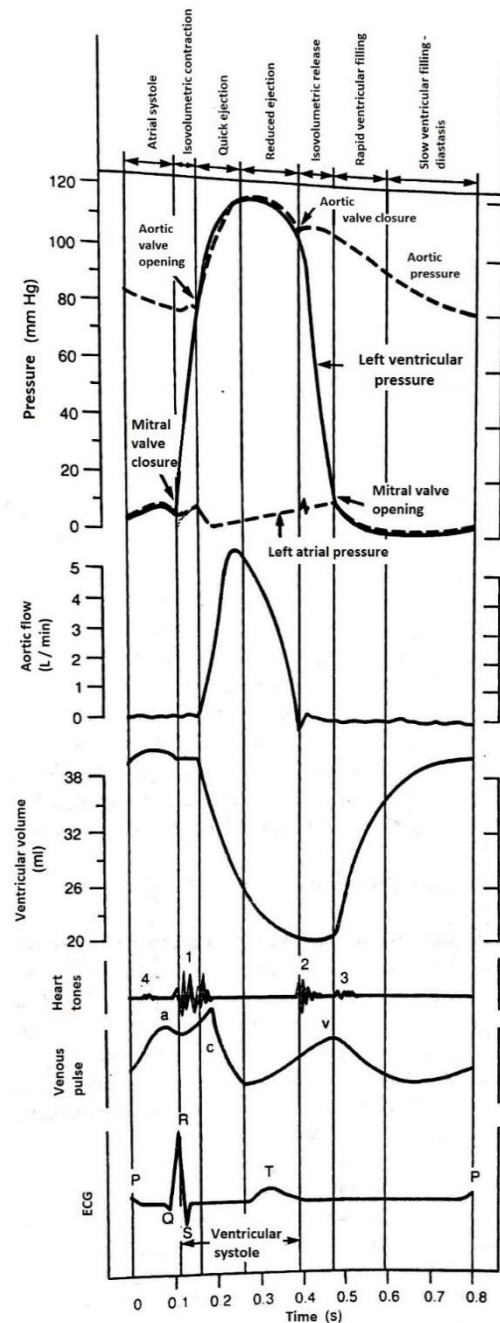
**Figure 1.8 Pressure pulses in the left atrium, aorta, and left ventricle, temporally correlated with aortic flow, ventricular volume, cardiac tones, venous pulse, and ECG, in a complete cardiac cycle of the dog.**

The second cardiac tone, which occurs at the closing of the semilunar valves (Figure 1.8), consists of high frequency vibrations (of a higher tone), of shorter duration and lower intensity, and has a more populating quality compared to the first tone. The second tone is caused by the sudden closing of the semilunar valves which, due to the stretching and elastic retention of the closed valves, causes vibrations of the blood column and of the vascular walls under tension.

The third cardiac tone, more appreciable in children with thin chest walls and in subjects with left ventricular insufficiency, consists of a few low frequency vibrations, better audible to the apex region. It occurs in the first stage of diastole and is believed to be caused by the vibrations of the ventricular walls, due to the sudden cessation of ventricular drift and the deceleration of blood entering the ventricles.

A fourth tone, or atrial tone, is occasionally audible in normal subjects. It is caused by the vibrations of the blood and cardiac chambers due to the atrial contraction (Figure 1.8).

An asynchronous closure of the valves can produce a split tone, at the apex of the heart for the AV valves, and at the base of the heart for the semilunar valves; malformations or deformations of the valves can produce heart murmurs.



## The cardiac cycle

### *Ventricular systole:*

- Isovolumetric contraction.

The beginning of the ventricular contraction coincides with the apex of the R wave of the ECG and with the initial vibration of the first cardiac tone. In the ventricular pressure curve, its beginning corresponds with the beginning of the first increase in ventricular pressure, immediately after the atrial contraction. The interval between the start of the ventricular systole and the opening of the

semilunar valves (when the ventricular pressure rises sharply) is called isovolumetric contraction, because for this period the ventricular volume remains constant (Figure 1.8).

- Ejection.

The opening of the semilunar valves marks the beginning of the ejection phase which can be divided into a shorter first phase (rapid ejection) and a second longer phase (slow or reduced ejection). The rapid ejection phase is characterized by:

- a sudden increase in ventricular and aortic pressure which ends with the maximum development of these pressures;
- a rapid reduction of the ventricular volume;
- a high blood flow in the aorta (Figure 1.8).

The rapid reduction of the pressure curve of the left atrium, which occurs at the beginning of the ejection, is caused by the lowering of the base of the heart and the elevation of the atrial chambers. During the phase of reduced ejection, or slow ejection, the outflow of blood from the aorta towards the periphery exceeds the volume of blood introduced by the ventricle into the aorta; therefore, aortic pressure declines. During the period of the ventricular systole, the blood returning to the atria causes a progressive increase in atrial pressure.

Note that during the first third of the ejection period, the ventricular pressure slightly exceeds the aortic pressure and the flow accelerates (continues to increase), whereas during the last two thirds of the ventricular ejection period exactly the opposite occurs. This inversion of the pressure gradient between the ventricle and the aorta, in the presence of a continuous flow of blood from the left ventricle to the aorta (caused by the inertia of the blood flow), is the result of the storage of potential energy in the dilated arterial walls, which causes a deceleration of blood flow in the aorta.

The effect of ventricular systole on the diameter of the ventricular ventricle is shown in the ECG of Figure 1.7. During ventricular systole (Figure 1.7 from C to D), the septum and the free wall of the left ventricle thicken and approach each other.

At the end of the ejection a volume of blood approximately equal to that expelled during the systole remains in the ventricular cavities. This residual volume is constant in normal hearts, but is reduced by increased heart rate or reduced resistance to flow, while increasing in opposite conditions. An increase in myocardial contractility may reduce the residual volume (by increasing the systolic volume or ejection pressure), especially in a hypodynamic heart. In severely hypodynamic or dilated hearts, as in cardiac collapse, the residual volume may become several times greater than the systolic volume. In addition to serving as a small variable reservoir of blood, the residual volume may allow a certain degree of momentary disparity between the outflow of the two ventricles.

#### *Ventricular diastole:*

- Isovolumetric release.

Closing the aortic valve causes an incision in the descending part of the aortic pressure curve and marks the end of the ventricular systole. The period between the closing of the semilunar valves and

the opening of the AV valves is called isovolumetric release and is characterized by a very rapid fall in the ventricular pressure, without volume variation.

- Quick filling phase.

Most ventricular filling occurs immediately after opening the AV valves, when the blood that had returned to the atria during the previous ventricular systole is suddenly released into the ventricles that are releasing. This period of the ventricular remnant is known as rapid filling (Figure 1.8). The atrial and ventricular pressures are reduced despite the increase in volume, as the released ventricles exert a progressively lower pressure on the blood that is filling their cavities.

- Diastases.

The rapid filling phase is followed by a reduced or slow filling phase, called diastase. During diastasis the blood returning from the periphery flows into the right ventricle and the blood drains from the lungs into the left one. This small but slow increase in ventricular filling is associated with a gradual increase in ventricular and venous pressure, and ventricular volume.

- Pressure - volume relationship.

Changes in pressure and ventricular volume over the course of the cardiac cycle are summarized in a schematic way in Figure 1.9: in this pressure-volume graph the time element is not considered; the diastolic filling begins in A and ends in C, when the mitral valve is closed. The initial reduction in pressure in the left ventricle (A to B), despite the rapid flow of blood from the atrium, is due to the progressive relaxation and distension of the ventricle chamber. During the remaining part of the diastole (from B to C) the increase in ventricular pressure reflects the ventricular filling and the elastic characteristics of the ventricle.

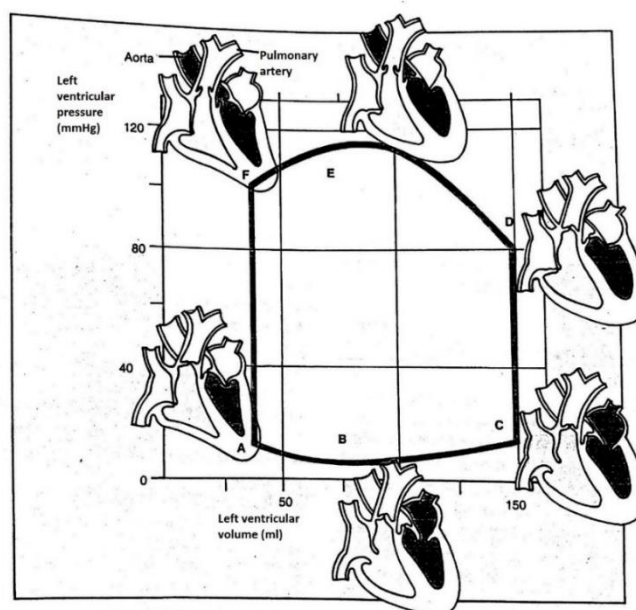


**Figure 1.9** The pressure-volume cycle of the left ventricle in a single cardiac cycle (from A to F).

Note that during diastole only a small pressure increase occurs with the increase in ventricular volume (from B to C). The isovolumetric contraction (from C to D) causes a rapid increase in

pressure without variation of the ventricular volume. In D the aortic valve opens and during the first phase of the injection (rapid ejection, from D to E) the large reduction in volume is followed by the reduced ejection (from E to F) and a slight reduction in intraventricular pressure. The aortic valve closes in F; the isovolumetric release (from F to A) takes place, characterized by a rapid pressure drop without volume variation. In A the mitral valve opens and the cardiac cycle is complete.

#### *Atrial systole:*

Begins immediately after the onset of the P wave of the ECG (wave of atrial depolarization), and the passage of blood from the atria to the ventricles, caused by a symmetrical wave of atrial contraction, completes the ventricular filling period (Figure 1.9). During the ventricular diastole, the atrial pressure slightly exceeds the ventricular pressure, indicating that the open AV valves are a low-resistance pathway.

Since there are no valves at the outlet of the hollow veins in the right atrium and of the pulmonary veins in the left atrium, the atrial contraction can push the blood in both directions. In reality, the reflux of blood in the tributary veins is modest, especially because of the inertia of the blood that flows to the heart.

Atrial contraction is not essential for ventricular filling. In patients with atrial fibrillation or complete heart block often the ventricular filling is adequate, despite the absence of atrial contraction. However, the contribution of atrial contraction largely depends on the heart rate and the structure of the AV valves. At low heart rates the filling is practically complete at the end of the diastasis and the atrial contraction contributes little to the filling. In tachycardia, diastasis is instead abbreviated, and the contraction contribution occurs immediately after the rapid filling phase, when the pressure gradient AV is maximum. If the tachycardia becomes so high that it interferes with the rapid filling phase, then atrial contraction is of great importance in rapidly pushing the blood into the ventricles during this short period of the cardiac cycle. In certain morbid states, the AV valves can become remarkably narrow (stenosis). Under such conditions, atrial contraction may have a far more important role for ventricular filling than a normal heart.

#### Conduction system

For the electrical stimulus with which excitement begins, conduction and then contraction, a specialized system, which constitutes the specific system of the heart, is located in some areas of the heart.

The cells that constitute it are a little different from the contractile muscle, having in part characteristics similar to those of the nervous system.

They belong to the specific system of the heart (Figure 1.10):

- a. The sinus or Keith-Flack node, placed near the outlet in the right atrium of the superior vena cava, this structure begins, depolarizing, the electrical activity of the heart;
- b. The atrioventricular junction, or node of Tawara-Aschoff, consisting of cells of different nature, to which comes the electrical stimulus that excited the atria and which in the junction slows down

before entering the beam of His due to the heterogeneous conduction of the different types of cells. His beam starts from the junction, enters the fibrous body of the interventricular septum and at the end of the interventricular membranous septum, between this and the non-coronary aortic cusp, is divided into a right and a left branch.

The left branch is further subdivided into an anterior fascicle and a posterior one at the height of the lower third of the septum, from the specific part, directed from the endocardium towards the epicardium in the ventricular walls, the Purkinje network, which is missing only in the third top of the septum: it ensures the almost simultaneous arrival of the electrical stimulus in every structure, even peripheral, of the heart.

The two branches run relatively to the surface in the septum, which is thus functionally divided into a septum belonging to the right branch and one to the left branch;

- c. The internodal atrial fibers that, although not as distinct as the bundle of His and its branches, ensure a constant atrial excitation.

The three interatrial beams are the anterior, middle and posterior bundles and connect the node to the atrioventricular junction. The anterior one, or Bachmann's beam, is the most constant as an anatomical presence and arrangement.

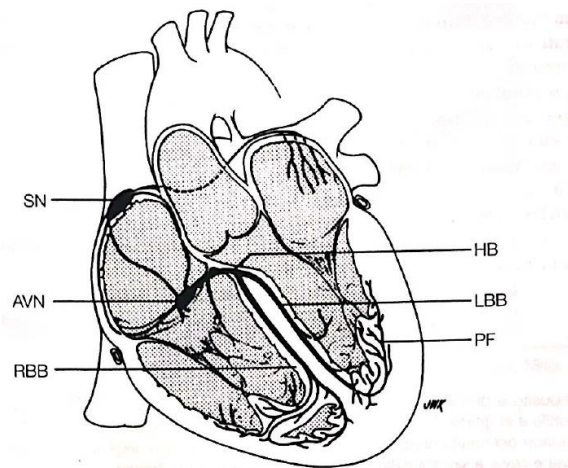


**Figure 1.10 Schematic representation of the heart conduction system. SN, sinus node; AVN, atrioventricular node; RBB, right branch; HB, His beam; LBB, left branch; PF, Purkinje fibers.**

## 1.1 Diseases of the circulatory system

Cardiovascular diseases (CVD) are the most common cause of death globally as of 2017, accounting for 45% of all deaths in Europe and 37% of all deaths in the EU. Of these more than three quarters are a result of coronary artery disease and stroke.

Risk factors include: smoking, being overweight, little exercise, high cholesterol, high blood pressure, and poorly controlled diabetes, among others. Cardiovascular diseases frequently do not have symptoms or may cause chest pain or shortness of breath. Diagnosis of heart disease is often done by the taking of a medical history, listening to the heart-sounds with a stethoscope, ECG, and ultrasound.

### 1.1.1 Valvular vices

Valve vices are abnormalities in the function of the cardiac valves due to anatomical alterations of the flaps and / or of the valvular apparatus.

Schematically, valvular defects can be classified according to three main criteria:

#### A. Nature of vice

- *Stenosis*. The valvular ostium is restricted and impedes the passage of blood in an anterograde direction to a more or less serious extent;
- *Failure*. The valve is not continent and therefore allows the blood to regurgitate backwards. Failure may be either direct or direct injury to the valve or secondary to dilatation of the cardiac cavity;
- *Steno-insufficiency*. The two functional alterations coexist and therefore there is an obstacle to the anterograde flow as well as a retrograde regurgitation; in the case of rheumatic valvular vices this is the most common condition.

#### B. Seat of the vice

Stenosis, insufficiency or steno-insufficiency may occur in each valve or be presented in multiple valves simultaneously. In the adult the most commonly affected valves are those of the left sections of the heart (mitral and aorta). In the case of rheumatic etiology, the association of mitroaortic vices is common. The valves of the right sections of the heart (tricuspid and pulmonary) are rarely the site of left-hand valvular vices. A primitive involvement of the valves of the right sections is more commonly congenital in nature.

#### C. Etiology of vice

Rheumatic endocarditis, even if in constant decline, remains the most common cause of valvular vices; other causes are congenital anomalies, infective endocarditis, ischemic heart disease, cardiomyopathies, primitive changes in the connective tissue.

Given the subject of the thesis, the different types of valvular stenosis and vices will be neglected to be able to deepen the aortic stenosis.

### 1.1.2 Aortic stenosis

In addition to aortic stenosis proper, there are also other obstacle conditions to the outflow of the left ventricle (due to structure other than the valve).

Schematically, an obstruction of the left ventricle can occur at four different levels (Figure 1.11).

Valve obstructions are mostly due to inflammatory or degenerative processes, which overlap in many cases with congenital malformations of varying severity; therefore, they occur in the adult or in the elderly, unless the malformation is very serious from birth.

The obstructions above and below, however, are always congenital and manifest in childhood or youth: they consist of diaphragms or narrowings in the immediate vicinity of the valvular ostium. From a clinical and physiopathological point of view, they are almost completely superimposable to congenital valvular stenosis. The characteristic (but not constant) obstruction of hypertrophic cardiomyopathy (a hereditary disease that manifests itself mostly in adulthood) occurs during the systolic concentration for approximation of the mitral anterior limb to the hypertrophic septum.

However, the subaortic stenosis of hypertrophic cardiomyopathy has peculiar physiopathological and clinical characteristics.

A. *Etiopathogenesis.* In more than half the cases of aortic stenosis, the valve has an anomalous congenital structure. In place of the three normal semilunar cusps divided by regular commissures (Figure 1.11), the valve may have only one cusp (monocuspid) with a small eccentric orifice. In this case the signs of aortic obstruction are present from birth. More frequently, the valve is bicuspid and the malformation (which affects almost 2% of the population) does not in itself lead to significant obstruction. The excessive turbulence of the blood around the valvular flaps however produces, over the years, the appearance of fibrosis, calcification and therefore imperfect opening of the valvular apparatus. The structural alteration also makes it easier to implant an infective endocarditis, after which the stenosis can worsen with a valve insufficiency due to partial destruction of the flaps. Sometimes the tricuspid valves can have irregular flaps of different sizes and with partial melting of the joints. If this creates an increase in turbulence in the flow, over time a stenosis may occur with the same mechanism mentioned above.

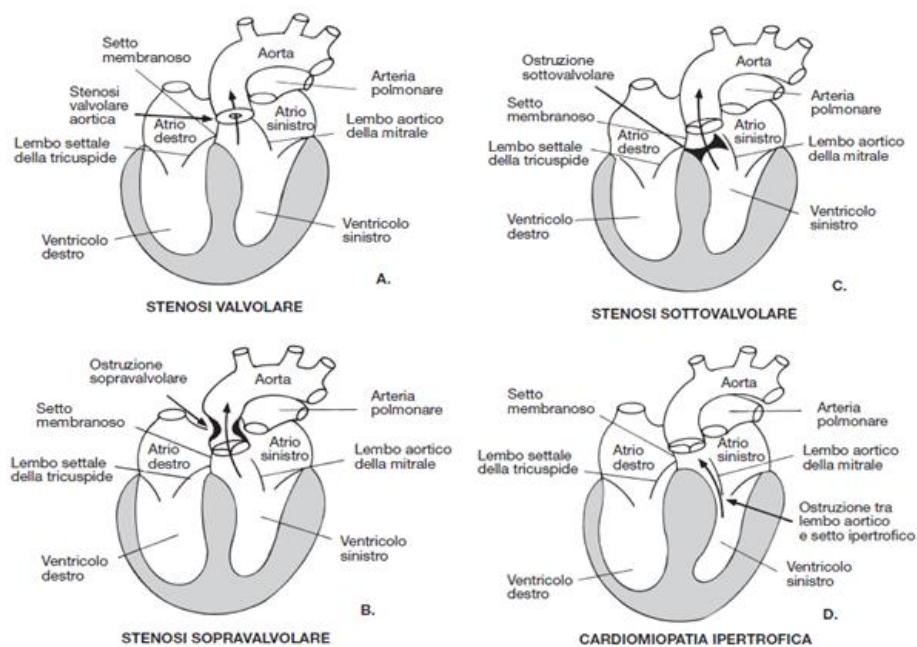


**Figure 1.11** An obstruction of the outflow of the left ventricle can occur at four different levels. A. Valvular, often with loss of commissures and with a small central orifice; B. Spore valvular, most often due to hourglass narrowing of the ascending aorta; C. Under-valvular, due to the presence of congenital fibrous diaphragms below the valvular plane; D. Between the septum and the aortic limb of the mitral, as occurs in hypertrophic cardiomyopathy, where the septum is hypertrophic and the aortic limb of the mitral is moved forward during the systole.

Finally, in some cases, the stenosis is produced on a completely normal valve at birth. The cause of this fact is unknown, but it is thought that it depends on processes similar to those that produce coronary atherosclerosis. In fact, this type of aortic stenosis is associated with the same risk factors of coronary atherosclerosis, such as hypertension and hypercholesterolemia.

Aortic stenosis of rheumatic origin is rarely isolated: it is mostly associated with aortic insufficiency and especially with mitral valvular vices. The inflammatory process produces fusion of the joints, hence stiffening and retraction of the valvular edges (hence the associated insufficiency) and formation of calcified nodules on the free surfaces. Degenerative aortic stenosis, which is attributed to the wear and tear of the valve, appears as a result of progressive fibrosis and calcification at the root of the valvular flaps (which can then open normally, even if the joints remain free) in older people (over 65 years), or atherosclerotic changes in people with severe hypercholesterolemia. Also those affected by Paget's disease are particularly predisposed to the early onset of degenerative aortic stenosis.

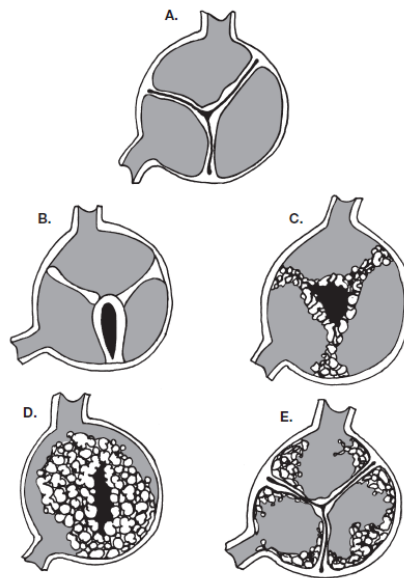


**Figure 1.12** Several valve morphologies in case of aortic stenosis. **A.** Normal tricuspid valve. **B.** Congenital stenosis with practically monocepatic valve and small eccentric orifice. **C.** Stenosis of rheumatic origin with vegetations and fusions of the flaps, which have thickened and retracted edges (coexistence insufficiency). **D.** Calcific aortic stenosis of a bicuspid valve. **E.** Senile aortic stenosis with calcification of cusps of an originally normal valve.

- B. Pathophysiology.** When the opening area (ostium) of the aortic valve is reduced compared to normal, the blood that is expelled into systole from the ventricle forms vortices around the valvular structures. These turbulences give rise to pathological noises (puffs) that can be heard on the chest. The vortices, over time, also produce calcific fibrosis of the valvular flaps, which tends to progressively aggravate the stenosis up to alter the cardiac function (hemodynamically significant stenosis). Valvular narrowing is an obstacle to blood ejection. In order to overcome this resistance and maintain a normal flow, the pressure in the left ventricle in systole must always exceed the

pressure in the aorta (Figure 1.13). This difference is called pressure gradient between ventricle and aorta and is proportional to the obstruction. When the valvular ostium is reduced to less than a quarter of normal, the pressure gradient rises above 50 mmHg. This is then called critical stenosis, concomitantly with which the first symptoms of the disease usually appear.

The systolic pressure overload stimulates a concentric hypertrophy of the left ventricle: the walls thicken considerably, while the cavity does not expand and therefore the total volume of the heart increases little. The increase in thickness of the walls counterbalances the increase in systolic ventricular pressure, so as to maintain the stress (or stress) of the wall, ie the afterload, at almost normal values. This is due to the Laplace law. Thanks to this the ventricle can maintain a normal performance for a long time, at least at rest, despite the obstruction. However, the mechanism of compensation for hypertrophy involves two costs.

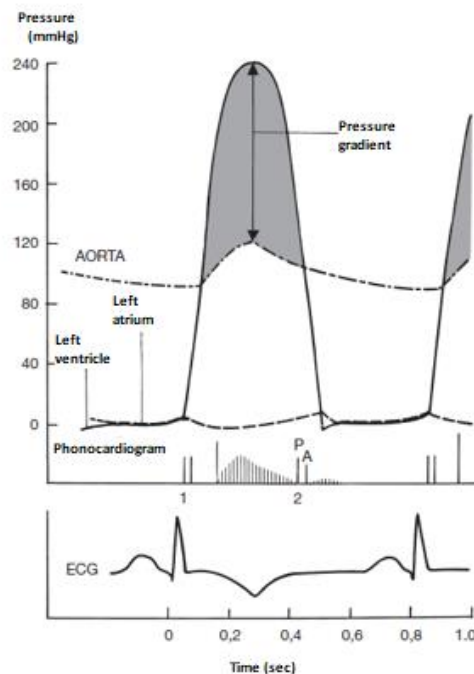


**Figure 1.13** In the diagram the pressure gradient is evident that is determined in systole between left ventricle and aorta. The ejection blow (below) reaches its maximum when the pressure gradient has the greatest amount.

1. The consumption of myocardial O<sub>2</sub> increases due to the increase in muscle mass. Added to this is an increased compression of the coronary arteries (due to the increase of the intracavitary pressure), which hinders the flow, and an extension of the systole. All these factors together can lead to myocardial ischemia (insufficient oxygen supply in relation to the needs), even in the absence of coronary artery disease.
2. Decreases the distensibility (compliance) of the left ventricle. Greater rigidity increases the ventricular diastolic pressure even in the absence of decompensation. To achieve full ventricular filling, the left atrium must exert a more energetic contraction and become hypertrophied. Atrial input becomes indispensable for good cardiac functioning: the onset of

atrial fibrillation or an atrioventricular block (two conditions that result in the loss of a useful atrial contraction) can therefore precipitate this precarious balance.

*Physical effort*, however, represents the most frequent situation, capable of putting a strain on the mechanisms of heart compensation with aortic stenosis. During the effort, therefore, three serious pathophysiological phenomena can be more easily determined.

1. Consumption of cardiac O<sub>2</sub> increases considerably under stress, while coronary perfusion is hampered by extrinsic compression from the hypertrophic live myocardium. This explains the appearance of stress angina.

2. Systolic ventricular pressure increases tremendously in an attempt to maintain the flow required by muscular exercise. This causes an abnormal stimulation of the ventricular baroreceptors (receptors sensitive to pressure variations), which in turn trigger a reflex of abrupt peripheral vasodilatation. This is probably a regulatory mechanism in the normal ventricular subject, reducing peripheral resistance. In the subject with aortic stenosis, however, the point of maximum resistance is placed on the valvular ostium and is not modifiable. The reflex of the ventricular baroreceptors then causes systemic resistance to collapse without managing to reduce ventricular pressure.

The reduction of the resistances can not be compensated by an adequate increase in the cardiac flow, due to the obstruction to the efflux. Therefore, pressure systems fall, rather than increase as normally happens under stress, until they show signs of cerebral hypoperfusion: lipothymia and syncope. The appearance of severe arrhythmias, especially ventricular, can prolong syncope or, in some cases, trigger it even at rest.

3. The increase in systolic ventricular pressure under stress increases the afterload (wall effort) until the ventricle can no longer expel all the blood it receives in diastole into systole. Then the pressures in the left atrium and in the pulmonary circulation rise and the signs of pulmonary congestion (exercise dyspnea) appear. With the aggravation of the situation, the left ventricular failure manifests itself by efforts of ever smaller entity and finally also at rest, with signs and symptoms of heart failure, initially only sinister and then global. The ventricle expands and this often leads to the appearance of a mitral insufficiency, which compromises the situation even more. Without a therapeutic intervention the patient reaches death within a few years from the onset of the first relevant symptoms (angina, syncope or dyspnea).

C. *Clinic*. The patient with aortic stenosis has no symptoms for many years, while the obstacle is progressively aggravated until reaching a critical entity. At this point the first disturbances appear, sign of the fact that the ventricle can no longer compensate for the negative effects of the obstruction.

The cardinal symptoms of aortic stenosis are three: dyspnea, angina, syncope. All generally arise in occasions of physical effort. In most cases the first symptom is exercise dyspnea, while other symptoms of left ventricular failure (orthopnea, paroxysmal dyspnea, pulmonary edema) intervene

only in advanced stages of the disease. Dyspnea is often associated with a sense of chest weight, which should not be confused with the actual angina pectoris present in many patients with aortic stenosis. This angina is not different from the stress angina typical of coronary artery disease: indeed, often a more or less severe coronary atherosclerosis is associated with aortic stenosis, especially in elderly people.

Syncope is the rarest symptom (present in about 10% of patients). It arises mostly under stress (unless it is triggered by an arrhythmia) and is preceded by premonitory symptoms. Often during the loss of consciousness there are convulsions and involuntary loss of urine and faeces.

The objective examination of the patient with aortic stenosis allows to detect signs on the pulse and the heart.

The pressure is normal, unless a hypertension of another origin coexists. In the advanced stages of the disease the systolic pressure can be "beheaded" (with reduction of the differential pressure) due to the decrease in systolic flow.

Arterial pulses are normal until the stenosis becomes hemodynamically significant: then they become late, ie they have a slow rise in the pressure wave, due to the obstruction that slows down the ejection. This is clearly evident with the registration of the carotid pulse (Figure 1.14). When the differential pressure falls, the pulse becomes small.

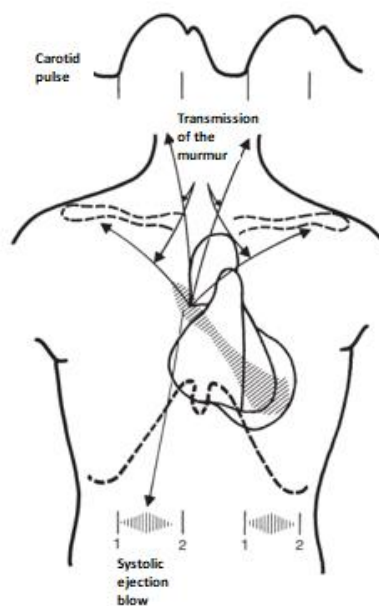


**Figure 1.14** The scheme indicates the focal points of maximum intensity of the ejection systolic murmur characteristic of aortic stenosis, with the typical irradiation towards the neck vessels. At the top, the carotid pulse track shows a slow ascent and a reduced performance (late and small pulse).

Precordial palpation allows a more energetic and prolonged toe to be detected only when significant left ventricular hypertrophy appears. Since hypertrophy is concentric in pure stenosis, and therefore the total volume of the heart has not increased, the stroke is almost in its normal location. When the heart dilates due to the appearance of severe decompensation (or due to the simultaneous presence of an aortic insufficiency), the impulse moves to the left and down. When the decompensation also

involves the right ventricle, a low left-sided xifloid or parasternal pulse appears. Finally, with palpation, a tremor (which is the tactile sensation corresponding to a low-frequency murmur) can also be detected in the high parasternal region or in the jugule.

Listening allows to detect numerous signs that generally make it possible to ascertain the presence and severity of the stenosis. The most characteristic sign is an audible systolic murmur in the right upper parasternal region, often irradiated towards the vessels of the neck and towards the cardiac apex. The murmur is due to the turbulence produced by the blood expelled through the narrow valvular ostium. Begins after I tone, it grows until it reaches a maximum at the height of the injection, then decreases and ceases before the 2nd tone. The murmur then follows a course parallel to the expulsion of blood during systole. The crescendo and decrescendo form (which confers a diamond configuration to the murmur recording; Figure 1.14) and the interruption before the 2nd tone are characteristic of the expulsive puffs and allow it to be distinguished from the regurgitated puffs (for example, from mitral insufficiency).

The murmur of aortic stenosis often disappears above the breastbone and reappears in the area of the tip, simulating the systolic murmur of mitral insufficiency (Gallivardin phenomenon).

The murmur of aortic stenosis is of low frequency (this is almost always accompanied by a tremor) and of a sour shade. Its intensity is not proportional to the degree of stenosis. On the contrary, in the terminal phases of the disease, when the ejection is very reduced due to the severe obstruction, the murmur can be intense even when the stenosis is completely insignificant on the hemodynamic plane. It is very common, especially in elderly people, the finding of an aortic expulsive murmur due to a modest valve degenerative calcification, without any valvular alteration. Therefore the presence of aortic stenosis can be indicated only by an overall clinical picture and not by an isolated systolic murmur.

In the initial stages of the disease (and especially in congenital cases) the murmur of aortic stenosis is preceded by an ejection click. It is a short and dry noise produced by the abrupt opening of the stiffened valve: it follows therefore a short distance from the first tone. When, with the progressive worsening of the disease, the valve structure is altered to the point of almost completely preventing the movements of the flaps, the click disappears. It is always absent from the beginning in cases of congenital over or under-valvular stenosis, in which, in fact, the valve functions normally.

The aortic component of the II tone ( $A_2$ ) is often reduced in intensity (due to the poor mobility of the flaps) or fused with the pulmonary component ( $P_2$ ), for the prolongation of the left injection caused by the obstruction. In some cases the prolongation of the left ejection phase can be such as to drop  $A_2$  after  $P_2$ . We speak then of paradoxical doubling of the second tone: in fact in these cases the doubling increases during expiration (which shortens the duration of right ejection and prolongs the left one by delaying even more  $A_2$ ) and is reduced or canceled during inhalation (which has opposite effects on ventricular ejection times). Physiological splitting, on the other hand, occurs during inspiration and disappears with exhalation, since normally  $P_2$  falls after  $A_2$ .

Another possible cause of paradoxical doubling of the II tone in patients with aortic stenosis is the left bundle branch block. Conduction disturbance, delaying the contraction of the left ventricle, can cause  $A_2$  to fall after  $P_2$ . Left bundle branch block is not uncommon in patients with aortic stenosis due to the possible "casting" of calcific infiltration of the valve to the contiguous ventricular conduction system.

Concentric hypertrophy involves a reduction in compliance of the left ventricle, which often manifests itself with an added presystolic tone (IV tone) at the most energetic atrial contraction. On the contrary, a third tone (or diastolic proto) appears only when the decompensation occurs. Then all the signs (cardiac, thoracic and general) of ventricular insufficiency are manifested, first only left and then, due to the pulmonary hypertension that is established, also right.

The diagnosis of aortic stenosis must be confirmed with a series of instrumental examinations that allow even better to assess the entity.

The electrocardiogram allows to appreciate the signs of right ventricular hypertrophy, induced by pressure overload, almost always present in significant stenoses.

Signs of left atrial dilatation are also often present, caused by the increased resistance of the hypertrophic ventricle to atrial emptying. In some cases there are atrioventricular or intraventricular conduction disturbances due to calcification.

The chest radiograph shows in most cases an almost normal heart (hypertrophy is concentric) with a rounded tip and the dilated ascending aorta (Figure 1.15).

This last sign, called poststenotic dilatation, is due to the mechanical effect on the aortic walls of the turbulences caused by the valve obstruction.

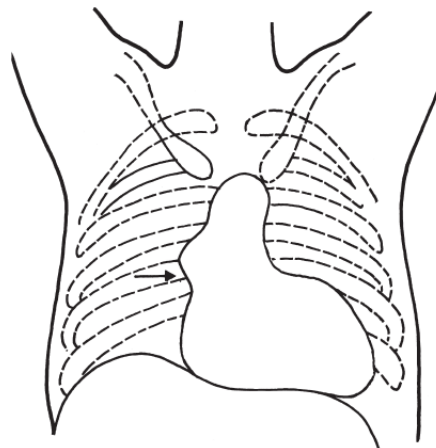


**Figure 1.15** Chest diagram in antero - posterior projection of a man with severe aortic stenosis. The arrow indicates the poststenotic dilatation of the ascending aorta. In this case, a fair degree of left ventricular hypertrophy is also visible.

The fluoroscopy test allows to highlight the valvular calcifications: if they are absent, it is unlikely that the stenosis is significant; conversely, in older people, there may be significant calcifications without major obstructions. When the decompensation begins, the ventricle and left atrium dilate and the radiological signs of pulmonary congestion appear.

With single or two-dimensional echocardiography, it is often possible to confirm the presence and severity of the stenosis (poor opening of the cusps in an enlarged aortic root), the presence of

calcifications (multiple and thickened echoes), concentric ventricular hypertrophy and any signs of decompensation. With echocardiography it is easy to recognize the presence of a bicuspid aortic valve, a congenital condition that often underlies progressive stenosis. The Doppler ultrasound, above all, allows to calculate with considerable precision the pressure gradient between ventricle and aorta. Finally, the ultrasound allows to identify any other associated valvular anomalies.

In order to arrive at a final decision regarding the advisability of surgery, however, it may be necessary to perform a left catheterization with angiocardiology and coronarography. The bloody examination allows to collect many useful elements: the pressure gradient between ventricle and aorta; the area of the valvular ostium; the precise site of the obstruction (in congenital non-valvular cases); the extent of hypertrophy and the functional state of the left ventricle. With the information that can be obtained today from echocardiography, cardiac catheterization is especially indicated to detect any atherosclerotic coronary lesions, present in 50% of males over 40 years of age.

- D. *Prognosis and indications of therapy.* As already mentioned, aortic stenosis remains silent and asymptomatic for many years, thanks to the reserves of compensations of the left ventricle. However, when the first serious symptoms appear (angina, syncope, dyspnea), a rapid decline begins, leading to death, in the absence of intervention, within 2-6 years on average. In 15-20% of cases death is sudden. The most difficult therapeutic decision is the choice of the best time to perform the replacement surgery of the diseased valve with a prosthesis (mechanical or biological) in patients with critical stenosis (pressure gradient above 50 mmHg and reduced orifice to  $\frac{1}{4}$  or less of normal).

Unlike mitral stenosis, balloon valvulotomy usually resulted in poor results. In fact, the frequency of serious complications, such as sudden death, stroke, rupture of the aorta and aortic insufficiency, is greater than 10%. Mortality after this treatment is 60% after 18 months, ie comparable to that of untreated subjects. Therefore, the best intervention is valve replacement. The only exception to this rule is the case of children or young people with non-calcified congenital valvular stenosis, in which it may be useful to perform a simple valvulotomy (cutting the commissures to enlarge the ostium) even in the asymptomatic phase. Heart failure and angina are treated with drugs in the usual way. Abstention from intense exertion and antibiotic prophylaxis against the risk of infective endocarditis (severe but not frequent complication of structural changes of the aortic valve) should be advised, even to the asymptomatic patient, in the case of cruel maneuvers such as dental extractions. Prophylaxis should continue even after valve replacement with a prosthesis.

## 2 Aortic root

The aortic root connects the heart to the systemic circulation and is a highly sophisticated and complex structure. Each component of the aortic root - although simple in its macroscopic morphology - has an optimal macroscopic and microscopic structure and anatomical architecture which contributes to the function of the aortic root as a whole: the intermittent, unidirectional channeling of large volumes of fluid, while maintaining laminar flow, minimal resistance and least possible tissue stress and damage, during varying hemodynamic conditions and demands. This well-coordinated dynamic behavior of all aortic root components has been shown to be of importance for specific flow characteristics, coronary perfusion and left ventricular function.

### 2.1 Anatomy of the aortic root

The aortic root is an ensemble consisting of distinct entities: the aortic valve leaflets, the leaflet attachments, the sinuses of Valsalva, the interleaflet trigones, the sinotubular junction and the annulus.

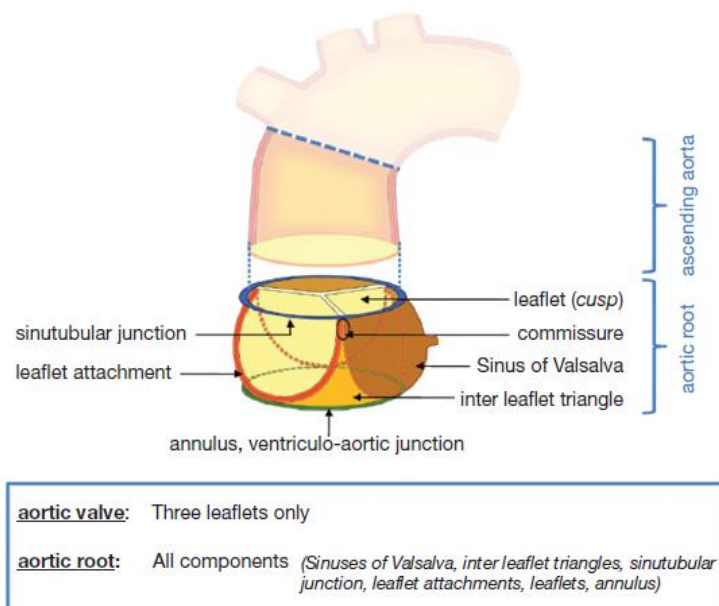


**Figure 2.1 Proposed nomenclature for the aortic root components.**

The three leaflets form the aortic valve and provide its main sealing mechanism. Anatomically the valve leaflets can be divided into three parts:

- The free margin, with a thickened circular node (nodule of Arantius), which provides the coaptation area to the corresponding neighboring valve leaflets
- The “belly” of the leaflet
- The basal parts of the leaflet or leaflet attachments

The aortic valve leaflets form the hemodynamic junction and physical boundary between the left ventricle and the aorta. All the structures distal to the hemodynamic junction are subject to arterial pressures, whereas

all the proximal parts are subjected to ventricular hemodynamics. The trileaflet design represents the optimal solution for low resistance valve opening. No other valve configuration can provide these characteristics, a fact prominently demonstrated in the setting of a bicuspid aortic valve, in which some kind of valve dysfunction or degree of stenosis always co-exists depending on the configuration.

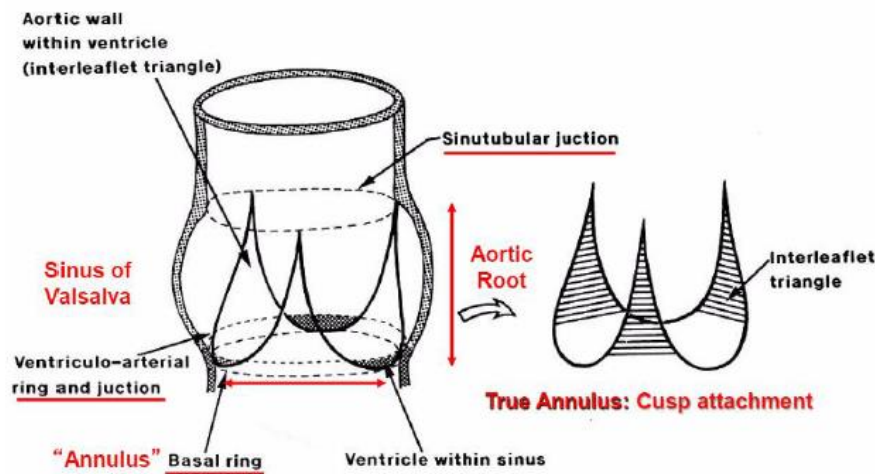


Figure 2.2 Schematic representation of the aortic root. AA = aortic annulus, ST = synotubular junction, H = commissural height.

The aortic root is therefore a complex structure in which each individual element (annulus, flaps, triangles "interleaflets", commissures, sinuses of Valsalva and sino-tubular junction) assumes a role of fundamental importance for correct functionality. The geometric relationship of the aortic root it is also of particular importance. The diameter of the annulus aortic, of the sinus, the sino-tubular junction and the ascending aorta are correlated with body surface and age. The relationships and proportions of these components, fundamental in ensuring a physiological functioning of the aortic valve, are shown in Figure 2.3.

The sinus may not be symmetrical (ex.: the non-coronary sinus is larger than the others) and small differences in size there may be amplitude and height of the valvular flaps.

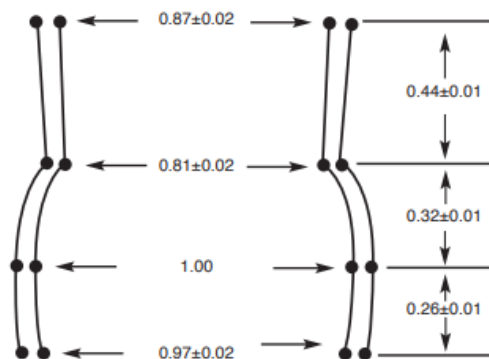
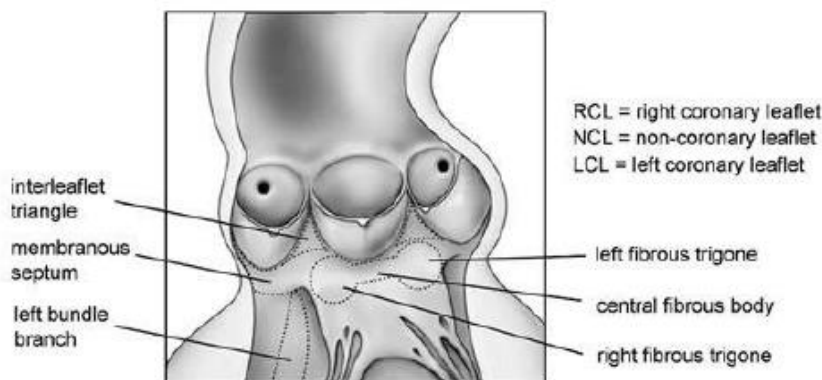


Figure 2.3 Normalized size of an un-pressurized human aortic root.

The opening and closing of the valve depends not only on the characteristics anatomical components of the various components but also from modifications in the form and size of the aortic root during the cardiac cycle. The isovolumetric contraction ventricular through the interleaflet triangles makes it expand slightly the commissures which, by placing the flaps under tension, start the opening of the valve even before the

blood flow passes through it. During systole, the aortic root takes on a more cylindrical appearance for favor ejection, while during diastole there is a simple elastic recoil to return to the starting conditions.

The systolic expansion of the root, evident above all at the sinuses of Valsalva, also allows the flaps to be open progressively until they reach their classic triangular appearance, without creases or wrinkles ever forming along their free margin.



**Figure 2.4** Anatomic section of the aortic root

This aspect is essential to ensure the longevity of their operation (Figure 2.5).

As well understood by Leonardo about 500 years ago, it is precisely for the presence of the vortices formed in the sinus ("eddy currents") that not only the flaps they do not come into contact with the aortic wall, but they promote the mechanism of valve closure. The shape of the sinuses and their continuity with the flaps Aortic is indeed essential for an effective, symmetrical and coordinated closure valve. Furthermore, most of the mechanical stress on the flaps during the diastole is "absorbed" by the sinuses of Valsalva through the cyclical changes dimensions.

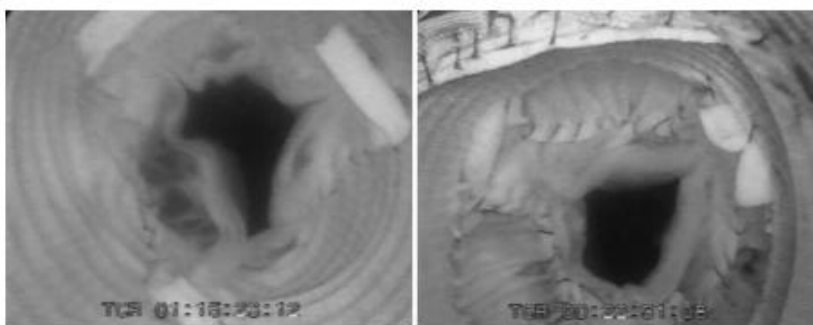


**Figure 2.5** Appearance of opening an aortic valve in the presence (right) or absence (left) of the sinuses of Valsalva.

## 2.2 Aortic root surgery

Several surgical techniques have been developed for the correction of dysfunctional or misaligned leaflets leading primarily to aortic insufficiency. The required height and size of the leaflets to warrant competent valve function are primarily determined by the root size. These considerations seem to be a major

determinant for the durability of aortic valve repair. Another important factor for the durability of the repair is adequate tissue quality, especially in the setting of bicuspid aortic valve disease.

As the leaflet attachments insert in the wall of the aortic root they form a crown shaped, thick fibrous structure, often termed the “annulus”. This description is unfortunate as the word annulus implies a circular structure in contrast to the “crown” shape of the leaflet attachment. The points where the leaflet attachments run parallel - distally upstream towards the ascending aorta - are called the commissures.

The three bulges of the aortic wall are named the sinuses of Valsalva, after the Italian anatomist Antonio Valsalva. Two of the three sinuses host the origin of the coronary arteries and the sinuses are termed accordingly the left, right and non-coronary sinus. They are limited proximally by the attachments of the valve leaflets and distally by the sinotubular junction. At their base, ventricular musculature is partly incorporated. The sinus wall itself is predominantly made up of aortic wall, although it is thinner than the native aorta. The precise function of the sinuses of Valsalva is unclear. There is evidence that the vortices created in the sinuses lead to stress reduction on the aortic leaflets and support coronary flow. In valve sparing aortic valve surgery, maintenance or recreation of the sinuses has been shown to effectively recreate the vortices in the sinuses and may be beneficial in terms of normal leaflet movement and valve durability (Figure 2.1). However, aortic root reimplantation without recreation of the aortic sinuses has not been shown to have deleterious effects on valve durability despite abnormal leaflet motion. In general, there is a need for aortic root replacement material that imitates the compliant characteristics of the normal aortic root. This would allow for an ideal, and low stress, movement of the leaflets and could be a future area of interest and research not only for prosthetic material design but also for tissue engineering.

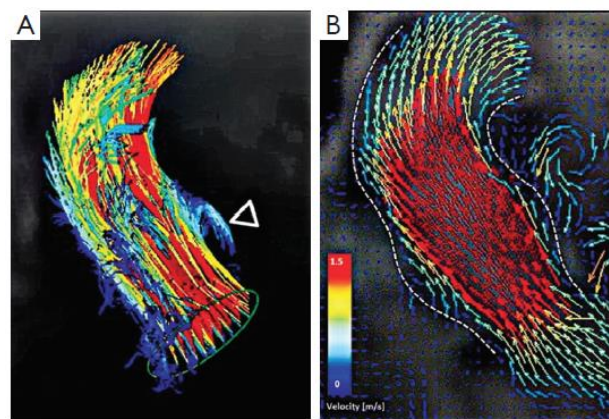


**Figure 2.6 Aortic root vortices visualized using flow-sensitive time-resolved ‘4D’ magnetic resonance imaging with flow sensitivity in all three directions.**

Under each commissure lies one of the three interleaflet triangles. Although histologically they consist of thinned aortic wall, hemodynamically they are extensions of the ventricular outflow tract and reach the level of the sinotubular junction in the area of the commissures.

The triangle between the right- and non-coronary sinuses faces the right atrium. It is in direct continuity with the membranous septum proximally which contains the His bundle. This area is of special importance during aortic valve procedures, as injury here can lead to temporary or permanent conduction abnormalities, which

may require the implantation of a permanent pacemaker. Under the left and non-coronary triangle, the aorto-mitral curtain leads to the anterior mitral valve leaflet.

The distal part of the sinuses toward the ascending aorta together with the commissures form a tubular structure called the "sinotubular junction" which separates the aortic root from the ascending aorta (Figure 2.1). In some cases, dilatation of the sinotubular junction is the cause of central aortic insufficiency and replacement of the ascending aorta with a short tubular graft can restore valve competence.

Although the word annulus implies a circular structure, no distinct histological entity or anatomical boundary fits this description. The circumference defined by the nadirs of the semi-lunar leaflet attachments is difficult to define as the annulus, because there is no real, anatomically or histologically distinct, circular structure. The term 'ventriculo-arterial junction', as a definition of the "annulus", is rather ambiguous as the 'anatomical ventriculo-arterial junction' represents the junction between the left ventricular myocardium and the arterial structure of the aorta. On the contrary, the 'hemodynamic ventriculo-arterial junction' is represented by the coronet shaped leaflet insertion, and defines the separation level of ventricular and arterial hemodynamics. From a strictly anatomic point of view, the 'anatomic/histologic ventriculo-arterial' as well as the 'hemodynamic ventriculo-arterial' junction lie somewhat more distally to the 'annulus' and define the area of interest less precisely.

Despite the absence of any anatomically or histologically distinct circular structure the popularity of the term 'annulus' probably stems from the fact that this is the area of the smallest diameter in the blood path between the left ventricle and the aorta and determines the fitting position of prosthetic valve sizes and, therefore, the size of the prosthetic valve to be implanted. In addition to this, the use of this definition gives a good impression of the operative technique in use, such as the positioning of the prostheses 'supra' or 'intra-annular', as this is the level measured by echocardiographers as the 'aortic valve annulus' and is the area which defines the size of the prosthesis to be implanted during aortic valve replacement procedures. However prosthetic valves are inserted somewhat more proximally, more towards the level of the anatomic ventricular-arterial junction, due to the placement of the sutures predominantly through the scalloped attachment of the excised leaflets, from the nadir of the sinus to midway up the commissures. In order to avoid any misunderstanding due to the numerous definition and terms employed, we have recently proposed the use of the term 'annulus' to describe the virtual, circular ring defined by the nadirs of the semi-lunar leaflet attachments (Figure 2.1).

There are basically two techniques of conservative surgery of the aortic root: "remodeling" (Figure 2.7 a and b) and "reimplantation". The "remodeling", conceived by M. Yacoub in 1983, allows, through an appropriate modeling of the prosthesis in Dacron, a reconstruction of the breasts, but does not ensure a complete stabilization of the aortic annulus, with the possibility therefore, in the medium and long term, of a progressive annular dilatation and a consequent valvular insufficiency.

In contrast, the "reimplantation" technique, devised by T. David a few years later, while guaranteeing an effective annular stabilization and at the same time also a lower risk of postoperative bleeding, almost abolishes altogether the breasts of Valsalva, with a consequent increase of stress on the aortic flaps and their

greater deterioration over time (Figure 2.7 c, d and e). Both the procedures, however, guarantee fluttering results in the medium and long term, although the technique of David (today very "modernized" and "modified" from the same or other authors) seems to ensure better and more stable results even in patients with Marfan syndrome. In recent years, therefore, important innovations have been introduced both in the techniques and in the materials, so you can get the creation of "pseudo-sini" of Valsalva and a more "physiological" anatomical reconstruction of the entire aortic root (annulus, "pseudo-sines", new sino-tubular junction) (Figure 2.8).

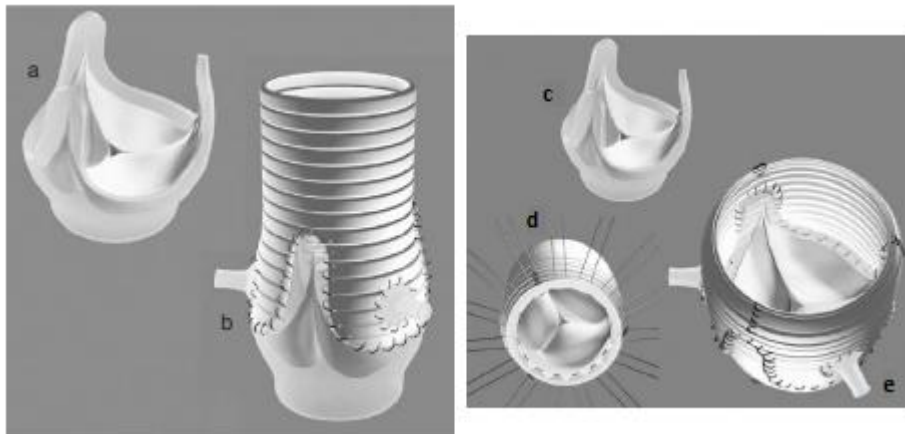


**Figure 2.7 Remodeling (a and b) and Reimplantation (c, d and e).**

The common goal of all these techniques is to preserve a valve aortic, "intrinsically healthy" in patients with a disease affecting the aortic root trying to reconstruct as much as possible all the components of the aortic root, and thus allowing a normal functioning of the valvular flaps.

In 2000, at the University of Rome Tor Vergata, a further and significant step forward was obtained not by a further modification of the surgical techniques, but from a modification and subsequent introduction into practice surgery of a new prosthetic duct in dacron (Gelweave Valsalva, Terumo-Vaskutek, Renfrewshire, Scotland, UK) that, recreating shape and size of the sinuses of Valsalva (Figure 2.9), combines the advantages of the "reimplantation" technique in terms of annular stabilization with the reconstruction of the Valsalva breasts, obtainable with the "remodeling".

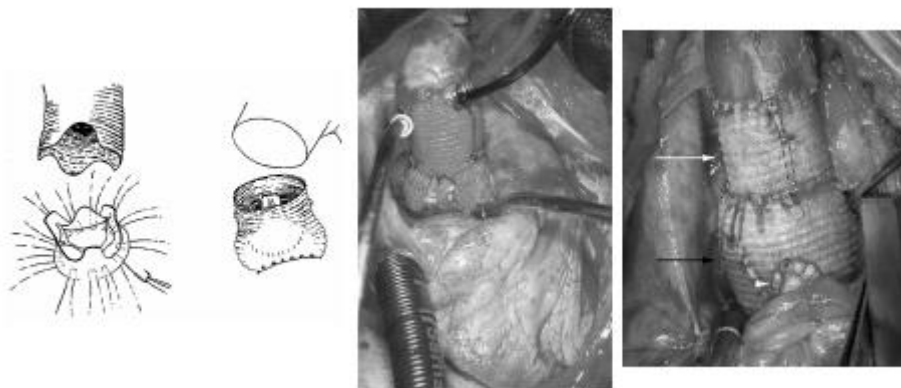


**Figure 2.8 Some examples of changes in surgical techniques and / or materials for the most anatomical aortic root reconstruction. Cochran (left), Robicsek (center) and Miller, 2004 (right).**

The new conduit, called "Valsalva" is a composite conduit formed by a proximal portion ("gonna") that can be expanded in the lateral direction (about 20-30%) by "stretching" the folds longitudinal, and from a distal portion expanding exclusively in the longitudinal direction, as indeed all the dacron ducts currently on the market.

The junction of these two portions creates a "breast-tubular neo-junction", while the base of the "gonna" corresponds to the annulus aortic (note that the height of the "gonna" is similar to the diameter of the distal portion: for example, diameter of the duct 30 mm, height of the "gonna" 30 mm).

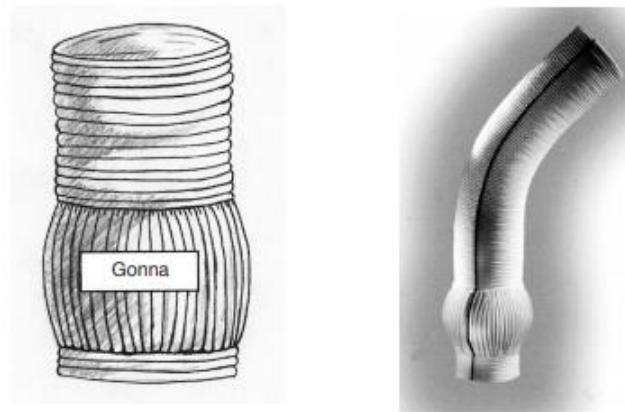


**Figure 2.9 Original drawing and realization of the dacron duct called "Valsalva" for the ability to rebuild, after implantation and pressurization, the shape of the sinuses of Valsalva.**

The surgical technique for the valve-sparing procedure using the conduit modified retraces without additional procedures the one described by T. David. The only precaution of the surgeon is to adapt the dimensions of the gonna to the patient's aortic flaps, so as to reconstruct an aortic root of normal dimensions and proportions. Achieving an ideal adaptation of the gonna and the new breast-tubular joint is the key moment of the whole surgical procedure and can be obtained by following various techniques. In some cases it is also possible to associate particular forms of reparation with this procedure aortic (eg shortening of free margins, sub-commissural application) in order to guarantee a perfect coaptation of the flaps and therefore best results at distance.

It is clear that for an effective and lasting clinical result it is important to select the ideal candidates for a "valve-sparing" procedure. The patients ideals should present an intrinsically "healthy" independent aortic valve whether it is competent or not. Indeed, the valvular insufficiency possibly present must be secondary to dimensional alterations due to the presence of an aneurysm or to the dissection of the same aortic wall. In both cases, in fact, at least in the initial phases, it is clear that the pathology is exclusively dependent on the aortic wall and not on the flaps valvular. However, there are cases in which significant aneurysmal dilatation (60 mm and above) and long lasting can cause deterioration structural flaps due to the prolonged and continuous tension placed on the same flaps. In these cases the flaps are found to be secondarily but intrinsically damaged by aneurysmal pathology and therefore can it will no longer work properly, even if a normal one is restored root anatomy. It is therefore increasingly evident how, in order to perform a conservation intervention of the aortic flaps in the presence of pathology aneurysm of the aortic root and

ascending aorta, it is necessary to pose surgical indication before the flaps are damaged by the same pathology dilated. In principle, action should be taken when, in presence of aneurysmal dilatation of the ascending aorta, begin to appear the first signs of valvular insufficiency.

A group of patients that particularly benefits from this type of approach are patients with Marfan syndrome. In particular in these patients, very often young, the techniques of "valve-sparing" allow to reduce the problems related to the use of valve prostheses. Recent experiences In fact, clinics seem to show encouraging results for the use of these techniques also in this group of high-risk patients 30.

It therefore appears clear that a correct approach to root surgery aortic should be aimed at ensuring optimal functionality of the flaps valvular. The fundamental points to be taken into consideration must therefore foresee the restoration of the normal proportions of the aortic root and of the breast-tubular junction, with the reconstruction of Valsalva's sinuses of normal form and function. The prosthetic conduit in dacron "Valsalva" allows to standardize the "theoretical" and "ideal" proportions of the aortic root guaranteeing a more physiological performance of the valve leaflets compared to traditional ducts. The possibility of being able to standardize an intervention that otherwise requires a specific experience from the individual surgeon certainly represents a not inconsiderable advantage, which contributes to the diffusion of this type of surgery. However, long-term durability remains to be defined term of this type of procedure.

### **3 Aortic valve replacement**

Severe aortic valve stenosis is the most common valvular heart disease in Western nations, mostly secondary to the aging process and increased life expectancy. In recent years, new therapeutic options have emerged with the introduction of transcatheter valves for specific subpopulations. All preoperative information required for patient selection and correct matching to a specific transcatheter valve size is obtained almost exclusively with noninvasive imaging methods.

In this chapter it is discussed the current state of treatment using this new technique, with emphasis on the relevant anatomy of the aortic root and the role of multidetector computed tomography (CT) in patient selection, device size selection, and the preprocedural evaluation of possible access routes.

#### **3.1 Definition and clinical consequences of aortic valve stenosis**

Aortic valve stenosis is defined as an obstruction of the left ventricular outflow tract (LVOT) at or near the level of the aortic valve. Critical aortic valve stenosis is reached when the valve area is less than 0.6 cm<sup>2</sup>.

Although the aortic valve stenosis can be sub – or supra- valvular, the valvular form is most frequently encountered in adults.

Aortic valve stenosis is a progressive disease that evolves from a non-symptomatic valve with thickened and calcified leaflets but without hemodynamic repercussions into an increasingly degenerative valve with extensive calcified and immobile leaflets. As the valve stenosis worsens, symptoms progress from mild to severe, with increasing fatigue and shortness of breath being common complaints and with the condition invariably leading to heart failure. The final symptomatic stage is short and rapidly progressive and is associated with a 2 – years survival rate of 50% or less.

#### **3.2 Evolving treatment options for severe aortic valve stenosis**

Traditionally, elective surgical aortic valve replacement has been considered the most effective treatment for advanced disease, significantly improving patient symptoms and survival compared with patients who are unwilling or unable to undergo surgery. Aortic valve bypass surgery, in which the left ventricular apex is connected to the descending aorta by means of a conduit valve, is also an option, although it is more rarely performed.

Unfortunately, not all patients are eligible for surgery. Several studies have identified various subgroups of patients with a substantially elevated risk for surgery-related complications or death, with some series reporting inoperability in up to 32% of cases. Factors contributing to a substantially increased surgical risk include frailty and old age, prior radiation therapy with significant chest damage, a heavily calcified aorta, severe pulmonary or hepatic disease, and chest deformities. Surgical risk is also increased in the presence of depressed renal function, previous stroke, peripheral vascular disease, and reduced left ventricular function. Because untreated symptomatic aortic valve stenosis has a dismal short-term prognosis, a less rigorous approach is needed for this subgroup of patients.

In recent years, alternative therapeutic options for patients deemed inoperable have emerged with the development of transcatheter-based therapies and specific aortic valve prostheses that can be transported to the aortic root using a nonsurgical endovascular, transaortic, or transapical approach. Once in place, these bioprosthetic valves functionally replace the native valve by displacing it to the aortic root wall during deployment. Given its less invasive nature, this procedure is less strenuous for patients and can therefore be applied in selected patients in a nonsurgical subgroup. The procedure is known as transcatheter aortic valve replacement (TAVR), also referred to as transcatheter aortic valve implantation or percutaneous aortic valve replacement.

Recently published data from individual centers, large prospective studies, observational registries, and multicenter randomized controlled trials have validated the efficacy of TAVR compared with the standard of care in patients with severe aortic valve stenosis. Therefore, TAVR is currently a valid treatment option in both the high-risk surgical cohort and the subgroup deemed to be at too high a risk for conventional surgery. These results, together with promising short- and medium-term outcomes, have led to the success and increasingly widespread clinical implementation of this intervention, with over 50,000 procedures now being performed worldwide each year. Because the clinical technique was implemented only recently, long-term outcomes are not yet known.

Nevertheless, not every patient who is refused or is at high risk for surgery is a good candidate for TAVR. A thorough clinical evaluation remains an important part of the global procedural assessment, since the overall condition of some patients may be so severely compromised by frailty, known and/or masked comorbidities, or a deteriorated mental state that even a successful TAVR procedure will have little chance of improving the patient's quality of life. Besides this clinical selection, certain technical and anatomic criteria must be met, and it is in this respect that noninvasive imaging techniques play a crucial role in the selection and further preprocedural workup of patients.

### **3.3 Definition of TAVR**

A TAVR procedure consists of deploying a bioprosthetic aortic valve in the aortic root after transporting the device from a chosen entry point. The approach can be retrograde (ie, using the femoral or subclavian artery as an endovascular access point) or antegrade percutaneous transapical through the apex of the left ventricle. A suprasternal approach through the brachiocephalic trunk, an anterior approach through a minimal right anterior thoracotomy, or a partial ministernotomy for transaortic placement through the ascending aorta is also possible.

Currently, two types of transcatheter valves are commercially available for TAVR. Edwards Lifesciences (Irvine, Calif) makes the balloon expandable Sapien and Sapien XT valves (Figure 3.1a). The Sapien XT valve is a slightly different version of the Sapien valve. It was introduced in Europe and features a cobalt-chromium lower-profile frame. Medtronic (Minneapolis, Minn) makes the self-expandable CoreValve revalving system (Figure 3.1b). These transcatheter valves have different physical properties that have been extensively described elsewhere. A brief summary is provided in Table 1.

Both devices have been clinically implemented worldwide and have received approval from the U.S. Food and Drug Administration for the American market for use in patients with severe symptomatic aortic stenosis who are considered to be at high surgical risk or are declined for surgery owing to excessive risk. Several device sizes exist, covering different diameter ranges of the native aortic annulus (Figure 3.2). With the current commercially available devices, TAVR is technically possible when the aortic annular diameter is between 18 and 29 mm (range for the two devices combined). Nevertheless, multiple vendors are currently developing other devices; thus, these size criteria will no doubt continue to evolve in the coming years.

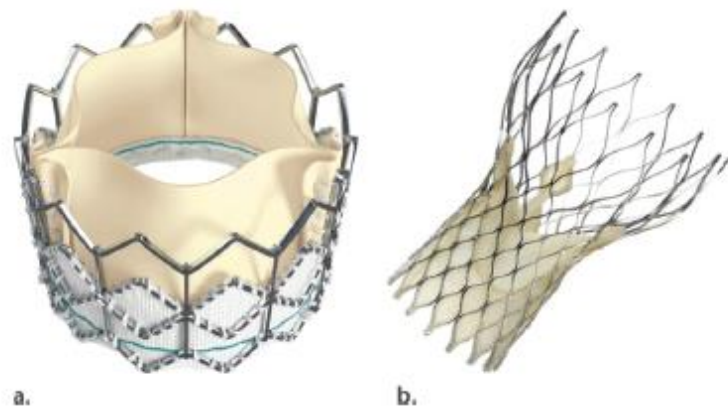


**Figure 3.1** Currently clinically implemented transcatheter valves. (a) The balloon-expandable Sapien XT valve (Edwards Lifesciences) consists of a cobalt-chromium frame and bovine pericardial leaflets. (b) The CoreValve (Medtronic) has a self-expanding nitinol frame and porcine pericardial leaflets.

**Table 1** Overview of Sapien XT and CoreValve Transcatheter Valves and Their Respective Delivery Systems

Parameter	Sapien XT	CoreValve
Manufacturer	Edwards Lifesciences	Medtronic
Aortic annular range (mm)	18–27	18–29
Deployment	Balloon-expandable	Self-expandable
Frame	Cobalt-chromium	Nitinol
Pericardial leaflets	Bovine	Porcine
Valve function	Intraannular	Supraannular
Access routes	Transfemoral, transaortic, transapical	Transfemoral, transaortic, transaxillary
Delivery sheath size	22–24 F, 16/18 F (Novaflex +)	18 F

Regardless of the device chosen, balloon aortic valvuloplasty is traditionally performed first, to dilate the stenotic native aortic valve and allow better passage of the transcatheter valve to its final position. Next, the position of the unexpanded prosthetic valve is checked; if this position is deemed adequate, deployment is initiated in a plane perpendicular to the aortic annular plane. The balloon-expandable Sapien valve is expanded during rapid ventricular pacing to minimize cardiac output and prevent device migration during deployment. Pacing is not typically performed during deployment of the CoreValve device, which has a self-expanding frame that conforms to the native aortic annulus.

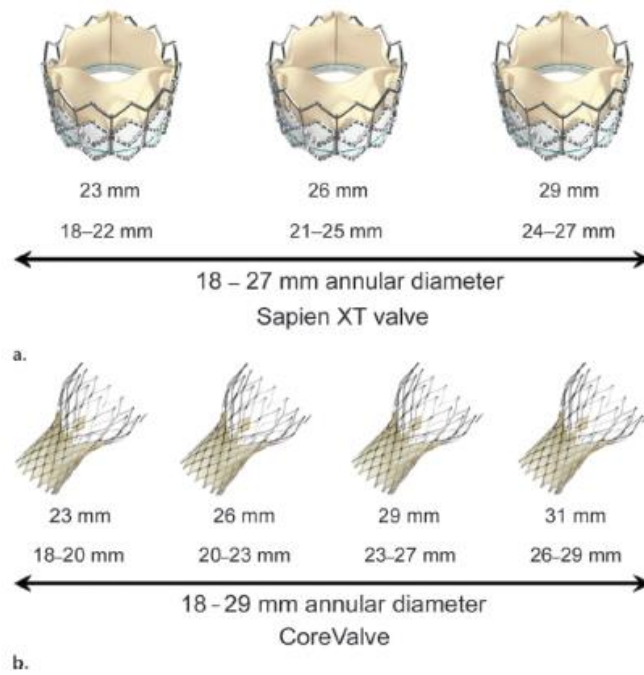


**Figure 3.2** Available transcatheter valve sizes from Edwards Lifesciences (a) and Medtronic (b) with their corresponding ranges of aortic annular diameters. The diameter of the aortic annulus must be between 18 and 29 mm, regardless of other parameters.

### 3.4 Preoperative imaging of potential access routes

#### Importance of the preoperative evaluation

Before the transcatheter valve is deployed in the aortic root, it must be transported to its target destination using a device-specific delivery system (Table 1). Both Sapien and CoreValve devices allow transfemoral and transaortic access.



**Figure 3.3** Inadequate access route patency. (a) Maximum intensity projection CT angiographic image reveals a subocclusive stenosis in the right external iliac artery (arrow) inhibiting endovascular access through the right iliac arterial axis, with diffuse atherosclerotic calcifications in the other aortoiliac vessels. (b) Volume-rendered CT image obtained in a different patient shows general tortuosity of the aortoiliac arterial vessels, a finding that is most prominent in the left common iliac artery (arrow).

Depending on the device chosen, a transaxillary (CoreValve) or transapical (Sapien) access route is also possible. All except the transfemoral approach require a surgical incision for initial access.

The final selection of access route will depend on a combination of the device chosen, the physical properties of the corresponding delivery system, and the adequacy of the investigated pathway. A carefully chosen access route is therefore one of the key components of procedural eligibility and success, since in a given case different pathways may be associated with potentially different risks for peri- and postprocedural vascular and embolic cerebrovascular complications. This underscores the need for individualized access route selection.

Both device- and anatomy-related obstacles may alter the chosen access pathway or even make the procedure impossible to perform via the endovascular pathway regardless of device-compatible aortic root dimensions (Figure 3.3). Therefore, multidetector CT plays an important role in examining the potential access routes and reporting any possible problems that may alter the chosen access strategy.

### Endovascular access

Commercially available device delivery systems come with different sheath sizes depending on the manufacturer and the production version of the device. Ideally, the minimum diameter of the native vessel should be smaller than the outer diameter of the chosen delivery sheath (Table 1). Lower-profile sheaths and delivery catheters improve procedural safety and expand patient eligibility. Currently, the two systems associated with the most worldwide experience and reported study results are (a) the third-generation femoral delivery systems from Medtronic, with a sheath size of 18 F (26); and (b) the Edwards Lifesciences Retroflex, with a 22–24-F sheath. Edwards Lifesciences has also created the Novaflex+ transfemoral delivery system with a 16/18-F low-profile introductory sheath. However, delivery catheters remain the subject of intense research and have been continuously improved ever since their introduction, with other systems currently being developed by different vendors.

Not surprisingly, a larger sheath size (22–24 F) has been associated with a higher incidence of vascular complications (22.9%–30.7%) compared with smaller systems (1.9%–13.3%). To allow proper tracking and meaningful comparisons of endpoints in trials, major and minor vascular complications have been formally defined by the Valve Academic Research Consortium. Prominent atherosclerotic (specifically, circumferential) wall calcifications, small native vessel diameter (smaller than the outer diameter of the delivery sheath being used), and marked tortuosity of the iliac arteries have been described as risk factors for procedural complications (Figure 3.3), with some series finding an unsuitable iliofemoral anatomy in 19.1%–35% of patients. When two or more of these features are present, an alternative transapical, transaxillary, or transaortic approach can be considered. Hayashida et al proposed the ratio of sheath size to femoral artery size (SFAR) as the most predictive variable in identifying patients at risk for vascular access injury. With use of a SFAR sliding scale depending on the burden of atherosclerotic calcification, a threshold of 1.05 was predictive of a higher rate of major complications as defined by the Valve Academic Research Consortium. Therefore, the authors suggest that routine application of SFAR improves patient selection, leads to better

outcomes, and lowers the morbidity profile for TAVR. The minimum recommended vessel diameters are shown in Table 2.

**Table 2 Recommended Minimum Vessel Diameter based on the Delivery Device**

Device	Valve Size (mm)	Introducer Profile (mm)	Recommended Minimum Vessel Diameter (mm)
Sapien valve with Retroflex 3-mm delivery system	23	22	>7
	26	24	≥8
Sapien XT valve with No-vaflex delivery system and e-sheath	23	16	≥6
	26	18	≥6.5
	29	20	≥7
CoreValve revalving system	23	18	≥6
	26	18	≥6
	29	18	≥6
	31	18	≥6

Note.—Adapted, with permission, from reference 36.

Information regarding the patency of the chosen endovascular route can be acquired during preprocedural evaluation with multidetector CT and conventional coronary angiography, but it can also be obtained from previous imaging studies (sometimes performed for unrelated reasons). Although there are no guidelines regarding how recent such a study should be, it is believed that a study should have been performed no more than 6 months ago, unless there are clinical grounds for a recent change in vascular status.

Conventional coronary angiography is always routinely performed in potential TAVR candidates for whom recent information about coronary patency is not available. In such cases, this examination is expanded to include an assessment of the aorta and iliac arteries.

Although conventional angiography allows a basic assessment of the luminal size of the involved peripheral arteries, it is less suitable for optimal assessment of the presence, amount, and morphologic features of atherosclerotic calcifications and vessel tortuosity. Multidetector CT is therefore considered a valuable tool for vascular assessment due to its intrinsic cross-sectional and three-dimensional (3D) multiplanar capabilities. In practice, precise multidetector CT–derived measurements of the common femoral, external iliac, and common iliac arteries are obtained at several levels using curved multiplanar reformation, measuring the transaxial diameter on a view obtained perpendicular to the long axis of the investigated vessel segment. Although there are no universally accepted guidelines regarding the anatomic level at which measurements along a vessel trajectory should be obtained, it is important to choose the measurement points so that information can be acquired concerning both average vessel diameter and narrow segments that may hinder passage of the transcatheter device. This information is relevant, since TAVR procedures have been successfully performed in patients with borderline vessel size and in those without extensive atherosclerotic burden or tortuosity but with relatively compliant arteries with a short-segment diameter up to 1–2 mm smaller than the intended sheath size. The degree of atherosclerosis remains a subjective matter, with no quantifiable parameters or published guidelines, and is therefore subject to interpretation by the radiologist, cardiologist, and cardiovascular surgeon. An accurate and complete description of the degree of atheroscle-

rotic burden by the radiologist is therefore necessary and should include the presence and extent of atherosclerotic plaques and stenosis. Finally, 3D volume-rendered images have been obtained of the aortoiliac arteries for further subjective evaluation of vessel tortuosity and general morphology.

Both left and right subclavian arteries may be used for endovascular access with a transaxillary approach. However, the left subclavian artery is often preferred because, similar to the femoral artery, it allows a more favorable orientation of the delivery system. Furthermore, a left-sided approach will minimize the potential obstructive effect of the delivery system on the ostium of the brachiocephalic artery and the subsequent risk of stroke. Nevertheless, caution is needed to prevent vascular complications such as dissection or occlusion of the vessels of the arm and head. Ipsilateral transvenous internal pacemaker leads and internal mammary artery grafts are not considered contraindications but do increase procedural complexity. Finally, some centers have experience—albeit limited—with a suprasternal approach through the brachiocephalic trunk.

### Transaortic access

Worldwide experience with the transaortic approach through an anterior right mini–thoracotomy or partial mini–sternotomy is increasing (Figure 3.4).

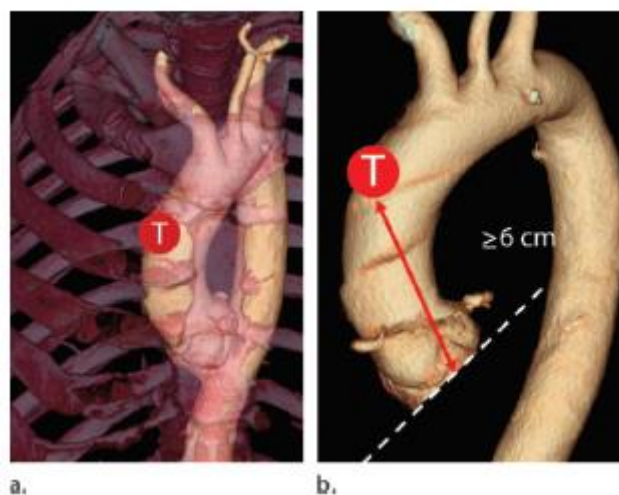


**Figure 3.4** Entry site for transaortic access for TAVR. (a) Volume-rendered CT image shows the approximate target point (*T*) for transaortic access through a minimal right sternotomy or thoracotomy, typically located at the level of the second intercostal space. (b) For CoreValve devices (Medtronic), a minimum distance of 6 cm (double-headed arrow) between the entry point (*T*) and the aortic annular plane (dashed line) is recommended to accommodate the device length.

Access is typically achieved at the level of the second right intercostal space, bypassing the aforementioned peripheral vascular territories and thereby providing an alternative route when other approaches have been deemed unsuitable. This procedure has been well tolerated by patients. As more experience with this access pathway is gained, the potential problem of not having an adequate endovascular access pathway is becoming less of an issue. However, the transaortic approach also has certain anatomic requirements, including a minimum distance of 6 cm between the basal aortic plane and the aortic access site for CoreValve implantation. Further preoperative CT evaluation for transaortic access must also include analysis of the selected delivery trajectory to optimize coaxial alignment with the native aortic valve, evaluation of the presence of calcification at the aortic access site, and correct identification of critical vessels such as the right internal mammary artery and possible bypass grafts along the delivery trajectory. Concomitant pleural

or lung parenchymal disease along the delivery trajectory as well as other unexpected findings may further compromise this entry point. Currently, there are no guidelines as to which lung diseases exclude this procedure, with the final decision being left to the interventional cardiologist and surgeon.

Although in practice aortic disease will be less critical in determining procedural feasibility, several procedural contraindications involving aortic disease have been described. These include severe aortic angulation, coarctation, aneurysm of the abdominal aorta with protruding mural thrombus, and previous aortofemoral bypass surgery.

### **3.5 CT acquisition**

#### Required anatomic coverage and preoperative information

In practice, the CT scanning protocol will be determined mainly on the basis of the required preoperative information, the patient's condition, and the need to reduce the required amount of contrast material. The last-named factor is especially important in the investigated population, since advanced age is often associated with depressed renal function. An overview of the required multidetector CT information is given in Table 3.

In general, the technical multidetector CT settings used for routine CT angiography of the coronary arteries constitute an excellent starting point. Next, the required scanning range should be determined. When only information concerning the aortic root is required, many centers use electrocardiography (ECG)-gated contrast material-enhanced multidetector CT of the heart with a scanning range identical to that used for routine multidetector CT of the coronary arteries. However, it can be argued that, especially in patients with impaired renal function, acquisition can be limited to the aortic root, since evaluating the status of the coronary arteries is not the purpose of the multidetector CT examination. Limiting the investigated anatomic range and acquisition time to the bare minimum allows a reduction in the required amount of intravenous contrast material. If evaluation of the patency of the subclavian arteries is also required, the scanning range should extend from the neck base to the thoracic diaphragm.

When evaluation of the iliac access route is also requested, the scanning protocol is also influenced by the acquisition speed of the available multidetector CT equipment, since this anatomic region is farther away from the aortic root. Last-generation multidetector CT scanners with a large anatomic coverage per rotation and/or high pitch modes will allow scanning of both the heart and aortoiliac vessels within a minimum time span and with a single reduced dose of contrast material.

With slower multidetector CT scanners, it may be necessary to perform two different multidetector CT examinations on separate days to achieve optimal arterial enhancement of the targeted vascular territory. Using a single-source 64-section multidetector CT system (Lightspeed 64; GE Healthcare, Milwaukee, Wis), two different but consecutive acquisitions have been combined during the same intravenous contrast material injection, as was also proposed by Blanke et al. First, a retrospectively ECG-triggered examination is performed, with anatomic coverage limited to the region of the aortic root. A nongated examination is subsequently performed from a supraclavicular level to below the common femoral artery. A single 120-mL dose

of contrast material has been administered with a high iodine concentration (a minimum of 350 mg/mL is recommended).

**Table 3 Required Information from Preprocedural CT Examinations**

Anatomic Level	Required Information
Aortic annulus	Systolic measurements (if available) are preferred Annular cross-sectional (long- and short-axis) diameters, circumference, and area; circumference- and area-derived diameters Recommended fluoroscopic projection angle for orthogonal view in annular plane if not determined during procedure (eg, at 3D rotational angiography)
Aortic valve (native)	Extent and distribution of valve calcifications, cuspidity (bicuspid, tricuspid, other variants)
Aortic root	Shortest distance from aortic annulus to ostia of left main and right coronary arteries
Left atrium	Exclusion of a left atrial appendage thrombus with either TEE or delayed phase imaging
Left ventricle	Evaluation for basal septal hypertrophy and wall thrombi
Ascending aorta	Extent of wall calcifications (especially if a transaortic approach is being considered) and presence or absence of atherosclerotic thrombi, angulation between ascending aorta and LVOT
Aortic arch, descending aorta, and abdominal aorta	Branch anatomy of aortic arch (subclavian approach), descriptive assessment of atherosclerosis (including tortuosity, intraluminal obstruction, and thrombi)
Subclavian arteries and brachiocephalic artery	Report on patency and luminal diameter (left subclavian artery is preferred)
Common and external iliac arteries and common femoral artery	Report on patency and luminal diameter, descriptive assessment of atherosclerosis (including tortuosity), report of any potential problems at the targeted femoral access site (eg, preexisting pseudoaneurysm)

Note.—TEE = transesophageal echocardiography.

Using this approach, the flexibility of ECG-triggered acquisition for optimal-quality images of the aortic root has been combined with a subsequent faster scan for evaluation of the pathways of the subclavian and iliac arteries. In addition, routinely 80 or 100 kV has been used as the default setting (depending on body weight), since lower kilovolt settings have been shown to reduce radiation dose for multidetector CT angiography without compromising image quality.

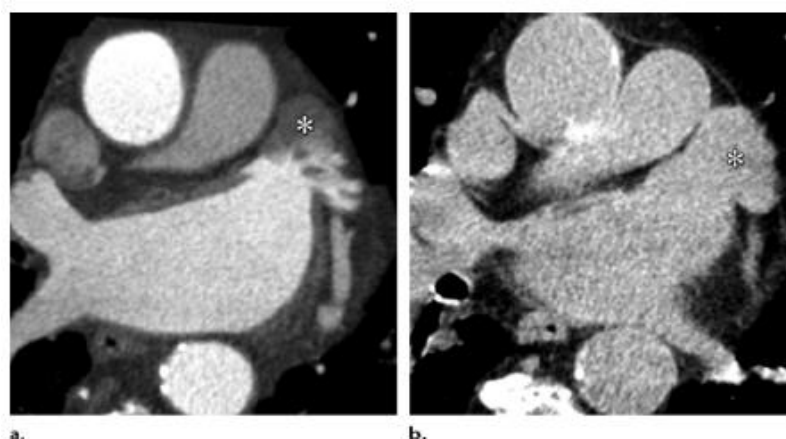


**Figure 3.5** Circulatory stasis in a large left atrial appendage producing a pseudothrombus during pre-TAVR evaluation. (a) Axial contrast-enhanced CT image demonstrates how slow flow can lead to incomplete filling of the left atrial appendage (\*) during the arterial phase. When detected, an atrial appendage thrombus must be either confirmed or excluded. This is traditionally achieved with TEE, although delayed phase CT images can also be used. (b) Axial contrast-enhanced delayed venous phase CT image shows final complete filling of the appendage (\*). The possibility of a left atrial appendage thrombus must always be reported immediately, since such a finding constitutes a procedural contraindication with a high risk of stroke.

Finally, atrial fibrillation is a known risk factor for the development of atrial thrombi, especially in the left atrial appendage. This is particularly important because the presence of thrombus in the left atrium is a procedural contraindication with an increased peri- and postprocedural risk of stroke (Figure 3.5).

Although echocardiography has traditionally been the preferred modality for screening for this abnormality, atrial thrombi can be detected with contrast-enhanced multidetector CT and should always be mentioned in the radiology report. However, caution should be exercised when evaluating the left atrial appendage on single-phase arterial scans, since circulatory stasis in a large appendage can produce a false-positive pseudothrombus. Performing a dual-phase examination with images acquired in a delayed contrast phase increases the sensitivity and specificity of CT for this abnormality. In this practice, is quickly review the incoming arterial phase images as they appear on the CT console, and when incomplete filling of the left atrial appendage is observed, an additional targeted scan is performed, typically an average of 2 minutes after contrast material injection.

#### ECG gating and the varying dimensions of the aortic annulus during the cardiac cycle

Given the inherent motion of the aortic root, an ECG-gated multidetector CT acquisition is necessary to achieve the best image quality with minimal motion artefacts. It also allows evaluation of the dimensions of the aortic root, which vary depending on the phase of the cardiac cycle. The aortic annulus is traditionally measured in the systolic phase, during which it manifests with its intrinsically largest diameter. Nevertheless, several authors have reported varying results concerning the optimal scanning window in the cardiac cycle. A multidetector CT-based study in healthy subjects reported a significant difference in the dimensions of the aortic annulus between systole and diastole (up to 5 mm in some cases). However, this is a different patient population than that with severely stenotic aortic valves, in which this variation is thought by some investigators to be minimal due to reduced wall compliance. Nevertheless, Hamdan et al, using four-dimensional multidetector CT data, reported that in both healthy subjects and patients with calcified aortic valves, the aortic annulus was generally elliptic but assumed a rounder shape in systole, thereby increasing the minimum diameter but without a significant change in perimeter. Based on these findings and the experience, is generally recommend ECG-triggered scanning of the aortic root with systolic measurements. Consequently, ECG-modulated milliamperage settings should be adjusted to deliver sufficient image quality in the systolic phase.

Still, ECG gating by itself can also induce artifacts. In practice, this implies that on most equipment, the best image quality will be achieved in patients with a slow and regular heartbeat. However, because the investigated cohort is almost invariably of advanced age with an associated higher incidence of significant comorbidity, the measures that are typically used to lower the heart rate (eg, the administration of additional b-blockers) are not always possible or are less clearly indicated. Moreover, the presence of atrial fibrillation is not rare in an advanced-age population, further adding to the technical complexity of acquiring high-quality images.

### Clinically relevant anatomy

The aortic root has a relatively central position in the heart, with a double-oblique orientation at 3D imaging (Figure 3.6). It extends from the LVOT to the sinotubular junction, which marks the transition from the aortic sinuses (of Valsalva) to the tubular ascending aorta. This junction can be identified as an area of abrupt change in caliber, better seen on coronal and sagittal reformatted images as an obtuse angulation. The aortic root also contains the aortic valve within the aortic sinus (Figure 3.7). Three distinct aortic valve leaflets can be visualized, with left and right coronary cusps named after the corresponding coronary arteries originating from their sinuses. A third cusp is appropriately named the noncoronary cusp, since no coronary artery originates from its sinus (Figure 3.8).



**LEFT:** Figure 3.6 Volume-rendered CT image shows the central position and oblique angulation of the aortic root and annular plane.

**RIGHT:** Figure 3.7 Coronal contrast-enhanced CT image shows the aortic root extending between the LVOT and the ascending aorta (*Ao asc*), with its borders formed by the sinotubular junction (dashed line) and the basal attachments of the aortic valve leaflets, which define the level of the annular plane (solid line). The aortic root contains the sinus of Valsalva (arrows) and aortic valve leaflets (\*).

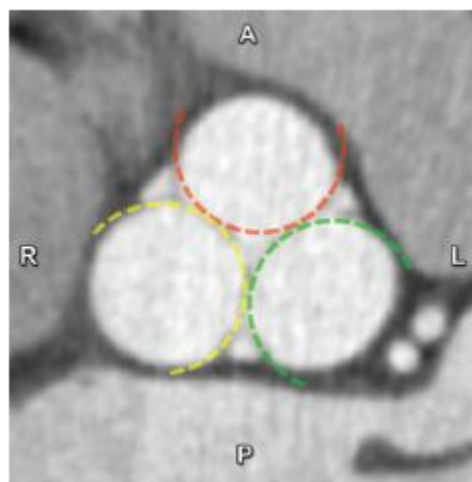


**Figure 3.8** Double-oblique contrast-enhanced CT image of the aortic root at the level of the sinuses of Valsalva demonstrates the anatomy of the aortic valve, consisting of left coronary (green), right coronary (red), and noncoronary (yellow) cusps.

Note the cloverleaf shape of the aortic root contour. *A* = anterior, *P* = posterior.

In contrast to these anatomic landmarks, the aortic annulus is not a real anatomic structure. Instead, the term *aortic annulus* is often used by surgeons to refer to the insertion site of the aortic valve cusps, which many authors have traditionally assumed is always circular. Nevertheless, this term is not adequately defined anatomically, with a nonstandard and variable interpretation. Consequently, some authors have suggested refraining from using the term. Still, its use is widespread and deeply embedded in scientific literature and communications.

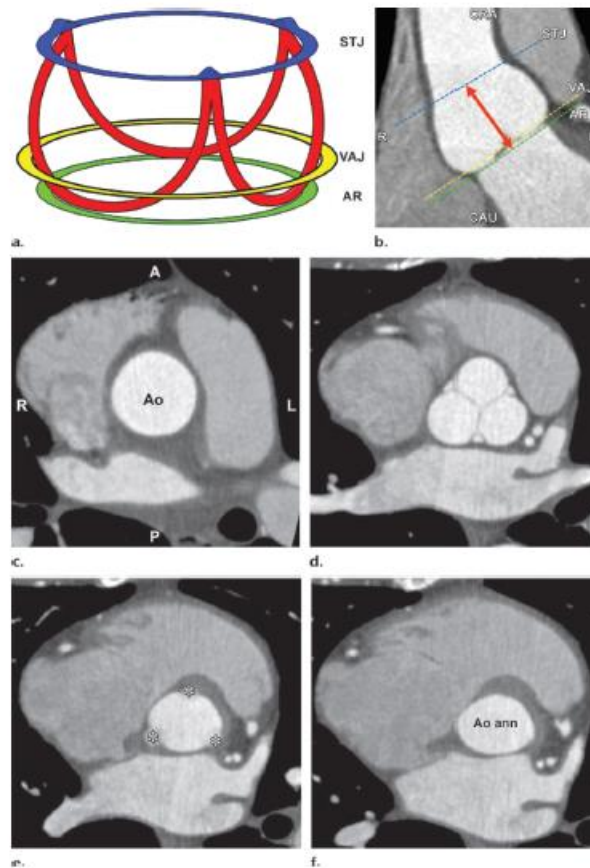


**Figure 3.9** a) Drawing illustrates the crownlike suspension of the aortic valve leaflets within the aortic root extending across the length of the aortic sinus. *AR* = virtual annular ring (green), formed by joining the basal attachments of the aortic valve leaflets; *STJ* = sinotubular junction (blue); *VAJ* = ventriculoarterial junction (yellow). Red = aortic leaflet insertion sites in the sinus of Valsalva forming a crownlike ring. (Reprinted, with permission, from reference 39.) (b) Coronal contrast-enhanced CT image demonstrates the levels of the sinotubular junction (*STJ*) (blue line), ventriculoarterial junction (*VAJ*) (yellow line), and annular ring (*AR*) (green line). Double-headed arrow = anatomic range of the sinuses of Valsalva. *CAU* = caudal, *CRA* = cranial. (c–f) Double-oblique reformatted images further clarify the changing shape of the aortic root contour. (c) The sinotubular junction forms the top of the crown, where the outlet of the aortic root in the ascending aorta (*Ao*) is a true circle. *A* = anterior, *P* = posterior. (d) The aortic root gradually becomes less circular, with a more cloverleaf shape at its midportion (ie, at the sinuses of Valsalva). At this level, the aortic valve leaflets are clearly seen. (e) The aortic valve leaflets (\*) are just barely visible at the level of the ventriculoarterial junction, where the left ventricular structures give rise to the fibroelastic walls of the aortic valvar sinuses. Note that the aortic root contour is now becoming increasingly ellipsoid. (f) The bottom of the aortic root is formed by the virtual ring, or aortic annulus (*Ao ann*), which has an oval shape in most patients.

In practice, the term *annulus* is commonly used to specifically indicate a virtual ring formed by the nadir of the attachment sites of the aortic valve leaflets. This attachment of the aortic valve leaflets to the aortic root wall is not circular; it has a more semilunar, crown-shaped appearance, extending from the sinotubular junction to the basal attachment plane of the aortic valve leaflets (the so-called annulus), located just below the ventriculoarterial junction. Given its conical form, the annulus is perhaps more appropriately described as a three-pronged coronet than as a ring.

Histologically, the aortic root consists of a ventricular component (at the level of the membranous septum) and an arterial component as the leaflet insertions extend up to the sinotubular junction.

At cross-sectional imaging, the aortic root contour is practically circular at the level of the sinotubular junction and assumes a more cloverleaf shape at the level of the aortic sinus, often becoming oval to ellipsoid at the annular plane and LVOT (Figure 3.9). Consequently, small differences in the choice of a measurement plane in the aortic root can produce notably different results.

### 3.6 Noninvasive imaging of the annulus: ongoing controversies and current insights

#### Multimodality imaging comparison

With TAVR, unlike with surgical valve replacement, annular sizing is not performed under direct inspection but on the basis of noninvasive imaging findings. Imaging guidance is needed to ensure the appropriate degree of oversizing to help avoid paravalvular regurgitation and reduce the potential risk of annular rupture. Historically, transthoracic echocardiography (TTE) and TEE have been used for preoperative sizing of the aortic annulus in different trials. However, because they are operator-dependent two-dimensional (2D) imaging techniques, they provide only limited data regarding the complex 3D geometry of the annulus (Figures 3.10, 3.11).

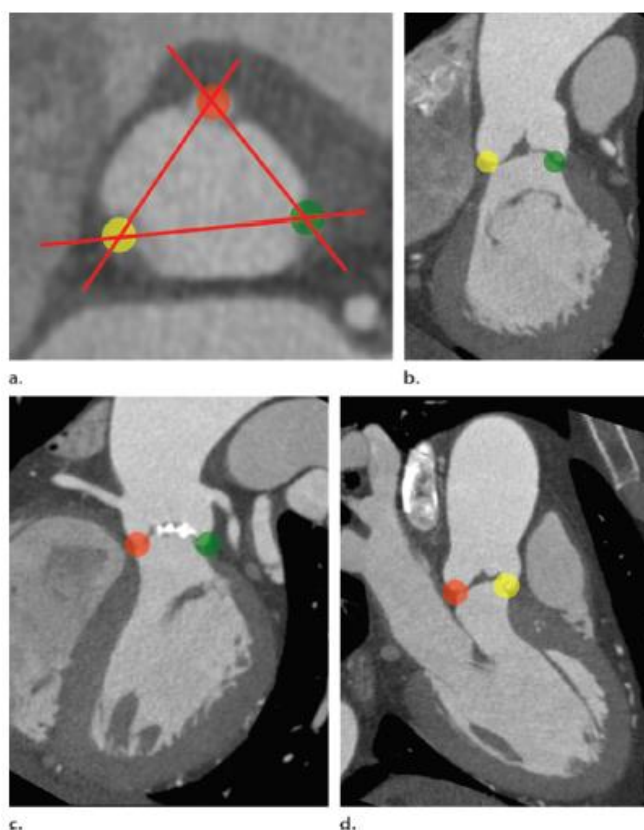


**Figure 3.10** Double-oblique reformatted CT images show the basal insertion sites of the right coronary cusp (orange dot), noncoronary cusp (yellow dot), and left coronary cusp (green dot). When these basal leaflet insertion sites are used as a reference for deriving a single 2D measurement of the annular plane (as in 2D echocardiography-derived measurements), the 3D anatomy is reduced to a 2D image. Furthermore, these images illustrate that none of the performed 2D measurements is along the true long or short axis of the aortic annulus, complicating simple comparisons between CT and echocardiographic measurements.

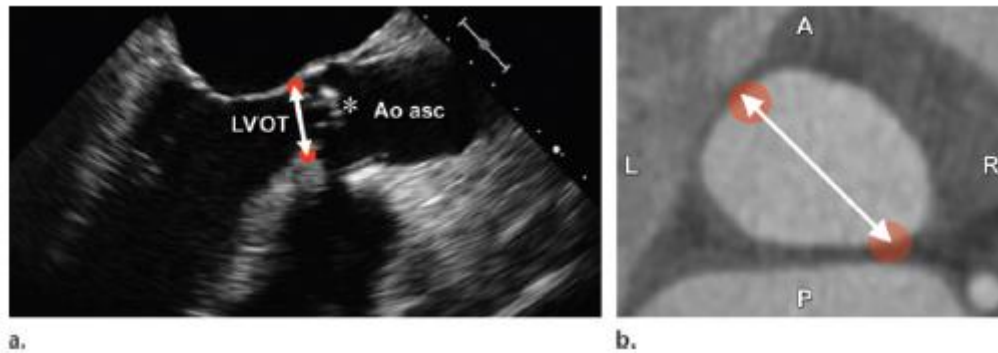


**Figure 3.11(a)** On an echocardiographic image, the diameter of the aortic annulus (double-headed arrow) is measured by identifying two opposing points (orange dots) on the basal insertion sites of the aortic valve leaflets (\*). *Ao asc* = ascending aorta. **(b)** Corresponding double-oblique reformatted image through the aortic annulus reveals that the pathway (double-headed arrow) between these points (orange dots) does not correspond to the true long axis of the aortic annulus. Echocardiography-derived measurements often lead to underestimation of the true size of the annulus. Furthermore, because conventional echocardiography is a 2D imaging modality with a varying degree of operator dependency, it is almost impossible to compare single echocardiography-derived measurements with their CT counterparts, since both the measurement plane and the chosen oblique diameter will differ between these imaging modalities. *A* = anterior, *P* = posterior.

Because of the noncircular nature of the annulus and the fact that echocardiography typically yields measurements that most closely approximate the short axis of the annulus, TEE measurements have been shown to understate the surgically measured annular size.

To further optimize the sizing process, the potential contributions of 3D imaging methods such as multidetector CT, 3D TEE, and (potentially) 3D rotational angiography have recently been fairly extensively investigated. Multidetector CT, with its isotropic voxels and multiplanar reformatting capabilities, seems intrinsically better suited than echocardiography for correctly characterizing the complex 3D anatomy of the aortic annulus. As such, it allows reconstruction of the dataset in the true plane of the aortic annulus, after which various measurements of the annulus can be obtained.

MR imaging is also increasingly being used for the evaluation of the aortic valve area, with encouraging results, and, according to some authors, yields measurements comparable to those obtained with multidetector CT. In some respects, MR imaging of the aortic root has clear benefits compared with multidetector CT, including (a) radiation-free imaging, (b) functional evaluation of the aortic valve, and (c) the use of gadolinium-based contrast material, which is significantly less nephrotoxic and produces less adverse reactions than its iodine-based multidetector CT counterpart. Nevertheless, the use of MR imaging is far less widespread than that of multidetector CT for obtaining annular measurements, probably because (among other reasons) MR imaging is a technically more complex examination, takes a longer time, and requires a higher degree of patient cooperation. However, on a case-by-case basis, MR imaging may be used instead of multidetector CT in patients with severely depressed renal function.

Nevertheless, comparisons between imaging methods are often the subject of debate, since experience with MR imaging and multidetector CT as selection and sizing tools is of fairly recent origin. As a result, there are currently no universally validated strict guidelines regarding the exact use of multidetector CT or any other 3D imaging tool for patient selection and device sizing across all platforms. Therefore, it is important to realize that in practice, the process of clinical patient evaluation, annular sizing, and evaluation of access route for final transcatheter heart valve selection and placement is multifactorial, integrating both clinical

data and information from all available imaging modalities. This approach allows the most complete clinical and technical assessment, leading to an informed procedure and optimal device selection.

#### Paravalvular regurgitation and the importance of the correct assessment of annular dimensions

Proper selection of a patient on clinical grounds (overall assessment of frailty and comorbidity factors, which influence life expectancy and the ability to undergo TAVR) and correct choice of a patient-specific transcatheter valve size are crucial for successful TAVR, minimizing peri- and postprocedural complications. Postprocedural regurgitant leakage of blood around the attachment sites of the prosthetic valve remains a relatively common complication with potential important clinical consequences. This regurgitant flow is called paravalvular aortic regurgitation (PAR), with approximately one in nine patients developing moderate to severe PAR after TAVR. PAR has also been associated with a worse long-term outcome. There is growing evidence that PAR may be related, at least in part, to preoperative undersizing of the aortic annulus, with the subsequent choice of an undersized transcatheter valve and incorrect device positioning. Furthermore, recent reports indicate that even mild PAR, which is generally considered to be of little clinical significance, is nevertheless an underappreciated contributor to late all-cause mortality.

As a result, a great deal of attention is being given to further refining annular sizing and subsequent transcatheter valve selection to help minimize the occurrence of moderate to severe PAR.

#### Annular measurements and multidetector CT: workflow and current viewpoints

The primary uses of multidetector CT in annular sizing are (a) obtaining a correct image orientation in the true plane of the aortic annulus, (b) correctly measuring the annulus using different methods, and (c) implementing these measurements in the selection of a transcatheter valve size.

The plane of the aortic annulus is defined by the three lowest insertion points of the aortic valve leaflets. Because this plane has a double-oblique orientation, standard coronal, sagittal, or even single-oblique reformatted images are not considered suitable. Furthermore, the insertion of the right coronary cusp leaflet is often inferior to those of the left and noncoronary cusp leaflets. Although these characteristics can make obtaining a correctly oriented image plane less straightforward and somewhat frustrating in inexperienced hands, a method describing a sequence of image reformations leading to an image plane precisely oriented along the aortic annulus has been described elsewhere. In this plane, the three lowest anchor points of the aortic valve leaflets are displayed on the same image.

Once a suitable plane has been obtained, several annular measurements can be taken. Investigators have approached annular sizing using various measurements of the annulus (Table 4). Currently, has been proposed calculating the mean annular diameter (preferably on the basis of systolic images) as follows (Figure 3.12): First, has been obtained annular cross-sectional long-axis ( $DL$ ) and short-axis ( $DS$ ) diameters. The annular perimeter is manually tracked using a planimetry tool on a workstation, after which the area ( $A$ ) and circumference ( $C$ ) of the aortic annulus are derived by the workstation software. Finally, the mean annular diameter ( $D$ ) is calculated based on these measurements. For the cross-sectional derived mean diameter ( $DCS$ ), this is carried out with simple averaging:  $DCS = (DL + DS)/2$ . The area-derived ( $DA$ ) and

circumference-derived (*DC*) diameters are calculated as follows:  $DA = 2 \times \sqrt{(A/p)}$ , and  $DC = C/p$ . However, it is important to realize that *DC* and *DA* are calculated under the assumption that the annulus is fully circular after device deployment, particularly with balloon-expandable valves. The discrepancy between these three measurements (*DCS*, *DA*, and *DC*) will therefore increase with remaining annular eccentricity, most notably with the circumference-based method. This further underscores the fact that transcatheter valve size selection is closely tied to the type of device used.

**Table 4 Overview of the Heterogeneity in Methods of Obtaining Annular Dimensions across Several Studies**

Authors/Year	No. of Patients	Method of Measurement at CT	CT Measurement (mm)	TTE Measurement (mm)	TEE Measurement (mm)
Yano et al/2012	55	Largest LVOT diameter	23.9 ± 3.19	20.3 ± 2.5	...
Altiok et al/2011	49	Coronal and sagittal aortic annular diameters	Coronal: 22.19 ± 1.96 Sagittal: 22.27 ± 2.01	...	Coronal: 23.6 ± 1.89 Sagittal: 23.46 ± 2.07
Pontone et al/2011	60	Maximum and minimum aortic annular diameters	Maximum: 25.1 ± 2.8 Minimum: 21.2 ± 2.2	21.6 ± 1.4	20.9 ± 2.0
Tzikas et al/2011	70	Coronal, sagittal, and mean aortic annular diameters	Coronal: 26.3 Sagittal: 21.8 Mean: 23.7	22.6	...
Dashkevich et al/2011	33	Mean aortic annular diameter	24.5 ± 2.6	...	23.4 ± 2.4
Mizia-stec et al/2011	20	Mean aortic annular diameter	26.9 ± 3.2	24 ± 3.6	26 ± 4.2
Messika-Zeitoun et al/2010	45	Long-axis, short-axis, and mean aortic annular diameters	Long-axis: 27.5 ± 3.1 Short-axis: 21.7 ± 2.3 Mean: 24.6 ± 2.4	23.1 ± 2.1	24.1 ± 2.1
Delgado et al/2010	53	Annular area measured with planimetry	4.65 ± 0.82*	3.89 ± 0.74*	Planimetry: 4.22 ± 0.77* Circular: 4.06 ± 0.79*
Halpern et al/2009	41	Aortic valve area measured with planimetry	3.1 ± 1.4*	2.5 ± 1.3*	...
Wood et al/2009	44	Coronal and sagittal aortic annular diameters in systole/diastole	Coronal: 25.7 ± 1.5 / 25.5 ± 2.5 Sagittal: 22.4 ± 1.3 / 21.5 ± 2.1	...	...
Tops et al/2008	169	Coronal and sagittal aortic annular diameters	Coronal: 26.3 ± 2.8 Sagittal: 23.5 ± 2.7	...	...
Willmann et al/2002	25	Mean aortic annular diameter	24.0 ± 2	...	...

Note.—When available, the corresponding echocardiography-derived measurements are obtained.

\*Units are in square centimeters.

Finally, these measurements must be incorporated into the transcatheter valve size selection process. Both Medtronic and Edwards Lifesciences have provided guidelines for valve size selection that depend on annular dimensions (Figure 3.2). However, these sizing scales are historically based on echocardiography-derived 2D measurements of the annulus. Therefore, these manufacturer-based recommendations cannot

simply be applied to multidetector CT–derived measurements without modification. Several studies have reported that the exclusive use of multidetector CT with an unmodified scale would influence patient eligibility and lead to the choice of a different transcatheter valve size compared with echocardiography in up to 40% of cases.

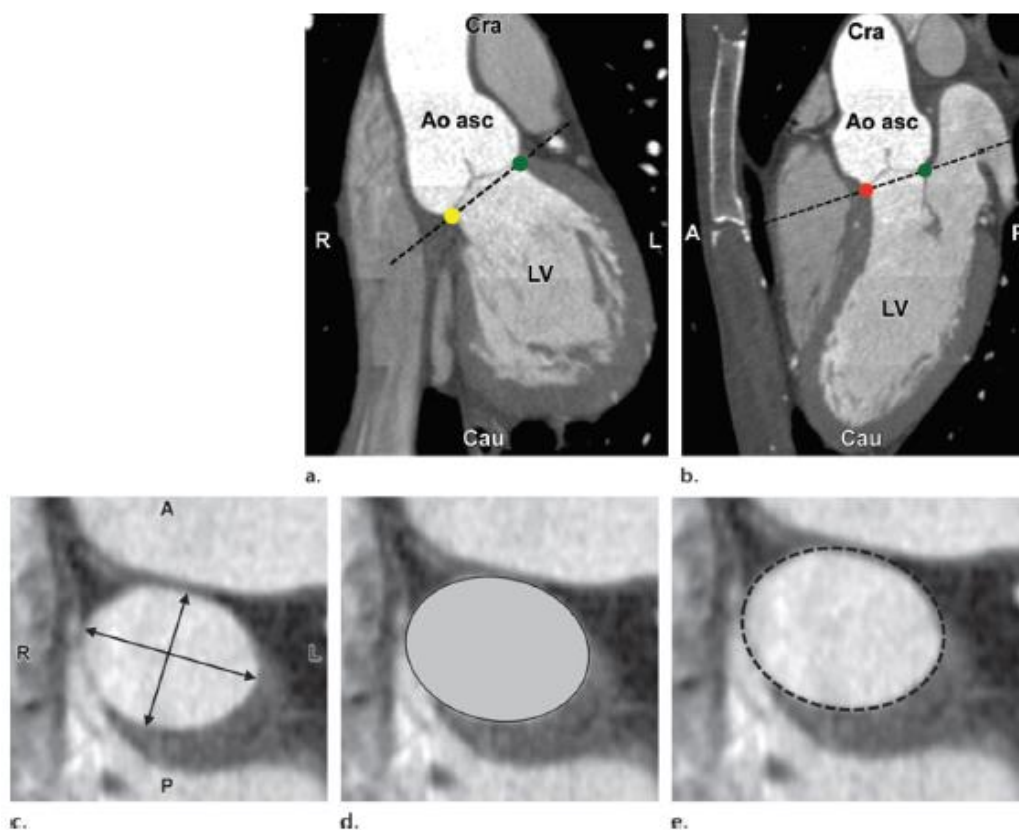


**Figure 3.12** Possible measurements of the aortic annulus. Before taking any measurement, a correctly reformatted image along the annular plane must be obtained. This is achieved by interactively manipulating the reconstruction planes on a workstation so that the nadirs of all three cusps are identified on one transverse image. (a, b) Standard coronal (a) and sagittal (b) images are in themselves not suitable but can be used as a starting point, with the final double-oblique imaging plane (dashed line) containing the basal attachment points of the left coronary (green dot), right coronary (orange dot), and noncoronary (yellow dot) cusps. *A* = anterior, *Ao asc* = ascending aorta, *Cau* = caudal, *Cra* = cranial, *P* = posterior. (c–e) The resulting cross-sectional image can then be used to measure the true long- and short-axis annular diameters (arrows in c), the annular area (shaded oval in d), and the annular perimeter (dashed line in e). From each of these different types of measurements, the mean area diameter can be derived using the appropriate formula. *A* = anterior, *P* = posterior.

These early data led to significant confusion regarding the appropriate integration of multidetector CT measurements in annular sizing and valve selection. To help mitigate this confusion, several investigators have sought to validate multidetector CT–based sizing guidelines for both the self-expanding and balloon-expandable platforms.

For balloon-expandable valves, Gurvitch et al have provided an early modified sizing-scale proposal based on the cross-sectional mean annular diameter, the area-derived mean diameter, and the expected differences between these multidetector CT–based diameters and the echocardiographic measurements. Using this modified scale, they found that the multidetector CT–based measurements would modify valve selection in only about 10% of patients, all of whom had moderate to severe PAR after a device size had been selected based on echocardiographic measurements. This suggests that multidetector CT can help in further reducing PAR in those cases in which echocardiography did not help identify the optimal valve size. On the basis of

these findings and other retrospective analyses, Willson et al (70) recently proposed a multidetector CT-based annular area sizing scheme with the goal of achieving an annular area oversizing of 10%. This sizing algorithm has recently been validated in a multicenter trial and shown to not only help reduce paravalvular regurgitation, but also the combined endpoint of in-hospital death, annular rupture, valve-in-valve implantation, and valve embolization.

For self-expandable valves, other authors have suggested perimeter-based multidetector CT sizing with a recommended oversizing of the annular circumference by approximately 10%–25%. This approach is probably more in keeping with the persistent annular eccentricity after deployment in this kind of valve.

Although these multidetector CT sizing proposals represent a thoughtful first step in more formal integration of multidetector CT in transcatheter valve selection, it is important to emphasize that, because Medtronic and Edwards Lifesciences valves have different properties (Table 1), the results of studies of one type of valve are not applicable across vendors. Furthermore, the value of echocardiography in the sizing process must not be underestimated, since available randomized trial data and the great majority of TAVR outcome data have been successfully based on (2D) TEE-derived measurements. Thus, valve size selection remains a multifactorial and multimodality process.

Finally, although 3D annular measurements obtained with multidetector CT have been shown to help predict PAR retrospectively (74), there is only limited prospective large-scale evidence that integrating multidetector CT in annular sizing and transcatheter valve selection will improve clinical outcomes.

### **3.7 Native aortic valve: further imaging features and relationship to the coronary artery ostia**

Multidetector CT has proved to be an excellent tool for the accurate assessment of the morphology of the aortic valve, with a recent study further indicating excellent correlation between the degree of valve calcification and the hemodynamic severity of aortic valve stenosis. TTE remains the primary tool for morphologic and functional evaluation of the aortic valve; in a recent study, however, CT proved superior in characterizing the morphology of the aortic valve, with better differentiation between bicuspid and tricuspid valves (76). This is important, since the procedure can be technically more challenging in bicuspid valves (77). There is increasing evidence that the presence, extent, and distribution of valve calcifications may have a role in the occurrence of peri- and postprocedural complications. Extensive valve calcification has been associated with moderate to significant valve regurgitation after TAVR, presumably due to interposition of these bulky calcifications between the deploying device and the native aortic valve (Figures 3.13, 3.14). Furthermore, owing to the same proposed mechanism of restricted deployment, extensive calcifications at the sinotubular junction can limit balloon expansion, possibly leading to inadequate device fixation and subsequent migration into the ascending aorta.

Displacement of the native aortic valve leaflets during deployment of the transcatheter valve carries a minimal but nevertheless important risk of subsequent occlusion of the coronary ostia, with a reported incidence of 0.6%–4.1%. Although this is typically a periprocedural complication, it has also been reported

to occur hours after valve implantation. Increased awareness of this rare complication is required in patients with large and heavily calcified valve leaflets and a short anatomic distance from the annular plane to the ostia of the coronary arteries (Figure 3.15). Furthermore, this distance has been shown to have significant interindividual variation ranging from 7.1 to 21.7 mm. As a general rule, a minimum distance of 10 mm between the annular plane and the coronary ostia is recommended. Finally, the size of the aortic sinus could also play a role in this complication, since this structure acts as a “reservoir” for displaced native aortic valves. However, there are no strict guidelines regarding a minimum required size for the aortic sinus that would preclude intervention. Preoperative risk evaluation is therefore based on an overall subjective assessment of (a) the amount and distribution of calcifications in the native aortic valve, and (b) the capacity of the aortic sinus to accommodate the displaced native valve after deployment.



**Figure 3.13** Double-oblique contrast-enhanced CT image through the aortic sinus reveals extensive leaflet calcifications, most prominently in the right coronary cusp. Prominent valve calcification may complicate device deployment and may be associated with an increased risk for postoperative paravalvular regurgitation. *A* = anterior, *P* = posterior.

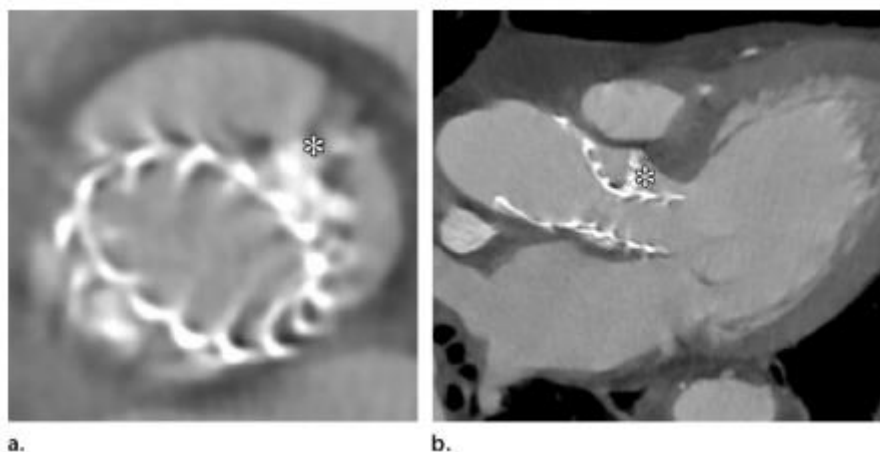


**Figure 3.14** Contrast-enhanced CT image at the level of the sinuses of Valsalva (a) and three-chamber view (b) show a CoreValve device in the aortic root. The obstructive effect of the extensive calcifications of the native aortic valve (\*) causes asymmetric deployment and positioning of the transcatheter valve. Despite a very convincing finding of severe paravalvular regurgitation at CT, echocardiography revealed only moderate regurgitation, underscoring the need to compare results from different imaging modalities to achieve the most complete assessment possible.



**Figure 3.15** Slightly oblique coronal contrast-enhanced CT image at the level of the aortic root shows that an adequate distance (white double-headed arrow) between the annular plane and the nearest coronary ostium—in this case, the left main ostium (\*)—is necessary to avoid the rare but devastating complication of ostial occlusion due to displaced native valve leaflets during prosthesis deployment. As a rule of thumb, a minimum distance of 10 mm is recommended. It is also recommended that this distance be greater than the length of the aortic valve leaflets (black double-headed arrow). *Cau* = caudal, *Cra* = cranial.

### 3.8 Determining the best fluoroscopic projection angle for device deployment

During the actual TAVR procedure, the 3D visualization offered by multidetector CT is reduced to the 2D projection image inherent in conventional angiography. Nevertheless, a correct periprocedural understanding on the part of the operator of the spatial orientation of the aortic root relative to the body axis is necessary to correctly position the prosthetic device along the centerline of the aortic root and perpendicular to the aortic annular plane. Without multidetector CT guidance, the operator needs to perform several intravenous contrast material injections to find the optimal fluoroscopic projection plane for deployment, with the nadirs of the three aortic valve cusps aligned in the same straight 2D projected plane (Figure 3.16). Besides adding complexity to the procedure, this step introduces an additional contrast volume load and increased risk for subsequent renal injury. Multidetector CT, with its excellent 3D capabilities, has been shown to help preoperatively predict a suitable angulation (left anterior oblique–right anterior oblique and cranial-caudal angles) of the angiography tube and achieve precise positioning of the prosthetic valve following angiography of the aortic root, thereby significantly improving the final transcatheter valve position compared with procedures performed without multidetector CT guidance. These tube angulation data can be obtained manually through manipulation of the multidetector CT dataset as explained by some authors, or derived using specialized software tools. In each individual case, there are several possible appropriate angles. This information is routinely derived and consistently reported at each preoperative CT examination using software-derived measurements (Advantage Windows AW 4.3, GE Healthcare). However, the

increasing availability of 3D rotational angiography systems also allows accurate assessment of the best projection plane, reducing the role of multidetector CT for this purpose.

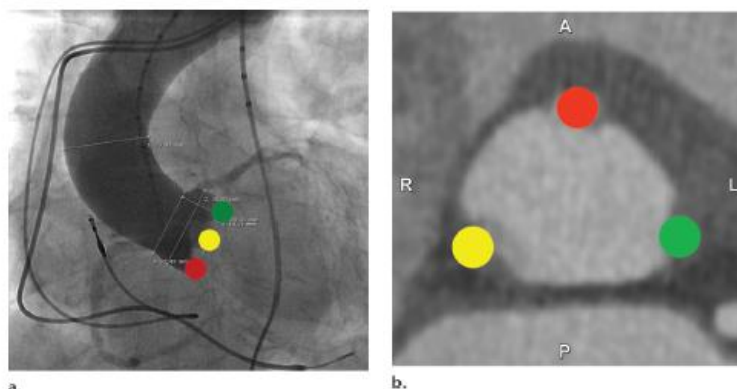


**Figure 3.16** For optimal device deployment, the inclination of the angiography tube must be such that, on the resulting fluoroscopic image (a), the basal insertion sites of all aortic valve leaflets are aligned in the same anatomic annular plane, corresponding with the correctly aligned double-oblique CT image (b). Green dot = left coronary cusp, orange dot = right coronary cusp, yellow dot = noncoronary cusp. On the basis of preprocedural CT-derived left anterior oblique–right anterior oblique and cranial-caudal angulation values, an accurate prediction of the best procedural fluoroscopic angulation for correct deployment of the transcatheter valve along an axis perpendicular to the aortic annular plane can be made. This approach obviates repeated angiographic test injections to determine the correct tube angulation, thereby reducing both the amount of contrast material used and the time required for the procedure. *A* = anterior, *P* = posterior.

### 3.9 Other preprocedural findings

Multidetector CT can help accurately evaluate the curvature of the ascending aorta and its anatomic relation to the left subclavian artery, since anatomic variations, increased angulation, and/or tortuosity of these vessels will increase the technical difficulty of the procedure. Likewise, augmented angulation between the ascending aorta and the aortic root–LVOT will complicate the accurate positioning of the transcatheter valve with endovascular access, since this angulation can induce some rotation of the transcatheter valve during deployment (although it is not a contraindication for the procedure) (Figure 3.17). Furthermore, the presence of a hypertrophic basal septum can theoretically undermine the stability of the transcatheter valve due to its mass effect during and after deployment (Figure 3.17b).

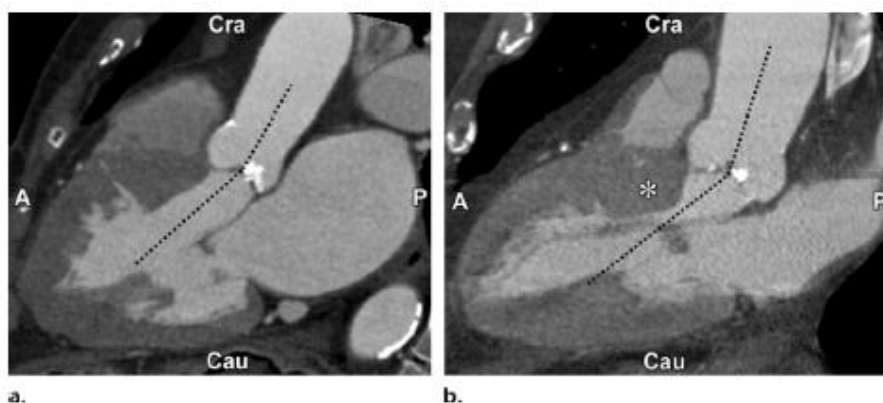


**Figure 3.17** CT evaluation of the angulation between the ascending aorta, aortic root, and LVOT. A practically straight line between the ascending aorta and the LVOT (dashed line in a) indicates a much more favorable anatomic situation than does a steeper angulation (dashed line in b), since the latter can complicate stable deployment of the prosthesis. The technical difficulty of the procedure is further increased by the presence of a hypertrophic basal septum (\* in b), potentially creating increased resistance during device deployment. *A* = anterior, *Cau* = caudal, *Cra* = cranial, *P* = posterior.

In transapical device deployment, the angle between the left ventricular apex and the aortic annular plane has been described as one of the determinants of success, since rigid delivery systems can make the procedure

more difficult at steeper angles. Although the aforementioned anatomic characteristics are not considered strict procedural contraindications, they are valuable for preoperative strategy evaluation and must always be included in the radiology report. Nevertheless, there are as yet no strict guidelines, with the final assessment being left to the performing surgeon and interventional cardiologist.

### **3.10 Incidental findings**

Because the investigated subgroup of TAVR candidates are invariably advanced in age, the presence of significant incidental findings that may alter the treatment course must always be considered. Therefore, with its large anatomic coverage, multidetector CT is an ideal screening tool, in one series helping detect significant incidental disease in up to 34.3% of cases and unsuspected malignancy in 4.1%. However, untreated symptomatic aortic valve stenosis has a dismal prognosis, with short-term survival rates even lower than those of some undetected malignancies. Therefore, treatment options must always be reviewed on a case-by-case basis.

### **3.11 Postprocedural imaging**

The exact role of multidetector CT in the postprocedural evaluation of patients who have undergone transcatheter valve implantation remains unclear. Although the role of multidetector CT in the detection of periaortic complications (eg, pseudoaneurysms) is unquestioned, its purpose in helping evaluate causes of valve dysfunction is currently the subject of debate and intense investigation. CT can be used to evaluate the position and expansion of the transcatheter valve in the aortic root (Figure 3.14); however, it is not yet known which morphologic parameters can help in the assessment of paravalvular regurgitation. This further underscores the need to compare results obtained with different imaging modalities to achieve the most complete evaluation possible.

### **3.12 Sutureless valves**

The increasing incidence of aortic stenosis and greater co-morbidities and risk profiles of the contemporary patient population has driven the development of minimally invasive aortic valve surgery and percutaneous transcatheter aortic valve implantation (TAVI) techniques to reduce surgical trauma. Recent technological developments have led to an alternative minimally invasive option which avoids the placement and tying of sutures, known as “sutureless” or rapid deployment aortic valves. Potential advantages for sutureless aortic prostheses include reducing cross-clamp and cardiopulmonary bypass (CPB) duration, facilitating minimally invasive surgery and complex cardiac interventions, whilst maintaining satisfactory hemodynamic outcomes and low paravalvular leak rates.

In this section it is shown an overview of the current sutureless valve solutions:

- Perceval

Consist in a bioprosthetic valve designed to replace a diseased native or a malfunctioning prosthetic aortic valve via open heart surgery, with the unique characteristic of allowing sutureless positioning and anchoring at the implant site. The choice of materials and configuration ensures the device biocompatibility and hemocompatibility. The Perceval prosthesis consists of a tissue component made from bovine pericardium and a self-expandable Nitinol stent, which has the dual role of supporting the valve and fixing it in place. Perceval tissue heart valve is supplied unmounted. Prior to implantation the prosthesis diameter is reduced to a suitable size for loading it on the holder. The valve is then positioned and released in the aortic root, where the stent design and its ability to apply a radial force to the annulus allow stable anchoring of the device.

The Perceval aortic model is available in four sizes: size S, size M, size L, and size XL.

The Perceval prosthesis is preserved in a buffered aldehyde-free sterile solution. Each is packaged individually in its own container. A plastic tag with the prosthesis identification data is attached to the device. The prosthesis is mounted on a support that holds it into the jar. The container is externally sealed with a transparent film, which should be removed just before preparing the prosthesis for implantation.

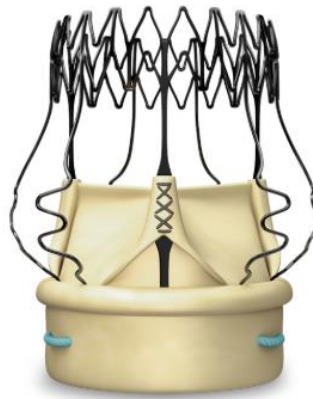


**Figure 3.18**

- **Intuity**

The pericardial stented aortic valve is based on the design and the proven performance of the PERIMOUNT valve family. A balloon expandable stainless steel cloth-covered frame is incorporated into the inflow aspect of the valve. The valve is implanted with the aid of a delivery system, which incorporates a balloon catheter to expand the frame within the left ventricular outflow tract (LVOT). The expandable frame works in conjunction with the sewing ring to position and stabilize the valve at implant. The system reduces the number of sutures required to secure the valve, while the frame establishes a seal within the LVOT. The system may be used in both traditional and less invasive surgical procedures for heart valve replacement.

The model 8300AB (Figure 3.18) is a stented trileaflet valve comprised of bovine pericardium treated with the Carpentier-Edwards ThermaFix process. The leaflets are mounted on a flexible cobalt-chromium alloy wireform. The inflow of the valve incorporates the cloth-covered balloon

expandable frame. The EDWARDS INTUITY Elite valve system is available in sizes 19, 21, 23, 25, and 27 mm.

The valve is packaged and terminally sterilized in glutaraldehyde. Glutaraldehyde is shown to both reduce the antigenicity of tissue xenograft valves and increase tissue stability. The wireform is made of cobalt-chromium alloy. The wireform is covered with a knitted polyester fabric. A thin, cobalt-chromium alloy/polyester film laminate band surrounds the base of the wireform. A silicone sewing ring which is covered with a porous, seamless polytetrafluoroethylene (PTFE) cloth is attached to the wireform. The scalloped sewing ring is designed to conform to the native aortic annulus. The compliant nature of the sewing ring facilitates coaptation between the valve and an often irregular or calcific tissue bed. The sewing ring has three suture markers to aid in valve orientation. A holder is attached to the valve by means of sutures to facilitate handling, deployment, and suturing the valve during the implant procedure. The holder is easily detached by the surgeon.



**Figure 3.19**

- **3F Enable**

Consists of a 3f Aortic Bioprosthesis Model 1000 (ATS Medical) mounted on a self-expanding nitinol frame (Figure 3.20). The nitinol frame contributes to the fixation of the device in the deployed location by outward radial forces inherent in the Nitinol material, thus reducing the number of sutures required to secure the bioprosthesis in the annulus. A polyester flange has been incorporated at the inflow aspect to minimize the potential of paravalvular leaks and migration. Access to the aortic valve is obtained through partial upper sternotomy in isolated aortic valve replacements or complete median sternotomy in combined procedures, respectively. Using a standard technique for cardiopulmonary bypass and cardioplegic arrest, transverse aortotomy is performed 2 cm above the sinotubular junction. Then the aortic valve is inspected, because the presence of a bicuspid valve is regarded as exclusion criteria according to the protocol. Attention is also paid to abnormalities of the coronary ostia and possible mismatch between the annulus and the sinotubular junction. After excision of the aortic valve and debridement of the aortic annulus, it is necessary size the aortic annulus with especially designed sizers. These sizers reflect the real annulus size, the external diameter of the corresponding Enable prosthesis (ATS Medical) is larger to enhance fixation. Because the fixation of the valve in place is obtained through outward radial forces of the nitinol frame, care has to be taken for exact sizing.



**Figure 3.20** *ATS 3f Enable*

If the implant chosen is too small for the annulus, paravalvular leakage or migration might occur; if it is too large, complete deployment might become impossible. The prosthesis requires rinsing in saline solution three times for 2 minutes each time. While rinsing the valve, a single-guiding suture (2-0 polyethylene) is placed under the left-to-aortic commissure or the annulus corresponding to the deepest point of the aortic sinus. With increasing implant experience, the technique was changed toward positioning the guiding suture in the annulus (aortic sinus), because two intraoperative conversions of clinical implants were caused by malpositioning in this region.

After the rinsing process is completed, the valve is placed in chilled physiological saline to make it pliable. It is carefully folded under water to avoid frame fracture. The valve is inserted in a deployment tool. The guiding suture is now attached to the superior portion of the flange, in a position corresponding to the placement in the annulus.

The valve is now inserted and deployed, and care must be taken to avoid rotation. Before the deployment is completed through rinsing with warm saline solution, exact positioning of the valve has to be performed. However, if malpositioning occurs after complete deployment, rinsing with chilled saline enhances repositioning until the valve is correctly placed. The guiding suture is then tied down. In 9 patients of the series, we removed it without having seen postoperative displacement of the valve. The aortotomy is then closed in the regular fashion.

Correct positioning of the valve prosthesis without paravalvular leakage is assessed intraoperatively by transesophageal echocardiography. Transthoracic echocardiography examinations are carried out at discharge, at 6 month, and at 12 month follow-up after surgery. Again, special attention is focused on the absence of paravalvular regurgitation, transvalvular gradients, and effective orifice area.

## 4 Materials and methods

This chapter focuses to the Persist study “Perceval Next Generation”, with which is intention to develop a new model of prosthesis. So, a specific analysis is performed on 100 patients through the visualization of the preoperative CT scan with the use of a specific program. Analyzing the various CTs, geometric parameters are evaluated to define a design that adapts to the patient’s anatomy.

The subject of the study are over 65 years old, both men and women coming from different center around the Europe, with problems at the level of the aortic root.

The data were obtained in the systole phase, except for some cases where it was not possible to distinguish between the systole phase and that of diastole or those in which the systole phase was not available. In fact the percentage of the cardiac cycle on which the measurements were extrapolated was specified. It is necessary to specify that the pre-operative CT scans, coming from different clinics and therefore having been carried out by different doctors, have different percentages. Consequently, on the basis of the analyzed CT scans, it was decided to stipulate a precise range for the two different phases:

- Systole for  $\leq 45\%$ ;
- Diastole for a percentage  $> 45\%$ .

### 4.1 CT scan analysis

A CT scan, also known as computed tomography scan, makes use of computer-processed combinations of many X-ray measurements taken from different angles to produce cross-sectional (tomographic) images (virtual “slices”) of specific areas of a scanned object, allowing the user to see inside the object without cutting.

In medical fields, it is used to diagnose pathologies or bone traumas, of articulations or other internal organs; it allow to obtain three-dimensional data about analyzed part and it is especially suitable for visualizing the structure and the tissue’s density.

This informations can be used to reconstruct the organ’s geometry.

4DCT is a type of CT scanning which records multiple images over time. It allows playback of the scan as a video, so that physiological processes can be observed and internal movement can be tracked. The name is derived from the addition of time (as the fourth dimension) to traditional 3D computed tomography. Alternatively, the phase of a particular process, such as respiration may be considered the fourth dimension.

To build a model of a cardiac element, using CT images as starting data, two softwares were used. Data concerning the scan (images in DICOM format) were appropriately treated.

To do that, different software can be used:

- *OsiriX*, is an image processing application for Mac dedicated to DICOM produced by equipment (MRI, CT, PET, PET-CT, ...). has been specifically designed for navigation and visualization of multimodality and multidimensional images: 2D Viewer, 4D Viewer (3D series with temporal

dimension, for example: Cardiac-CT) and 5D Viewer (3D series with temporal and functional dimensions, for example: Cardiac-PET-CT). The 3D Viewer offers all modern rendering modes: Multiplanar reconstruction (MPR), Surface Rendering, Volume Rendering and Maximum intensity projection (MIP). All these modes support 4D data and are able to produce image fusion between two different series (for example: PET-CT).

OsiriX is simultaneously a DICOM PACS workstation for imaging and an image processing software package for research (radiology and nuclear imaging), functional imaging, 3D imaging, confocal microscopy and molecular imaging.

It supports a complete plug-in architecture that allows one to expand the capabilities of OsiriX for personal needs. OsiriX is released under a proprietary license and runs under macOS.

- *3Mensio*, offers software for pre-operative sizing and planning. The 3mensio Workstation contains two modules: Structural Heart and Vascular. 3mensio Structural Heart contains dedicated workflows to assess structures in the heart in order to plan different procedures. 3mensio Vascular is dedicated to sizing and planning of EVAR, TEVAR and FEVAR procedures in a quick, easy and reliable way.
- *Mimics*, (Materialize's Interactive Medical Control System) (Materialize, Belgium), is a software that allows to use 2D images (DICOM format) for the realization of 3D models. The aim is to reconstruct the cardiac element starting from the image of its different section, and with Mimics it is possible identify the level curves of the heart's geometrical model.

The basic steps consist in importing images, selecting images related to the phase of the cardiac cycle of interest, the systole (around 30% of the complete cycle), thresholding and calculation of the parts, and then export in 3-Matic.

The thresholding is a technique for image segmentation which, in this case, associates pixels with gray values associated, included in a range to define, a single color. This allows to identify in a simpler way, section by section, the tissues to be considered in the reconstruction (aorta, left ventricle and left atrium).

In a previous thesis work, Cristina La morella has used a specific analysis on patients through the visualization of preoperative CT scan with the use of OsiriX, evaluating the geometrical parameters useful for the definition of the anatomy of the aortic area.

In this thesis work, for the evaluation of the geometrical aortic parameters, has been used Mimics software, which transform the raw data of the tomographs into suitable files for construction of the contour lines and the surface of the aorta of interest.

Mimics allows the passage from information concerning many images to an image that mathematically defines the contours and surfaces of the structure to rebuilt.

This operation requires manual intervention that mainly serves to decide the grey level of reference to distinguish the components of the tissue and to verify the effective success of the contour recognition.

The three-dimensional model obtained can be exported to Materialize 3-Matic.

The measures of interest were:

ANNULUS PLANE	VALSALVA SINUSES PLANE	SINOTUBULAR JUNCTION PLANE
Area (mm <sup>2</sup> )	Diameter of the circle passing through the 3 commissures (mm)	Area (mm <sup>2</sup> )
Perimeter (mm)	Radius of the non coronary cusp (mm)	Perimeter (mm)
Dmax (mm)	Radius of the right coronary cusp (mm)	Dmax (mm)
Dmin (mm)	Radius of the left coronary cusp (mm)	Dmin (mm)

from which derivated measures have been calculated:

ANNULUS PLANE	VALSALVA SINUSES PLANE	SINOTUBULAR JUNCTION PLANE
Dequivalent (Annulus perimeter/ $\pi$ )	HVS VS plane distance ratio	HSTJ hSTJ(mean)/Deq
D'equivalent (4*Annulus Area/ $\pi$ ) <sup>0.5</sup>	HRVS 2*r0/Deq	STJ 2*rSTJ/Deq
e= 2*Dmin/Dmax-1"	HRNC 2*rNC/Deq	/
$\alpha$ angle between Dmax and NC sinus (degrees)	HRRC 2*rRC/Deq	/
/	HRLC 2*rLC/Deq	/

With:

- e = eccentricity;
- r0 = radius of the circumference defined by the nadirs of the semi-lunar leaflet attachments;
- rNC = radius of the non coronary cusp;
- rRC = radius of the right coronary cusp;
- rLC = radius of the left coronary cusp;
- hSTJ = distance between the annulus plane and the sinotubular junction plane;
- rSTJ = radius of the sinotubular junction.

## 4.2 Procedure

Start the Mimics software, click File - *New Project Wizard*, select the folder where the images in DICOM format are located, select a *Target Folder* in which save the project you are about to create and click *Next*. Upload the images and convert them. Remove the check from *Check all studies* and select the images related to the cardiac systole. Click on *Convert*:

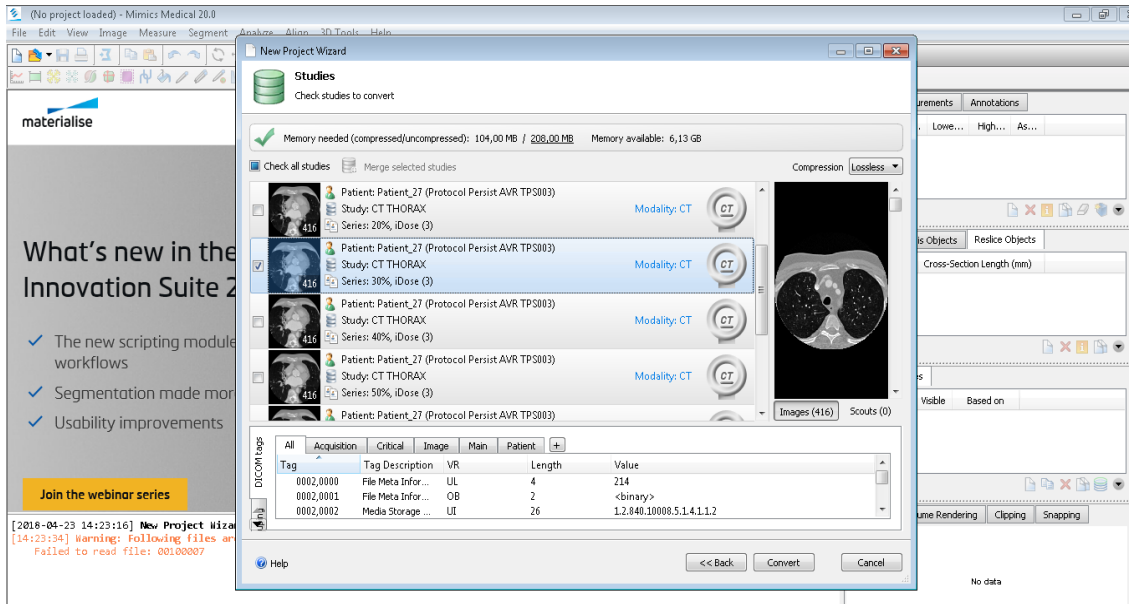


Figure 4.1

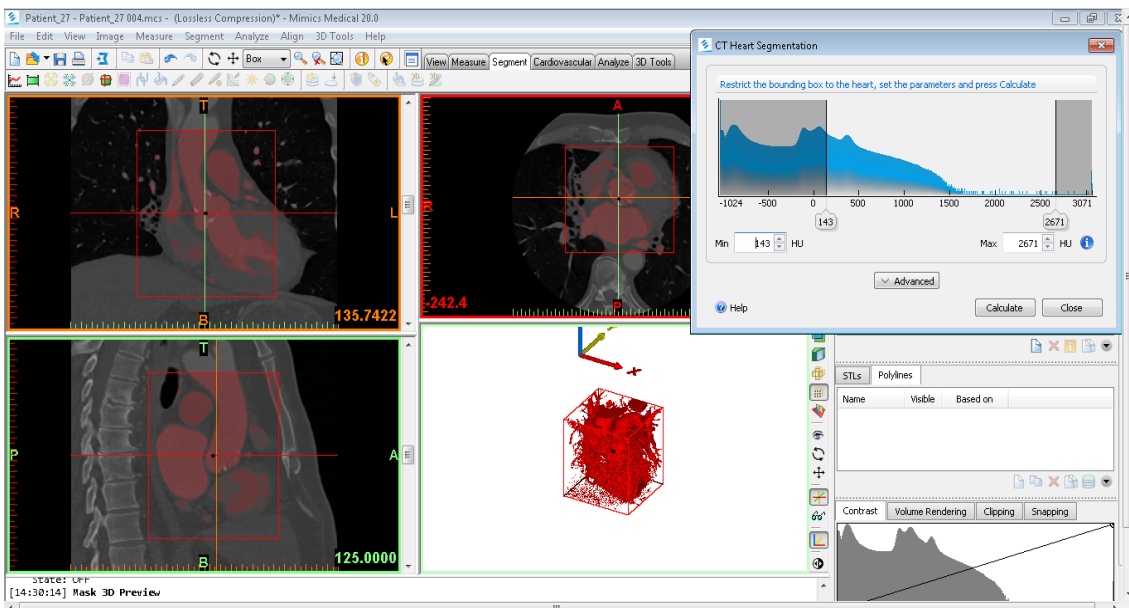


Figure 4.2

A *Change Orientation* window will appear, click Ok.

If everything performed correctly, the three views of the chest in question appear corresponding to the sagittal, coronal and axial plane.

Next step is identify the aorta, the left ventricle and the left atrium: click on *Segment - Cardiovascular - CT Heart*. Mimics opens a window from which is possible narrowing the contours of the heart field and select

the thresholding values (Figure 4.2) that identifying areas of the images whose pixels have a value of gray included in a fixed range of values.

For the tissue of our interest the ideal would be thresholding values around 200, if necessary decrease or increase to better identify the tissues.

It is possible activate a 3D view with the *Toggle mask 3D preview* command (indicated by the arrow) to display a 3D preview of the model.

Once this is done, go to *Advanced* which allow to select the points for manual segmentation: click on *Add* and for each mask (LV, LA, RV, RA, Aorta, PA, Other) identify the required tissue using the three views (Figure 4.3).

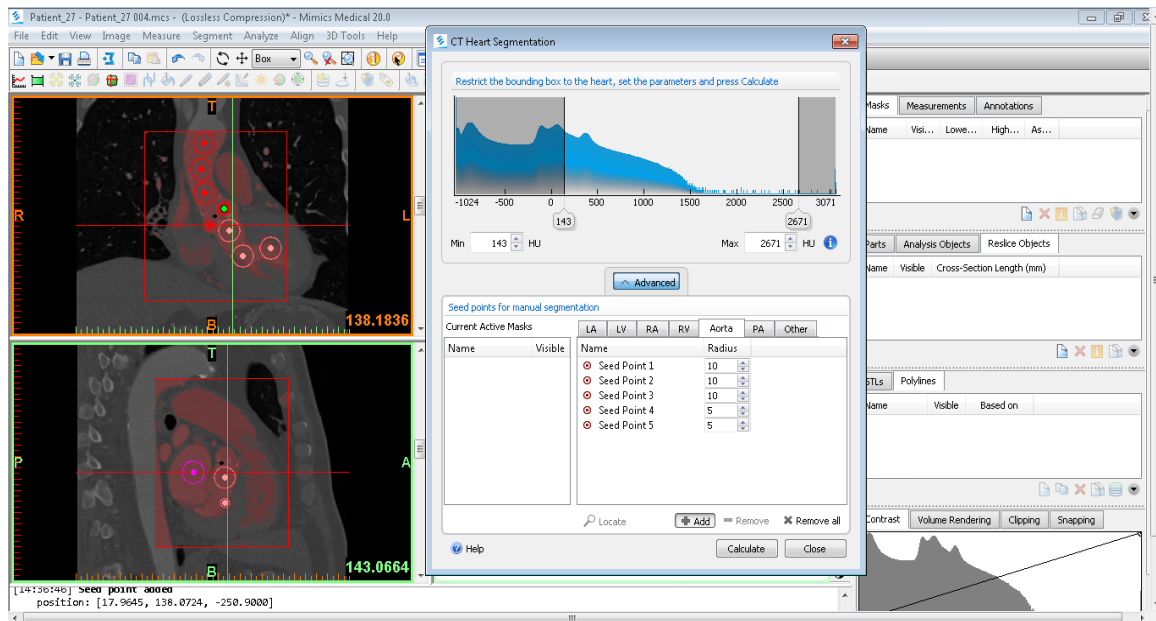


Figure 4.3

For our purpose, it is sufficient to identify the masks for the left ventricle, the left atrium and the aorta.

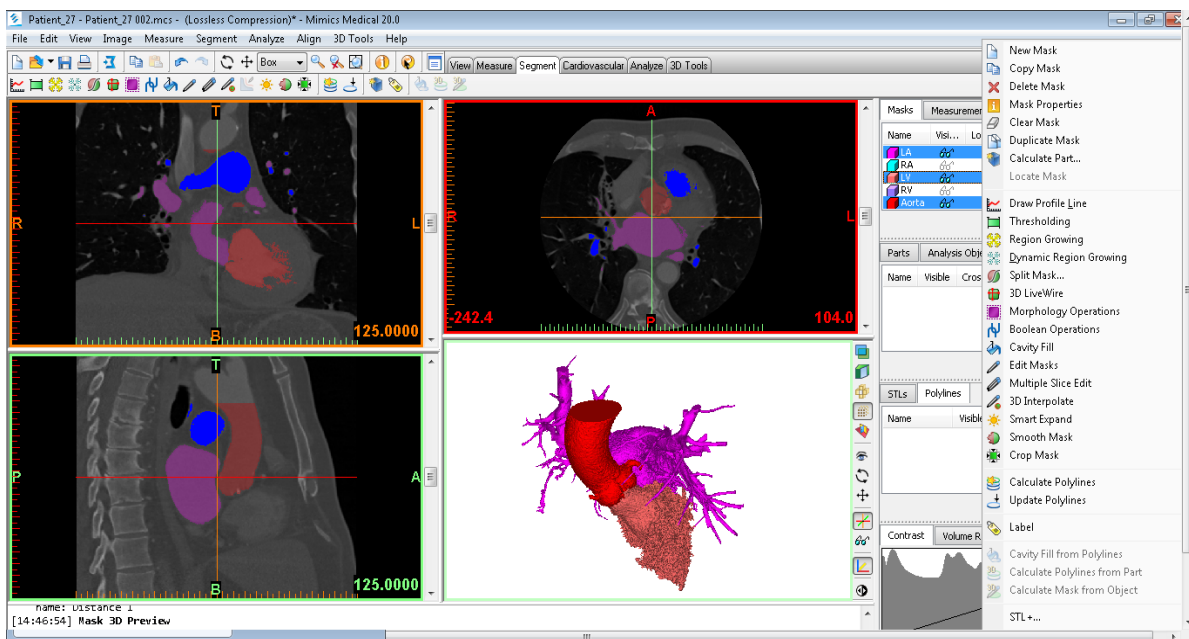


Figure 4.4

After this operation, press *Calculate* and then, at the end of calculation finished, if satisfy with results, press *Close*.

The calculated masks appear in the Masks section in the upper right-hand corner, each of which can be *cleaned* using the *Edit Masks* command, by right-clicking on the mask of interest (Figure 4.4).

Then it is possible to calculate the parts of the masks of interest with the *Calculate Part* command, remembering to select the *High option*.

Press *Calculate* and then *Close*.

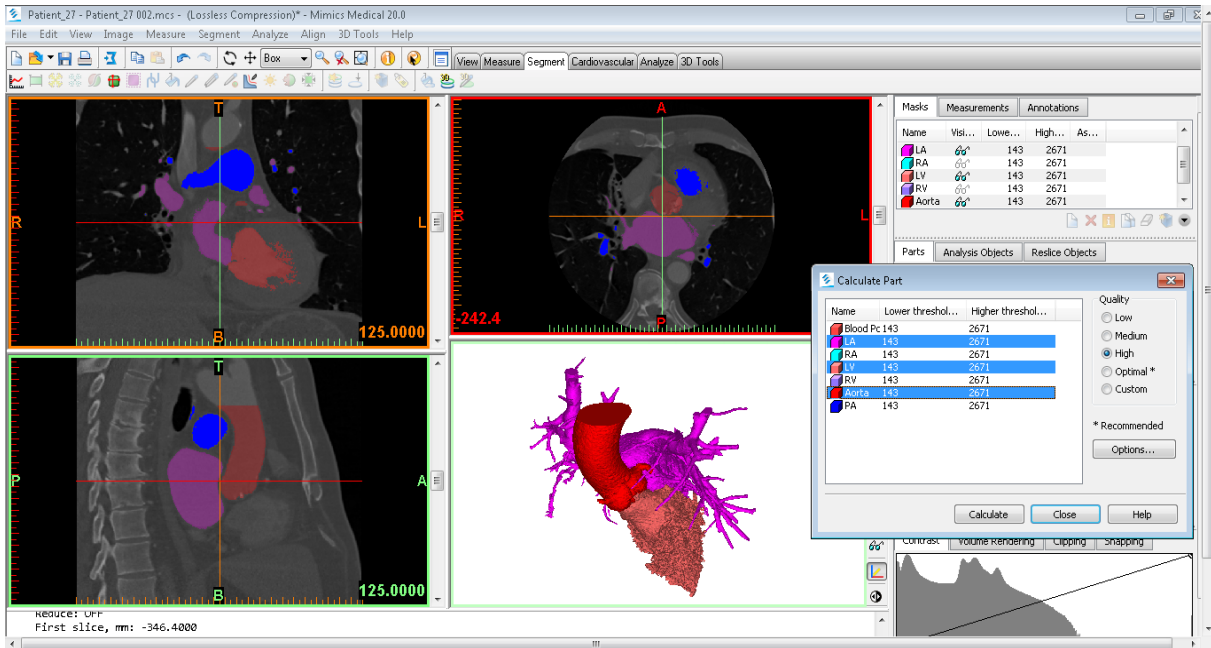


Figure 4.5

It is possible to improve the quality of the part through the 3D Tools - *Wrap* command:

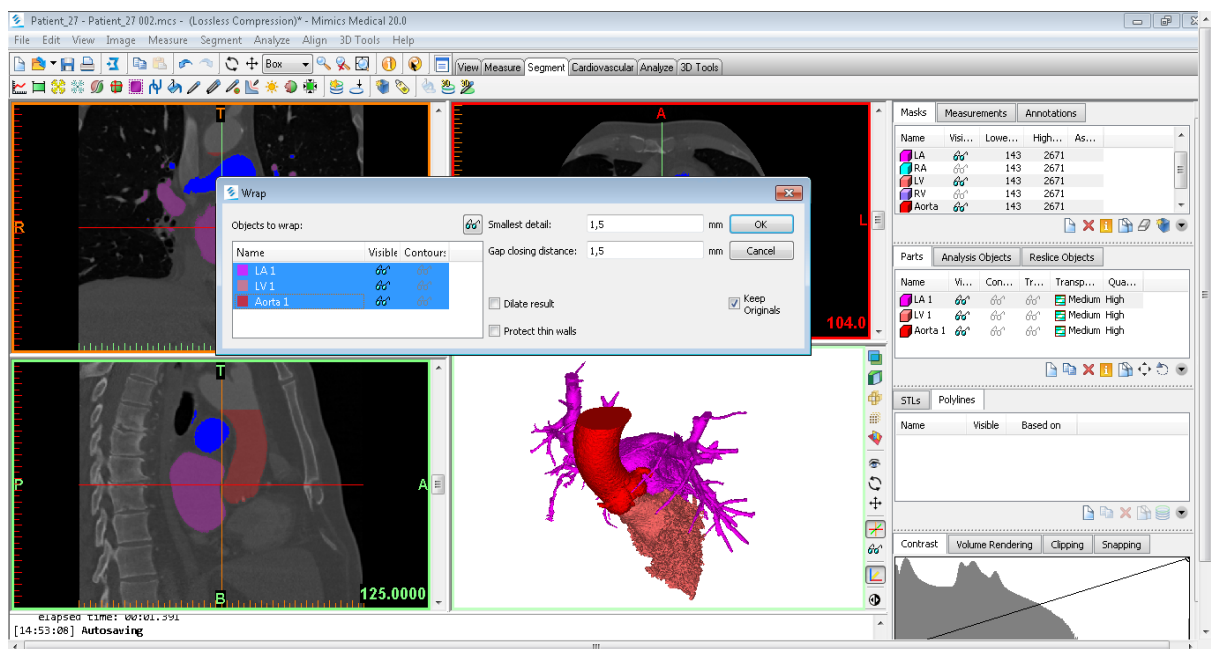


Figure 4.6

Once completed these operations, the model is ready to be exported to 3Matic: *File - Export - 3Matic*. In order to work better on the aorta it is recommended to hide the ventricle and the atrium: right-click and select *Hide*.

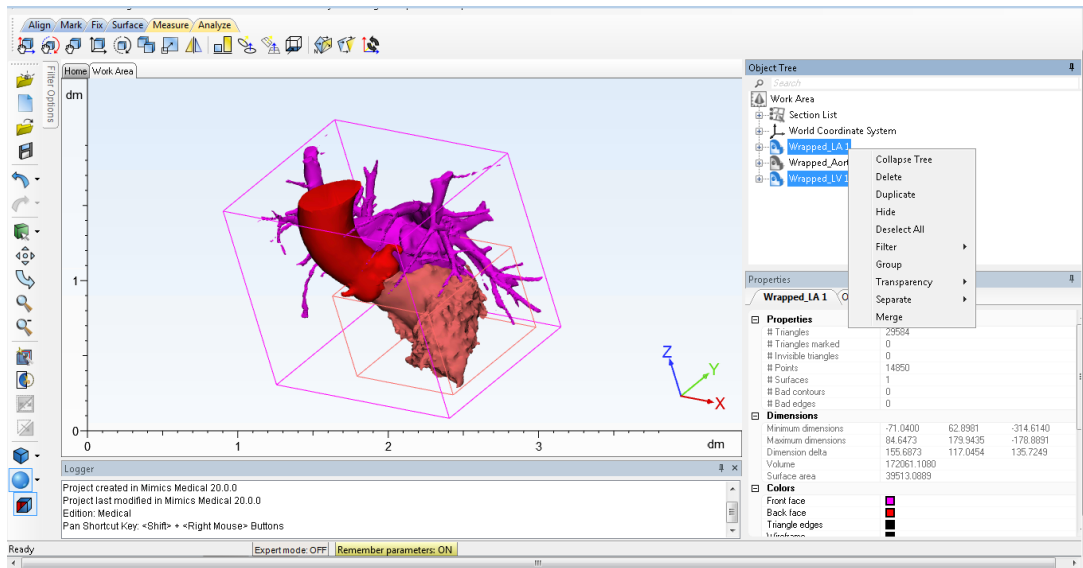


Figure 4.7

Now it is necessary create the planes of the annulus aortic, of the sinuses of Valsalva and of the sinotubular junction necessary for measuring the desired parameters.

Annulus aortic plane:

use the *Analyze - Create Datum Plane* command; in *Operations* select as *3 Points method*.

Locate the three points on the 3D model, corresponding to the anatomical points, placed at the base of each attack of the aortic leaflets; press *Apply*.

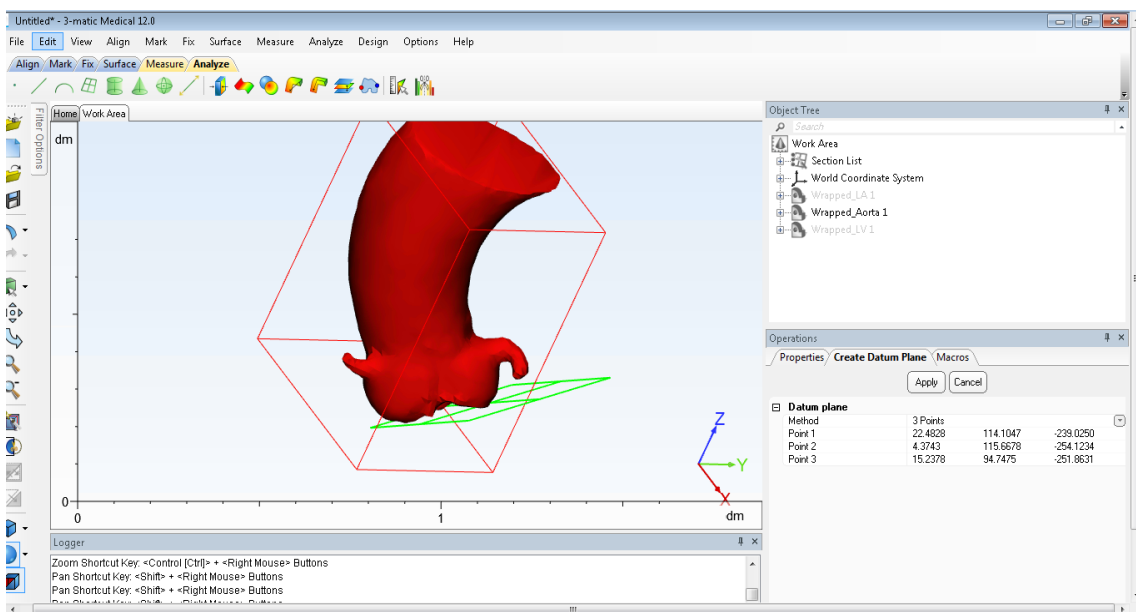


Figure 4.8

The plan created *Datum Plane-001* appear in the *Object Tree*; for convenience it is better rename it: *Annulus Plane*.

In *Properties*, increase the values of *DeltaX* and *DeltaY* in order to have a plan that includes the whole annulus section.

### Sinus of Valsalva plan:

this plane must be parallel to the annulus plane, then repeat the *Analyze - Create Datum Plane* operation, but this time, in *Operation*, select the *Through 1 point method, parallel to a plane*.

Take the point at the maximum protrusion of the non-coronary sinus and select the aortic plane.

Rename the VS plane and increase its size in *Properties*.

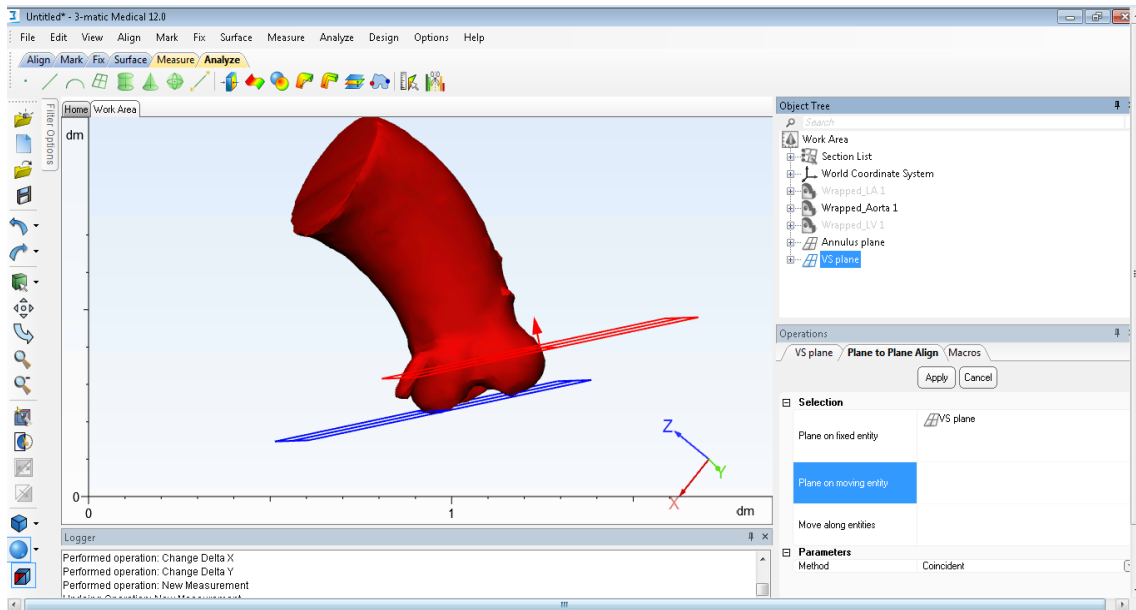


Figure 4.9

Therefore, it is possible to measure the distance between the two planes: *Measure - Distance*, in *Measure distance parameters* select *From Plane To Plane*. Select the two plans and press *Apply*.

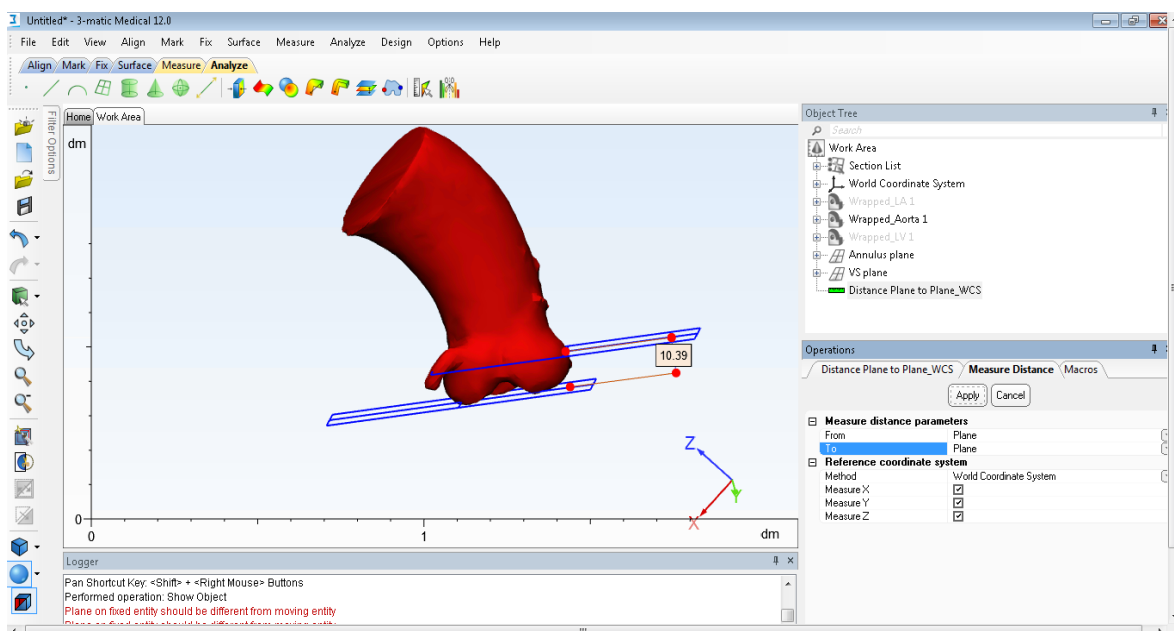


Figure 4.10

Plan of the tubular up joint (STJ):

in this case it is necessary to identify the three points of the junction at the end of the three coronary sinuses with the *Analyze - Create Point - Apply* command.

Obtained these three points, it is possible to measure, with the *Measure - Distance* command, the distance between STJ and the annulus plane in correspondence with the non - coronary sinus, the left sinus and the right sinus, by selecting Measure distance parameters: *From Point To Plane*.

Remember to always click on *Apply* at the end of each measurement and analysis.

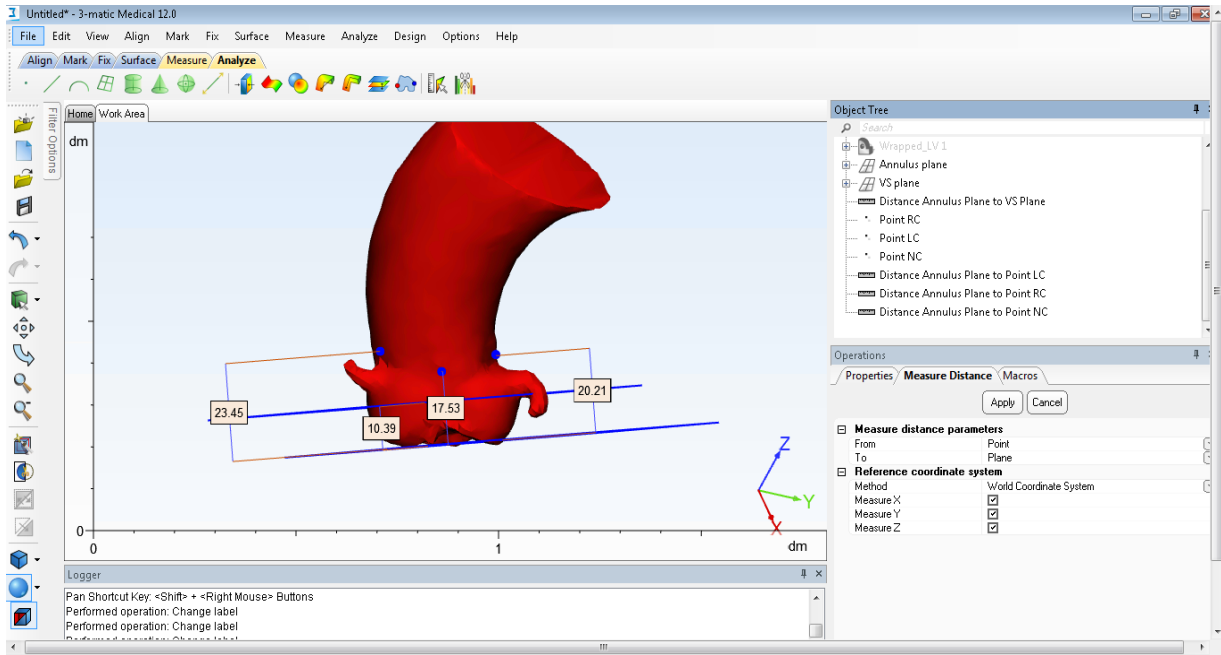


Figure 4.11

Once this is done, create the plan using the three points: *Analyze - Create Datum Plane*; in *Operations* select as *3 Points method*. In *Properties*, always increase the values of *DeltaX* and *DeltaY*.

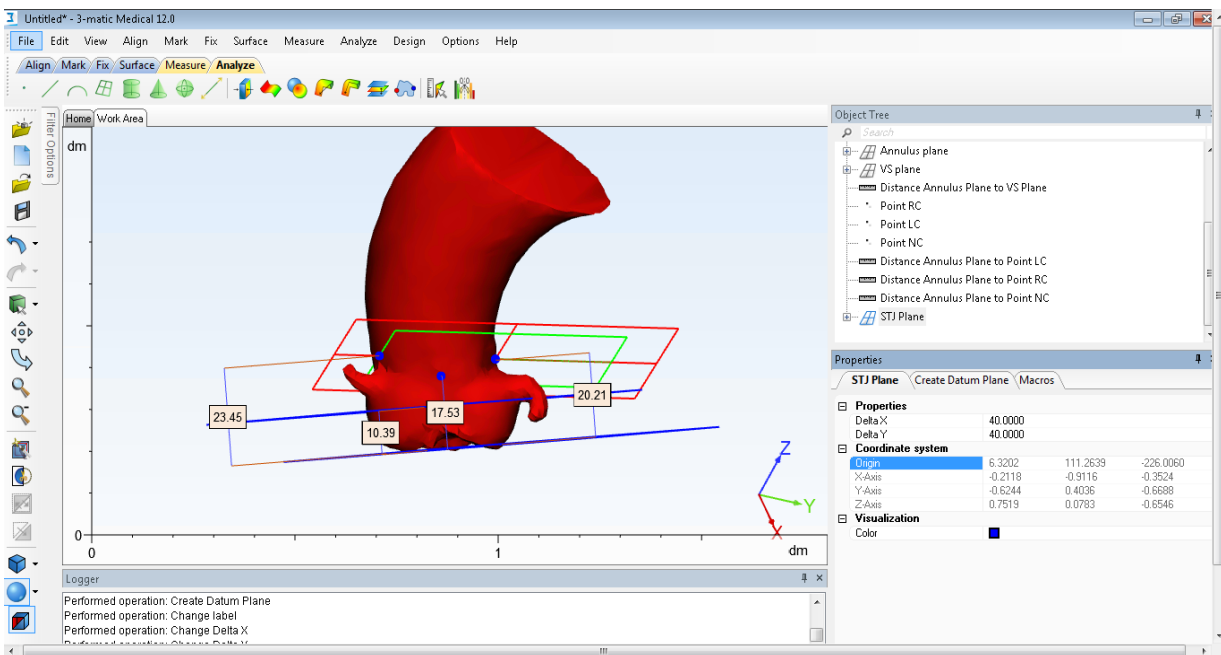


Figure 4.12

With 3Matic it is also possible to measure  $\beta$ , ie the angle between the mitral valve plane and the annulus plane reactivating the ventricle and the atrium (in this way it is easier visualize the points that identify the mitral plane).

Create the plan: *Analyze - Create Datum Plane*; in *Operations* select *3 Points* method.

Locate the three points on the 3D model and press *Apply*.

To measure the angle, click on *Measure - Angle*, in Measure angle parameters choose *Plane to Plane* method, select the annulus and mitral plane and press *Apply*.

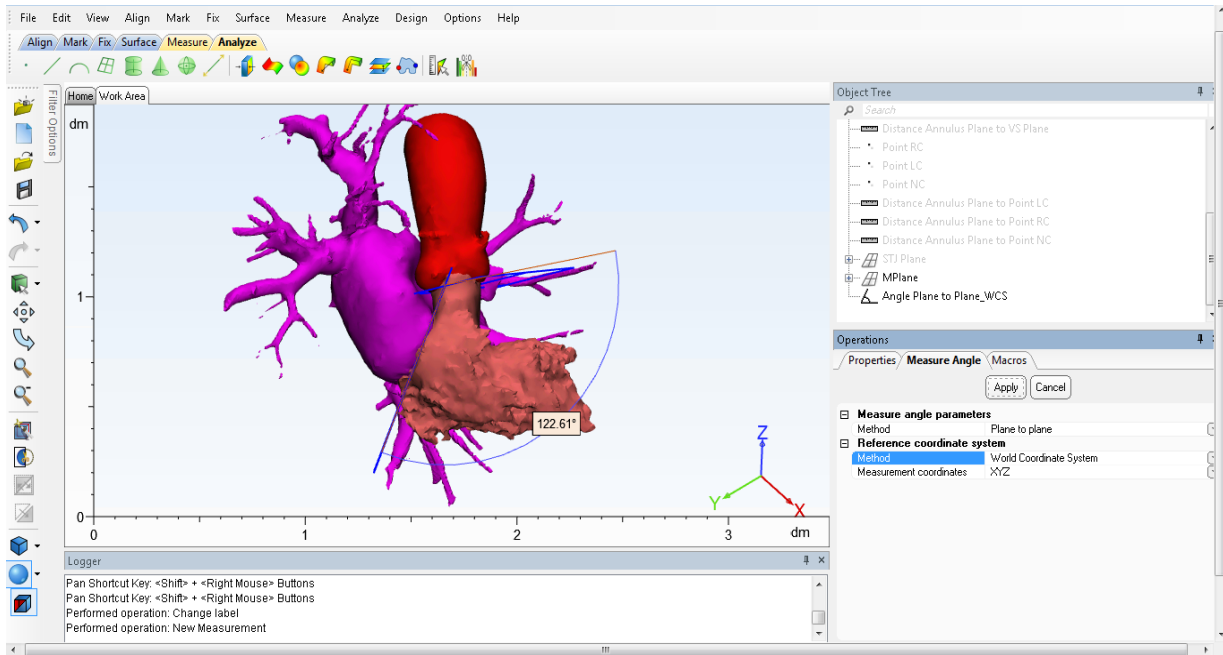


Figure 4.13

To get the values of the other necessary parameters it is necessary to go back in Mimics.

Copy the Annulus, Sinus Valsalva and STJ planes with *CTRL + C* and paste them into Mimics with *CTRL + V*. They will appear in *Analysis Object*.

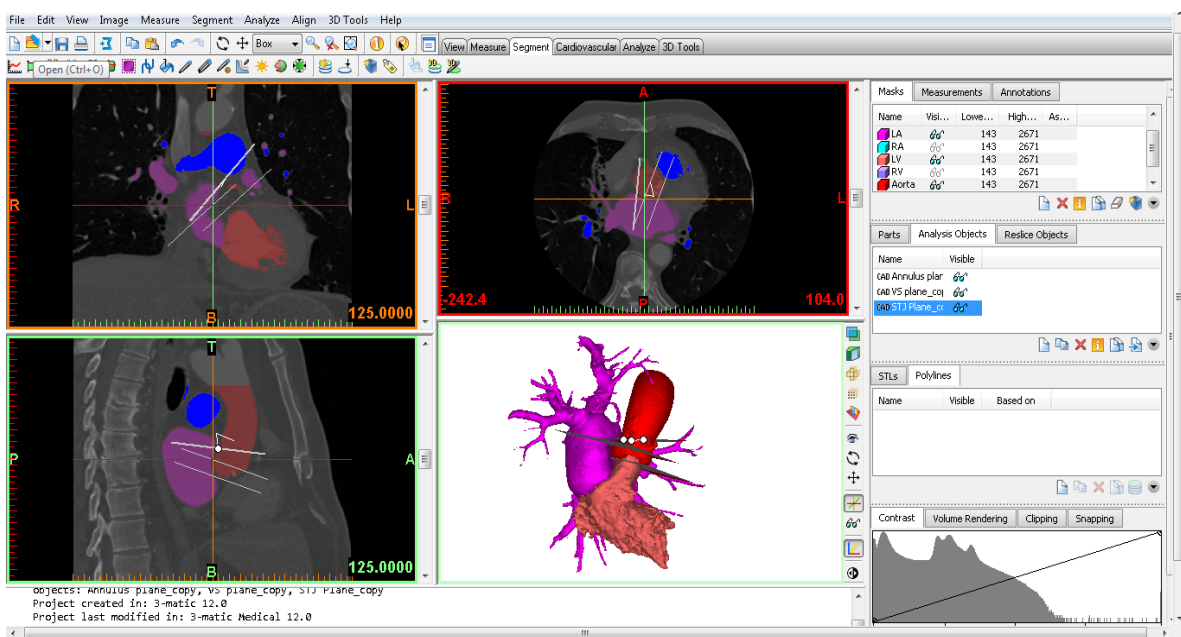


Figure 4.14

Measure of  $P_a$ ,  $L_{max}$ ,  $L_{min}$ ,  $\alpha$ :

Select Annulus Plane, right-click and select *Create reslice plane (s)*. *RPI* appears in *Reslice Object*.

The slice corresponding to the annulus plane appears on the three views of the sagittal, coronal and axial planes.

From the axial plane it is possible to measure the perimeter of the annulus with *Measure - Area*:

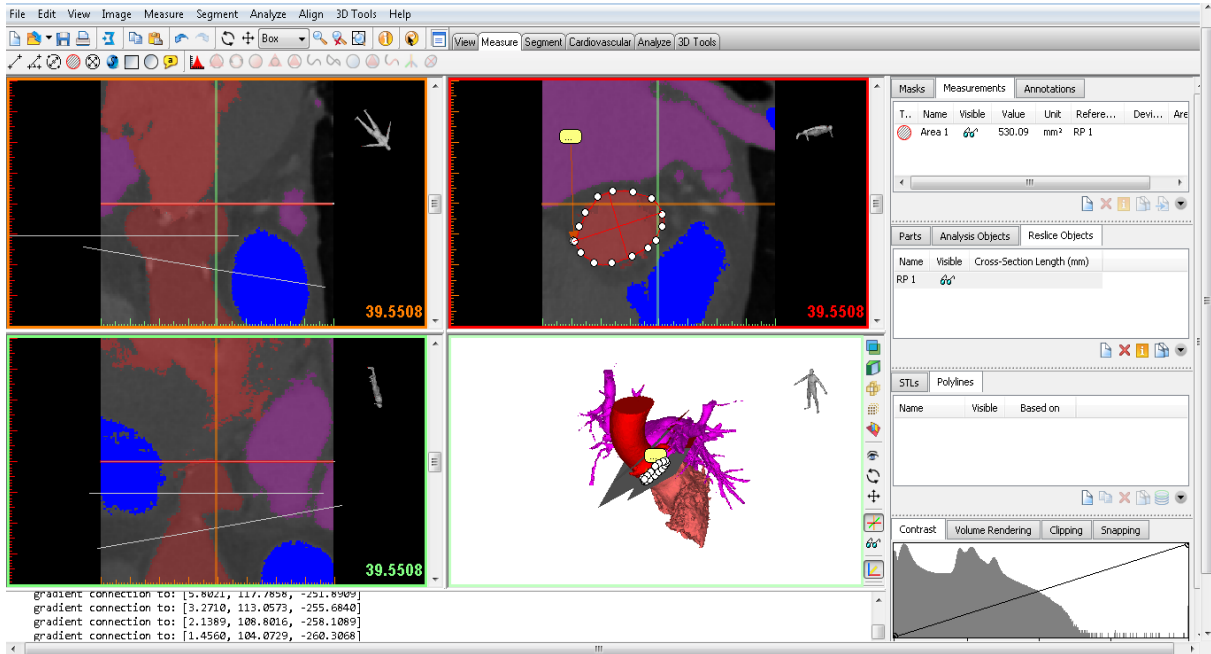


Figure 4.15

All the measurements of interest appear in the yellow box: perimeter, maximum and minimum diameter. This measurement can be done keeping the mask active; in case of any ambiguity, deactivate the mask and check that the points taken for the measurement are correct.

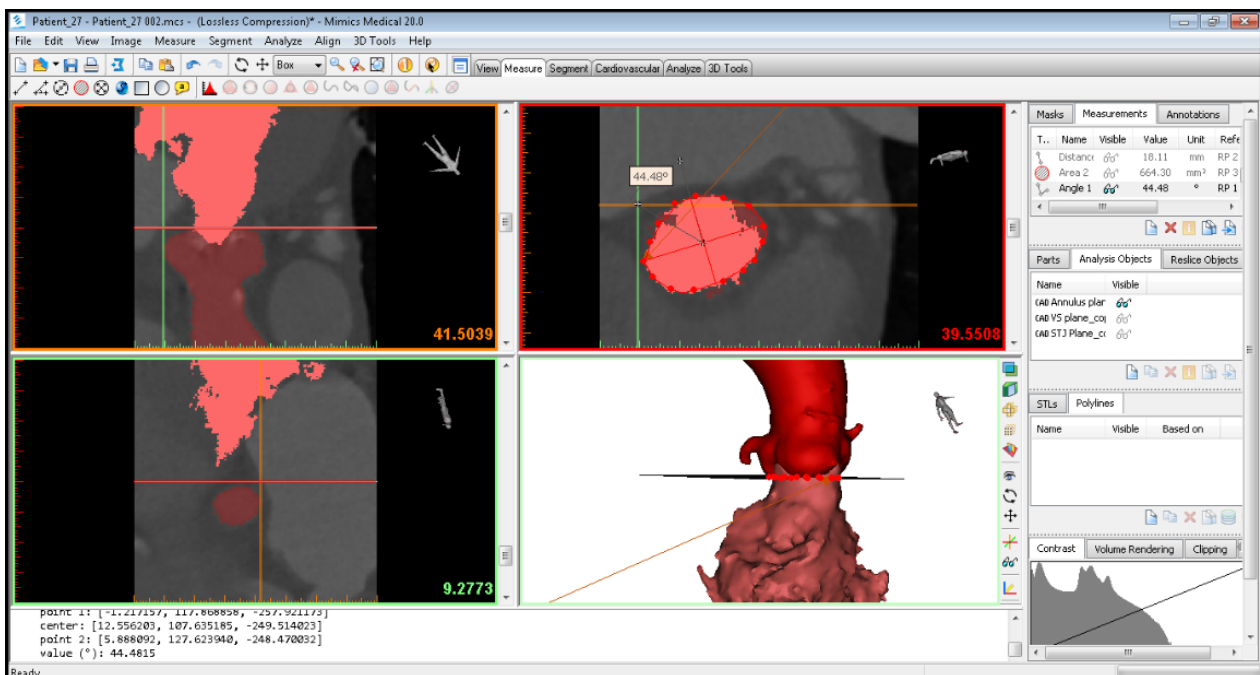


Figure 4.16

For the angle  $\alpha$ , index of the crushing of the annulus: from the 3D model move the pointer on the nadir of the non-coronary sinus, doing so on the axial plane this point is indicated by the origin of the orange-green axes; with *Measure - Angle*, take the first point in the origin of the orange-green axes, the second point in the intersection of the annulus axes and the third point on the minor semiaxis in the direction of crushing, proceeding towards the right coronary sinus (Figure 4.16). If the angle changes verso in performing this procedure, the value obtained is negative, so, it is necessary to consider its implementation (so as to obtain positive values).

Measure of  $R_0$ ,  $R_1$ ,  $R_2$ ,  $R_3$ :

Repeat the same operation for the sinus plane: select VS Plane, right-click and select *Create reslice plane (s)*. RP2 will appear in *Reslice Object*.

Also from the axial plane, with *Measure - Diameter*, it is possible to trace a circle inscribed in the aorta by selecting three points corresponding to the three coronary joints.

The diameter value appears on the screen.

With *Measure - Distance* trace the rays from the circumscribed circle to the three sinuses.

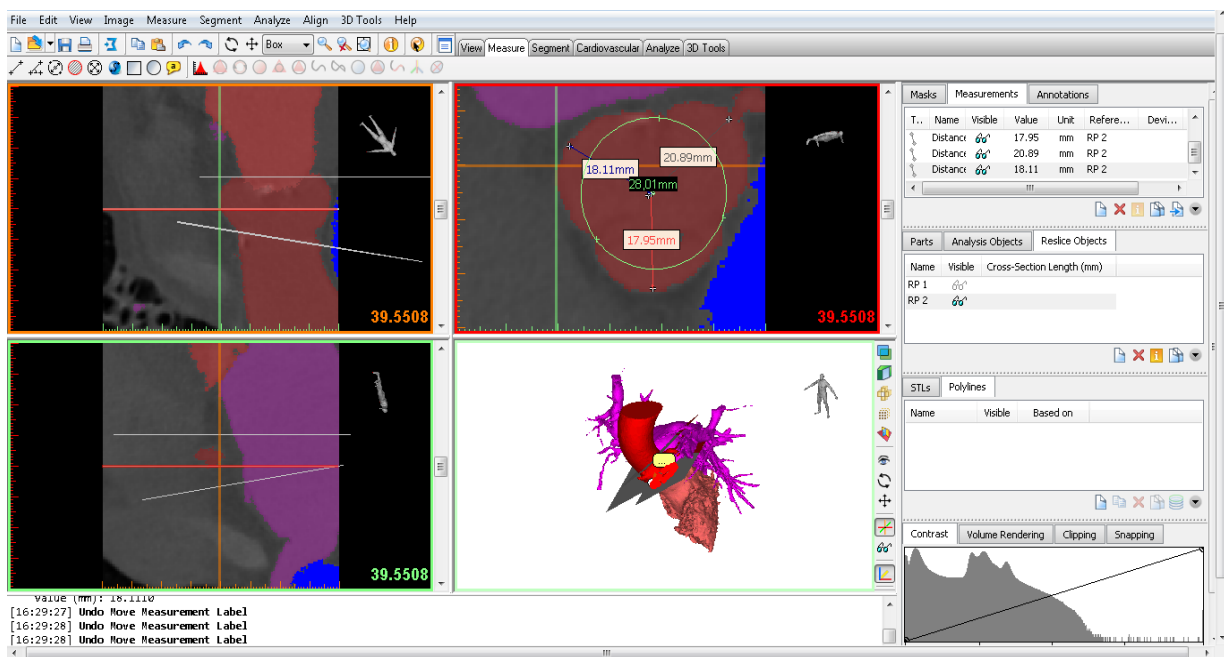


Figure 4.17

A<sub>1</sub>'s measure:

Repeat the operation for the synotubular junction plane: select Annulus Plane, right click and select *Create reslice plane (s)*. RP3 appears in *Reslice Object*. On the three views of the sagittal, coronal and axial planes, the section corresponding to the STJ appears. From the axial plane it is possible measure the perimeter of the junction with *Measure - Area*:

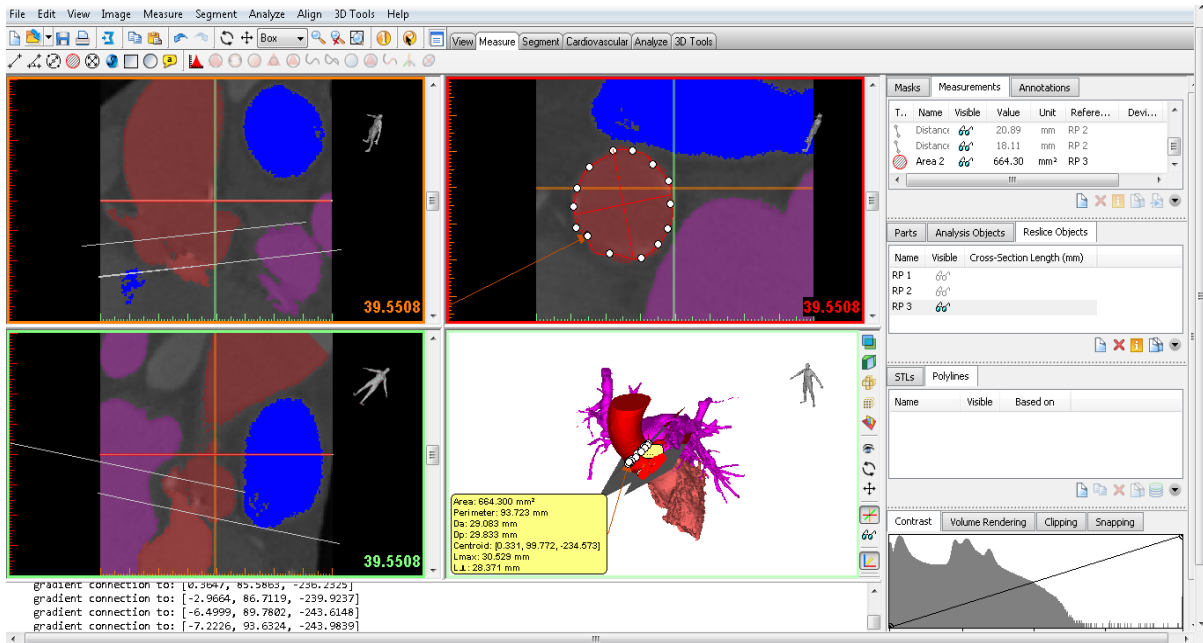


Figure 4.18

From the yellow box it is possible to measure the junction area.

## 5 Results

Here are presented the geometrical parameters obtained from CT scans by used the procedure in Mimics previously explained.

### 5.1 Database measured

The database measured contains all the geometrical parameters directly obtained from CT scans.

#### 5.1.1 Annulus plane

Patient number	Cycle phase	% phase	Annulus Perimeter (mm)	Annulus Area (mm <sup>2</sup> )	Annulus D <sub>max</sub> (mm)	Annulus D <sub>min</sub> (mm)	$\alpha$ (degrees)
1	Systole	40	75,89	417,04	25,52	21,24	237
2	Systole	36	93,28	625,24	30,23	26,65	197
3	Systole	44	95,07	607,81	31,11	26,35	197
4	Systole	35	78,47	422,1	26,39	21,29	226
5	Systole	33	78,53	430,10	25,68	24,44	67
6	Systole	38	85,76	532,87	28,85	23,68	244
7	Systole	29	78,05	434,19	26,11	22,69	213
8	Systole	45	82,46	502,67	27,525	24,554	209
9	Systole	41	90,01	564,45	30,86	23,87	1
10	Systole	41	78,49	426,30	28,47	20,34	163
11	Systole	40	85,98	448,53	26,48	20,58	231
12	Systole	44	74,29	391,77	25,03	20,41	206
13	Systole	43	73,14	358,85	24,06	20,10	58
14	Systole	40	72,33	384,26	24,76	20,37	221
15	Systole	39	89,96	553,93	30,22	24,96	34
16	Systole	35	71,36	355,91	23,89	20,22	180
17	Systole	47	83,45	519,64	26,92	25,88	173
18	Systole	26	80,87	456,16	27,90	22,08	11
19	Systole	30	79,81	465,66	25,83	25,49	149
20	Systole	38	77,60	434,58	26,81	21,24	39
21	Systole	38	70,67	361,83	23,95	20,55	45
22	Systole	38	80,69	447,77	25,40	23,53	127
23	Systole	33	96,76	647,29	31,99	26,07	54
24	Systole	42	81,76	466,38	28,39	24,36	43
25	Systole	39	87,62	547,28	30,93	24,21	74
26	Systole	47	83,10	509,33	27,05	26,35	38
27	Systole	33	75,17	398,92	26,63	19,58	33
28	Systole	30	86,56	517,56	30,20	23,84	215
29	Systole	30	79,57	453,58	26,87	22,65	190
30	Systole	30	83,13	498,22	28,95	22,91	57
31	Systole	30	87,95	560,60	30,56	27,67	39
32	Systole	30	86,48	513,16	31,56	22,93	214
33	Systole	30	98,19	716,68	31,66	28,64	51
34	Diastole	65	70,74	353,87	24,94	18,72	32
35	Diastole	65	90,31	568,05	30,39	24,67	206
36	Diastole	65	67,13	315,69	24,05	16,21	27
37	Diastole	65	82,55	487,33	28,79	22,91	53

38	Diastole	65	77,10	426,95	26,10	21,87	29
39	Diastole	65	82,91	519,57	28,34	23,08	44
40	Diastole	65	79,84	482,69	28,58	22,10	31
41	Diastole	65	71,87	365,69	25,53	18,97	49
42	Diastole	65	76,35	422,43	25,30	21,87	202
43	Diastole	65	87,75	583,03	29,39	26,56	202
44	Diastole	65	72,36	389,21	24,15	22,29	23
45	Diastole	65	69,32	365,39	23,22	20,96	55
46	NA	/	76,33	444,39	26,60	23,28	211
47	Diastole	65	73,17	409,94	24,78	22,12	54
48	Diastole	65	68,19	353,19	22,56	21,24	68
49	Diastole	65	73,00	395,39	24,87	22,68	59
50	Diastole	65	81,08	485,16	27,62	22,62	291
51	Diastole	65	77,50	445,54	24,54	23,67	87
52	Diastole	65	83,59	521,09	28,09	24,59	222
53	Diastole	65	68,74	353,06	24,73	20,37	210
54	Diastole	65	74,87	420,62	25,00	22,94	50
55	NA	/	86,20	487,35	30,41	22,19	219
56	NA	/	102,43	680,84	34,04	29,77	279
57	NA	/	83,23	511,74	27,42	25,60	62
58	NA	/	103,52	733,80	36,57	25,35	258
59	NA	/	90,61	608,24	31,20	26,51	161
60	NA	/	90,74	619,90	29,91	26,39	219
61	NA	/	82,70	512,95	27,79	24,50	110
62	NA	/	107,17	854,42	37,95	29,55	50
63	Diastole	68	72,78	394,23	25,66	20,12	34
64	NA	/	103,61	781,57	34,67	31,01	276
65	Systole	25	84,84	528,04	28,14	23,21	30
66	Diastole	75	78,86	448,30	26,48	21,71	21
67	Diastole	75	75,30	420,79	27,43	20,17	69
68	Systole	30	68,63	349,91	22,80	19,52	197
69	Systole	25	89,24	543,99	28,60	24,94	189
70	Systole	25	73,36	406,68	24,28	21,39	236
71	NA	/	65,51	312,67	22,49	19,57	24
72	NA	/	79,68	475,60	28,37	22,27	49
73	NA	/	92,84	618,75	30,80	27,93	54
74	Diastole	60	96,38	696,23	32,54	28,59	208
75	Diastole	60	82,17	475,06	27,34	24,42	138
76	Diastole	60	81,44	480,92	30,88	20,53	52
77	Diastole	60	82,56	475,99	27,78	24,70	28
78	Systole	35	88,89	569,45	31,05	22,33	54
79	NA	/	99,24	666,03	32,58	29,10	210
80	Systole	35	82,70	506,38	28,76	23,54	51
81	NA	/	69,98	355,62	24,23	18,56	88
82	NA	/	80,89	456,28	27,38	22,93	71
83	NA	/	84,57	495,20	28,59	24,47	150
84	NA	/	86,32	521,31	29,62	23,05	93
85	NA	/	77,43	436,03	27,58	21,72	40
86	NA	/	76,40	432,01	25,04	22,76	90
87	NA	/	77,44	442,79	27,45	20,53	70
88	NA	/	81,14	509,20	27,53	24,33	180

89	NA	/	93,08	631,09	30,68	28,20	54
90	NA	/	87,33	530,69	30,77	23,57	278

### 5.1.2 Valsalva sinus plane

Patient number	Cycle phase	% phase	Distance between VS plane (max protrusion) and annulus plane (parallel) (mm)	Diameter of the circle inscribed in the aorta at the VS plane (radius r0) (mm <sup>2</sup> )	rNC radius of the circle circumscribed to the non coronary sinus (mm)	rRC radius of the circle circumscribed to the right sinus (mm)	rLC radius of the circle circumscribed to the left sinus (mm)
1	Systole	40	10,95	26,68	17,46	18,43	16,06
2	Systole	36	8,26	27,93	17,06	16,22	14,54
3	Systole	44	9,18	27,82	20,00	19,32	18,58
4	Systole	35	6,01	21,15	12,19	17,92	12,19
5	Systole	33	9,42	26,52	18,88	19,62	16,04
6	Systole	38	8,13	27,00	20,55	19,83	17,15
7	Systole	29	9,03	26,36	18,72	19,02	17,41
8	Systole	45	7,68	29,67	18,74	19,32	19,26
9	Systole	41	9,71	26,24	20,21	17,51	17,85
10	Systole	41	9,56	26,47	19,79	15,33	16,77
11	Systole	40	7,43	23,51	16,08	20,56	15,09
12	Systole	44	7,89	22,17	18,72	12,8	18,48
13	Systole	43	7,27	23,02	15,37	13,64	13,62
14	Systole	40	5,44	20,54	13,68	15,02	13,13
15	Systole	39	9,57	23	23,32	15,31	16,67
16	Systole	35	7,35	19,65	15,64	13,52	15,25
17	Systole	47	8,79	29,67	20,2	19,3	18,30
18	Systole	26	8,89	23,72	19,07	17,24	17,14
19	Systole	30	8,91	20,05	14,27	15,74	14,13
20	Systole	38	8,17	22,56	15,93	16,82	18,06
21	Systole	38	9,93	23,91	15,34	15,86	15,90
22	Systole	38	10,08	25,54	21,08	16,62	14,75
23	Systole	33	9,17	25,63	21,61	18,08	19,61
24	Systole	42	9,88	27,42	17,58	18,14	18,33
25	Systole	39	8,71	26,57	19,7	17,15	15,43
26	Systole	47	12,8	31,1	20,8	20,21	21,11
27	Systole	33	7,25	23,47	16,26	16,61	14,27
28	Systole	30	10,15	29,56	19,52	19,38	17,87
29	Systole	30	7,25	28,71	18,35	17,5	20,70
30	Systole	30	9,97	28,22	16,21	19,88	17,05
31	Systole	30	10,05	26,63	18,64	16,37	17,25
32	Systole	30	10,65	30,23	19,83	18,04	18,09
33	Systole	30	10,03	30,9	27,44	19,43	19,33
34	Diastole	65	6,42	22,41	14,51	16,87	15,24
35	Diastole	65	8,55	27,28	22,49	21,7	19,31
36	Diastole	65	9,07	18,93	15,89	13,25	13,94
37	Diastole	65	11,42	26,38	18,29	20,85	19,29
38	Diastole	65	7,5	23,85	15,86	15,68	15,23
39	Diastole	65	11,64	26,47	19,45	17,64	20,24

40	Diastole	65	7,72	25,8	17,87	17,66	15,78
41	Diastole	65	9,1	22,29	16,15	16,73	14,04
42	Diastole	65	7,69	22,5	16,48	18,42	14,49
43	Diastole	65	7,09	29,47	24,31	18,79	19,17
44	Diastole	65	8,34	24,02	16,01	14,71	15,11
45	Diastole	65	8,39	22,49	15,35	14,24	13,31
46	NA	/	8,51	28,93	19,1	18,53	17,63
47	Diastole	65	8,27	21,65	15,5	16,64	13,98
48	Diastole	65	7,12	21,65	14,02	15,95	12,71
49	Diastole	65	7,76	22,6	16,44	13,83	15,60
50	Diastole	65	8,92	24,12	20,72	17,1	16,85
51	Diastole	65	9,15	25,17	18,08	15,79	17,11
52	Diastole	65	11,96	27	18,44	19,98	17,34
53	Diastole	65	6,1	23,36	16,58	15,31	14,91
54	Diastole	65	9,76	26,11	14,62	20,31	13,88
55	NA	/	9,68	29,03	18,44	19,9	16,65
56	NA	/	9,3	29,62	18,45	20,65	19,31
57	NA	/	13,52	26,68	22,85	17,36	17,75
58	NA	/	10,45	30,66	18,76	21,97	19,50
59	NA	/	8,33	26,95	20,03	16,91	17,70
60	NA	/	7,31	25,97	15,97	21,95	18,75
61	NA	/	7,48	24,75	16,61	17,79	14,50
62	NA	/	9,21	26,87	16,51	19,44	17,77
63	Diastole	68	8,27	24,11	15,81	18,23	18,17
64	NA	/	6,83	25,07	14,29	14,5	15,41
65	Systole	25	8,88	25,73	17,08	18,46	16,22
66	Diastole	75	8,34	22,05	18,18	18,42	19,11
67	Diastole	75	8,18	21,84	14,94	15,28	14,64
68	Systole	30	7	18,31	14,81	13,7	14,06
69	Systole	25	8,2	27,21	20,26	18,15	18,29
70	Systole	25	6,7	26,28	16,73	15,11	14,12
71	NA	/	6,62	20,01	15,91	14,04	12,79
72	NA	/	7,64	23,43	17,19	17,63	15,25
73	NA	/	10,88	28,67	19,41	19,41	20,30
74	Diastole	60	11,65	28,39	23,69	19,71	18,75
75	Diastole	60	10,88	27,65	21,26	17,12	18,07
76	Diastole	60	10,77	24,76	21,08	19,04	15,28
77	Diastole	60	6,94	24,47	17,28	16,57	15,91
78	Systole	35	8,5	25,21	18,51	17,76	17,24
79	NA	/	7,34	24,62	19,76	20,39	15,82
80	Systole	35	7,3	26,44	18,4	21,54	17,46
81	NA	/	6,02	22,02	16,7	16,36	17,25
82	NA	/	9,51	26,4	18,97	17,71	17,06
83	NA	/	8,02	24,01	16,74	19,47	17,41
84	NA	/	6,94	23,57	18,09	17,88	15,84
85	NA	/	6,85	21,4	16,36	16,28	14,79
86	NA	/	8,98	25,94	16,07	18,29	18,51
87	NA	/	6,25	22,46	15,95	12,44	15,36
88	NA	/	7,42	24,71	16,76	18,87	15,74
89	NA	/	8,26	28,15	18,66	20,25	19,59
90	NA	/	6,32	24,73	22,72	19,33	18,52

### 5.1.3 STJ

Patient number	Cycle phase	% phase	Distance of the STJ to the annulus plane at the non coronary sinus (mm)	Distance of the STJ to the annulus plane at the right sinus (mm)	Distance of the STJ to the annulus plane at the left sinus (mm)	Area of the STJ circle (radius rSTJ) (mm <sup>2</sup> )
1	Systole	40	21,80	18,90	22,40	581,75
2	Systole	36	18,67	19,96	17,44	606,38
3	Systole	44	20,82	21,89	23,67	646,63
4	Systole	35	18,1	18,56	19,76	646,72
5	Systole	33	14,03	15,79	19,94	594,19
6	Systole	38	25,84	20,37	25,52	723,97
7	Systole	29	21,98	20,53	18,82	588,52
8	Systole	45	23,12	19,23	21,98	707,68
9	Systole	41	22,13	20,15	12,51	627,18
10	Systole	41	18,46	18,72	16,81	617,52
11	Systole	40	16,27	23,52	11,08	697,60
12	Systole	44	16,12	24,44	17,81	671,80
13	Systole	43	18,90	19,24	23,76	564,29
14	Systole	40	12,52	27,32	15,00	595,07
15	Systole	39	22,24	14,56	18,52	592,38
16	Systole	35	15,12	17,42	15,44	454,12
17	Systole	47	18,76	21,16	25,18	688,44
18	Systole	26	20,87	17,90	17,81	564,41
19	Systole	30	12,98	13,93	17,46	497,49
20	Systole	38	12,22	14,27	14,45	674,20
21	Systole	38	22,65	19,07	24,98	556,92
22	Systole	38	19,11	22,51	16,57	498,31
23	Systole	33	19,74	22,50	23,98	838,19
24	Systole	42	18,66	20,86	18,12	726,36
25	Systole	39	21,94	18,28	23,33	638,14
26	Systole	47	24,85	23,15	22,58	738,85
27	Systole	33	19,85	21,00	20,03	522,76
28	Systole	30	21,13	21,39	23,84	525,72
29	Systole	30	16,28	20,12	17,82	646,26
30	Systole	30	16,97	23,46	19,71	668,32
31	Systole	30	20,89	22,20	22,14	663,92
32	Systole	30	25,98	19,78	22,91	743,72
33	Systole	30	32,92	26,29	23,27	855,91
34	Diastole	65	16,05	15,41	14,14	595,77
35	Diastole	65	21,40	22,43	17,04	976,51
36	Diastole	65	17,53	17,59	20,98	464,14
37	Diastole	65	20,68	21,74	20,75	675,46
38	Diastole	65	17,46	18,26	16,44	492,86
39	Diastole	65	24,16	22,42	19,56	713,82
40	Diastole	65	16,01	18,17	21,70	698,28
41	Diastole	65	23,45	16,01	14,07	491,96
42	Diastole	65	18,73	17,95	22,57	589,73
43	Diastole	65	18,26	22,66	21,96	956,76

44	Diastole	65	16,50	20,03	14,89	482,72
45	Diastole	65	16,41	17,22	17,27	476,60
46	NA	/	22,82	18,02	17,58	546,71
47	Diastole	65	17,09	20,47	22,26	567,73
48	Diastole	65	13,67	16,34	18,95	447,50
49	Diastole	65	16,57	18,11	21,31	552,97
50	Diastole	65	18,98	16,49	16,87	582,20
51	Diastole	65	21,70	19,26	17,18	672,61
52	Diastole	65	23,75	24,04	26,48	643,35
53	Diastole	65	14,76	19,87	16,50	583,22
54	Diastole	65	16,94	24,07	18,84	627,79
55	NA	/	24,24	20,53	23,56	676,74
56	NA	/	23,49	22,36	15,09	941,72
57	NA	/	26,71	21,33	19,42	662,31
58	NA	/	26,69	23,77	23,94	990,32
59	NA	/	25,95	19,63	18,12	679,01
60	NA	/	18,50	13,22	18,93	734,75
61	NA	/	19,17	20,73	18,53	706,36
62	NA	/	23,21	21,78	25,26	637,72
63	Diastole	68	18,34	21,02	22,51	564,91
64	NA	/	21,29	16,25	15,24	992,54
65	Systole	25	19,42	19,61	15,01	682,16
66	Diastole	75	19,33	18,65	17,47	816,88
67	Diastole	75	19,29	15,52	17,31	483,09
68	Systole	30	14,95	16,99	17,47	478,38
69	Systole	25	23,32	18,92	18,72	554,39
70	Systole	25	16,04	17,26	12,02	647,13
71	NA	/	16,35	17,72	19,87	474,16
72	NA	/	18,80	21,40	21,13	638,23
73	NA	/	25,55	21,52	21,03	753,12
74	Diastole	60	27,61	22,07	20,19	805,41
75	Diastole	60	23,49	25,75	30,95	815,32
76	Diastole	60	20,92	20,28	23,55	648,98
77	Diastole	60	19,83	17,16	13,09	612,46
78	Systole	35	17,63	20,63	18,75	715,49
79	NA	/	19,05	16,08	17,12	773,99
80	Systole	35	24,38	23,37	22,27	633,58
81	NA	/	17,45	16,85	15,01	576,27
82	NA	/	19,73	21,66	20,69	595,43
83	NA	/	20,43	20,03	20,50	501,98
84	NA	/	18,20	20,23	14,21	523,23
85	NA	/	19,41	20,89	22,15	644,46
86	NA	/	22,79	18,11	26,36	639,40
87	NA	/	11,71	13,76	13,48	534,41
88	NA	/	16,62	21,40	16,85	699,04
89	NA	/	20,75	14,51	17,24	761,06
90	NA	/	20,77	16,99	17,37	600,15

## 5.2 Database calculated

The database calculated contains the derived parameters.

### 5.2.1 Annulus plane

Patient number	Cycle phase	% phase	Dequivalent (Annulus perimeter/ $\pi$ )	D'equivalent (4*Annulus Area/ $\pi$ ) <sup>0.5</sup>	e= $\frac{2*D_{min}}{D_{max}-1}$	$\alpha$ angle between $D_{max}$ and NC sinus (degrees)
1	Systole	40	24,2	23,0	0,66	237
2	Systole	36	29,7	28,2	0,76	197
3	Systole	44	30,3	27,8	0,69	197
4	Systole	35	25,0	23,2	0,61	226
5	Systole	33	25,0	23,4	0,90	67
6	Systole	38	27,3	26,0	0,64	244
7	Systole	29	24,8	23,5	0,74	213
8	Systole	45	26,2	25,3	0,78	209
9	Systole	41	28,7	26,8	0,55	1
10	Systole	41	25,0	23,3	0,43	163
11	Systole	40	27,4	23,9	0,55	231
12	Systole	44	23,6	22,3	0,63	206
13	Systole	43	23,3	21,4	0,67	58
14	Systole	40	23,0	22,1	0,65	221
15	Systole	39	28,6	26,6	0,65	34
16	Systole	35	22,7	21,3	0,69	180
17	Systole	47	26,6	25,7	0,92	173
18	Systole	26	25,7	24,1	0,58	11
19	Systole	30	25,4	24,3	0,97	149
20	Systole	38	24,7	23,5	0,58	39
21	Systole	38	22,5	21,5	0,72	45
22	Systole	38	25,7	23,9	0,85	127
23	Systole	33	30,8	28,7	0,63	54
24	Systole	42	26,0	24,4	0,72	43
25	Systole	39	27,9	26,4	0,57	74
26	Systole	47	26,5	25,5	0,95	38
27	Systole	33	23,9	22,5	0,47	33
28	Systole	30	27,6	25,7	0,58	215
29	Systole	30	25,3	24,0	0,69	190
30	Systole	30	26,5	25,2	0,58	57
31	Systole	30	28,0	26,7	0,81	39
32	Systole	30	27,5	25,6	0,45	214
33	Systole	30	31,3	30,2	0,81	51
34	Diastole	65	22,5	21,2	0,50	32
35	Diastole	65	28,7	26,9	0,62	206
36	Diastole	65	21,4	20,0	0,35	27
37	Diastole	65	26,3	24,9	0,59	53
38	Diastole	65	24,5	23,3	0,68	29
39	Diastole	65	26,4	25,7	0,63	44
40	Diastole	65	25,4	24,8	0,55	31
41	Diastole	65	22,9	21,6	0,49	49

42	Diastole	65	24,3	23,2	0,73	202
43	Diastole	65	27,9	27,2	0,81	202
44	Diastole	65	23,0	22,3	0,85	23
45	Diastole	65	22,1	21,6	0,81	55
46	NA	/	24,3	23,8	0,75	211
47	Diastole	65	23,3	22,8	0,79	54
48	Diastole	65	21,7	21,2	0,88	68
49	Diastole	65	23,2	22,4	0,82	59
50	Diastole	65	25,8	24,9	0,64	291
51	Diastole	65	24,7	23,8	0,93	87
52	Diastole	65	26,6	25,8	0,75	222
53	Diastole	65	21,9	21,2	0,65	210
54	Diastole	65	23,8	23,1	0,84	50
55	NA	/	27,4	24,9	0,46	219
56	NA	/	32,6	29,4	0,75	279
57	NA	/	26,5	25,5	0,87	62
58	NA	/	33,0	30,6	0,39	258
59	NA	/	28,8	27,8	0,70	161
60	NA	/	28,9	28,1	0,76	219
61	NA	/	26,3	25,6	0,76	110
62	NA	/	34,1	33,0	0,56	50
63	Diastole	68	23,2	22,4	0,57	34
64	NA	/	33,0	31,5	0,79	276
65	Systole	25	27,0	25,9	0,65	30
66	Diastole	75	25,1	23,9	0,64	21
67	Diastole	75	24,0	23,1	0,47	69
68	Systole	30	21,8	21,1	0,71	197
69	Systole	25	28,4	26,3	0,74	189
70	Systole	25	23,4	22,8	0,76	236
71	NA	/	20,9	20,0	0,74	24
72	NA	/	25,4	24,6	0,57	49
73	NA	/	29,6	28,1	0,81	54
74	Diastole	60	30,7	29,8	0,76	208
75	Diastole	60	26,2	24,6	0,79	138
76	Diastole	60	25,9	24,7	0,33	52
77	Diastole	60	26,3	24,6	0,78	28
78	Systole	35	28,3	26,9	0,44	54
79	NA	/	31,6	29,1	0,79	210
80	Systole	35	26,3	25,4	0,64	51
81	NA	/	22,3	21,3	0,53	88
82	NA	/	25,7	24,1	0,68	71
83	NA	/	26,9	25,1	0,71	150
84	NA	/	27,5	25,8	0,56	93
85	NA	/	24,6	23,6	0,58	40
86	NA	/	24,3	23,5	0,82	90
87	NA	/	24,7	23,7	0,50	70
88	NA	/	25,8	25,5	0,77	180
89	NA	/	29,6	28,3	0,84	54
90	NA	/	27,8	26,0	0,53	278

## 5.2.2 Valsalva sinus plane

Patient number	Cycle phase	% phase	HVS VS plane distance ratio	HRVS 2*r0/Deq	HRNC 2*rNC/Deq	HRRC 2*rRC/Deq	HRLC 2*rLC/Deq
1	Systole	40	0,45	1,10	1,45	1,53	1,33
2	Systole	36	0,28	0,94	1,15	1,09	0,98
3	Systole	44	0,30	0,92	1,32	1,28	1,23
4	Systole	35	0,24	0,85	0,98	1,43	0,98
5	Systole	33	0,38	1,06	1,51	1,57	1,28
6	Systole	38	0,30	0,99	1,51	1,45	1,26
7	Systole	29	0,36	1,06	1,51	1,53	1,40
8	Systole	45	0,29	1,13	1,43	1,47	1,47
9	Systole	41	0,34	0,92	1,41	1,22	1,25
10	Systole	41	0,38	1,06	1,58	1,23	1,34
11	Systole	40	0,27	0,86	1,18	1,50	1,10
12	Systole	44	0,33	0,94	1,58	1,08	1,56
13	Systole	43	0,31	0,99	1,32	1,17	1,17
14	Systole	40	0,24	0,89	1,19	1,30	1,14
15	Systole	39	0,33	0,80	1,63	1,07	1,16
16	Systole	35	0,32	0,87	1,38	1,19	1,34
17	Systole	47	0,33	1,12	1,52	1,45	1,38
18	Systole	26	0,35	0,92	1,48	1,34	1,33
19	Systole	30	0,35	0,79	1,12	1,24	1,11
20	Systole	38	0,33	0,91	1,29	1,36	1,46
21	Systole	38	0,44	1,06	1,36	1,41	1,41
22	Systole	38	0,39	0,99	1,64	1,29	1,15
23	Systole	33	0,30	0,83	1,40	1,17	1,27
24	Systole	42	0,38	1,05	1,35	1,39	1,41
25	Systole	39	0,31	0,95	1,41	1,23	1,11
26	Systole	47	0,48	1,18	1,57	1,53	1,60
27	Systole	33	0,30	0,98	1,36	1,39	1,19
28	Systole	30	0,37	1,07	1,42	1,41	1,30
29	Systole	30	0,29	1,13	1,45	1,38	1,63
30	Systole	30	0,38	1,07	1,23	1,50	1,29
31	Systole	30	0,36	0,95	1,33	1,17	1,23
32	Systole	30	0,39	1,10	1,44	1,31	1,31
33	Systole	30	0,32	0,99	1,76	1,24	1,24
34	Diastole	65	0,29	1,00	1,29	1,50	1,35
35	Diastole	65	0,30	0,95	1,56	1,51	1,34
36	Diastole	65	0,42	0,89	1,49	1,24	1,30
37	Diastole	65	0,43	1,00	1,39	1,59	1,47
38	Diastole	65	0,31	0,97	1,29	1,28	1,24
39	Diastole	65	0,44	1,00	1,47	1,34	1,53
40	Diastole	65	0,30	1,02	1,41	1,39	1,24
41	Diastole	65	0,40	0,97	1,41	1,46	1,23

42	Diastole	65	0,32	0,93	1,36	1,52	1,19
43	Diastole	65	0,25	1,06	1,74	1,35	1,37
44	Diastole	65	0,36	1,04	1,39	1,28	1,31
45	Diastole	65	0,38	1,02	1,39	1,29	1,21
46	NA	/	0,35	1,19	1,57	1,53	1,45
47	Diastole	65	0,36	0,93	1,33	1,43	1,20
48	Diastole	65	0,33	1,00	1,29	1,47	1,17
49	Diastole	65	0,33	0,97	1,41	1,19	1,34
50	Diastole	65	0,35	0,93	1,61	1,33	1,31
51	Diastole	65	0,37	1,02	1,47	1,28	1,39
52	Diastole	65	0,45	1,01	1,39	1,50	1,30
53	Diastole	65	0,28	1,07	1,52	1,40	1,36
54	Diastole	65	0,41	1,10	1,23	1,70	1,16
55	NA	/	0,35	1,06	1,34	1,45	1,21
56	NA	/	0,29	0,91	1,13	1,27	1,18
57	NA	/	0,51	1,01	1,73	1,31	1,34
58	NA	/	0,32	0,93	1,14	1,33	1,18
59	NA	/	0,29	0,93	1,39	1,17	1,23
60	NA	/	0,25	0,90	1,11	1,52	1,30
61	NA	/	0,28	0,94	1,26	1,35	1,10
62	NA	/	0,27	0,79	0,97	1,14	1,04
63	Diastole	68	0,36	1,04	1,36	1,57	1,57
64	NA	/	0,21	0,76	0,87	0,88	0,93
65	Systole	25	0,33	0,95	1,26	1,37	1,20
66	Diastole	75	0,33	0,88	1,45	1,47	1,52
67	Diastole	75	0,34	0,91	1,25	1,28	1,22
68	Systole	30	0,32	0,84	1,36	1,25	1,29
69	Systole	25	0,29	0,96	1,43	1,28	1,29
70	Systole	25	0,29	1,13	1,43	1,29	1,21
71	NA	/	0,32	0,96	1,53	1,35	1,23
72	NA	/	0,30	0,92	1,36	1,39	1,20
73	NA	/	0,37	0,97	1,31	1,31	1,37
74	Diastole	60	0,38	0,93	1,54	1,28	1,22
75	Diastole	60	0,42	1,06	1,63	1,31	1,38
76	Diastole	60	0,42	0,96	1,63	1,47	1,18
77	Diastole	60	0,26	0,93	1,32	1,26	1,21
78	Systole	35	0,30	0,89	1,31	1,26	1,22
79	NA	/	0,23	0,78	1,25	1,29	1,00
80	Systole	35	0,28	1,00	1,40	1,64	1,33
81	NA	/	0,27	0,99	1,50	1,47	1,55
82	NA	/	0,37	1,03	1,47	1,38	1,33
83	NA	/	0,30	0,89	1,24	1,45	1,29
84	NA	/	0,25	0,86	1,32	1,30	1,15
85	NA	/	0,28	0,87	1,33	1,32	1,20
86	NA	/	0,37	1,07	1,32	1,50	1,52

87	NA	/	0,25	0,91	1,29	1,01	1,25
88	NA	/	0,29	0,96	1,30	1,46	1,22
89	NA	/	0,28	0,95	1,26	1,37	1,32
90	NA	/	0,23	0,89	1,63	1,39	1,33

### 5.2.3 STJ

Patient number	Cycle phase	% phase	HSTJ hSTJ(mean)/ Deq	STJ 2*rSTJ/ Deq
1	Systole	40	0,87	1,13
2	Systole	36	0,63	0,94
3	Systole	44	0,73	0,95
4	Systole	35	0,75	1,15
5	Systole	33	0,66	1,10
6	Systole	38	0,88	1,11
7	Systole	29	0,82	1,10
8	Systole	45	0,82	1,14
9	Systole	41	0,57	0,99
10	Systole	41	0,72	1,12
11	Systole	40	0,62	1,09
12	Systole	44	0,82	1,24
13	Systole	43	0,89	1,15
14	Systole	40	0,79	1,20
15	Systole	39	0,64	0,96
16	Systole	35	0,70	1,06
17	Systole	47	0,82	1,11
18	Systole	26	0,73	1,04
19	Systole	30	0,58	0,99
20	Systole	38	0,55	1,19
21	Systole	38	0,99	1,18
22	Systole	38	0,76	0,98
23	Systole	33	0,72	1,06
24	Systole	42	0,74	1,17
25	Systole	39	0,76	1,02
26	Systole	47	0,89	1,16
27	Systole	33	0,85	1,08
28	Systole	30	0,80	0,94
29	Systole	30	0,71	1,13
30	Systole	30	0,76	1,10
31	Systole	30	0,78	1,04
32	Systole	30	0,83	1,12
33	Systole	30	0,88	1,06
34	Diastole	65	0,68	1,22
35	Diastole	65	0,71	1,23
36	Diastole	65	0,88	1,14
37	Diastole	65	0,80	1,12
38	Diastole	65	0,71	1,02
39	Diastole	65	0,84	1,14
40	Diastole	65	0,73	1,17
41	Diastole	65	0,78	1,09

42	Diastole	65	0,75	1,13
43	Diastole	65	0,75	1,25
44	Diastole	65	0,74	1,08
45	Diastole	65	0,77	1,12
46	NA	/	0,80	1,09
47	Diastole	65	0,86	1,15
48	Diastole	65	0,75	1,10
49	Diastole	65	0,80	1,14
50	Diastole	65	0,68	1,06
51	Diastole	65	0,79	1,19
52	Diastole	65	0,93	1,08
53	Diastole	65	0,78	1,25
54	Diastole	65	0,84	1,19
55	NA	/	0,83	1,07
56	NA	/	0,62	1,06
57	NA	/	0,85	1,10
58	NA	/	0,75	1,08
59	NA	/	0,74	1,02
60	NA	/	0,58	1,06
61	NA	/	0,74	1,14
62	NA	/	0,69	0,84
63	Diastole	68	0,89	1,16
64	NA	/	0,53	1,08
65	Systole	25	0,67	1,09
66	Diastole	75	0,74	1,28
67	Diastole	75	0,72	1,03
68	Systole	30	0,75	1,13
69	Systole	25	0,72	0,94
70	Systole	25	0,65	1,23
71	NA	/	0,86	1,18
72	NA	/	0,81	1,12
73	NA	/	0,77	1,05
74	Diastole	60	0,76	1,04
75	Diastole	60	1,02	1,23
76	Diastole	60	0,83	1,11
77	Diastole	60	0,64	1,06
78	Systole	35	0,67	1,07
79	NA	/	0,55	0,99
80	Systole	35	0,89	1,08
81	NA	/	0,74	1,22
82	NA	/	0,80	1,07
83	NA	/	0,75	0,94
84	NA	/	0,64	0,94
85	NA	/	0,84	1,16
86	NA	/	0,92	1,17
87	NA	/	0,53	1,06
88	NA	/	0,71	1,16
89	NA	/	0,59	1,05
90	NA	/	0,66	0,99

### 5.3 Mean, standard deviation, maximum and minimum

Here are shown two tables with mean, standard deviation (SD) minimum and maximum for each parameters of relevance.

- Database measured:

		<i>Mean</i>	<i>Sd</i>	<i>Min</i>	<i>Max</i>
	<b>% phase</b>	48	16	25	75
<i>Annulus plane</i>	<b>Annulus perimeter (mm)</b>	82,07	8,96	65,51	107,17
	<b>Annulus area (mm<sup>2</sup>)</b>	489	106	313	854
	<b>Annulus D<sub>max</sub></b>	27,88	3,06	22,49	37,95
	<b>Annulus D<sub>min</sub></b>	23,32	2,83	16,21	31,01
	<b><math>\alpha</math></b>	120	84	1	291
<i>Valsalva sinuses plane</i>	<b>distance between VS plane (max protrusion) and annulus plane (parallel) (mm)</b>	8,61	1,60	5,44	13,52
	<b>Diameter of the circle inscribed in the aorta at the VS plane (radius r0) (mm<sup>2</sup>)</b>	25,25	2,90	18,31	31,10
	<b>rNC radius of the circle circumscribed to the non coronary sinus (mm)</b>	18,04	2,63	12,19	27,44
	<b>rRC radius of the circle circumscribed to the right sinus (mm)</b>	17,58	2,22	12,44	21,97
	<b>rLC radius of the circle circumscribed to the left sinus (mm)</b>	16,64	2,06	12,19	21,11
<i>STJ plane</i>	<b>Distance of the STJ to the annulus plane at the non coronary sinus (mm)</b>	19,82	3,82	11,71	32,92
	<b>Distance of the STJ to the annulus plane at the right sinus (mm)</b>	19,70	2,92	13,22	27,32
	<b>Distance of the STJ to the annulus plane at the left sinus (mm)</b>	19,32	3,75	11,08	30,95
	<b>Area of the STJ circle (radius rSTJ) (mm<sup>2</sup>)</b>	644	122	448	993

- Database derived:

		<i>Mean</i>	<i>Sd</i>	<i>Min</i>	<i>Max</i>
	% phase	48	16	25	75
<i>Annulus plane</i>	Dequivalent (Annulus perimeter/ $\pi$ )	26,12	2,85	20,85	34,11
	Dequivalent (Annulus perimeter/ $\pi$ )	24,83	2,61	19,95	32,98
	$e=2*D_{min}/D_{max}-1$	0,68	0,14	0,33	0,97
	$\alpha$ (angle between $D_{max}$ and NC sinus) (degrees)	120	84	1	291
<i>Valsalva sinuses plane</i>	HVS VS plane distance ratio	0,33	0,06	0,21	0,51
	HRVS $2*r_0/Deq$	0,97	0,09	0,76	1,19
	HRNC $2*r_{NC}/Deq$	1,39	0,16	0,87	0,88
	HRRC $2*r_{RC}/Deq$	1,35	0,14	0,88	1,70
	HRLC $2*r_{LC}/Deq$	1,28	0,14	0,93	1,63
<i>STJ plane</i>	HSTJ hSTJ(mean)/ Deq	0,75	0,10	0,53	1,02
	STJ $2*r_{STJ}/Deq$	1,10	0,08	0,84	1,28

## 6 Discussion

In this chapter will be discussed the statistical analysis carried out on the data calculated from the visualization of CT scans and tabulated in chapter 5.

In order to test the validity of the procedure, the engineers Bussone and Bondji have developed their own database (respectively of 33 and 58 subjects), whose data can be used, together with those obtained by me, to make a comparison and verify the repeatability of the data, ie the procedure is not operator depended.

For simplicity, the data obtained will refer to an *operator*, which in my case will be the operator A, for the engineer Bussone will be of the operator B and finally those of the engineer Bondji will refer to the operator C; for these measures was performed also the analysis of variance (ANOVA)

Next, normality and outliers tests and also regressions were performed on data from operator A.

### 6.1 Data repeatability

A comparison between the two A / B and A / C data groups is necessary to understand what is inherent in terms of statistical differences or statistical equalities.

For this reason, a *2-Sample t test* for the mean has been performed:

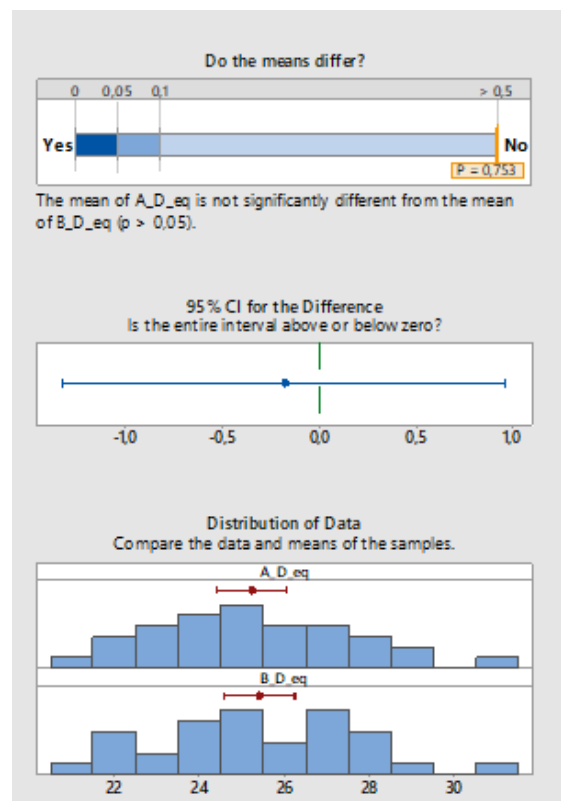
#### 6.1.1 A/B

- D equivalent (Annulus perimeter/ $\pi$ )

Test: there is not enough evidence to conclude that the means differ at the 0.05 level of significance.

CI: quantifies the uncertainty associated with estimating the difference in means from sample data. We can be 95% confident that the true difference is between -1.3290 and 0.96567.

Distribution of data: compare the location and the means of samples.

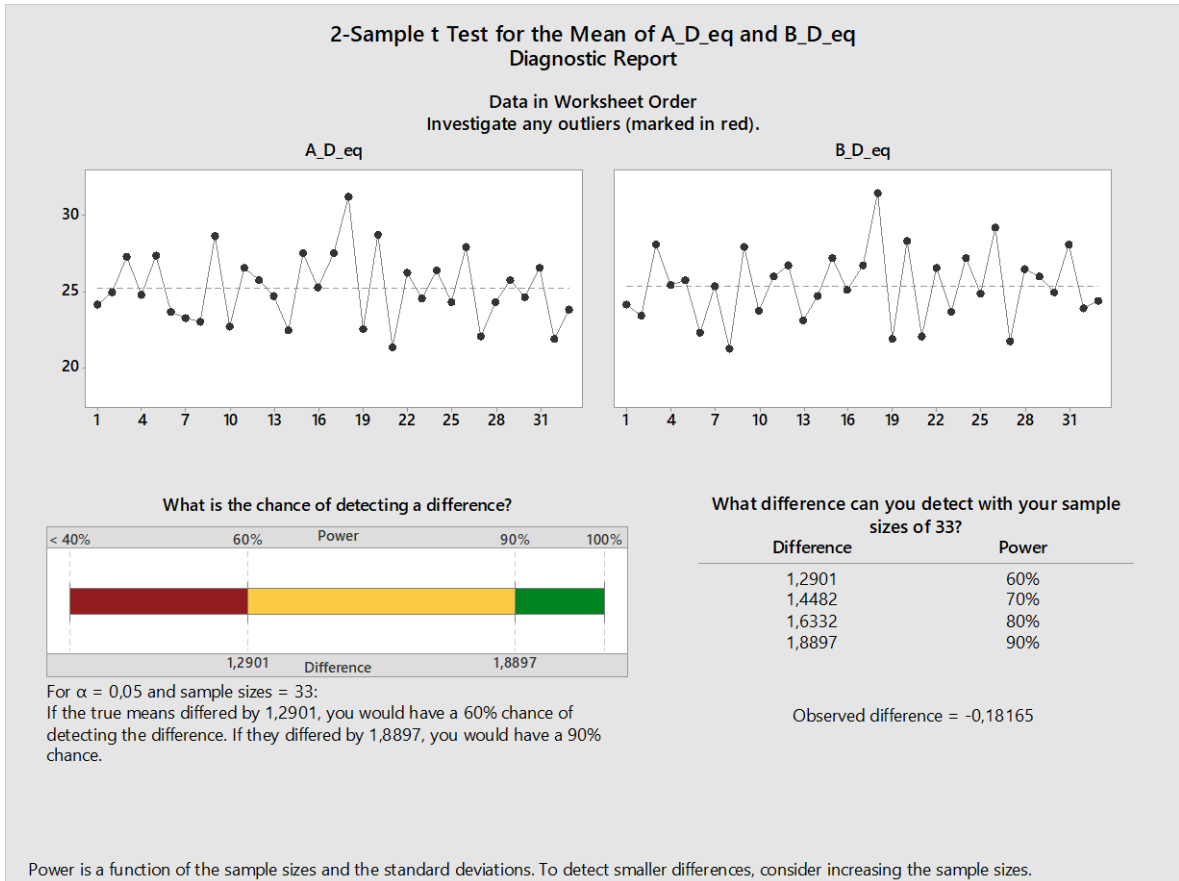


Individual Samples		
Statistics	A_D_eq	B_D_eq
Sample size	33	33
Mean	25,223	25,404
95% CI	(24,41; 26,04)	(24,564; 26,244)
Standard deviation	2,2944	2,3693

Difference Between Samples	
Statistics	*Difference
Difference	-0,18165
95% CI	(-1,3290; 0,96567)

\*Difference = A\_D\_eq - B\_D\_eq



Report: there are no unusual data points. Unusual data can have strong influence on the results. Because both sample sizes are at least 15, **normality is not an issue**. The test is accurate with non-normal data when the sample sizes are large enough.

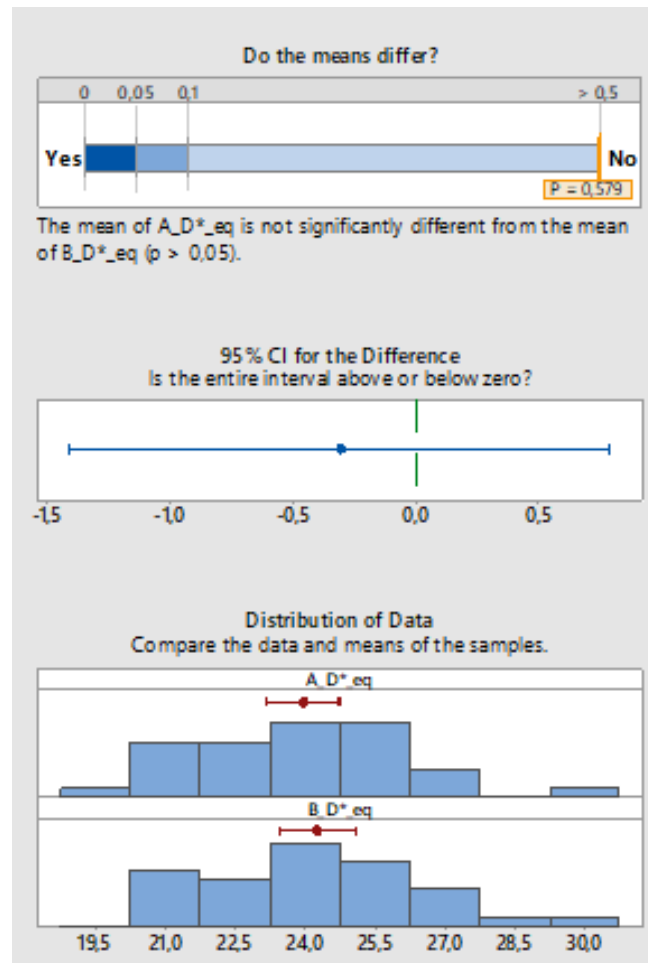
*This data does not provide sufficient evidence to conclude that the mean of A\_Deq differs from B\_Deq.* This may result from having sample sizes that are too small. Based on this sample sizes, standard deviations, and  $\alpha$ , we would have a 90% chance of detecting a difference of 1.8897.

- D\*equivalent  $[(4 \cdot \text{Annulus area} / \pi) \cdot 0.5]$

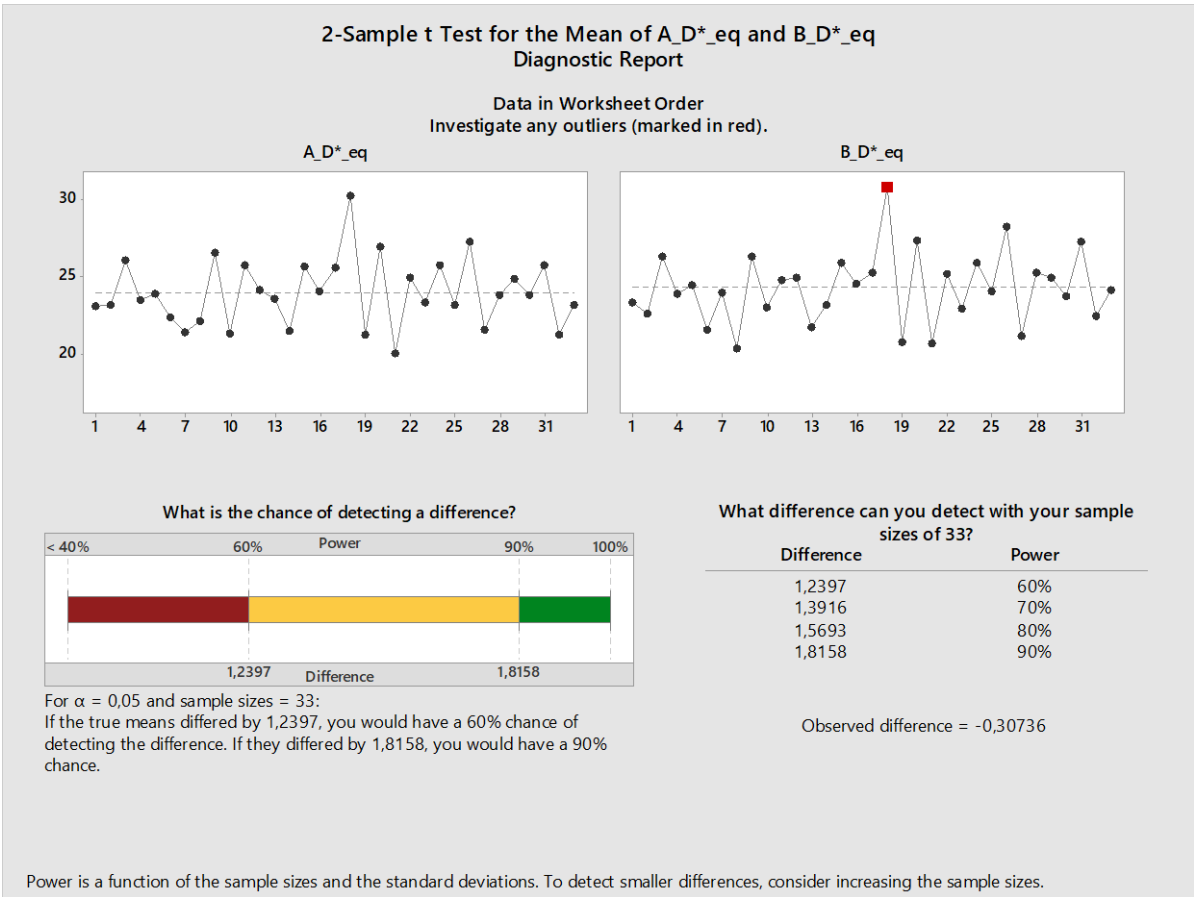
Test: there is not enough evidence to conclude that the means differ at the 0.05 level of significance.

CI: quantifies the uncertainty associated with estimating the difference in means from sample data. We can be 95% confident that the true difference is between -1.4098 and 0.79509.

Distribution of data: compare the location and the means of samples.



Individual Samples		
Statistics	A_D*_eq	B_D*_eq
Sample size	33	33
Mean	23,949	24,256
95% CI	(23,18; 24,72)	(23,440; 25,072)
Standard deviation	2,1790	2,3013
Difference Between Samples		
Statistics	*Difference	
Difference	-0,30736	
95% CI	(-1,4098; 0,79509)	
*Difference = A_D*_eq - B_D*_eq		



Report: one point is unusual compared with the others in B\_D\*\_eq. Because unusual data can have a strong influence on the results, we should try to identify the cause of its unusual nature. Correct any data or measurement errors. Consider removing data that are associated with special causes and repeating the analysis.

Because both sample sizes are at least 15, **normality is not an issue**. The test is accurate with non-normal data when the sample sizes are large enough.

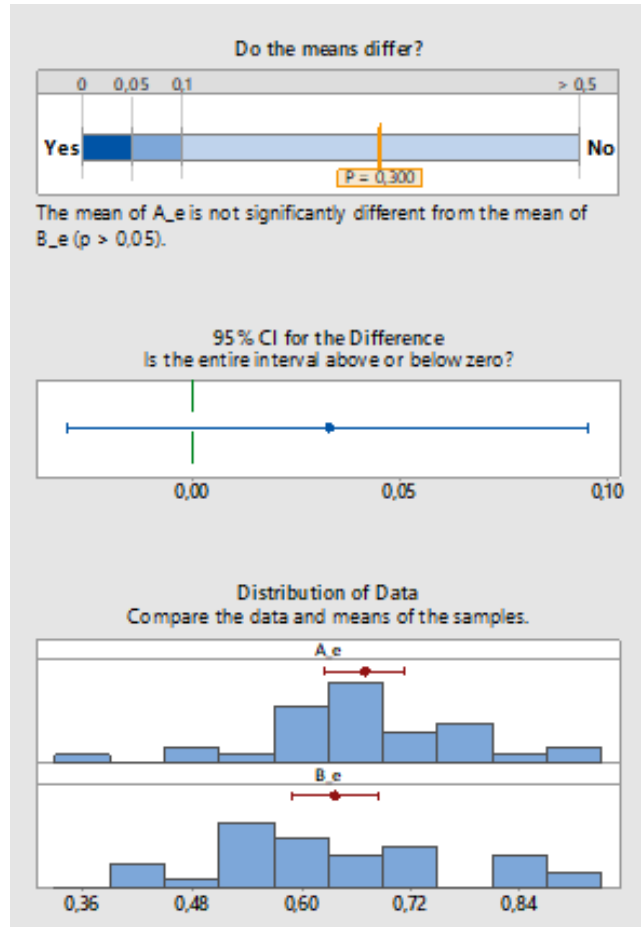
*This data does not provide sufficient evidence to conclude that the mean of A\_D\*\_eq differs from B\_D\*\_eq.* This may result from having sample sizes that are too small. Based on this sample sizes, standard deviations, and  $\alpha$ , we would have a 90% chance of detecting a difference of 1.8458.

- $e (2 * D_{\min} / D_{\max} - 1)$

Test: there is not enough evidence to conclude that the means differ at the 0.05 level of significance.

CI: quantifies the uncertainty associated with estimating the difference in means from sample data. We can be 95% confident that the true difference is between -0.029876 and 0.095501.

Distribution of data: compare the location and the means of samples.

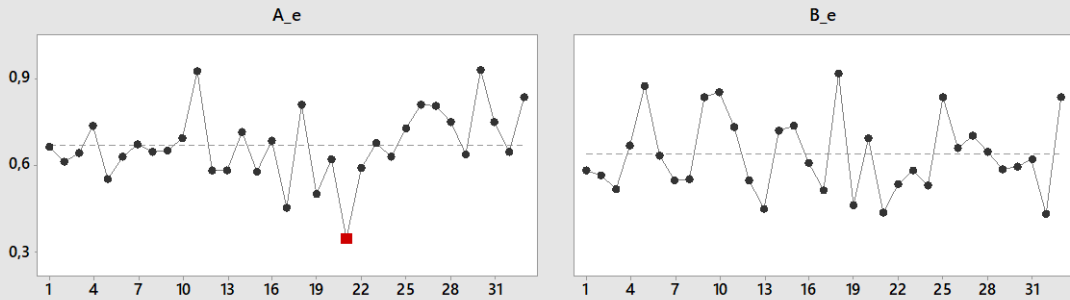


Individual Samples		
Statistics	A_e	B_e
Sample size	33	33
Mean	0,66959	0,63678
95% CI	(0,6265; 0,7127)	(0,58961; 0,68395)
Standard deviation	0,12156	0,13304
Difference Between Samples		
Statistics	*Difference	
Difference	0,032812	
95% CI	(-0,029876; 0,095501)	

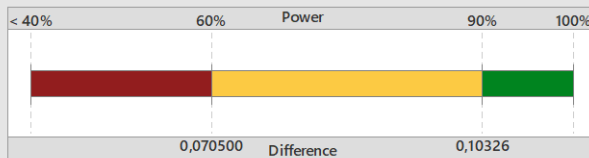
\*Difference = A\_e - B\_e

## 2-Sample t Test for the Mean of A\_e and B\_e Diagnostic Report

Data in Worksheet Order  
Investigate any outliers (marked in red).



What is the chance of detecting a difference?



For  $\alpha = 0,05$  and sample sizes = 33:  
If the true means differed by 0,070500, you would have a 60% chance of detecting the difference. If they differed by 0,10326, you would have a 90% chance.

What difference can you detect with your sample sizes of 33?

Difference	Power
0,070500	60%
0,079137	70%
0,089244	80%
0,10326	90%

Observed difference = 0,032812

Power is a function of the sample sizes and the standard deviations. To detect smaller differences, consider increasing the sample sizes.

Report: one point is unusual compared with the others in A\_e. Because unusual data can have a strong influence on the results, we should try to identify the cause of its unusual nature. Correct any data or measurement errors. Consider removing data that are associated with special causes and repeating the analysis.

Because both sample sizes are at least 15, **normality is not an issue**. The test is accurate with non-normal data when the sample sizes are large enough.

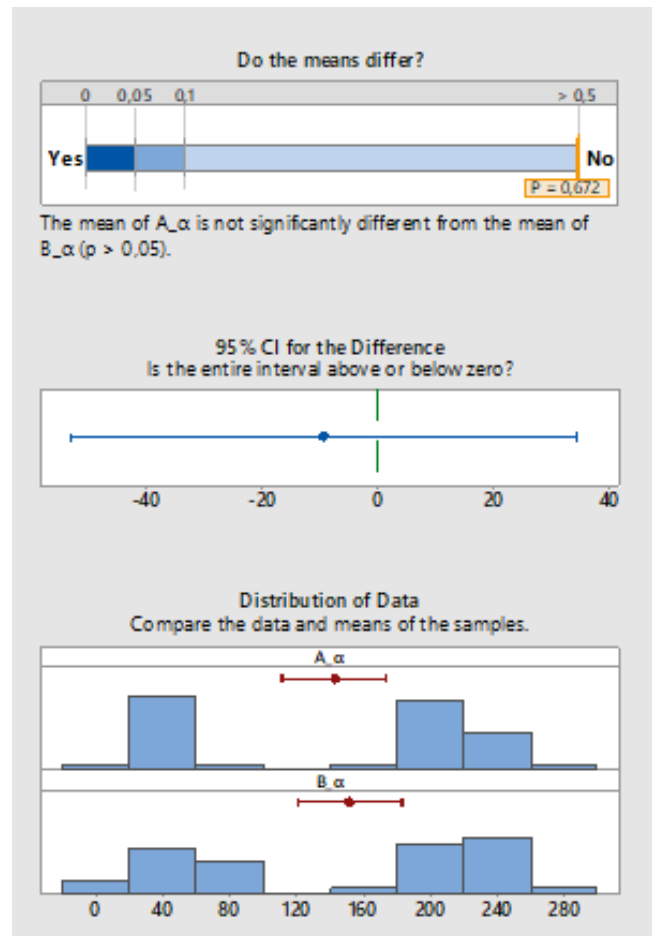
*This data does not provide sufficient evidence to conclude that the mean of A\_e differs from B\_e.* This may result from having sample sizes that are too small. Based on this sample sizes, standard deviations, and  $\alpha$ , we would have a 90% chance of detecting a difference of 0.10326.

- $\alpha$

Test: there is not enough evidence to conclude that the means differ at the 0.05 level of significance.

CI: quantifies the uncertainty associated with estimating the difference in means from sample data. We can be 95% confident that the true difference is between -53.065 and 34.460.

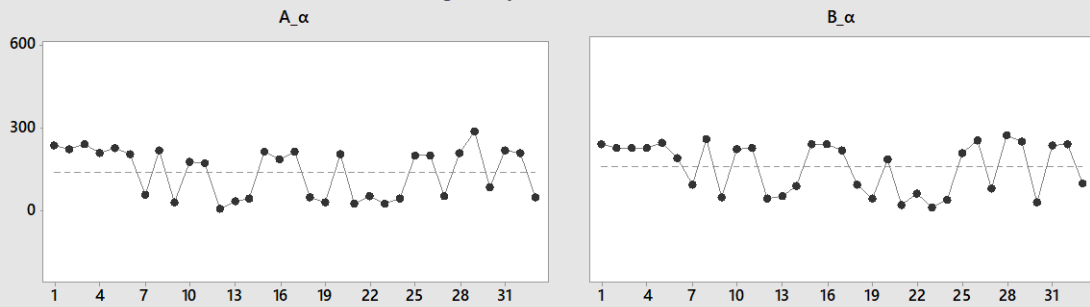
Distribution of data: compare the location and the means of samples.



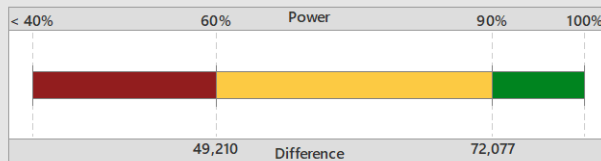
Individual Samples		
Statistics	A_α	B_α
Sample size	33	33
Mean	142,67	151,97
95% CI	(111,1; 174,2)	(120,41; 183,53)
Standard deviation	88,915	88,996
Difference Between Samples		
Statistics	*Difference	
Difference	-9,3027	
95% CI	(-53,065; 34,460)	
*Difference = A_α - B_α		

## 2-Sample t Test for the Mean of A\_α and B\_α Diagnostic Report

Data in Worksheet Order  
Investigate any outliers (marked in red).



What is the chance of detecting a difference?



For  $\alpha = 0,05$  and sample sizes = 33:  
If the true means differed by 49,210, you would have a 60% chance of detecting the difference. If they differed by 72,077, you would have a 90% chance.

What difference can you detect with your sample sizes of 33?

Difference	Power
49,210	60%
55,238	70%
62,293	80%
72,077	90%

Observed difference = -9,3027

Power is a function of the sample sizes and the standard deviations. To detect smaller differences, consider increasing the sample sizes.

Report: there are no unusual data points. Unusual data can have strong influence on the results.

Because both sample sizes are at least 15, **normality is not an issue**. The test is accurate with non-normal data when the sample sizes are large enough.

*This data does not provide sufficient evidence to conclude that the mean of A\_α differs from B\_α.*

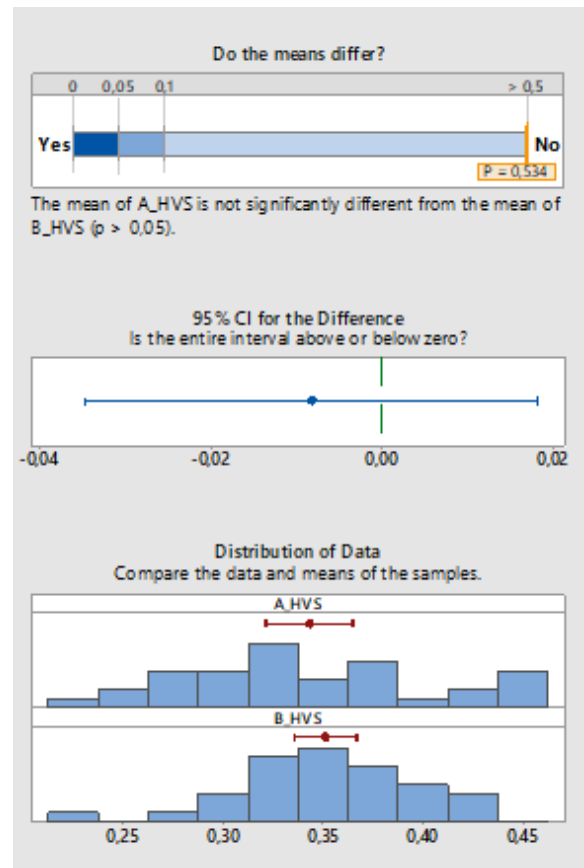
This may result from having sample sizes that are too small. Based on this sample sizes, standard deviations, and  $\alpha$ , we would have a 90% chance of detecting a difference of 72.077.

- HVS

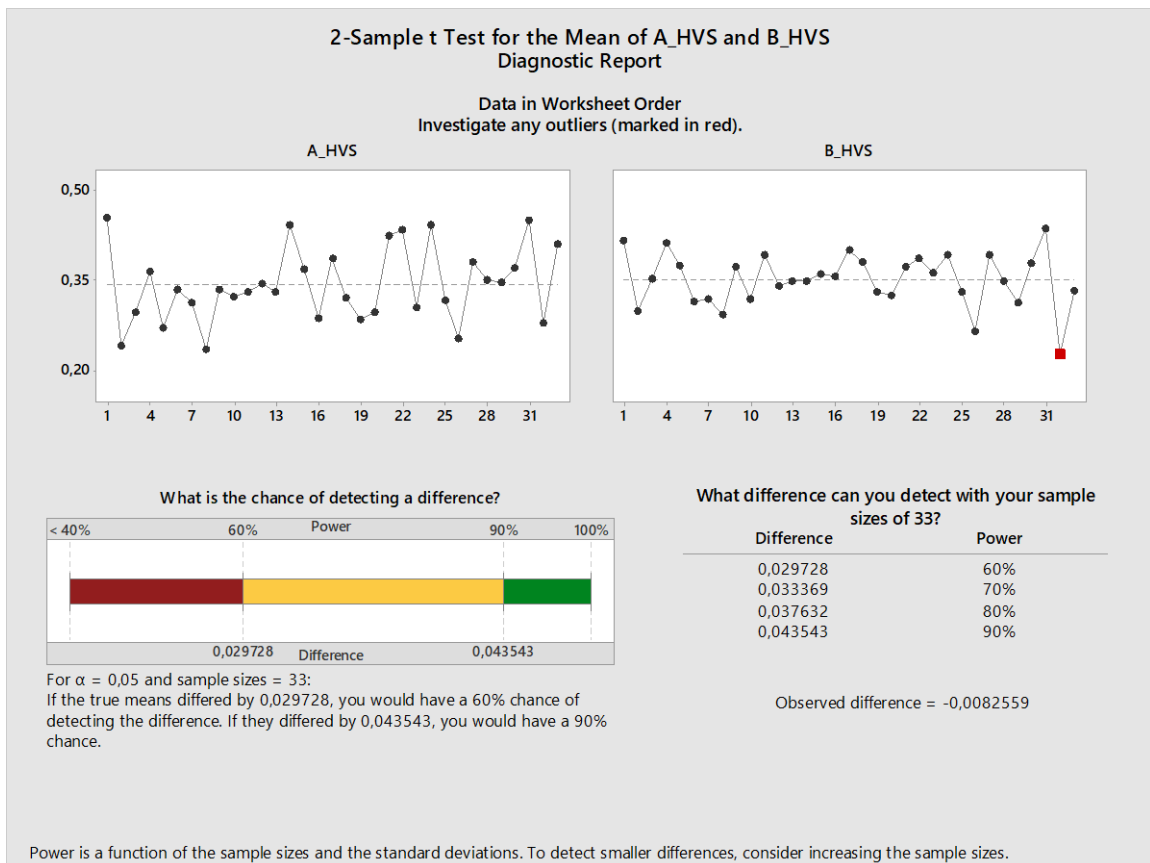
Test: there is not enough evidence to conclude that the means differ at the 0.05 level of significance.

CI: quantifies the uncertainty associated with estimating the difference in means from sample data. We can be 95% confident that the true difference is between -0.034696 and 0.018184.

Distribution of data: compare the location and the means of samples.



Individual Samples		
Statistics	A_HVS	B_HVS
Sample size	33	33
Mean	0,34306	0,35131
95% CI	(0,3212; 0,3649)	(0,33563; 0,36700)
Standard deviation	0,061648	0,044238
Difference Between Samples		
Statistics	*Difference	
Difference	-0,0082559	
95% CI	(-0,034696; 0,018184)	
*Difference = A_HVS - B_HVS		



Report: one data point is unusual compared with the others in B\_HVS. Because unusual data can have a strong influence on the results, we should try to identify the cause of its unusual nature. Correct any data entry or measurement errors. Consider removing data that are associated with special causes and repeating the analysis.

Because both sample sizes are at least 15, **normality is not an issue**. The test is accurate with non-normal data when the sample sizes are large enough.

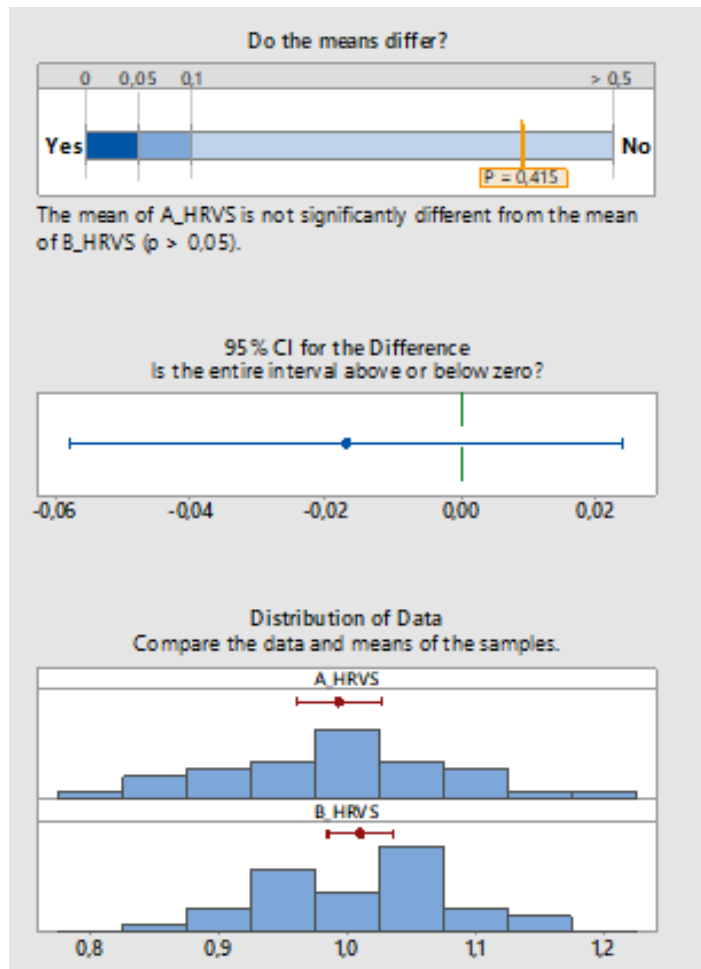
*This data does not provide sufficient evidence to conclude that the mean of A\_HVS differs from B\_HVS.* This may result from having sample sizes that are too small. Based on this sample sizes, standard deviations, and  $\alpha$ , we would have a 90% chance of detecting a difference of 0.043543.

- HRVS

Test: there is not enough evidence to conclude that the means differ at the 0.05 level of significance.

CI: quantifies the uncertainty associated with estimating the difference in means from sample data. We can be 95% confident that the true difference is between -0.057798 and 0.024184.

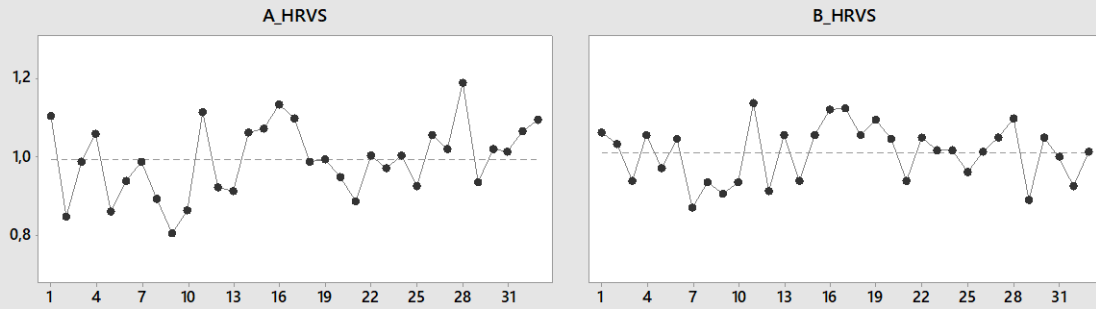
Distribution of data: compare the location and the means of samples.



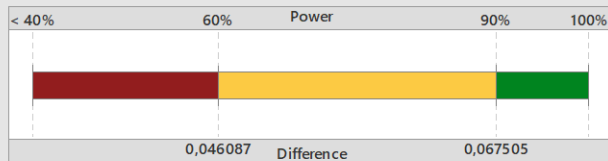
Individual Samples		
Statistics	A_HRVS	B_HRVS
Sample size	33	33
Mean	0,99356	1,0104
95% CI	(0,9607; 1,026)	(0,98455; 1,0362)
Standard deviation	0,092521	0,072787
Difference Between Samples		
Statistics	*Difference	
Difference	-0,016807	
95% CI	(-0,057798; 0,024184)	
*Difference = A_HRVS - B_HRVS		

## 2-Sample t Test for the Mean of A\_HRVs and B\_HRVs Diagnostic Report

Data in Worksheet Order  
Investigate any outliers (marked in red).



What is the chance of detecting a difference?



For  $\alpha = 0,05$  and sample sizes = 33:  
If the true means differed by  $0,046087$ , you would have a 60% chance of detecting the difference. If they differed by  $0,067505$ , you would have a 90% chance.

What difference can you detect with your sample sizes of 33?

Difference	Power
0,046087	60%
0,051733	70%
0,058341	80%
0,067505	90%

Observed difference =  $-0,016807$

Power is a function of the sample sizes and the standard deviations. To detect smaller differences, consider increasing the sample sizes.

Report: there are no unusual data points. Unusual data can have strong influence on the results.

Because both sample sizes are at least 15, **normality is not an issue**. The test is accurate with non-normal data when the sample sizes are large enough.

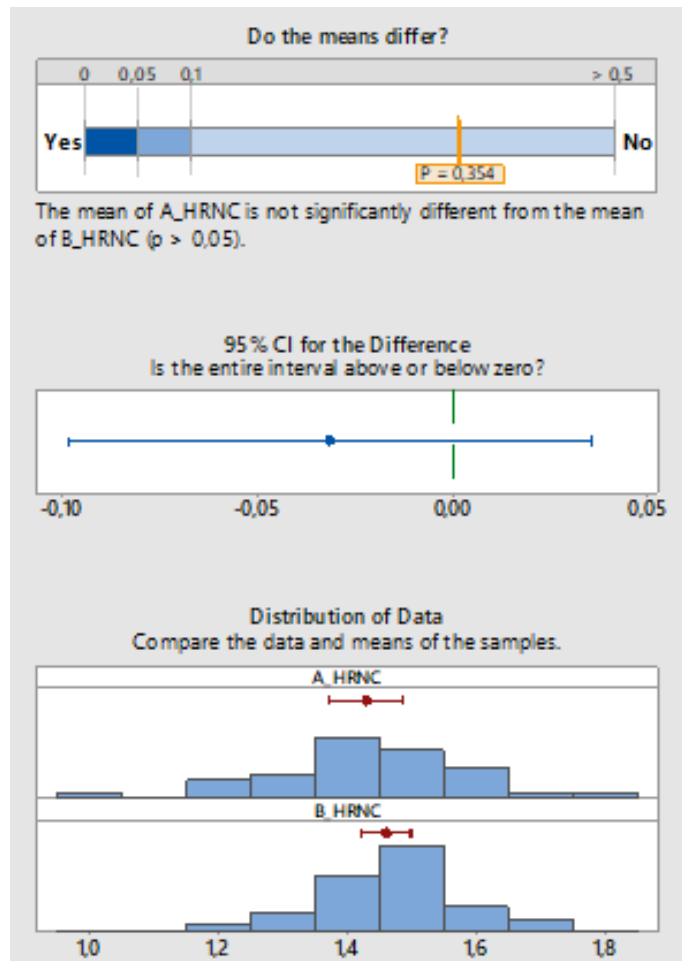
*This data does not provide sufficient evidence to conclude that the mean of A\_HRVs differs from B\_HRVs.* This may result from having sample sizes that are too small. Based on this sample sizes, standard deviations, and  $\alpha$ , we would have a 90% chance of detecting a difference of  $0,067505$ .

- HRNC

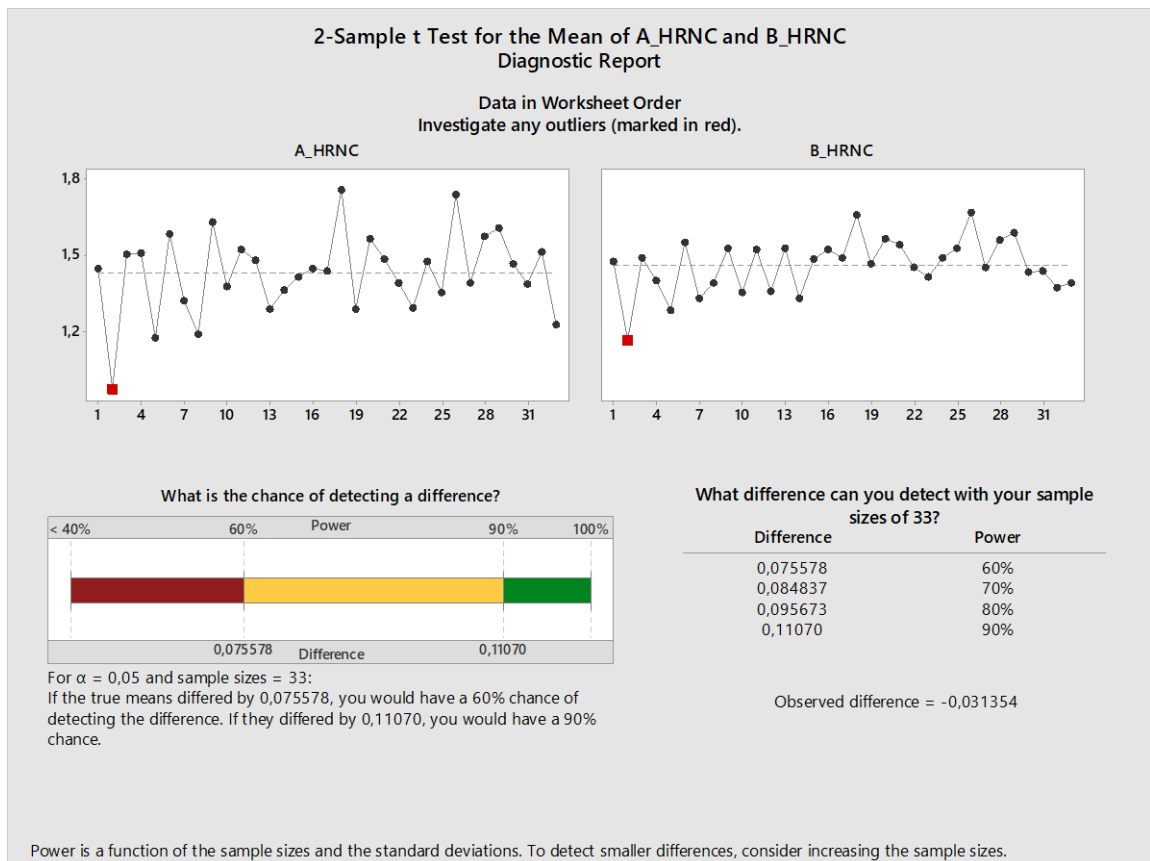
Test: there is not enough evidence to conclude that the means differ at the 0.05 level of significance.

CI: quantifies the uncertainty associated with estimating the difference in means from sample data. We can be 95% confident that the true difference is between -0.098594 and 0.035887.

Distribution of data: compare the location and the means of samples.



Individual Samples		
Statistics	A_HRNC	B_HRNC
Sample size	33	33
Mean	1,4299	1,4612
95% CI	(1,373; 1,487)	(1,4237; 1,4987)
Standard deviation	0,16113	0,10576
Difference Between Samples		
Statistics	*Difference	
Difference	-0,031354	
95% CI	(-0,098594; 0,035887)	
*Difference = A_HRNC - B_HRNC		



Report: some of the data points are unusual compared to the others in the same sample. Because unusual data can have a strong influence on the results, we should try to identify the cause of its unusual nature. These points are marked in red on the Diagnostic Report. Correct any data entry or measurement errors. Consider removing data that are associated with special causes and repeating the analysis.

Because both sample sizes are at least 15, **normality is not an issue**. The test is accurate with non-normal data when the sample sizes are large enough.

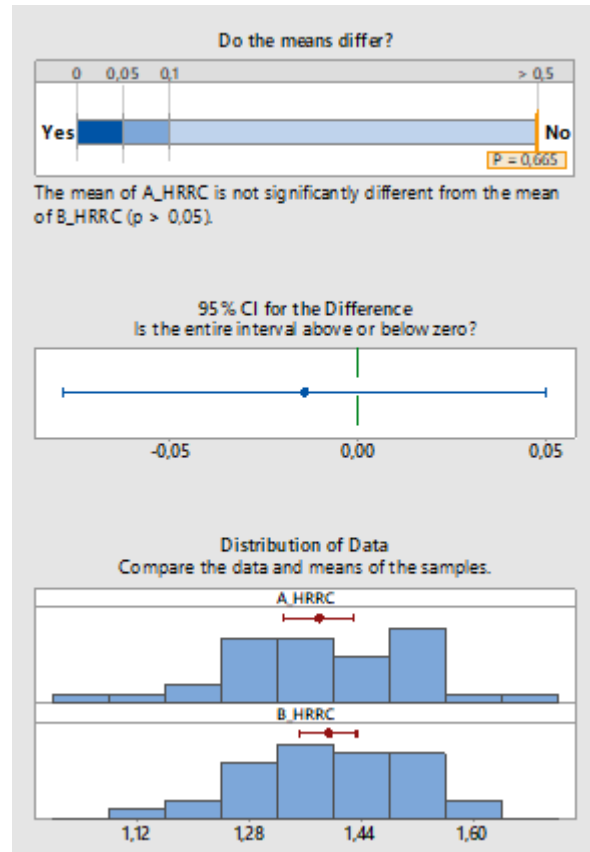
*This data does not provide sufficient evidence to conclude that the mean of A\_HRNC differs from B\_HRNC.* This may result from having sample sizes that are too small. Based on this sample sizes, standard deviations, and  $\alpha$ , we would have a 90% chance of detecting a difference of 0.11070.

- HRRC

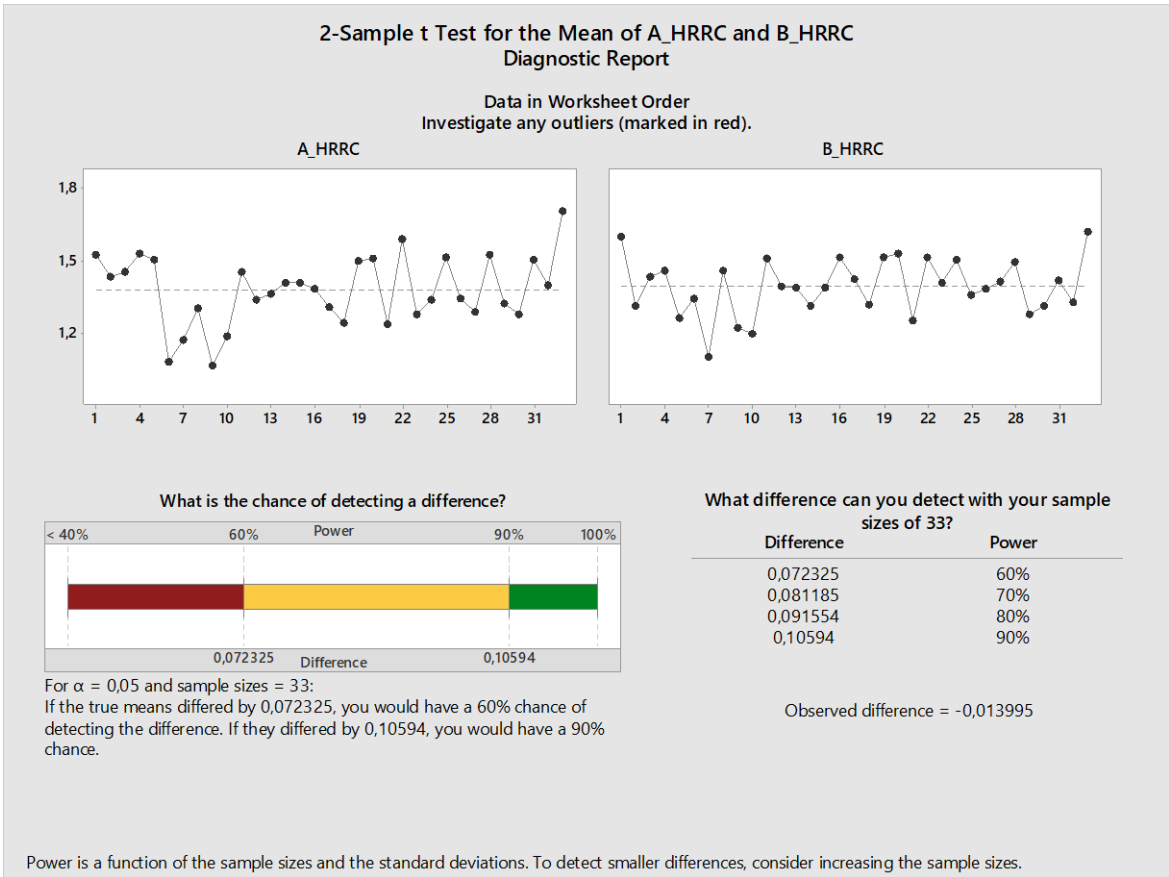
Test: there is not enough evidence to conclude that the means differ at the 0.05 level of significance.

CI: quantifies the uncertainty associated with estimating the difference in means from sample data. We can be 95% confident that the true difference is between -0.078315 and 0.050324.

Distribution of data: compare the location and the means of samples.



Individual Samples		
Statistics	A_HRRC	B_HRRC
Sample size	33	33
Mean	1,3791	1,3931
95% CI	(1,328; 1,430)	(1,3518; 1,4345)
Standard deviation	0,14335	0,11659
Difference Between Samples		
Statistics	*Difference	
Difference	-0,013995	
95% CI	(-0,078315; 0,050324)	
*Difference = A_HRRC - B_HRRC		



Report: there are no unusual data points. Unusual data can have strong influence on the results.

Because both sample sizes are at least 15, **normality is not an issue**. The test is accurate with non-normal data when the sample sizes are large enough.

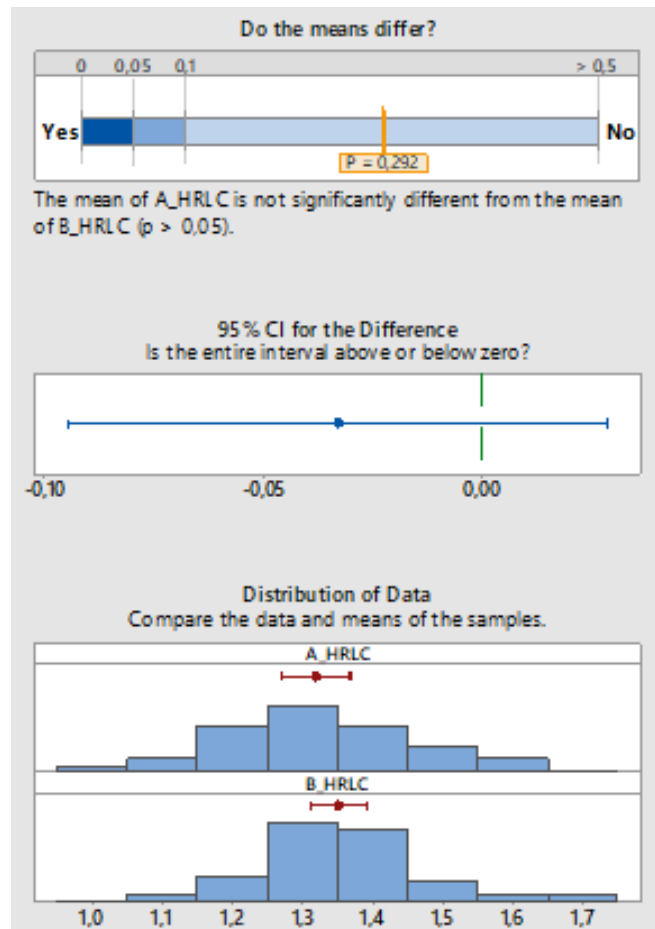
*This data does not provide sufficient evidence to conclude that the mean of A\_HRRC differs from B\_HRRC.* This may result from having sample sizes that are too small. Based on this sample sizes, standard deviations, and  $\alpha$ , we would have a 90% chance of detecting a difference of 0.10594.

- HRLC

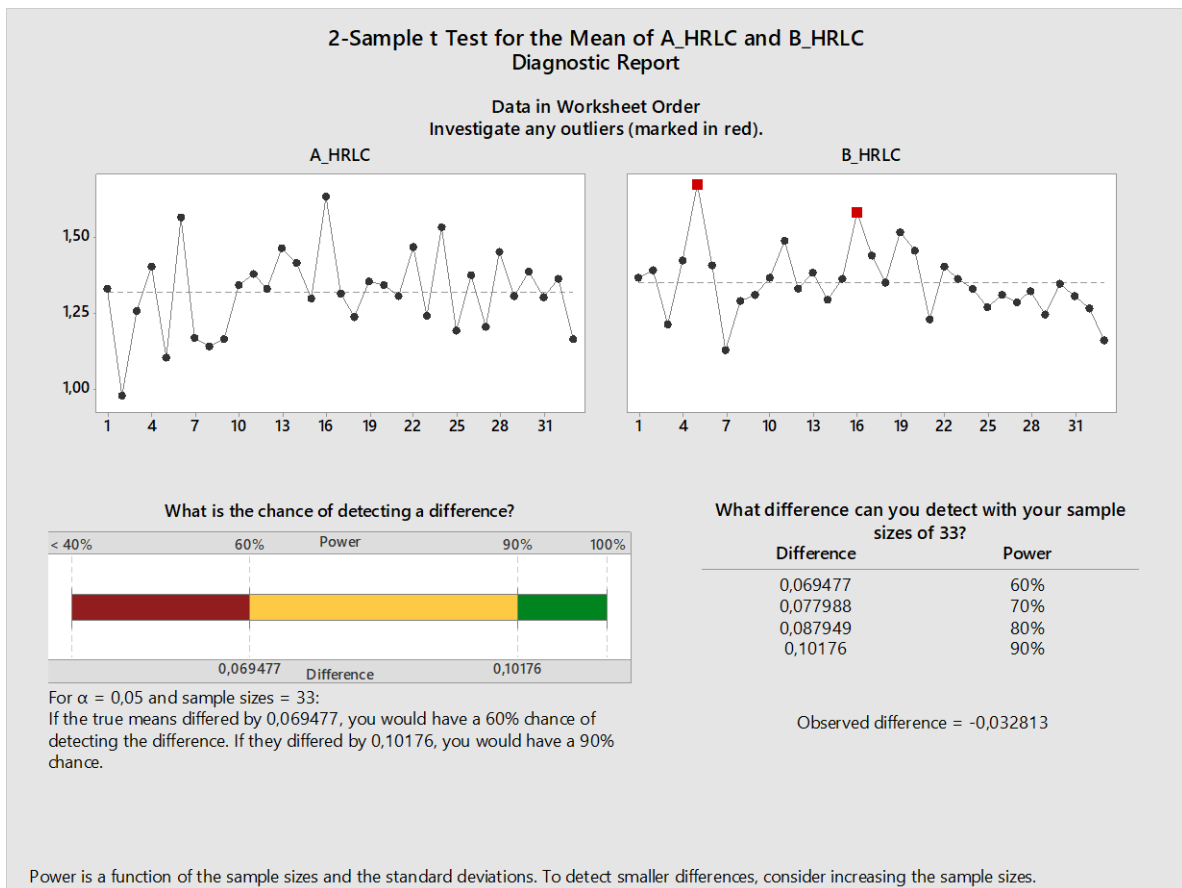
Test: there is not enough evidence to conclude that the means differ at the 0.05 level of significance.

CI: quantifies the uncertainty associated with estimating the difference in means from sample data. We can be 95% confident that the true difference is between -0.094597 and 0.028972.

Distribution of data: compare the location and the means of samples.



Individual Samples		
Statistics	A_HRLC	B_HRLC
Sample size	33	33
Mean	1,3184	1,3512
95% CI	(1,269; 1,367)	(1,3116; 1,3908)
Standard deviation	0,13800	0,11163
Difference Between Samples		
Statistics	*Difference	
Difference	-0,032813	
95% CI	(-0,094597; 0,028972)	
*Difference = A_HRLC - B_HRLC		



Report: some of the data points are unusual compared to the others in the same sample. Because unusual data can have a strong influence on the results, we should try to identify the cause of its unusual nature. These points are marked in red on the Diagnostic Report. Correct any data entry or measurement errors. Consider removing data that are associated with special causes and repeating the analysis.

Because both sample sizes are at least 15, **normality is not an issue**. The test is accurate with non-normal data when the sample sizes are large enough.

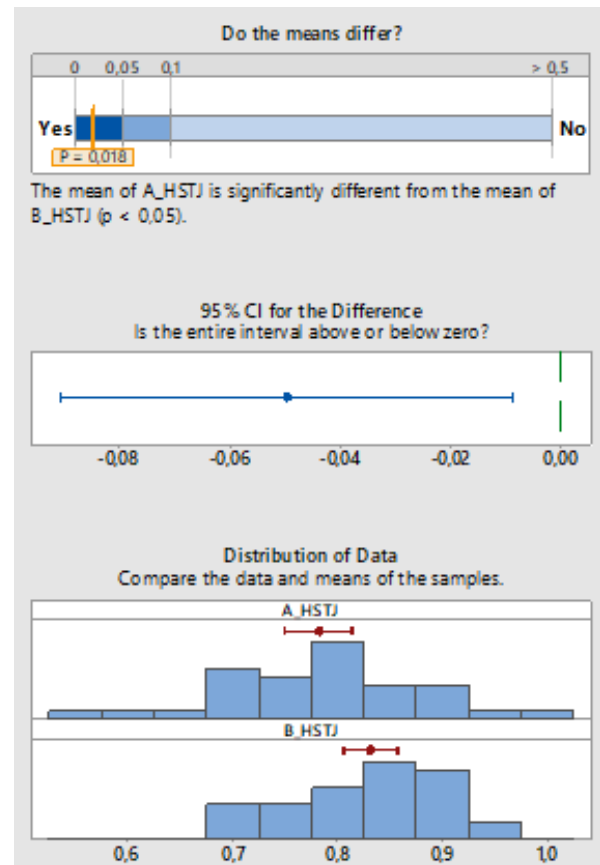
*This data does not provide sufficient evidence to conclude that the mean of A\_HRLC differs from B\_HRLC.* This may result from having sample sizes that are too small. Based on this sample sizes, standard deviations, and  $\alpha$ , we would have a 90% chance of detecting a difference of 0.10176.

- HSTJ

Test: we can conclude that the means differ at the 0.05 level of significance.

CI: quantifies the uncertainty associated with estimating the difference in means from sample data. We can be 95% confident that the true difference is between -0.090525 and 0.0088283.

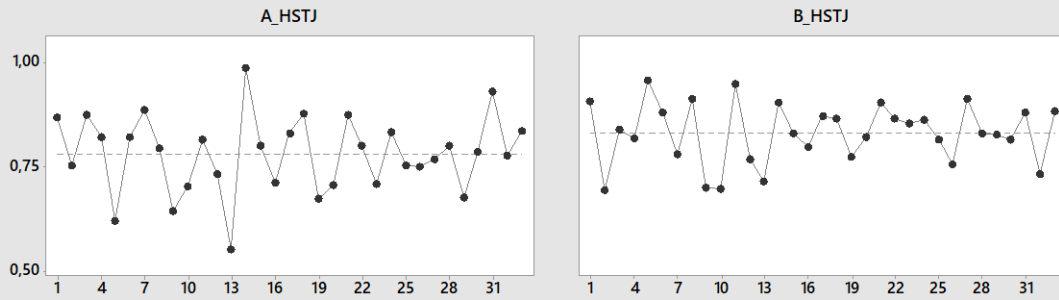
Distribution of data: compare the location and the means of samples.



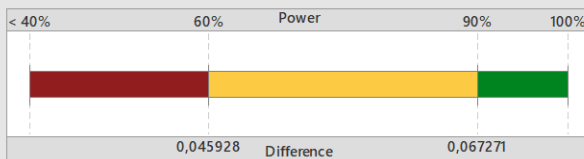
Individual Samples		
Statistics	A_HSTJ	B_HSTJ
Sample size	33	33
Mean	0,78169	0,83136
95% CI	(0,7490; 0,8144)	(0,80569; 0,85704)
Standard deviation	0,092295	0,072411
Difference Between Samples		
Statistics	*Difference	
Difference	-0,049677	
95% CI	(-0,090525; -0,0088283)	
*Difference = A_HSTJ - B_HSTJ		

## 2-Sample t Test for the Mean of A\_HSTJ and B\_HSTJ Diagnostic Report

Data in Worksheet Order  
Investigate any outliers (marked in red).



What is the chance of detecting a difference?



For  $\alpha = 0,05$  and sample sizes = 33:  
If the true means differed by 0,045928, you would have a 60% chance of detecting the difference. If they differed by 0,067271, you would have a 90% chance.

What difference can you detect with your sample sizes of 33?

Difference	Power
0,045928	60%
0,051554	70%
0,058139	80%
0,067271	90%

Observed difference = -0,049677

Power is a function of the sample sizes and the standard deviations. To detect smaller differences, consider increasing the sample sizes.

Report: there are no unusual data points. Unusual data can have strong influence on the results.

Because both sample sizes are at least 15, **normality is not an issue**. The test is accurate with non-normal data when the sample sizes are large enough.

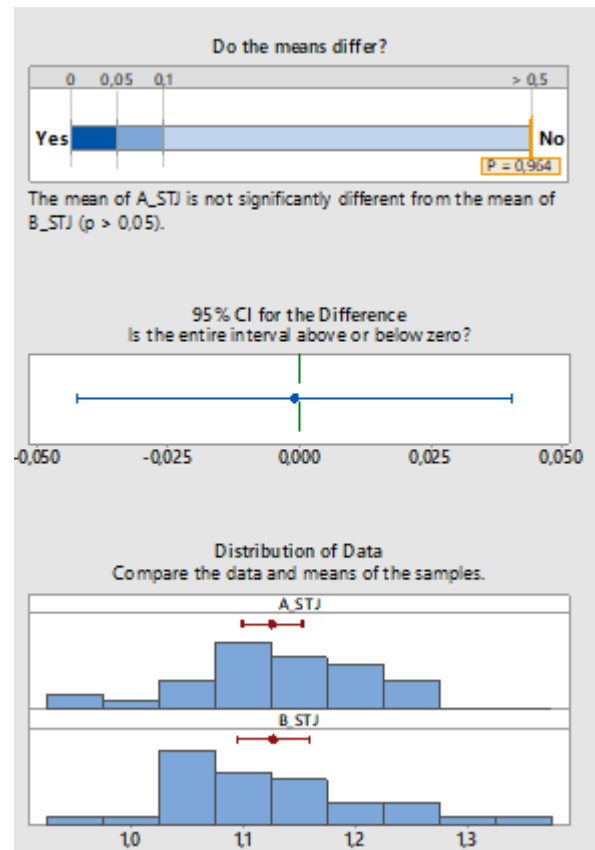
*The sample is sufficient to detect a difference between the means.*

- STJ

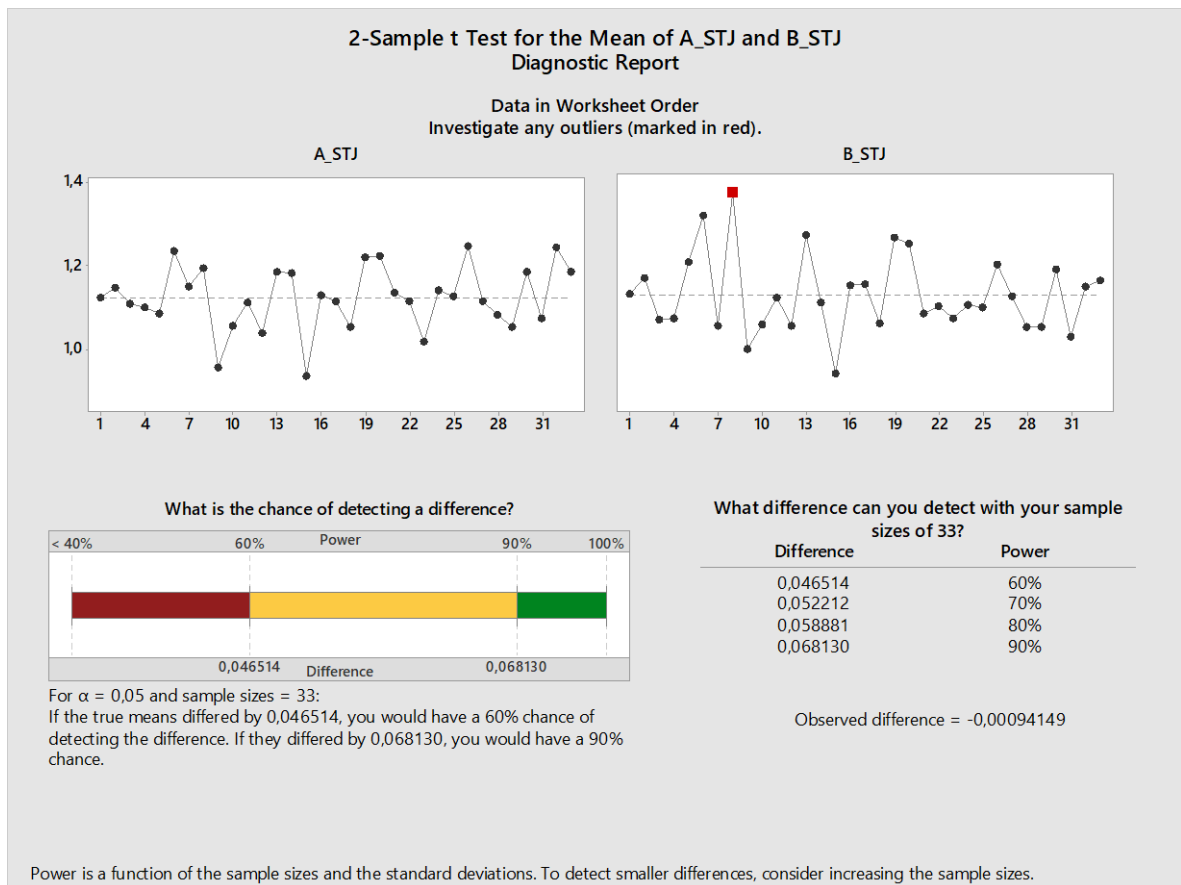
Test: there is not enough evidence to conclude that the means differ at the 0.05 level of significance.

CI: quantifies the uncertainty associated with estimating the difference in means from sample data. We can be 95% confident that the true difference is between -0.042312 and 0.040429.

Distribution of data: compare the location and the means of samples.



Individual Samples		
Statistics	A_STJ	B_STJ
Sample size	33	33
Mean	1,1256	1,1266
95% CI	(1,099; 1,153)	(1,0941; 1,1590)
Standard deviation	0,075868	0,091484
Difference Between Samples		
Statistics	*Difference	
Difference	-0,00094149	
95% CI	(-0,042312; 0,040429)	
*Difference = A_STJ - B_STJ		



Report: one data point is unusual compared with the others in B\_STJ. Because unusual data can have a strong influence on the results, we should try to identify the cause of its unusual nature. Correct any data entry or measurement errors. Consider removing data that are associated with special causes and repeating the analysis.

Because both sample sizes are at least 15, **normality is not an issue**. The test is accurate with non-normal data when the sample sizes are large enough.

*This data does not provide sufficient evidence to conclude that the mean of A\_STJ differs from B\_STJ. This may result from having sample sizes that are too small. Based on this sample sizes, standard deviations, and  $\alpha$ , we would have a 90% chance of detecting a difference of 0.068130.*

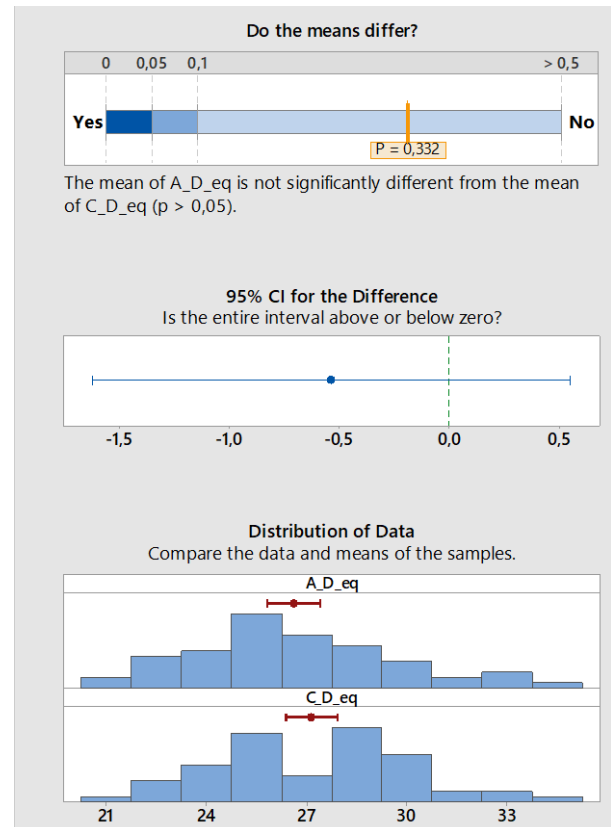
## 6.1.2 A/C

- D equivalent (Annulus perimeter/ $\pi$ )

Test: there is not enough evidence to conclude that the means differ at the 0.05 level of significance.

CI: quantifies the uncertainty associated with estimating the difference in means from sample data. We can be 95% confident that the true difference is between -1.6216 and 0.55271.

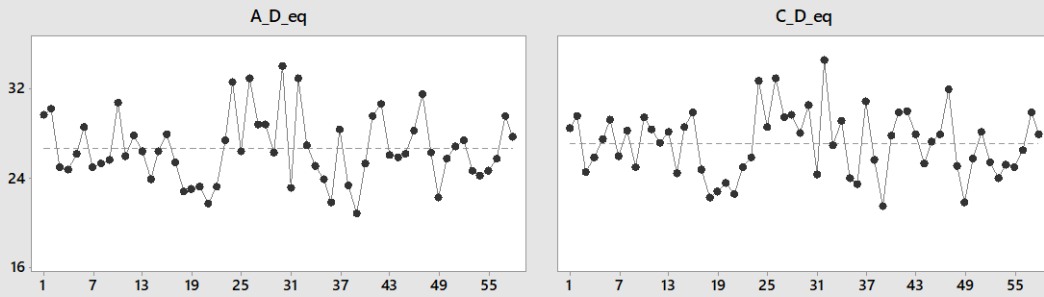
Distribution of data: compare the location and means of samples.



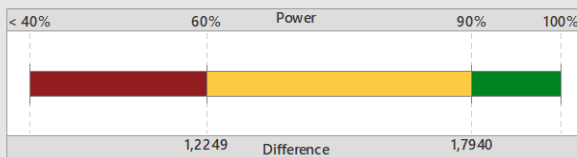
Individual Samples		
Statistics	A_D_eq	C_D_eq
Sample size	58	58
Mean	26,615	27,149
95% CI	(25,82; 27,41)	(26,386; 27,912)
Standard deviation	3,0081	2,9011
Difference Between Samples		
Statistics	*Difference	
Difference	-0,53447	
95% CI	(-1,6216; 0,55271)	
*Difference = A_D_eq - C_D_eq		

## 2-Sample t Test for the Mean of A\_D\_eq and C\_D\_eq Diagnostic Report

Data in Worksheet Order  
Investigate any outliers (marked in red).



What is the chance of detecting a difference?



For  $\alpha = 0,05$  and sample sizes = 58:  
If the true means differed by 1,2249, you would have a 60% chance of detecting the difference. If they differed by 1,7940, you would have a 90% chance.

What difference can you detect with your sample sizes of 58?

Difference	Power
1,2249	60%
1,3749	70%
1,5505	80%
1,7940	90%

Observed difference = -0,53447

Power is a function of the sample sizes and the standard deviations. To detect smaller differences, consider increasing the sample sizes.

Report: there are no unusual data points. Unusual data can have a strong influence on the results.

Because both sample size are at least 15, **normality is not an issue**. The test is accurate with non-normal data when the sample sizes are large enough.

*Data does not provide sufficient evidence to conclude that the mean of A\_D\_eq differs from C\_D\_eq.*

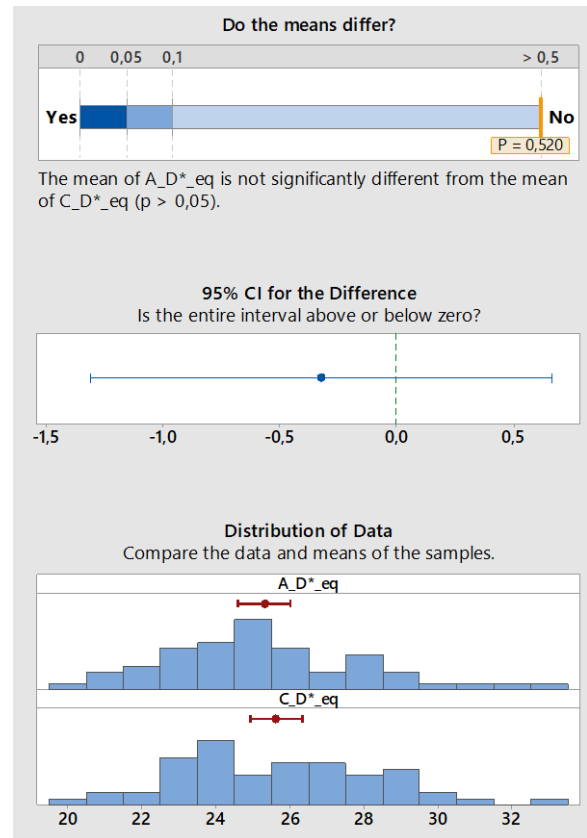
This may result from having sample sizes that are too small. Based on our sample sizes, standard deviation, and  $\alpha$ , we would have 90% chance of detecting a difference of 1.7940.

- D equivalent  $[(4 \cdot \text{Annulus area} / \pi) \cdot 0.5]$

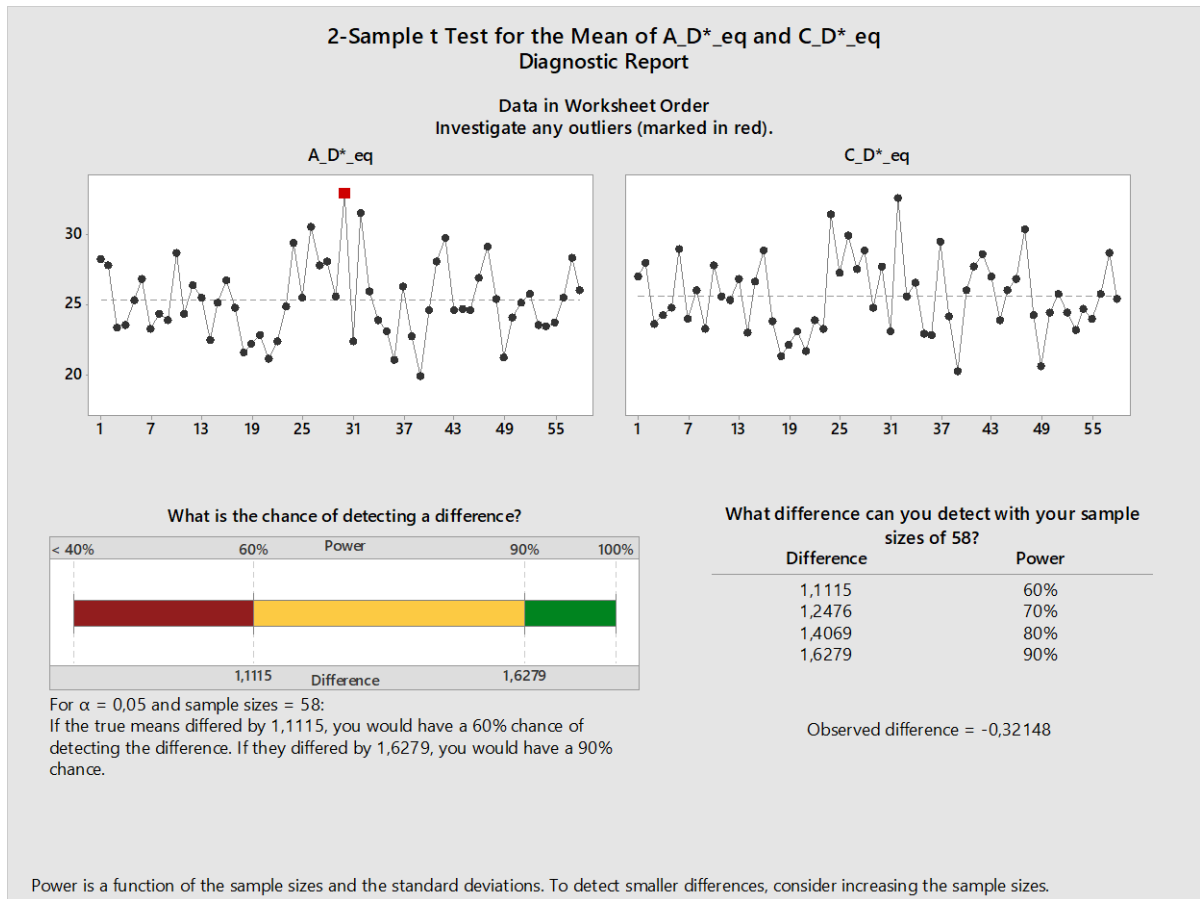
Test: there is not enough evidence to conclude that the means differ at the 0.05 level of significance.

CI: quantifies the uncertainty associated with estimating the difference in means from sample data. We can be 95% confident that the true difference is between -1.3080 and 0.66502.

Distribution of data: compare the location and means of samples.



Individual Samples		
Statistics	A_D*_eq	C_D*_eq
Sample size	58	58
Mean	25,305	25,627
95% CI	(24,59; 26,02)	(24,929; 26,324)
Standard deviation	2,7087	2,6540
Difference Between Samples		
Statistics	*Difference	
Difference	-0,32148	
95% CI	(-1,3080; 0,66502)	
*Difference = A_D*_eq - C_D*_eq		



Report: one data point is unusual compared to the others in A\_D\*\_eq. Because unusual data can have a strong influence on the results, we should try to identify the cause of its unusual nature. Correct any data entry or measurement errors. Consider removing data that are associated with special causes and repeating the analysis.

Because both sample sizes are at least 15, **normality is not an issue**. The test is accurate with non-normal data when the sample sizes are large enough.

*Our data does not provide sufficient evidence to conclude that the mean of A\_D\*\_eq differs from C\_D\*\_eq.* This may result from having sample sizes that are too small. Based on our sample sizes, standard deviation, and  $\alpha$ , we would have 90% chance of detecting a difference of 1.6279.

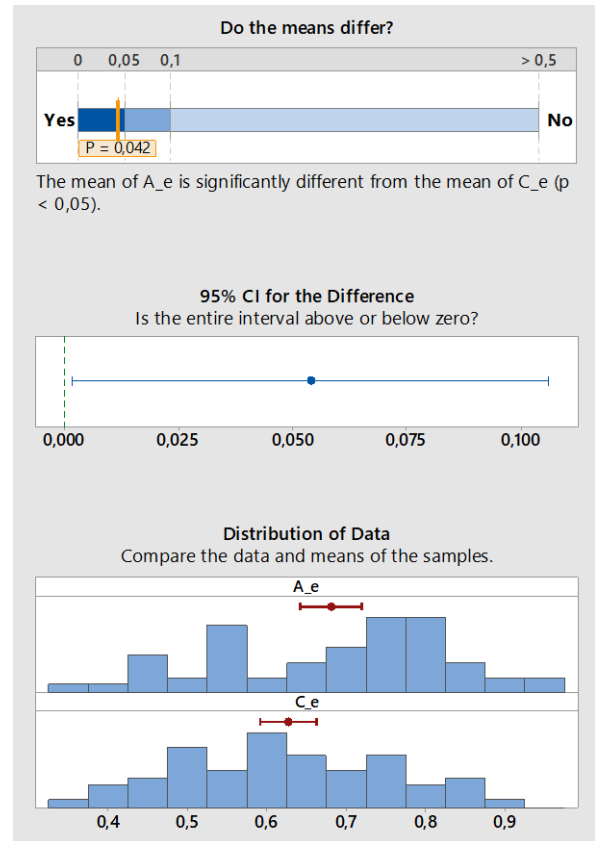
- $e (2 * D_{\min} / D_{\max} - 1)$

Test: we can conclude that the means differ at the 0.05 level of significance.

CI: quantifies the uncertainty associated with estimating the difference in means from sample data.

We can be 95% confident that the true difference is between 0.0018943 and 0.10606.

Distribution of data: compare the location and means of samples.

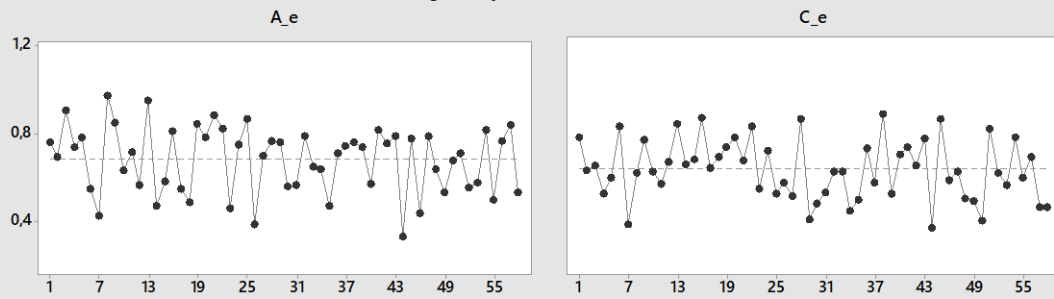


Individual Samples		
Statistics	A_e	C_e
Sample size	58	58
Mean	0,68107	0,62710
95% CI	(0,6416; 0,7205)	(0,59222; 0,66197)
Standard deviation	0,14993	0,13264
Difference Between Samples		
Statistics	*Difference	
Difference	0,053976	
95% CI	(0,0018943; 0,10606)	

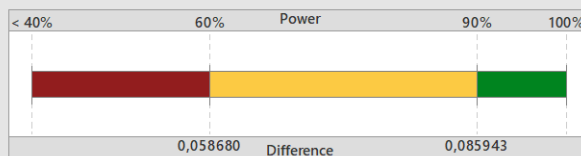
\*Difference = A\_e - C\_e

## 2-Sample t Test for the Mean of A\_e and C\_e Diagnostic Report

Data in Worksheet Order  
Investigate any outliers (marked in red).



What is the chance of detecting a difference?



For  $\alpha = 0,05$  and sample sizes = 58:  
If the true means differed by 0,058680, you would have a 60% chance of detecting the difference. If they differed by 0,085943, you would have a 90% chance.

What difference can you detect with your sample sizes of 58?

Difference	Power
0,058680	60%
0,065867	70%
0,074278	80%
0,085943	90%

Observed difference = 0,053976

Power is a function of the sample sizes and the standard deviations. To detect smaller differences, consider increasing the sample sizes.

Report: there are no unusual data points. Unusual data can have a strong influence on the results.

Because both sample size are at least 15, **normality is not an issue**. The test is accurate with non-normal data when the sample sizes are large enough.

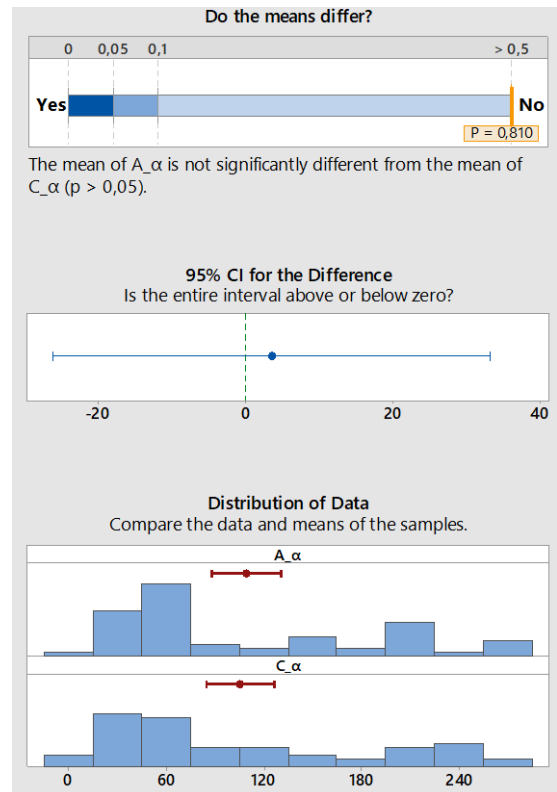
*The sample is sufficient to detect a difference between the means.*

- $\alpha$

Test: there is not enough evidence to conclude that the means differ at the 0.05 level of significance.

CI: quantifies the uncertainty associated with estimating the difference in means from sample data. We can be 95% confident that the true difference is between -25.998 and 33.183.

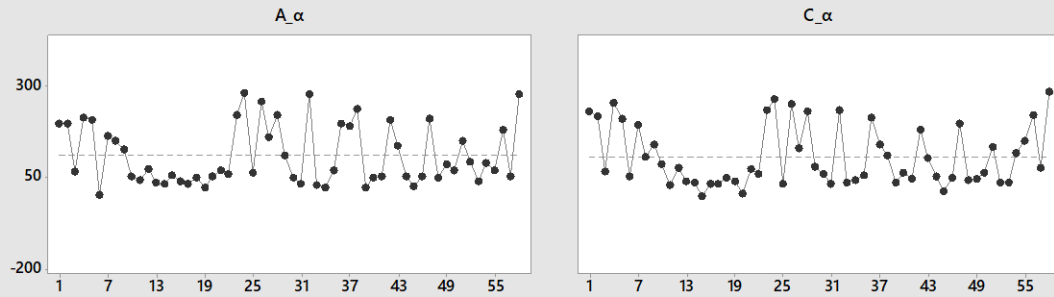
Distribution of data: compare the location and means of samples.



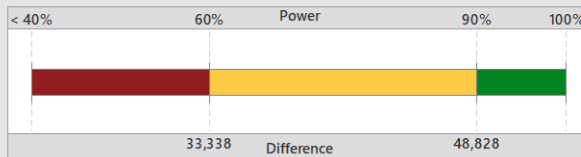
Individual Samples		
Statistics	A_α	C_α
Sample size	58	58
Mean	109,30	105,71
95% CI	(88,21; 130,4)	(84,506; 126,91)
Standard deviation	80,223	80,640
Difference Between Samples		
Statistics	*Difference	
Difference	3,5928	
95% CI	(-25,998; 33,183)	
*Difference = A_α - C_α		

## 2-Sample t Test for the Mean of A<sub>α</sub> and C<sub>α</sub> Diagnostic Report

Data in Worksheet Order  
Investigate any outliers (marked in red).



What is the chance of detecting a difference?



For  $\alpha = 0,05$  and sample sizes = 58:  
If the true means differed by 33,338, you would have a 60% chance of detecting the difference. If they differed by 48,828, you would have a 90% chance.

What difference can you detect with your sample sizes of 58?

Difference	Power
33,338	60%
37,422	70%
42,201	80%
48,828	90%

Observed difference = 3,5928

Power is a function of the sample sizes and the standard deviations. To detect smaller differences, consider increasing the sample sizes.

Report: there are no unusual data points. Unusual data can have a strong influence on the results.

Because both sample size are at least 15, **normality is not an issue**. The test is accurate with non-normal data when the sample sizes are large enough.

*Our data does not provide sufficient evidence to conclude that the mean of A<sub>α</sub> differs from C<sub>α</sub>.*

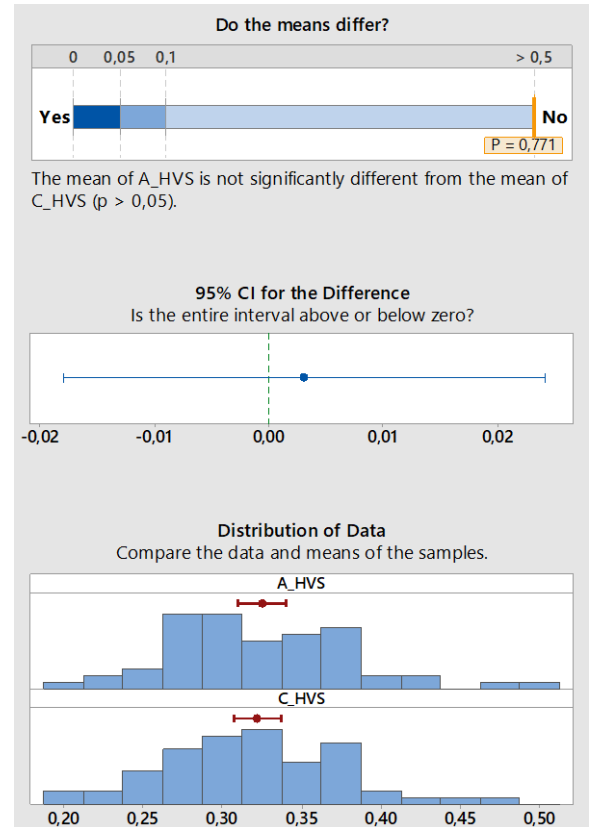
This may result from having sample sizes that are too small. Based on our sample sizes, standard deviation, and  $\alpha$ , we would have 90% chance of detecting a difference of 48.828.

- HVS

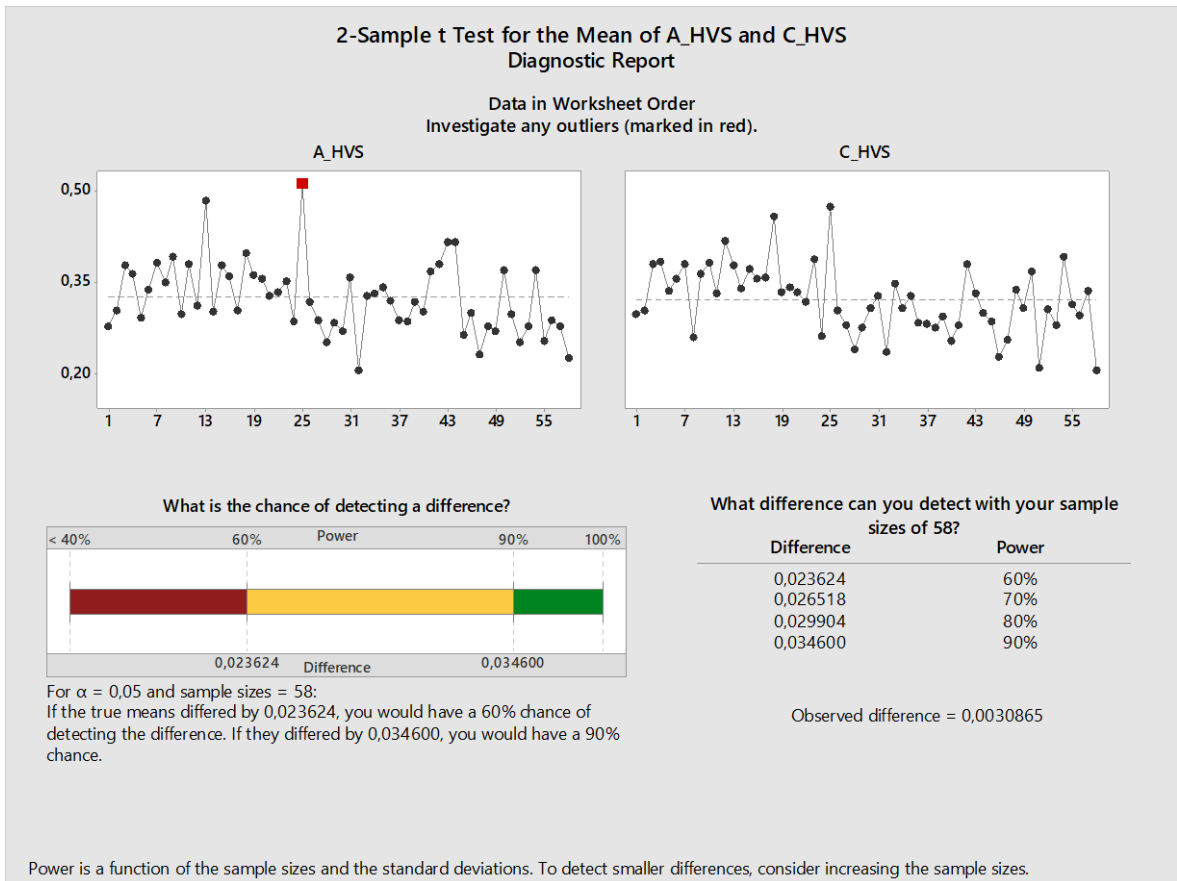
Test: there is not enough evidence to conclude that the means differ at the 0.05 level of significance.

CI: quantifies the uncertainty associated with estimating the difference in means from sample data. We can be 95% confident that the true difference is between -0.017881 and 0.024054.

Distribution of data: compare the location and means of samples.



Individual Samples		
Statistics	A_HVS	C_HVS
Sample size	58	58
Mean	0,32505	0,32196
95% CI	(0,3097; 0,3404)	(0,30736; 0,33656)
Standard deviation	0,058429	0,055522
Difference Between Samples		
Statistics	*Difference	
Difference	0,0030865	
95% CI	(-0,017881; 0,024054)	
*Difference = A_HVS - C_HVS		



Report: one data point is unusual compared to the others in A\_HVS. Because unusual data can have a strong influence on the results, we should try to identify the cause of its unusual nature. Correct any data entry or measurement errors. Consider removing data that are associated with special causes and repeating the analysis.

Because both sample sizes are at least 15, **normality is not an issue**. The test is accurate with non-normal data when the sample sizes are large enough.

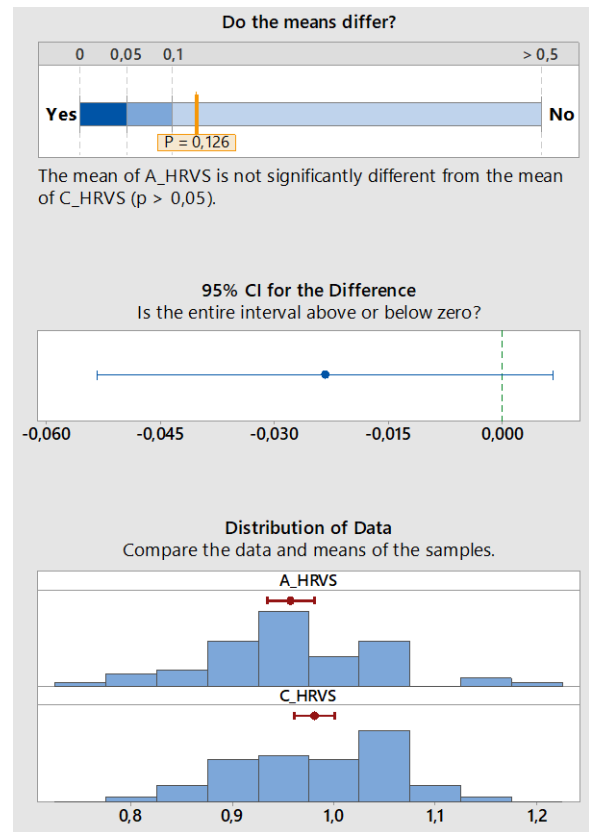
*Data does not provide sufficient evidence to conclude that the mean of A\_HVS differs from C\_HVS.* This may result from having sample sizes that are too small. Based on our sample sizes, standard deviation, and  $\alpha$ , we would have 90% chance of detecting a difference of 0.034600.

- HRVS

Test: there is not enough evidence to conclude that the means differ at the 0.05 level of significance.

CI: quantifies the uncertainty associated with estimating the difference in means from sample data. We can be 95% confident that the true difference is between -0.053274 and 0.0066426.

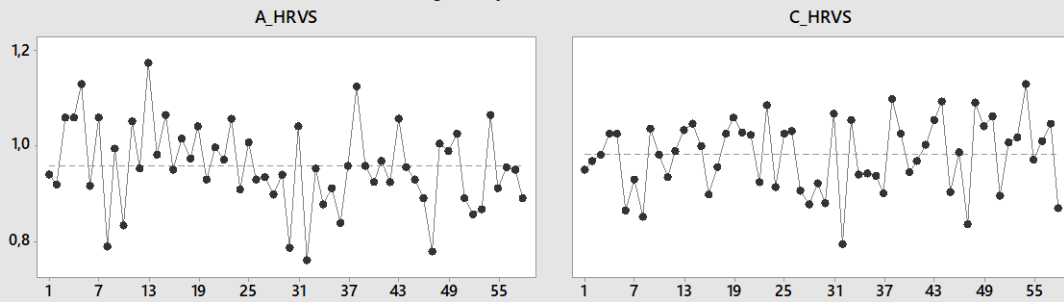
Distribution of data: compare the location and means of samples.



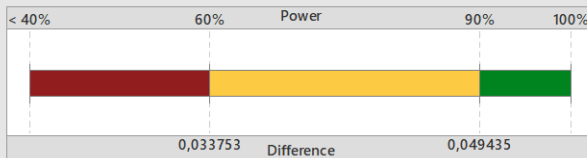
Individual Samples		
Statistics	A_HRVS	C_HRVS
Sample size	58	58
Mean	0,95775	0,98106
95% CI	(0,9347; 0,9808)	(0,96139; 1,0007)
Standard deviation	0,087531	0,074803
Difference Between Samples		
Statistics	*Difference	
Difference	-0,023316	
95% CI	(-0,053274; 0,0066426)	
*Difference = A_HRVS - C_HRVS		

## 2-Sample t Test for the Mean of A\_HRVs and C\_HRVs Diagnostic Report

Data in Worksheet Order  
Investigate any outliers (marked in red).



What is the chance of detecting a difference?



For  $\alpha = 0,05$  and sample sizes = 58:  
If the true means differed by 0,033753, you would have a 60% chance of detecting the difference. If they differed by 0,049435, you would have a 90% chance.

What difference can you detect with your sample sizes of 58?

Difference	Power
0,033753	60%
0,037887	70%
0,042726	80%
0,049435	90%

Observed difference = -0,023316

Power is a function of the sample sizes and the standard deviations. To detect smaller differences, consider increasing the sample sizes.

Report: there are no unusual data points. Unusual data can have a strong influence on the results.

Because both sample size are at least 15, **normality is not an issue**. The test is accurate with non-normal data when the sample sizes are large enough.

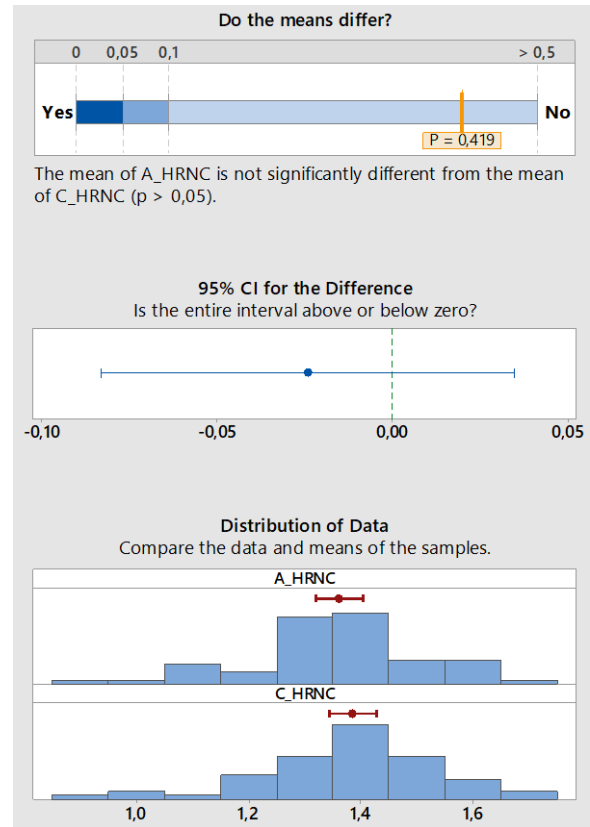
*Our data does not provide sufficient evidence to conclude that the mean of A\_HRVs differs from C\_HRVs.* This may result from having sample sizes that are too small. Based on our sample sizes, standard deviation, and  $\alpha$ , we would have 90% chance of detecting a difference of 0.049435.

- HRNC

Test: there is not enough evidence to conclude that the means differ at the 0.05 level of significance.

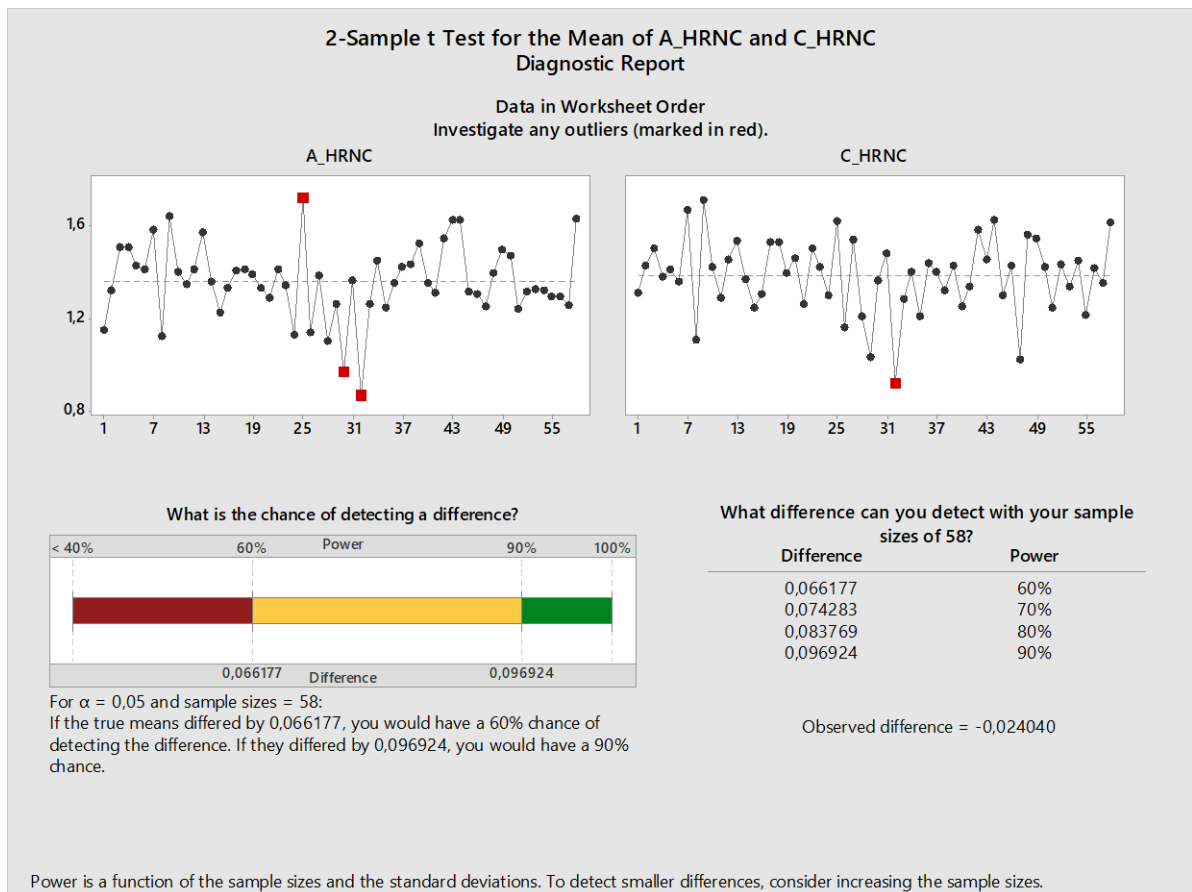
CI: quantifies the uncertainty associated with estimating the difference in means from sample data. We can be 95% confident that the true difference is between -0.082778 and 0.034698.

Distribution of data: compare the location and means of samples.



Individual Samples		
Statistics	A_HRNC	C_HRNC
Sample size	58	58
Mean	1,3618	1,3858
95% CI	(1,319; 1,404)	(1,3442; 1,4274)
Standard deviation	0,16110	0,15821
Difference Between Samples		
Statistics	*Difference	
Difference	-0,024040	
95% CI	(-0,082778; 0,034698)	

\*Difference = A\_HRNC - C\_HRNC



Report: some of the data points are unusual compared to the others in the same sample. Because unusual data can have a strong influence on the results, we should try to identify the cause of its unusual nature. These points are marked in red on the Diagnostic Report. Correct any data entry or measurement errors. Consider removing data that are associated with special causes and repeating the analysis.

Because both sample sizes are at least 15, **normality is not an issue**. The test is accurate with non-normal data when the sample sizes are large enough.

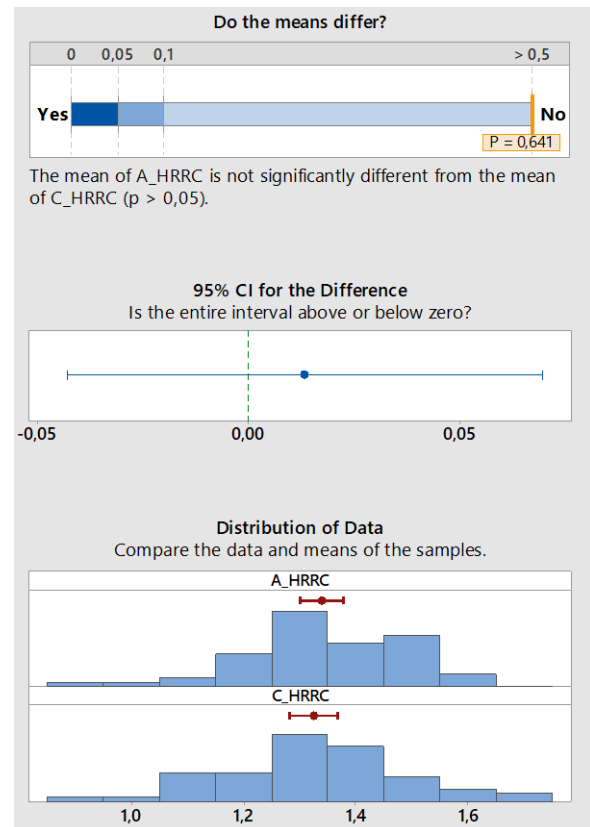
*Our data does not provide sufficient evidence to conclude that the mean of A\_HRNC differs from C\_HRNC.* This may result from having sample sizes that are too small. Based on our sample sizes, standard deviation, and  $\alpha$ , we would have 90% chance of detecting a difference of 0.096924.

- HRRC

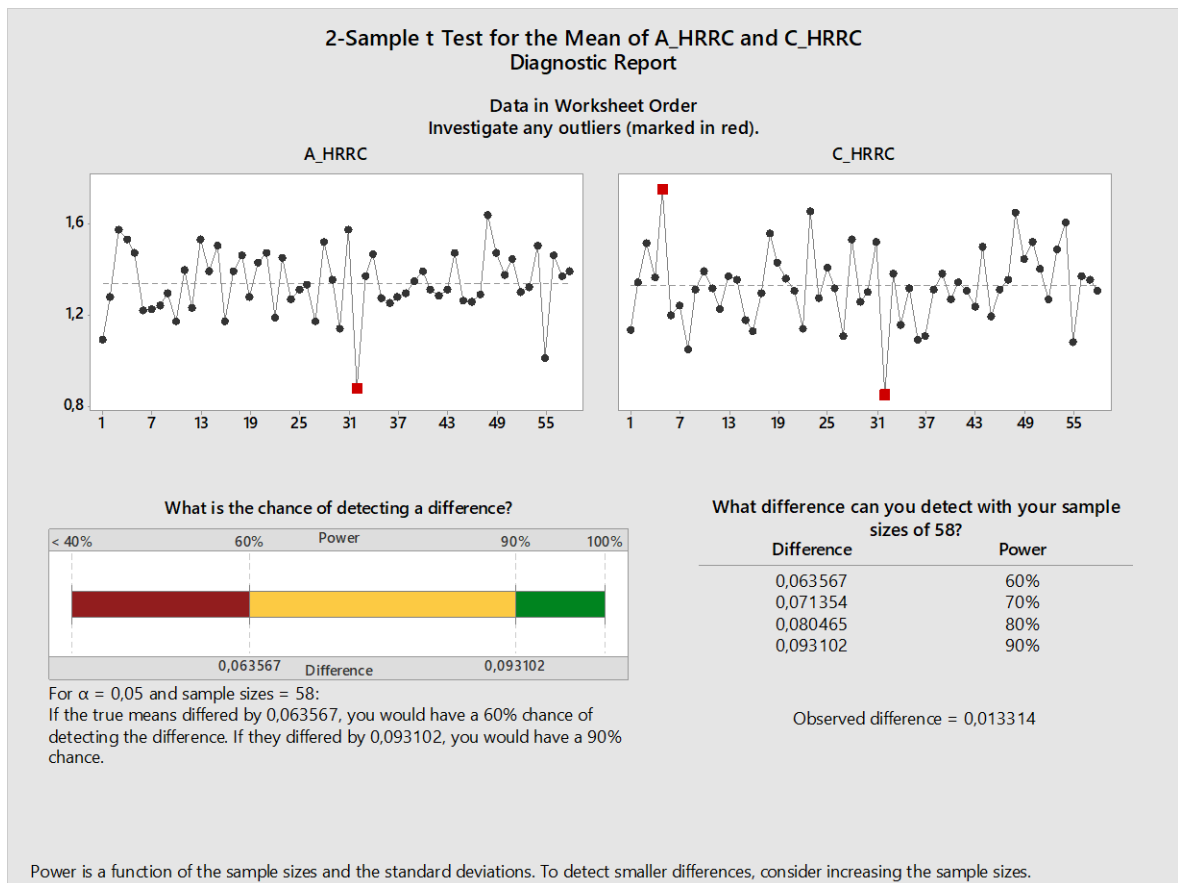
Test: there is not enough evidence to conclude that the means differ at the 0.05 level of significance.

CI: quantifies the uncertainty associated with estimating the difference in means from sample data. We can be 95% confident that the true difference is between -0.043108 and 0.069737.

Distribution of data: compare the location and means of samples.



Individual Samples		
Statistics	A_HRRC	C_HRRC
Sample size	58	58
Mean	1,3391	1,3258
95% CI	(1,302; 1,376)	(1,2827; 1,3689)
Standard deviation	0,14197	0,16391
Difference Between Samples		
Statistics	*Difference	
Difference	0,013314	
95% CI	(-0,043108; 0,069737)	
*Difference = A_HRRC - C_HRRC		



Report: some of the data points are unusual compared to the others in the same sample. Because unusual data can have a strong influence on the results, we should try to identify the cause of its unusual nature. These points are marked in red on the Diagnostic Report. Correct any data entry or measurement errors. Consider removing data that are associated with special causes and repeating the analysis.

Because both sample sizes are at least 15, **normality is not an issue**. The test is accurate with non-normal data when the sample sizes are large enough.

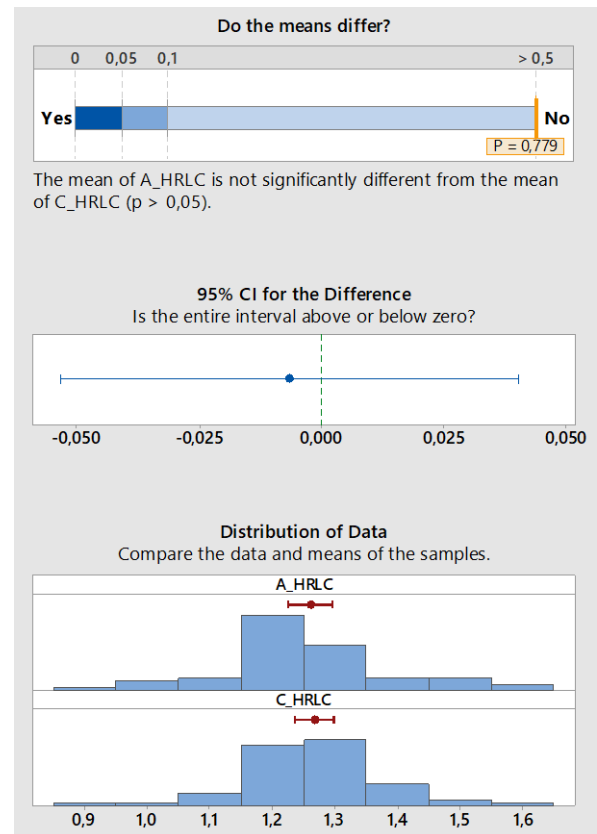
*Our data does not provide sufficient evidence to conclude that the mean of A\_HRRC differs from C\_HRRC.* This may result from having sample sizes that are too small. Based on our sample sizes, standard deviation, and  $\alpha$ , we would have 90% chance of detecting a difference of 0.093102.

- HRLC

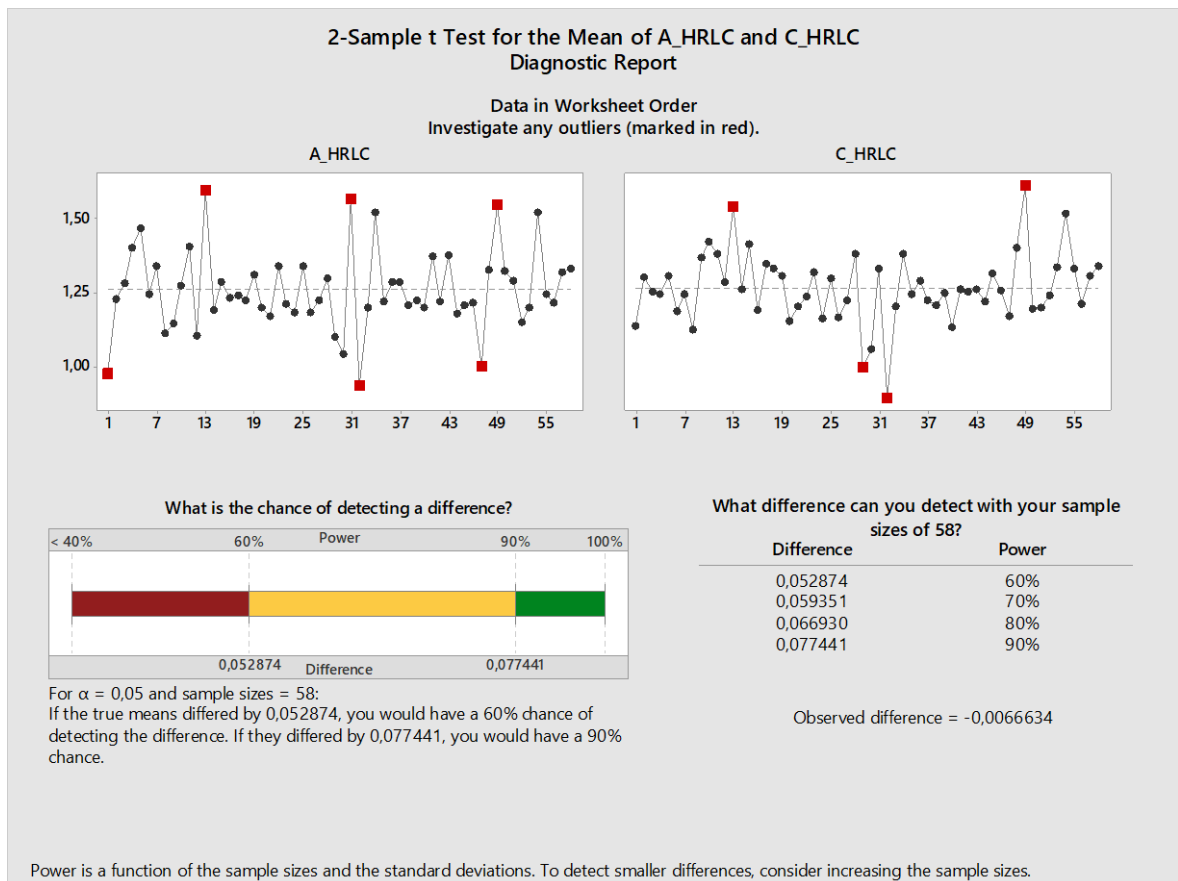
Test: there is not enough evidence to conclude that the means differ at the 0.05 level of significance.

CI: quantifies the uncertainty associated with estimating the difference in means from sample data. We can be 95% confident that the true difference is between -0.053592 and 0.040265.

Distribution of data: compare the location and means of samples.



Individual Samples		
Statistics	A_HRLC	C_HRLC
Sample size	58	58
Mean	1,2609	1,2675
95% CI	(1,225; 1,296)	(1,2362; 1,2989)
Standard deviation	0,13540	0,11918
Difference Between Samples		
Statistics	*Difference	
Difference	-0,0066634	
95% CI	(-0,053592; 0,040265)	
*Difference = A_HRLC - C_HRLC		



Report: some of the data points are unusual compared to the others in the same sample. Because unusual data can have a strong influence on the results, we should try to identify the cause of its unusual nature. These points are marked in red on the Diagnostic Report. Correct any data entry or measurement errors. Consider removing data that are associated with special causes and repeating the analysis.

Because both sample sizes are at least 15, **normality is not an issue**. The test is accurate with non-normal data when the sample sizes are large enough.

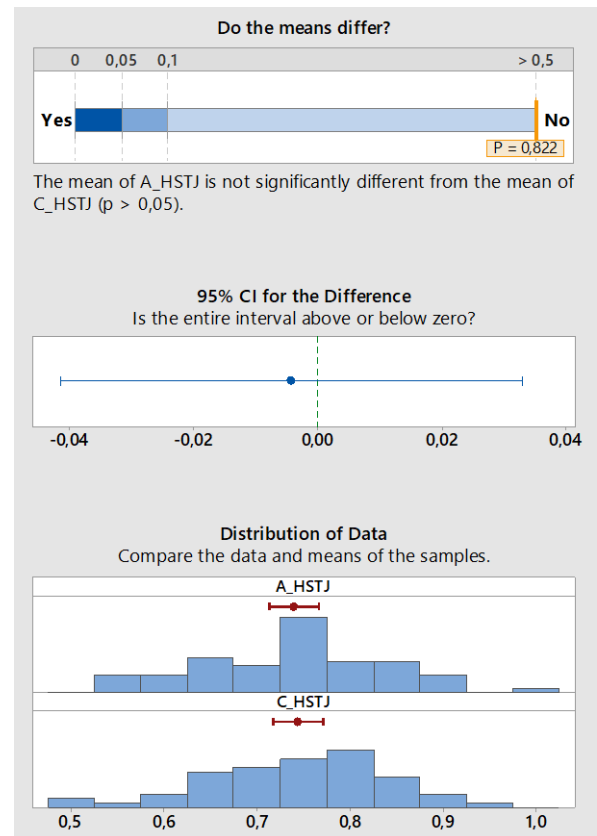
*Our data does not provide sufficient evidence to conclude that the mean of A\_HRRC differs from C\_HRRC.* This may result from having sample sizes that are too small. Based on our sample sizes, standard deviation, and  $\alpha$ , we would have 90% chance of detecting a difference of 0.077441.

- HSTJ

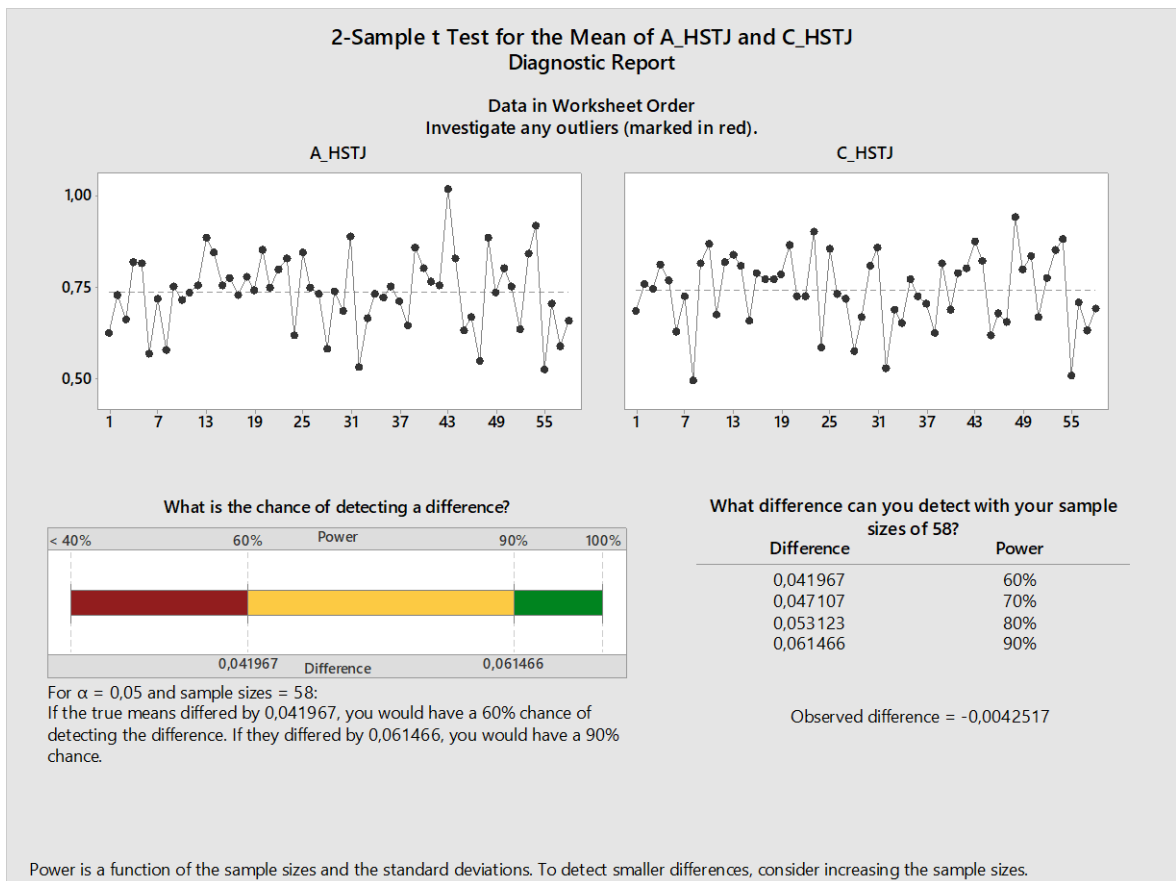
Test: there is not enough evidence to conclude that the means differ at the 0.05 level of significance.

CI: quantifies the uncertainty associated with estimating the difference in means from sample data. We can be 95% confident that the true difference is between -0.041501 and 0.032997.

Distribution of data: compare the location and means of samples.



Individual Samples		
Statistics	A_HSTJ	C_HSTJ
Sample size	58	58
Mean	0,73964	0,74389
95% CI	(0,7127; 0,7666)	(0,71757; 0,77021)
Standard deviation	0,10237	0,10012
Difference Between Samples		
Statistics	*Difference	
Difference	-0,0042517	
95% CI	(-0,041501; 0,032997)	
*Difference = A_HSTJ - C_HSTJ		



Report: there are no unusual data points. Unusual data can have a strong influence on the results. Because both sample size are at least 15, **normality is not an issue**. The test is accurate with non-normal data when the sample sizes are large enough.

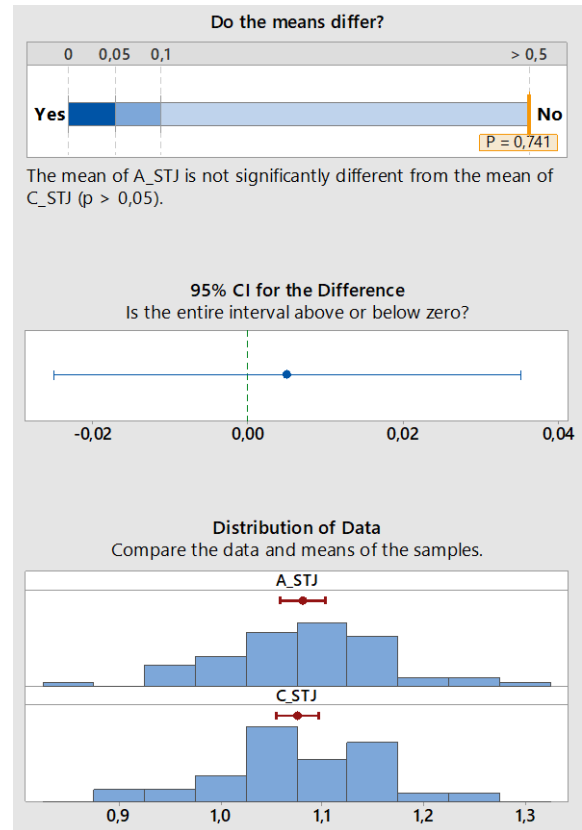
*Data does not provide sufficient evidence to conclude that the mean of A\_HSTJ differs from C\_HSTJ.* This may result from having sample sizes that are too small. Based on our sample sizes, standard deviation, and  $\alpha$ , we would have 90% chance of detecting a difference of 0.061466.

- STJ

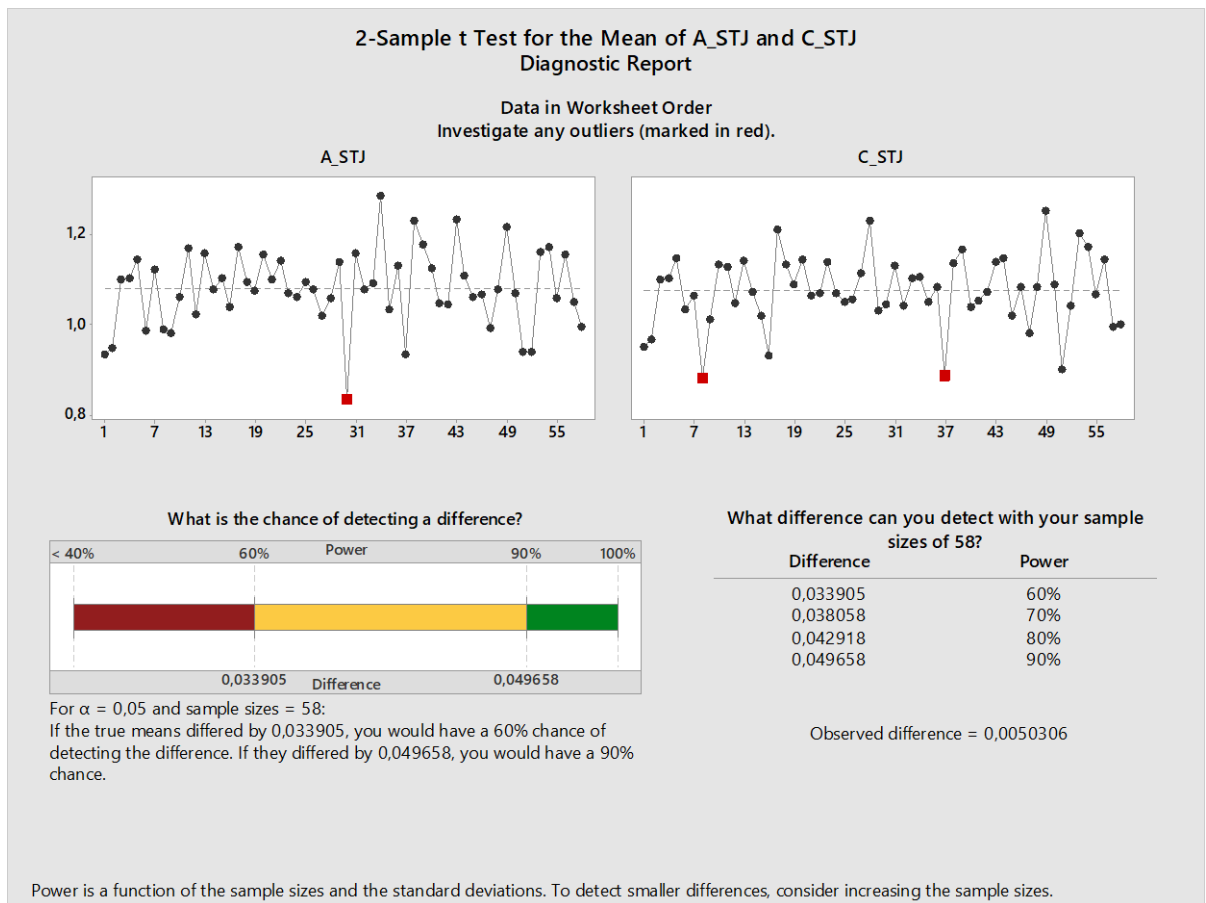
Test: there is not enough evidence to conclude that the means differ at the 0.05 level of significance.

CI: quantifies the uncertainty associated with estimating the difference in means from sample data. We can be 95% confident that the true difference is between -0.025062 and 0.035123.

Distribution of data: compare the location and means of samples.



Individual Samples		
Statistics	A_STJ	C_STJ
Sample size	58	58
Mean	1,0806	1,0755
95% CI	(1,058; 1,103)	(1,0548; 1,0963)
Standard deviation	0,084613	0,078878
Difference Between Samples		
Statistics	*Difference	
Difference	0,0050306	
95% CI	(-0,025062; 0,035123)	
*Difference = A_STJ - C_STJ		



Report: some of the data points are unusual compared to the others in the same sample. Because unusual data can have a strong influence on the results, we should try to identify the cause of its unusual nature. These points are marked in red on the Diagnostic Report. Correct any data entry or measurement errors. Consider removing data that are associated with special causes and repeating the analysis.

Because both sample sizes are at least 15, **normality is not an issue**. The test is accurate with non-normal data when the sample sizes are large enough.

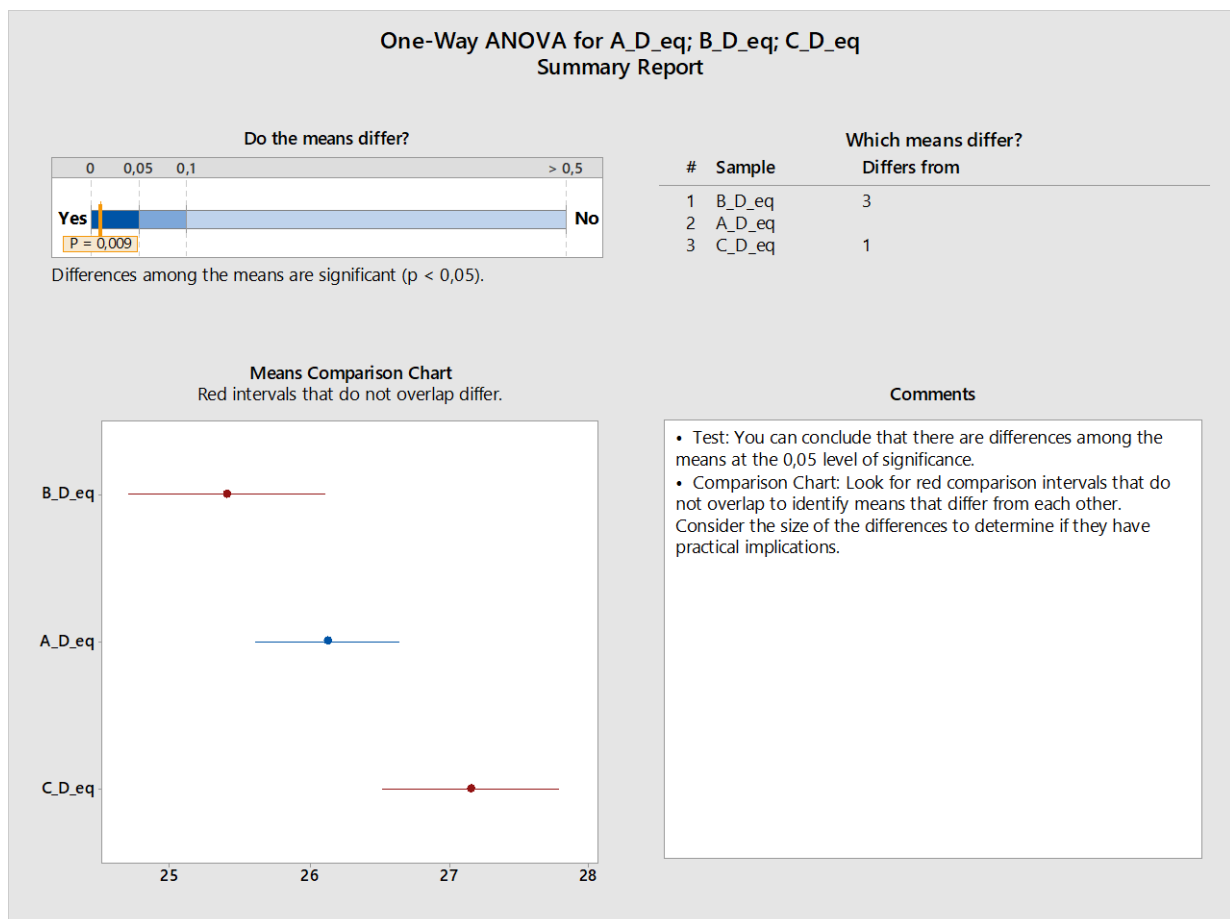
*Data does not provide sufficient evidence to conclude that the mean of A\_STJ differs from C\_STJ.* This may result from having sample sizes that are too small. Based on our sample sizes, standard deviation, and  $\alpha$ , we would have 90% chance of detecting a difference of 0.049658.

## 6.2 Analysis of variance (ANOVA)

Analysis of variance (ANOVA) is a collection of statistical models and their associated estimation procedures (such as the "variation" among and between groups) used to analyze the differences among group means in a sample. In the ANOVA setting, the observed variance in a particular variable is partitioned into components attributable to different sources of variation. In its simplest form, ANOVA provides a statistical test of whether the population means of several groups are equal, and therefore generalizes the t-test to more than two groups. ANOVA is useful for comparing (testing) three or more group means for statistical significance. It is conceptually similar to multiple two-sample t-tests, but is more conservative.

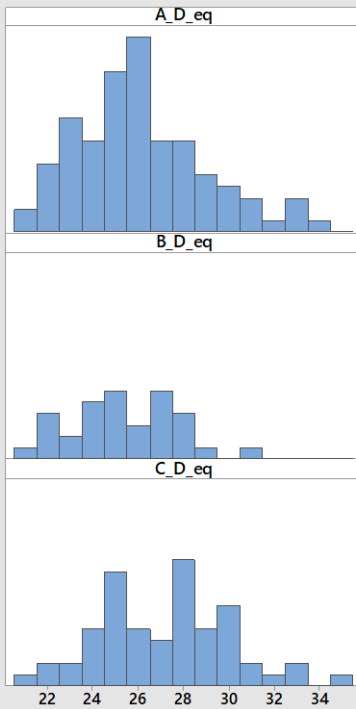
Here, I verified the variances among the parameters of interests calculated by operators A (me), B and C.

- D equivalent:

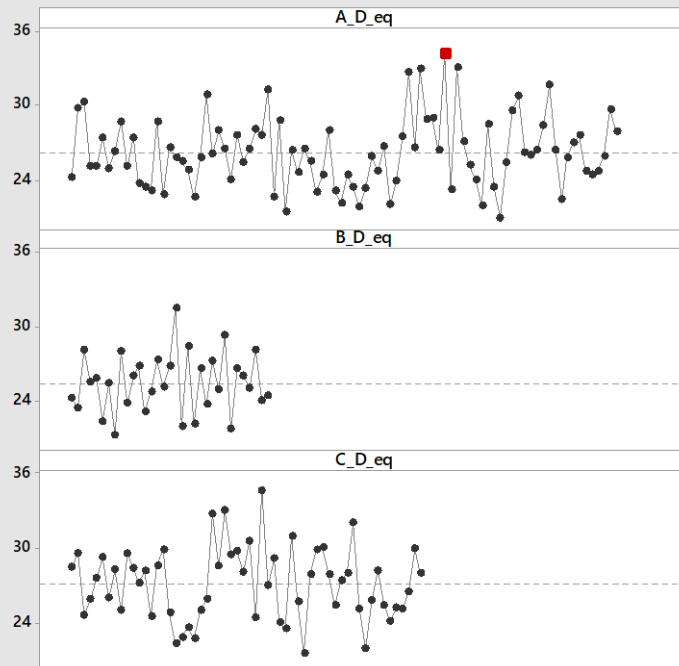


### One-Way ANOVA for A\_D\_eq; B\_D\_eq; C\_D\_eq Diagnostic Report

**Distribution of Data**  
Compare the location and spread.

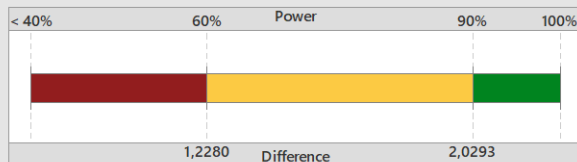


**Data in Worksheet Order**  
Investigate any outliers (marked in red).



### One-Way ANOVA for A\_D\_eq; B\_D\_eq; C\_D\_eq Power Report

What is the chance of detecting a difference?



Based on your samples and  $\alpha$  level (0,05), you have at least a 90% chance of detecting a difference of 2,0293, and at most a 60% chance of detecting a difference of 1,2280.

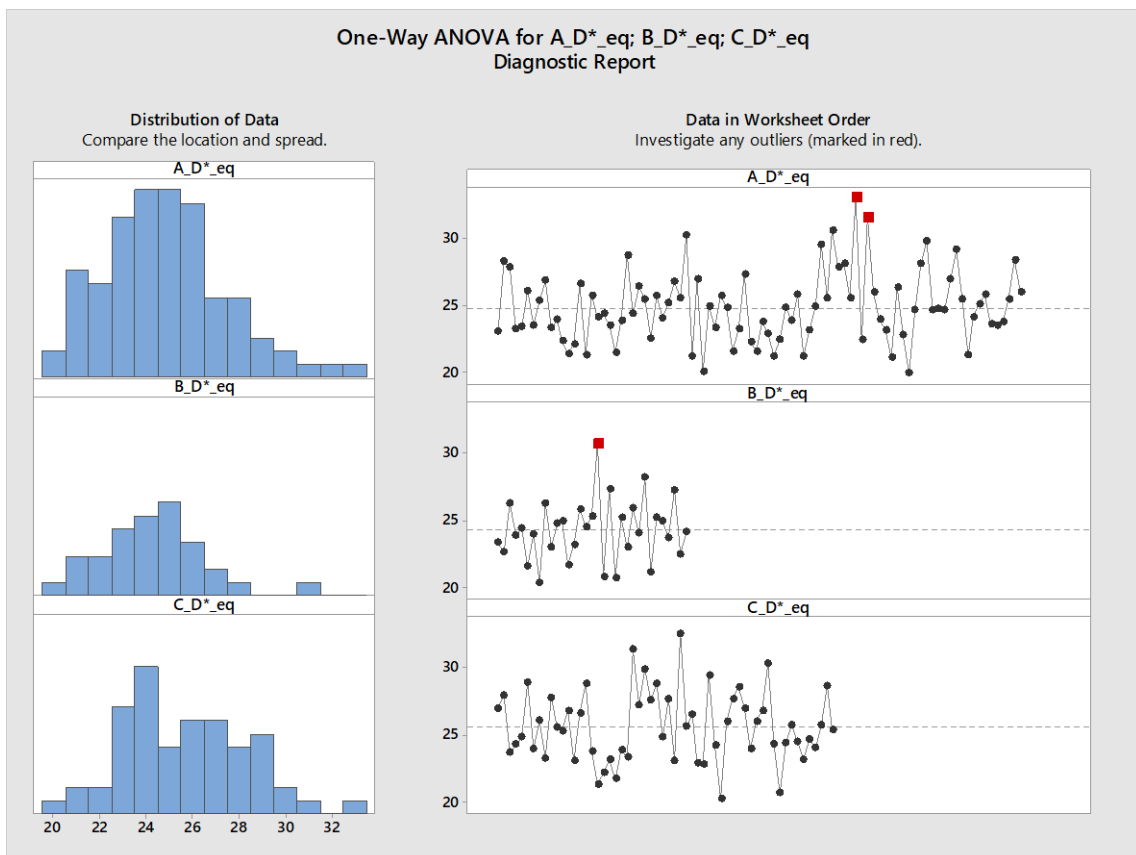
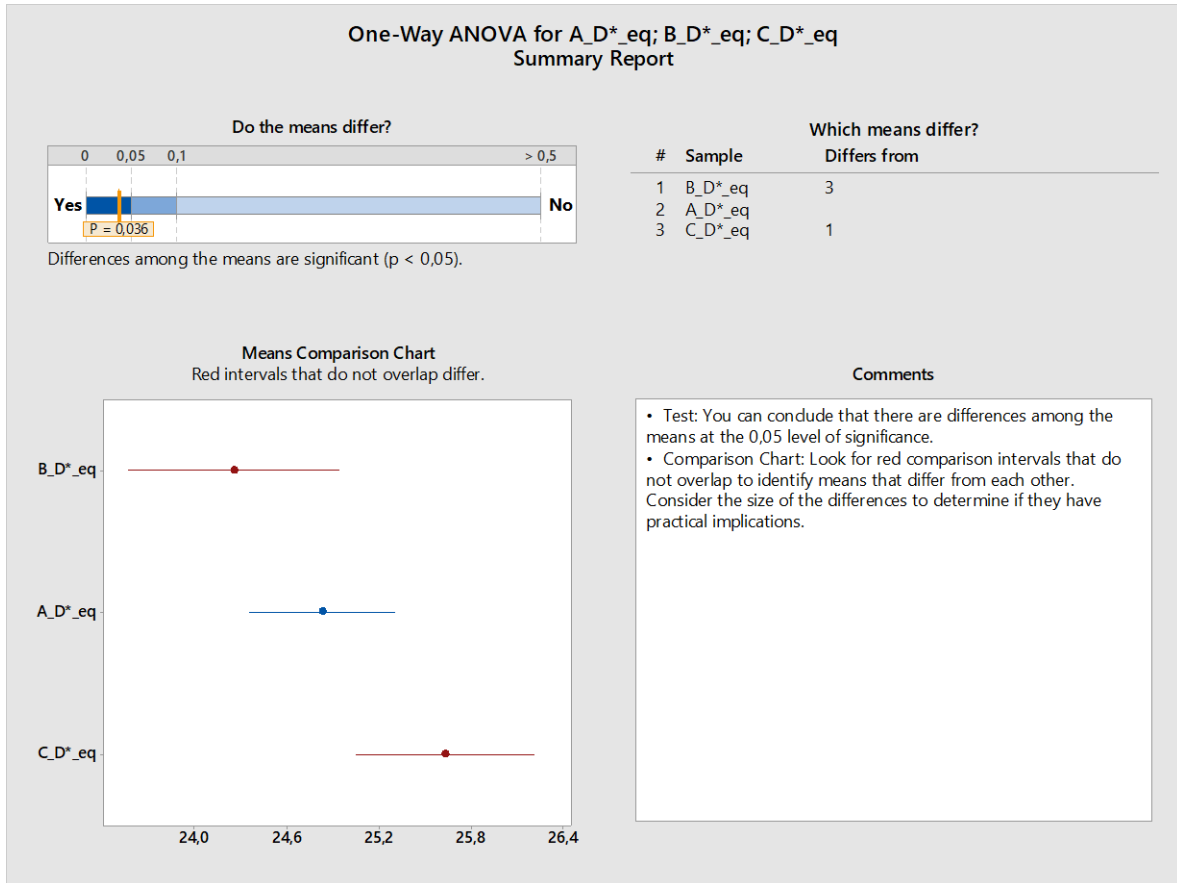
What difference can you detect with your sample sizes?

Difference	Power
1,2280	47,3 - 60,0%
1,4200	60,0 - 73,5%
1,5816	70,0 - 82,8%
1,7700	80,0 - 90,6%
2,0293	90,0 - 96,7%

Power is a function of the sample sizes and the standard deviations. To detect differences smaller than 1,7700, consider increasing the sample sizes.

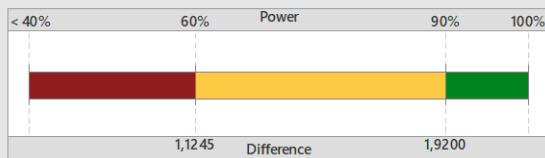
Sample	Sample Size	Statistics		Individual 95% CI for Mean
		Mean	Standard Deviation	
A_D_eq	90	26,124	2,8509	(25,527; 26,721)
B_D_eq	33	25,404	2,3693	(24,564; 26,244)
C_D_eq	58	27,149	2,9011	(26,386; 27,912)

- D\*equivalent:



### One-Way ANOVA for A\_D\*\_eq; B\_D\*\_eq; C\_D\*\_eq Power Report

What is the chance of detecting a difference?



Based on your samples and  $\alpha$  level (0,05), you have at least a 90% chance of detecting a difference of 1,9200, and at most a 60% chance of detecting a difference of 1,1245.

What difference can you detect with your sample sizes?

Difference	Power
1,1245	44,7 - 60,0%
1,3435	60,0 - 76,5%
1,4965	70,0 - 85,3%
1,6748	80,0 - 92,4%
1,9200	90,0 - 97,6%

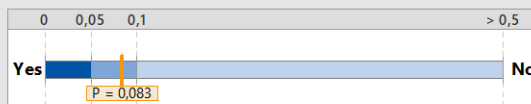
Power is a function of the sample sizes and the standard deviations. To detect differences smaller than 1,6748, consider increasing the sample sizes.

Sample	Sample Size	Statistics		
		Mean	Standard Deviation	Individual 95% CI for Mean
A_D*_eq	90	24,828	2,6118	(24,281; 25,375)
B_D*_eq	33	24,256	2,3013	(23,440; 25,072)
C_D*_eq	58	25,627	2,6540	(24,929; 26,324)

• e:

### One-Way ANOVA for A\_e; B\_e; C\_e Summary Report

Do the means differ?



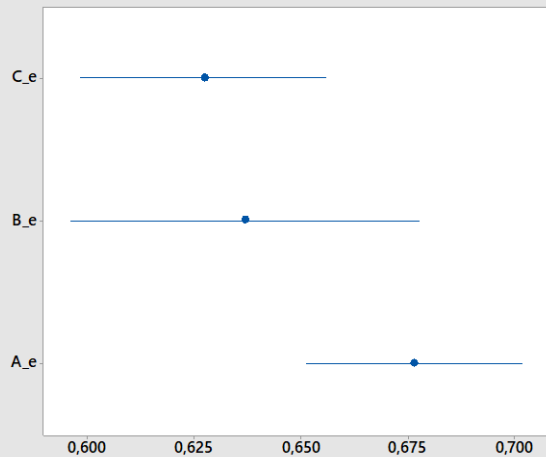
Differences among the means are not significant ( $p > 0,05$ ).

Which means differ?

#	Sample	Differs from
1	C_e	
2	B_e	None Identified
3	A_e	

Means Comparison Chart

Blue indicates there are no significant differences.

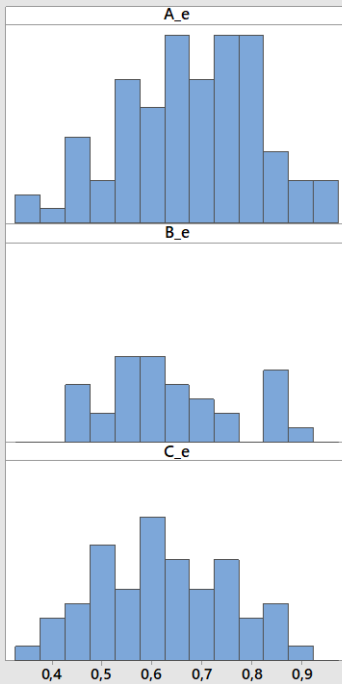


Comments

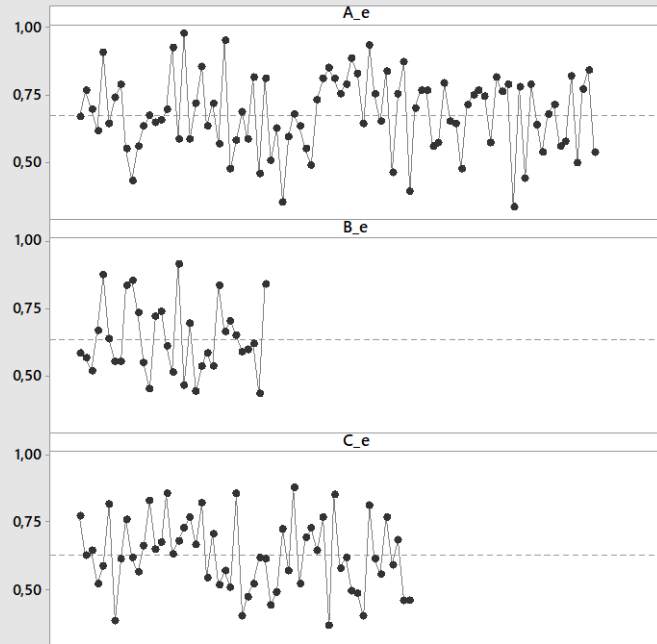
- Test: There is not enough evidence to conclude that there are differences among the means at the 0,05 level of significance.
- Comparison Chart: Blue intervals indicate that the means do not differ significantly.

### One-Way ANOVA for A\_e; B\_e; C\_e Diagnostic Report

**Distribution of Data**  
Compare the location and spread.

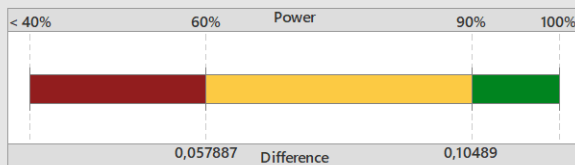


**Data in Worksheet Order**  
Investigate any outliers (marked in red).



### One-Way ANOVA for A\_e; B\_e; C\_e Power Report

What is the chance of detecting a difference?



Based on your samples and  $\alpha$  level (0,05), you have at least a 90% chance of detecting a difference of 0,10489, and at most a 60% chance of detecting a difference of 0,057887.

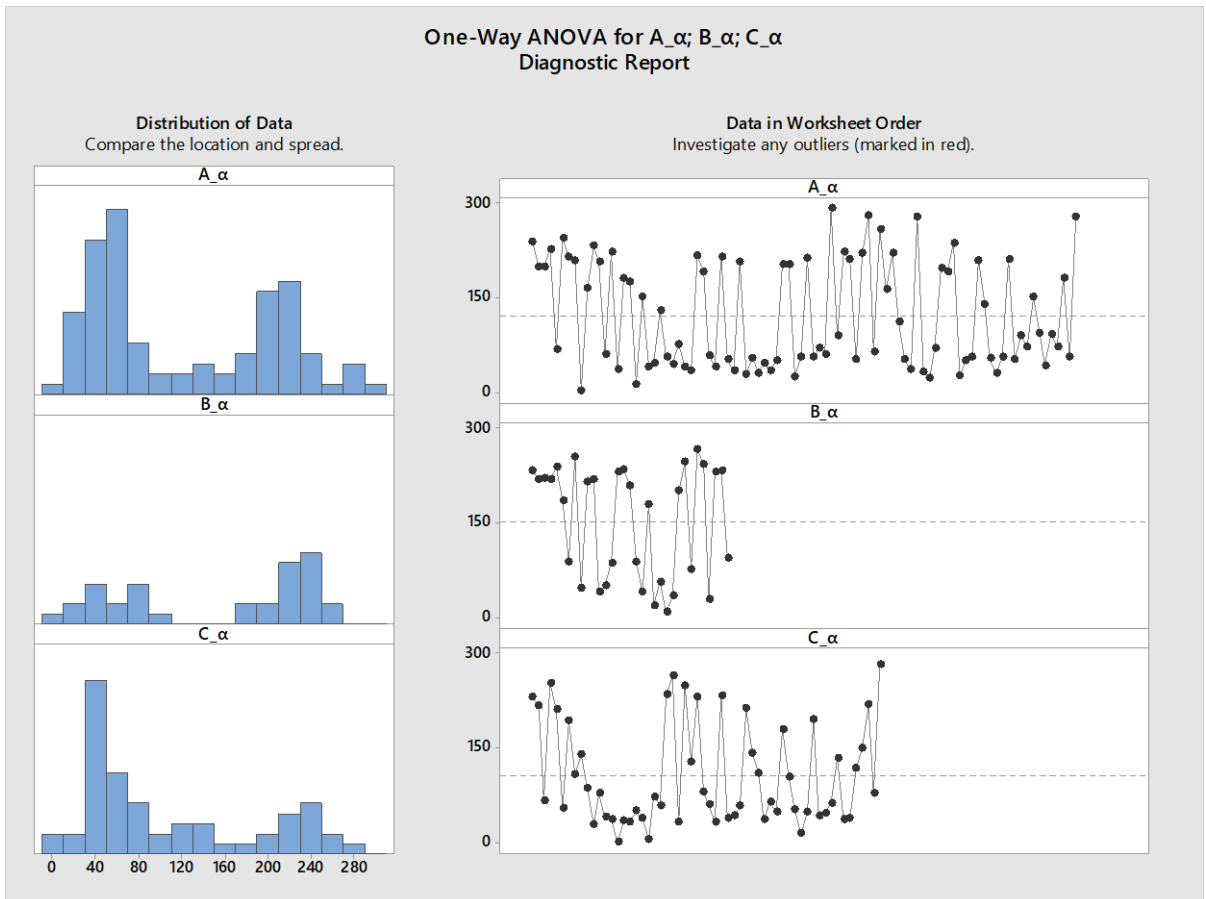
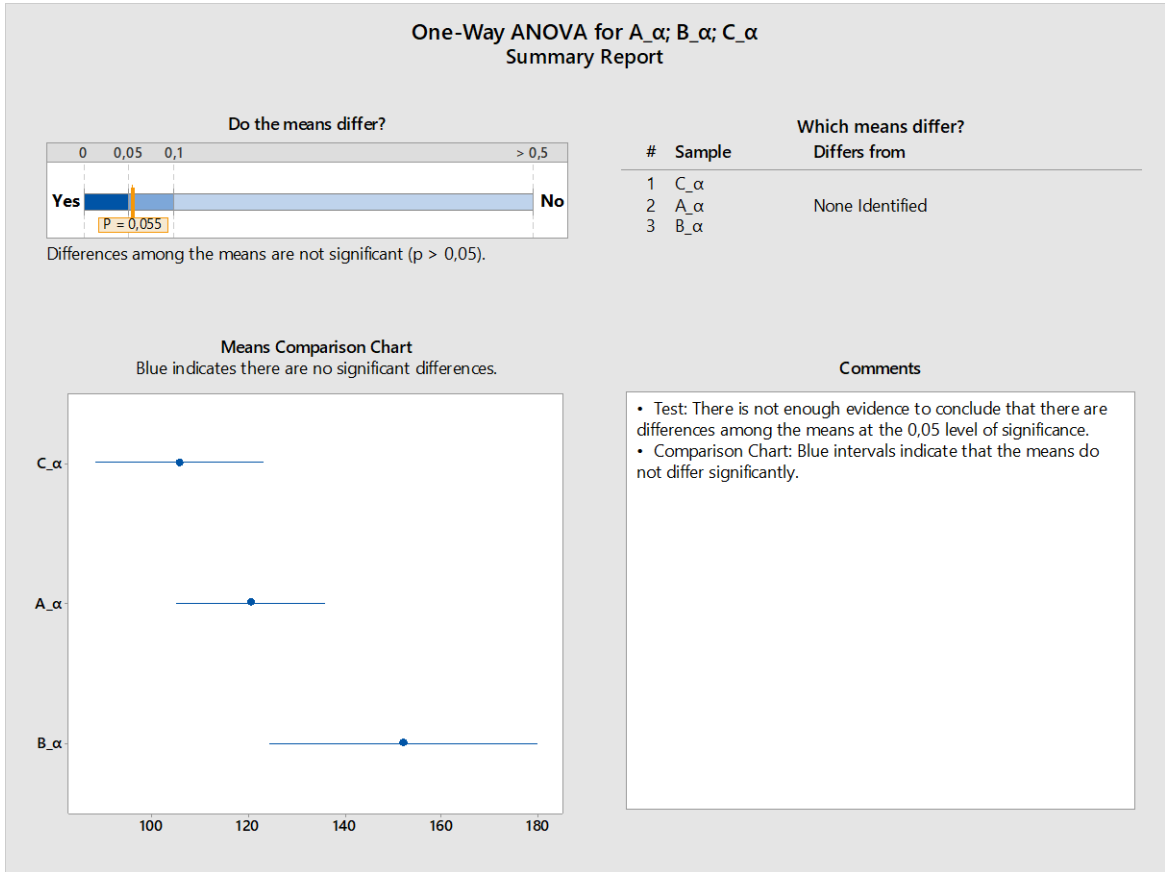
What difference can you detect with your sample sizes?

Difference	Power
0,057887	40,3 - 60,0%
0,073389	60,0 - 81,6%
0,081762	70,0 - 89,4%
0,091510	80,0 - 95,1%
0,10489	90,0 - 98,7%

Power is a function of the sample sizes and the standard deviations. To detect differences smaller than 0,091510, consider increasing the sample sizes.

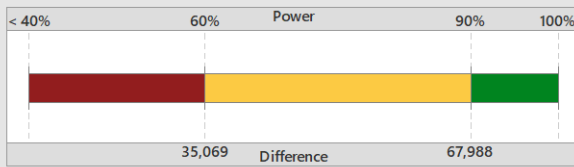
Sample	Sample Size	Statistics		
		Mean	Standard Deviation	Individual 95% CI for Mean
A_e	90	0,67623	0,14035	(0,64683; 0,70563)
B_e	33	0,63678	0,13304	(0,58961; 0,68395)
C_e	58	0,62710	0,13264	(0,59222; 0,66197)

- $\alpha$ :



### One-Way ANOVA for A\_α; B\_α; C\_α Power Report

What is the chance of detecting a difference?



Based on your samples and  $\alpha$  level (0,05), you have at least a 90% chance of detecting a difference of 67,988, and at most a 60% chance of detecting a difference of 35,069.

What difference can you detect with your sample sizes?

Difference	Power
35,069	35,8 - 60,0%
47,566	60,0 - 86,7%
53,000	70,0 - 93,2%
59,323	80,0 - 97,3%
67,988	90,0 - 99,5%

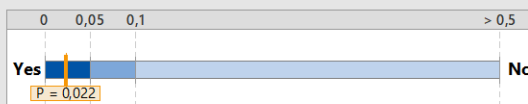
Power is a function of the sample sizes and the standard deviations. To detect differences smaller than 59,323, consider increasing the sample sizes.

Sample	Sample Size	Statistics		
		Mean	Standard Deviation	Individual 95% CI for Mean
A_α	90	120,39	84,455	(102,70; 138,08)
B_α	33	151,97	88,996	(120,41; 183,53)
C_α	58	105,71	80,640	(84,506; 126,91)

- HVS

### One-Way ANOVA for A\_HVS; B\_HVS; C\_HVS Summary Report

Do the means differ?

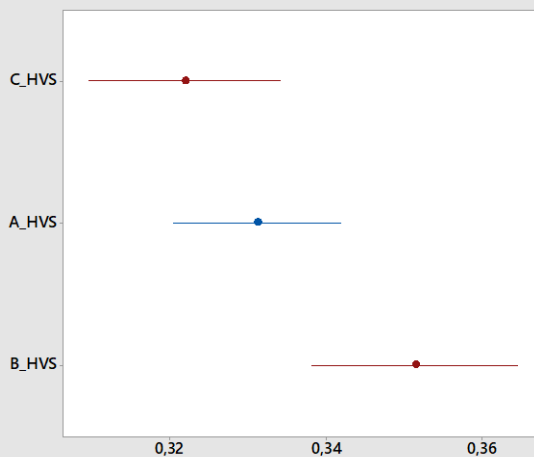


Differences among the means are significant ( $p < 0,05$ ).

Which means differ?

#	Sample	Differs from
1	C_HVS	3
2	A_HVS	
3	B_HVS	1

Means Comparison Chart  
Red intervals that do not overlap differ.

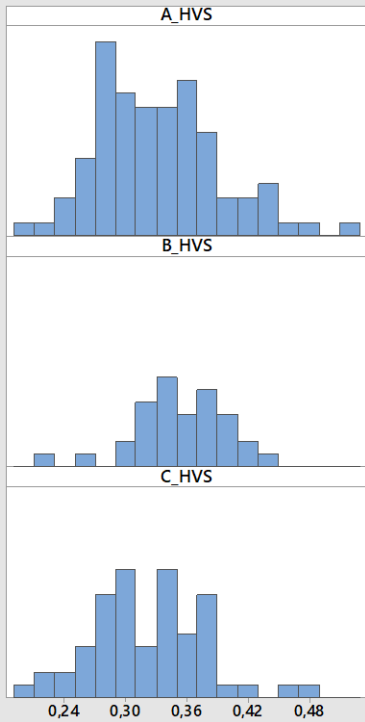


Comments

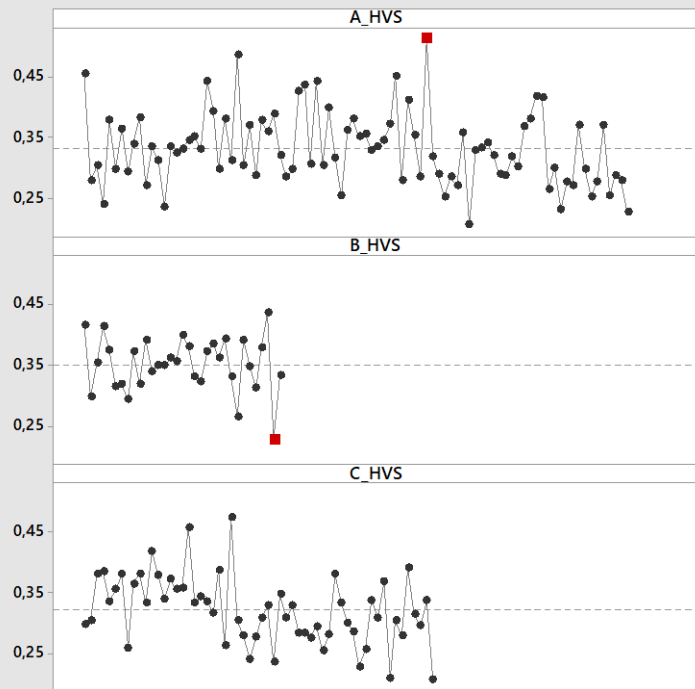
- Test: You can conclude that there are differences among the means at the 0,05 level of significance.
- Comparison Chart: Look for red comparison intervals that do not overlap to identify means that differ from each other. Consider the size of the differences to determine if they have practical implications.

### One-Way ANOVA for A\_HVS; B\_HVS; C\_HVS Diagnostic Report

**Distribution of Data**  
Compare the location and spread.

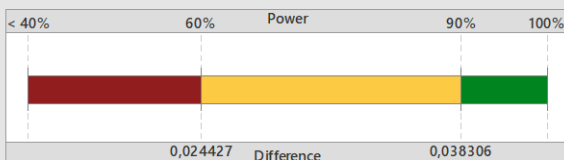


**Data in Worksheet Order**  
Investigate any outliers (marked in red).



### One-Way ANOVA for A\_HVS; B\_HVS; C\_HVS Power Report

What is the chance of detecting a difference?



Based on your samples and  $\alpha$  level (0,05), you have at least a 90% chance of detecting a difference of 0,038306, and at most a 60% chance of detecting a difference of 0,024427.

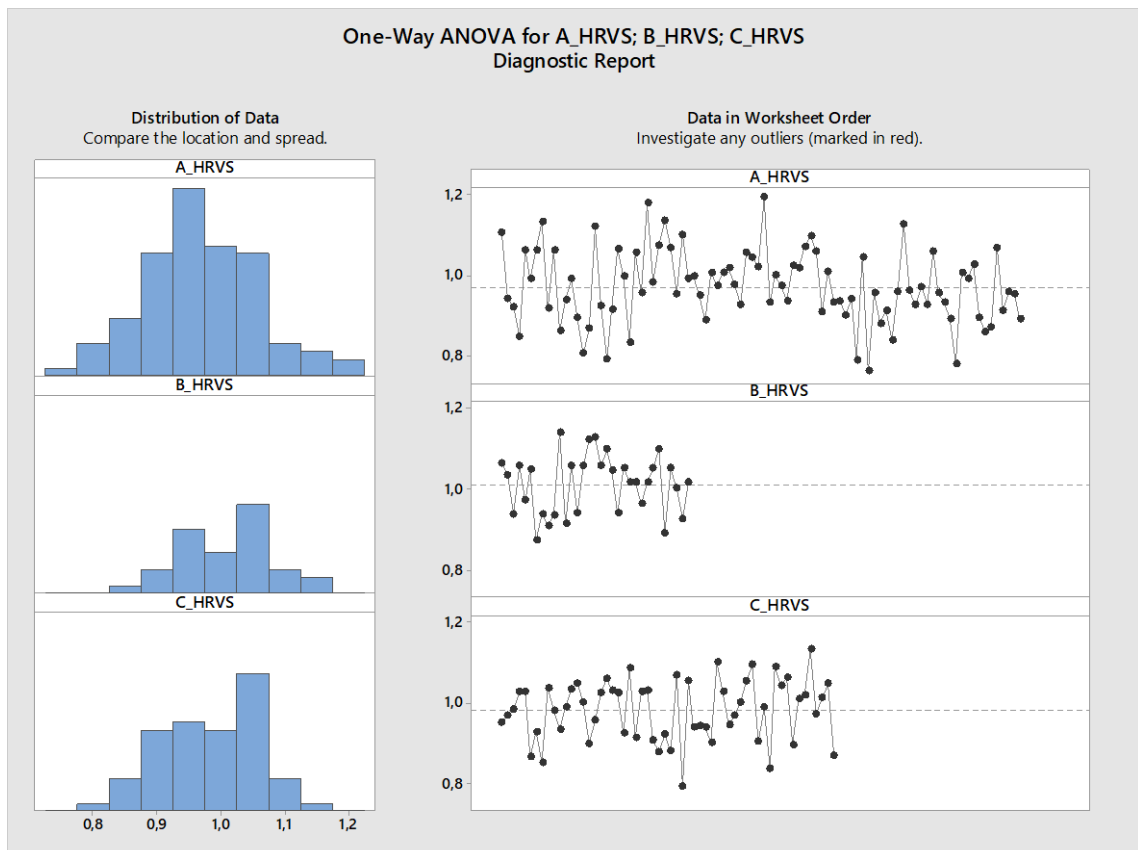
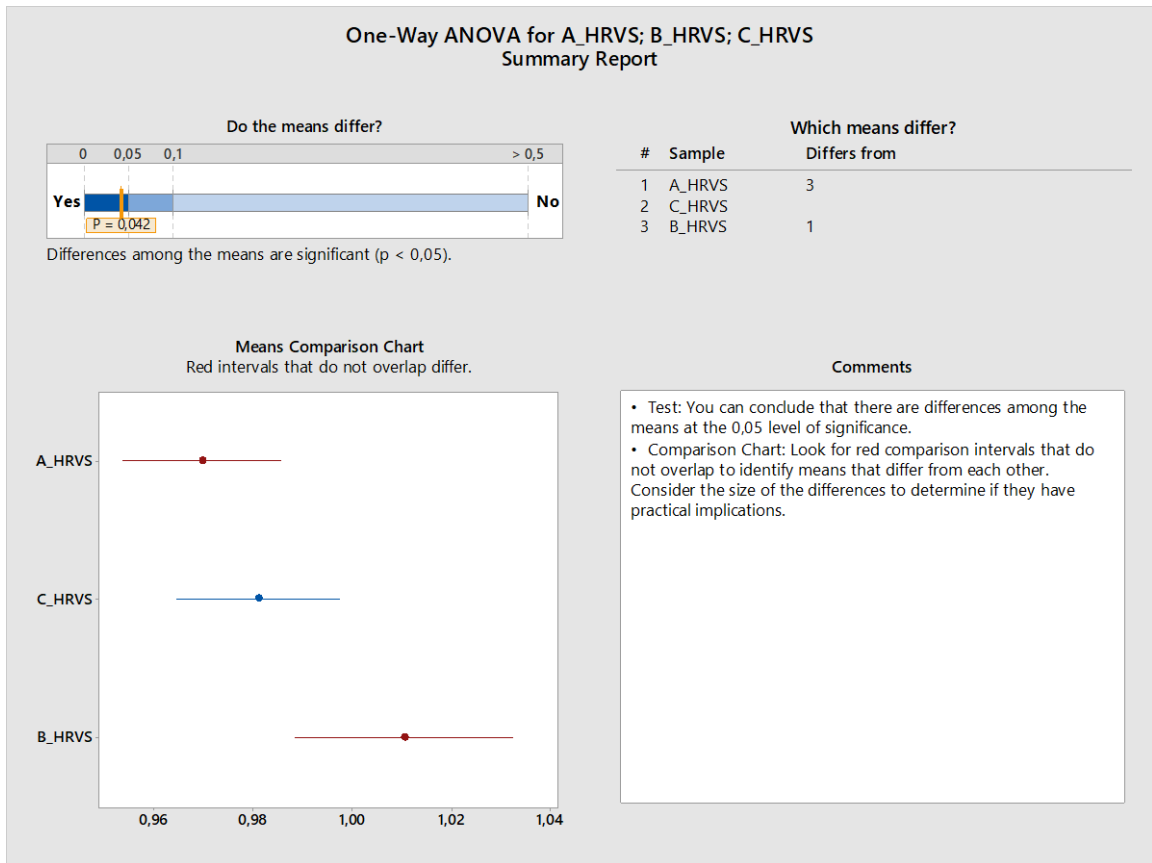
What difference can you detect with your sample sizes?

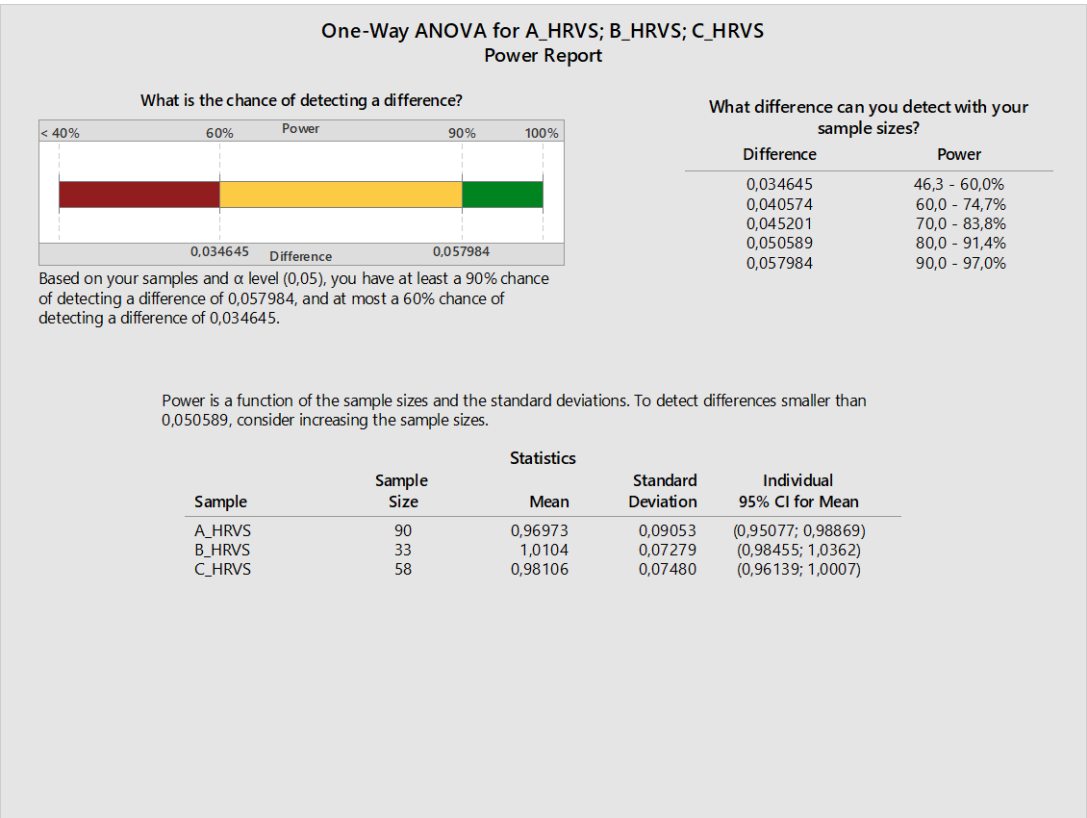
Difference	Power
0,024427	51,7 - 60,0%
0,026805	60,0 - 68,7%
0,029856	70,0 - 78,5%
0,033412	80,0 - 87,3%
0,038306	90,0 - 94,8%

Power is a function of the sample sizes and the standard deviations. To detect differences smaller than 0,033412, consider increasing the sample sizes.

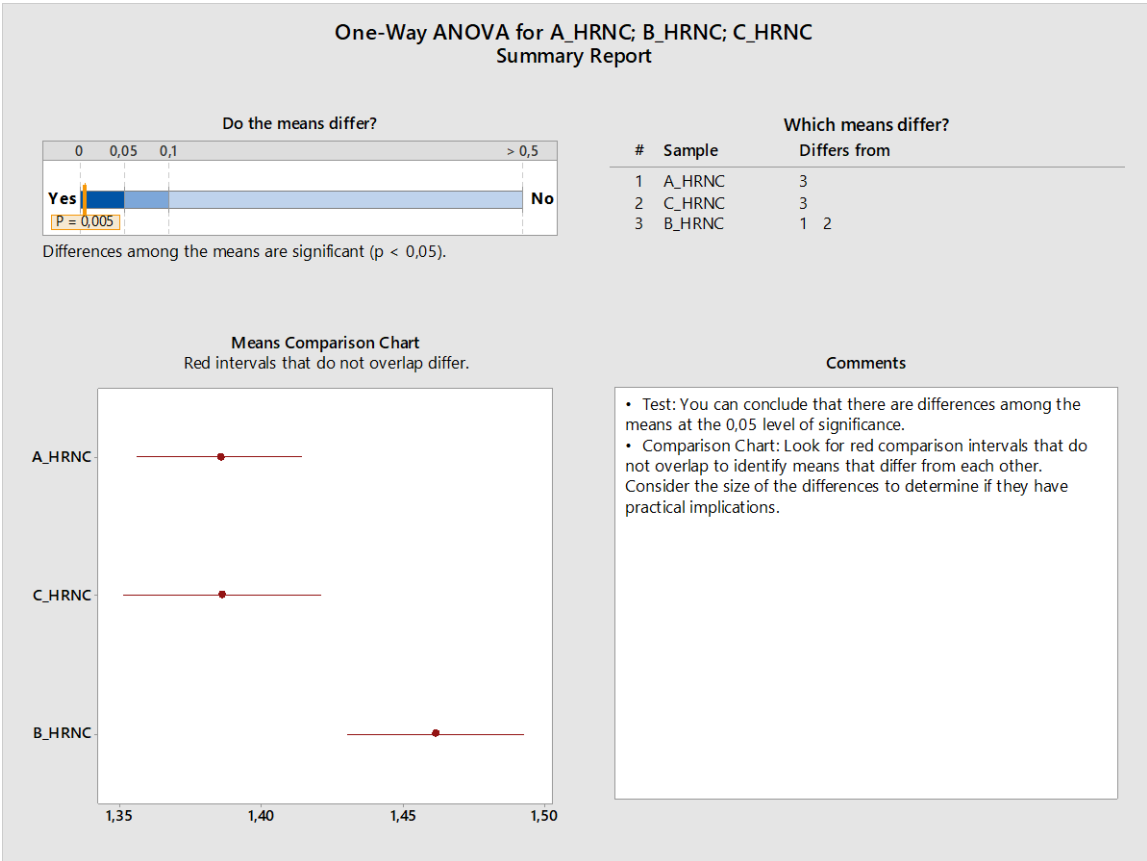
Sample	Sample Size	Statistics		
		Mean	Standard Deviation	Individual 95% CI for Mean
A_HVS	90	0,33122	0,06015	(0,31862; 0,34382)
B_HVS	33	0,35131	0,04424	(0,33563; 0,36700)
C_HVS	58	0,32196	0,05552	(0,30736; 0,33656)

- HRVS



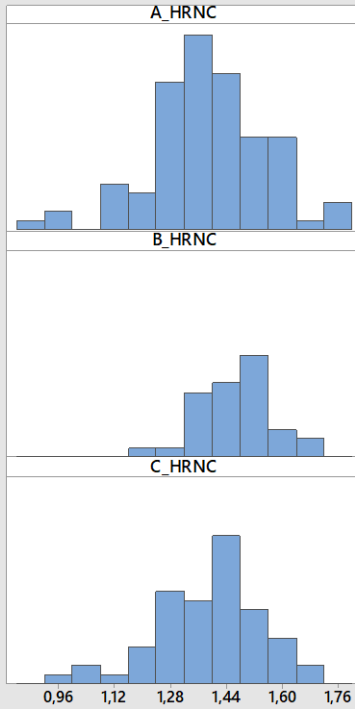


- HRNC

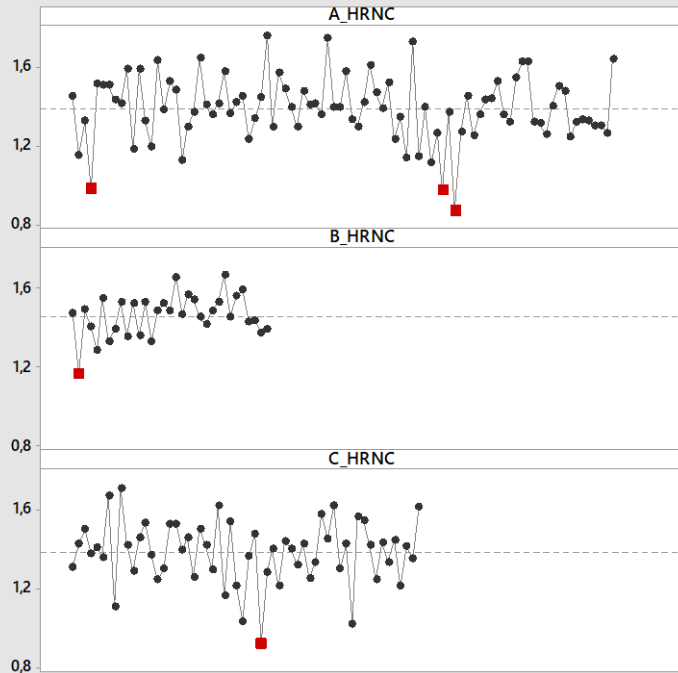


### One-Way ANOVA for A\_HRNC; B\_HRNC; C\_HRNC Diagnostic Report

**Distribution of Data**  
Compare the location and spread.

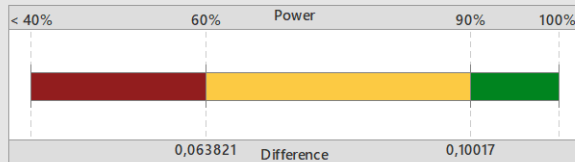


**Data in Worksheet Order**  
Investigate any outliers (marked in red).



### One-Way ANOVA for A\_HRNC; B\_HRNC; C\_HRNC Power Report

What is the chance of detecting a difference?



Based on your samples and  $\alpha$  level (0,05), you have at least a 90% chance of detecting a difference of 0,10017, and at most a 60% chance of detecting a difference of 0,063821.

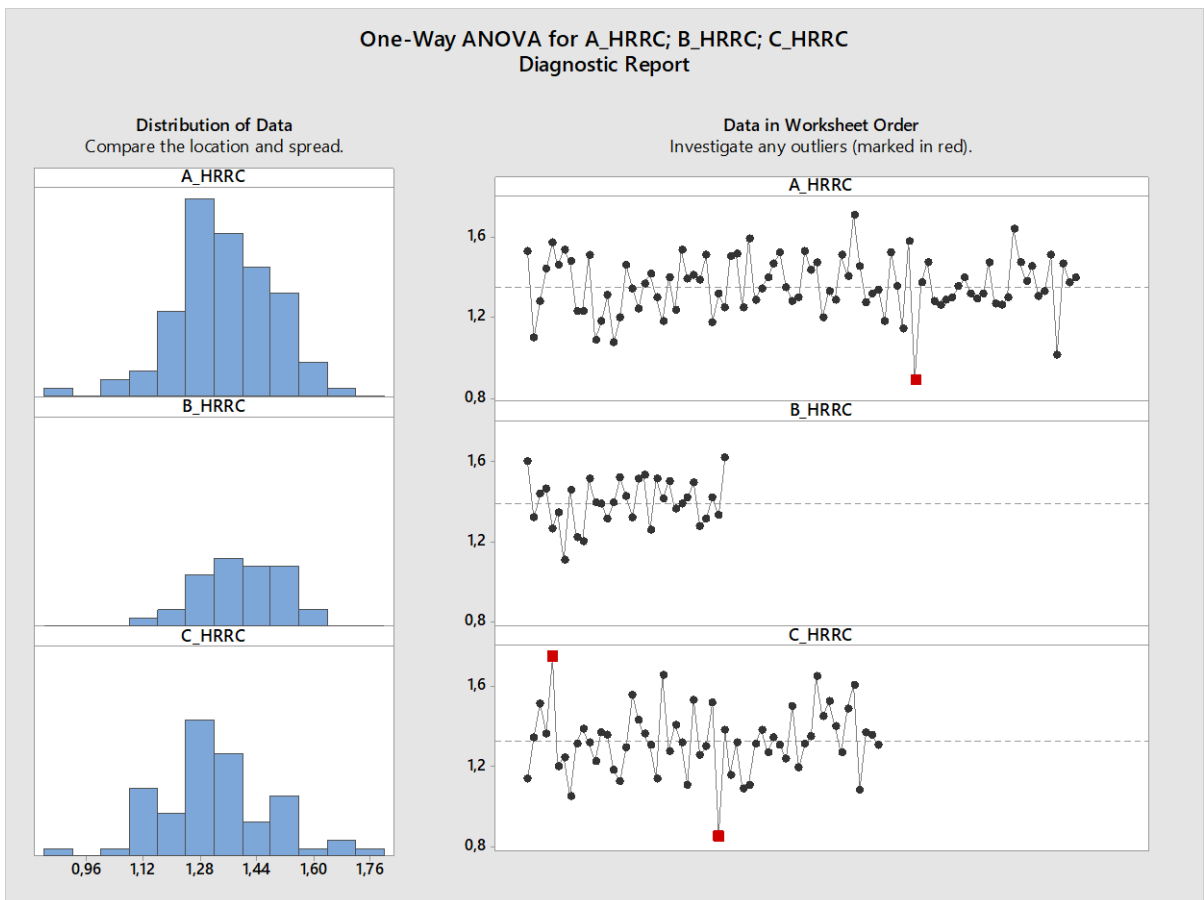
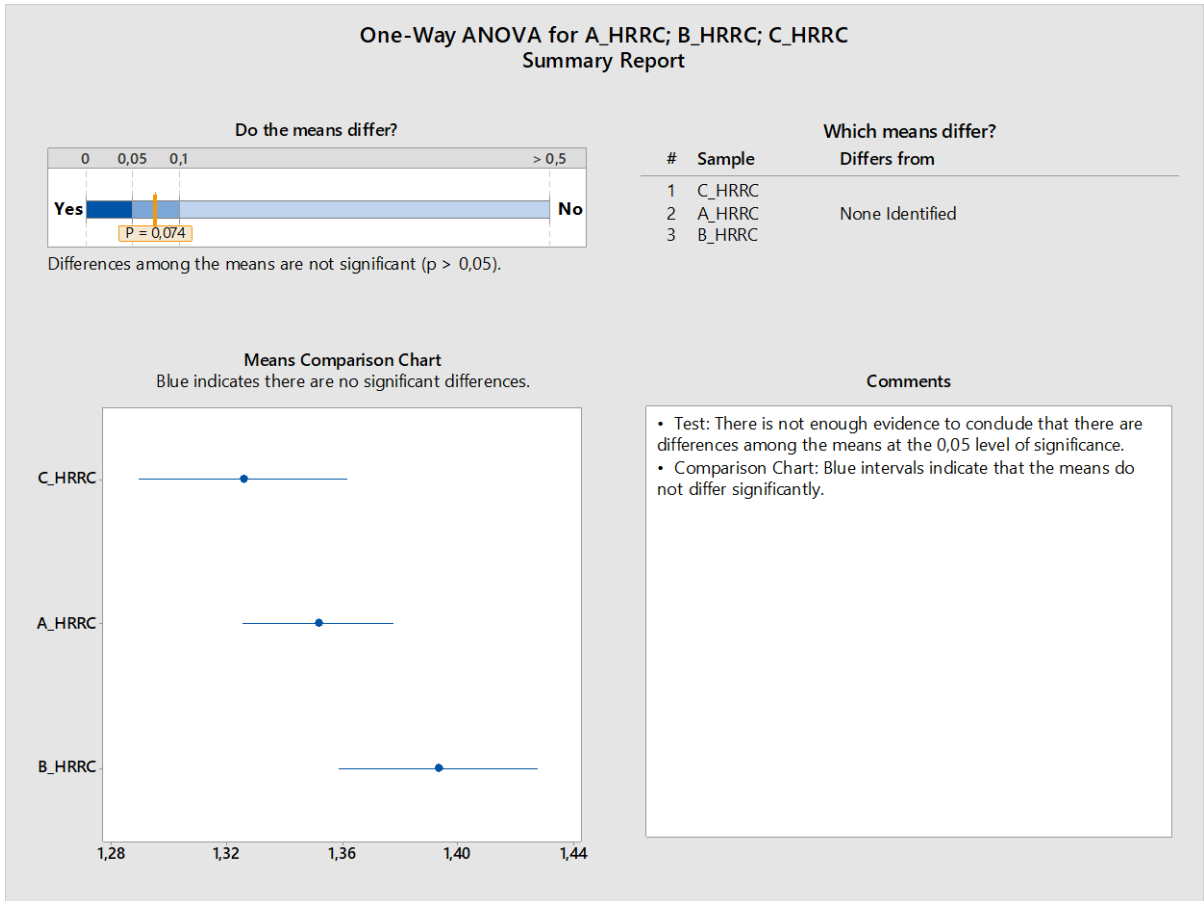
What difference can you detect with your sample sizes?

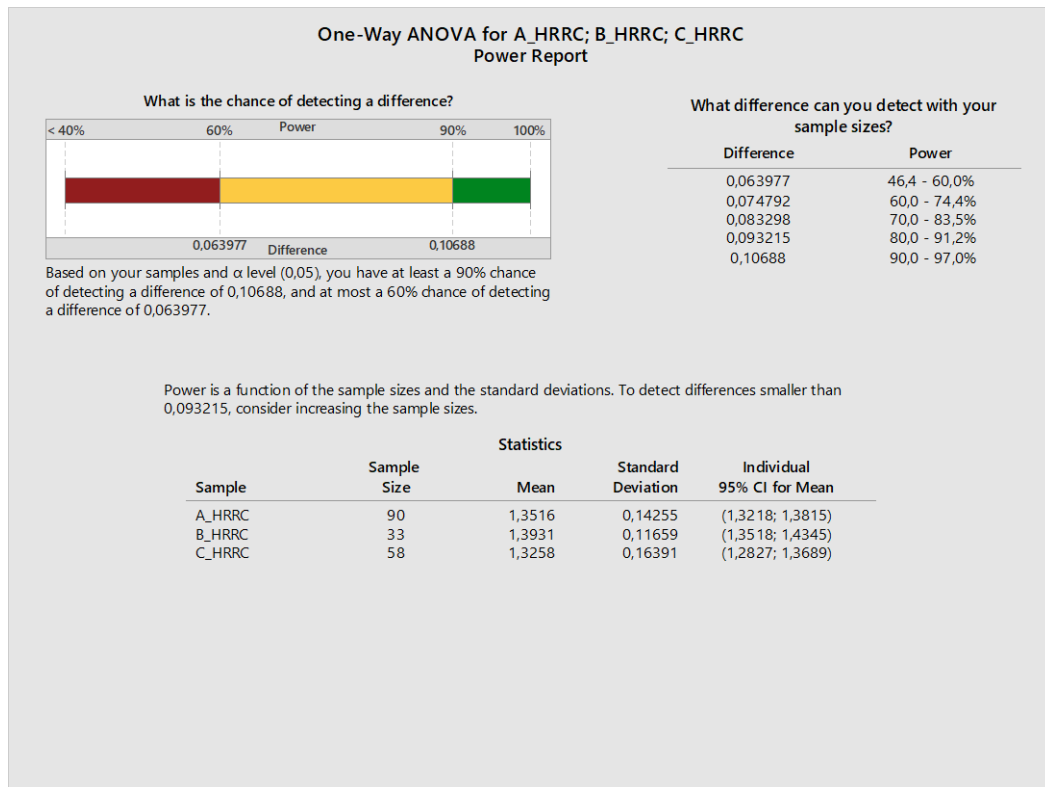
Difference	Power
0,063821	51,6 - 60,0%
0,070099	60,0 - 68,7%
0,078070	70,0 - 78,5%
0,087363	80,0 - 87,3%
0,10017	90,0 - 94,8%

Power is a function of the sample sizes and the standard deviations. To detect differences smaller than 0,087363, consider increasing the sample sizes.

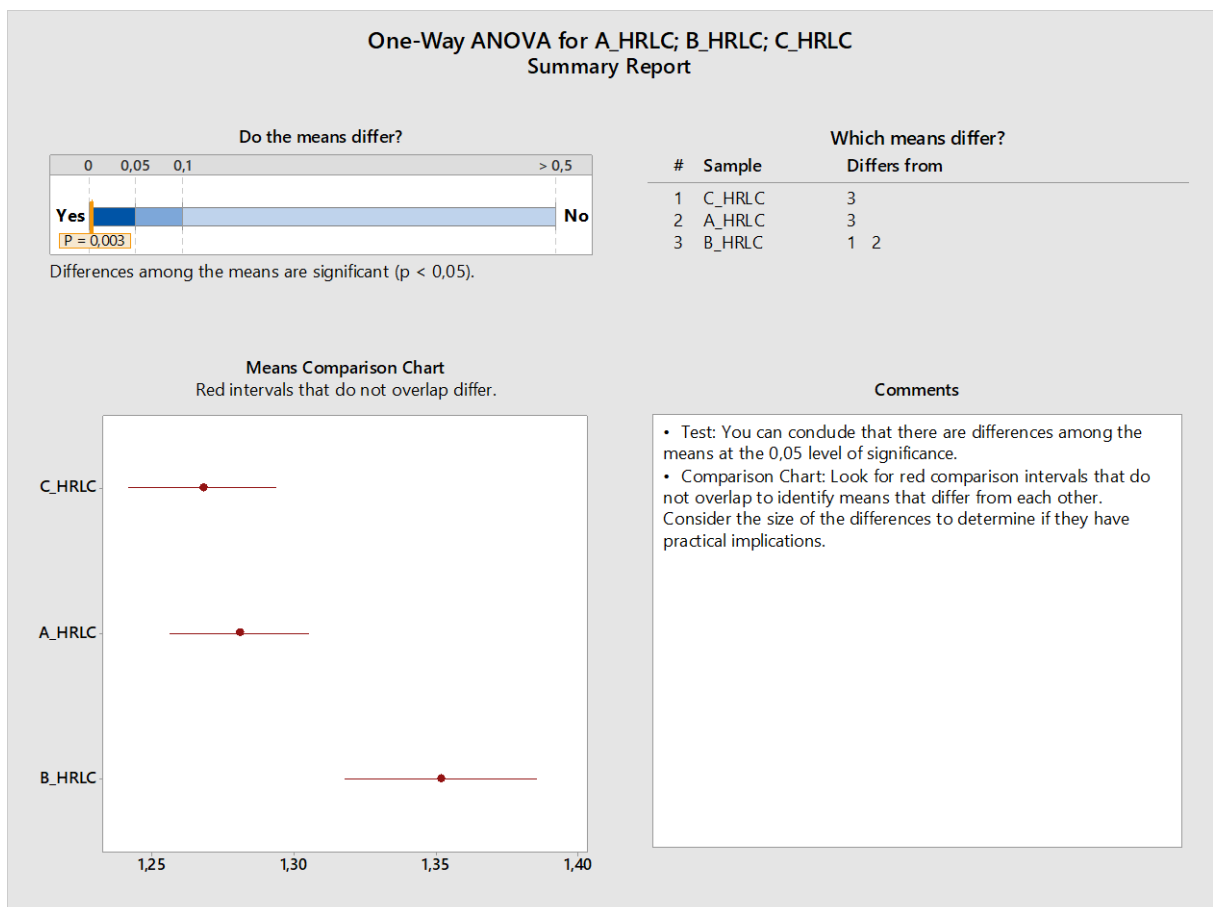
Sample	Sample Size	Statistics		
		Mean	Standard Deviation	Individual 95% CI for Mean
A_HRNC	90	1,3851	0,16398	(1,3508; 1,4195)
B_HRNC	33	1,4612	0,10576	(1,4237; 1,4987)
C_HRNC	58	1,3858	0,15821	(1,3442; 1,4274)

- HRRC



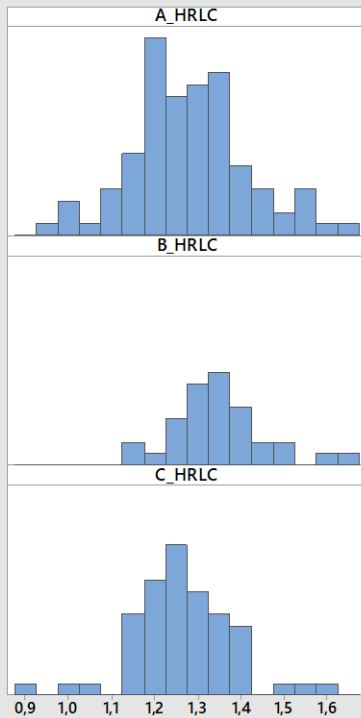


- HRLC

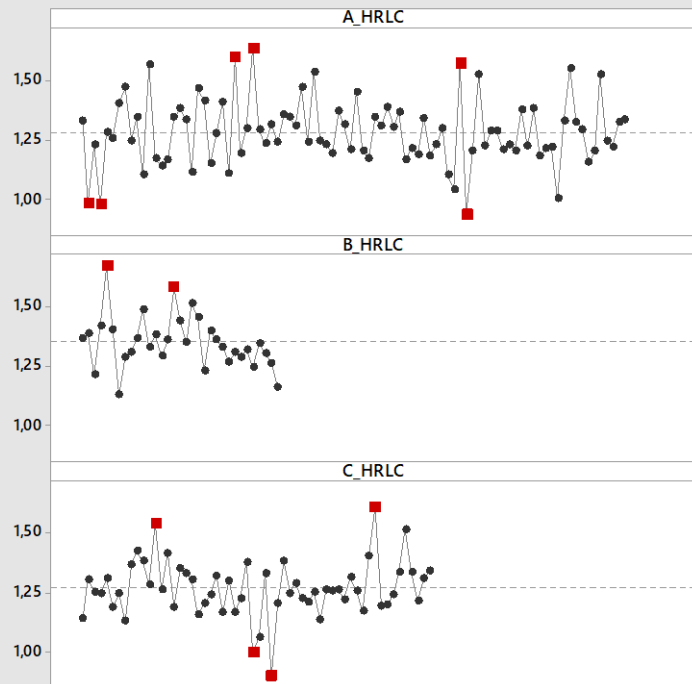


### One-Way ANOVA for A\_HRLC; B\_HRLC; C\_HRLC Diagnostic Report

**Distribution of Data**  
Compare the location and spread.

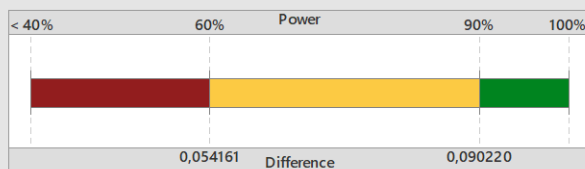


**Data in Worksheet Order**  
Investigate any outliers (marked in red).



### One-Way ANOVA for A\_HRLC; B\_HRLC; C\_HRLC Power Report

What is the chance of detecting a difference?



Based on your samples and  $\alpha$  level (0,05), you have at least a 90% chance of detecting a difference of 0,090220, and at most a 60% chance of detecting a difference of 0,054161.

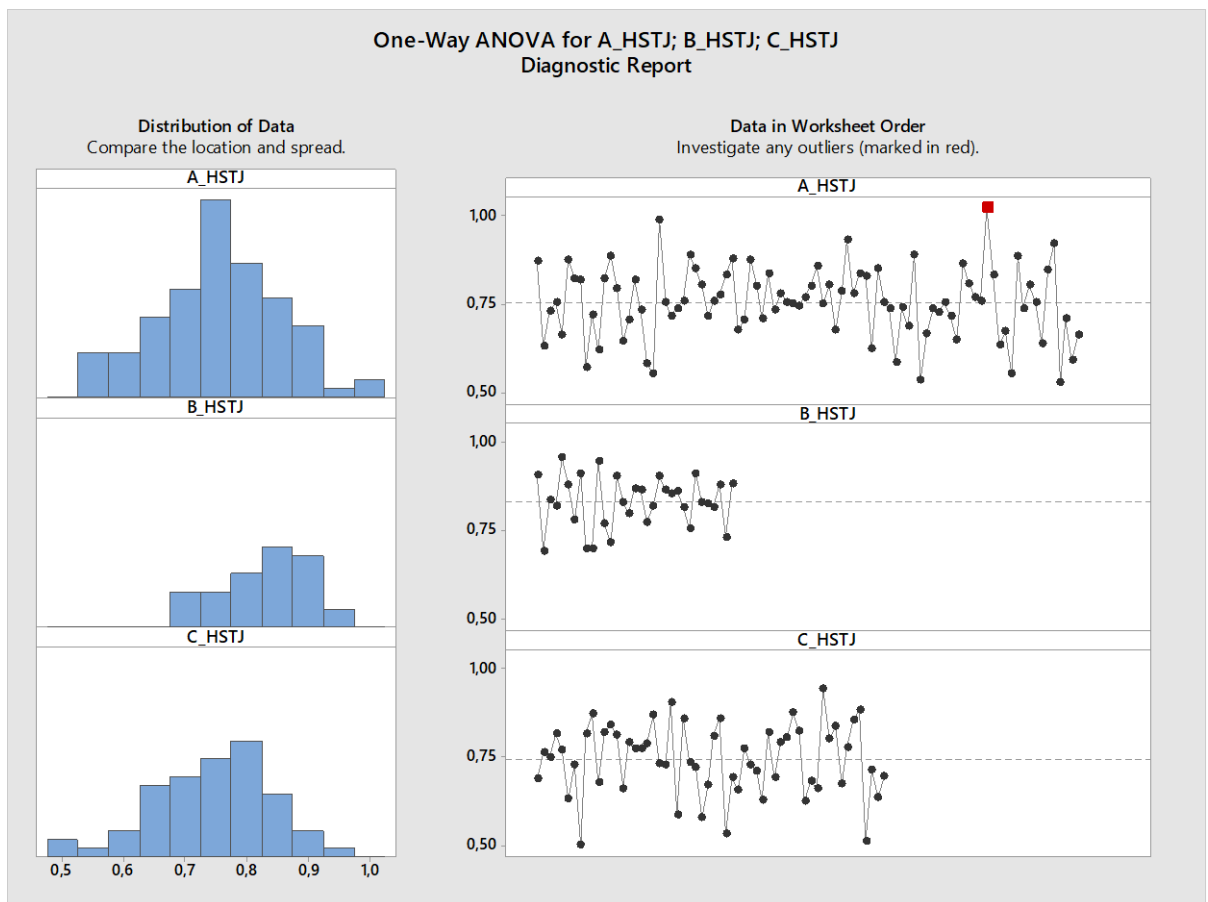
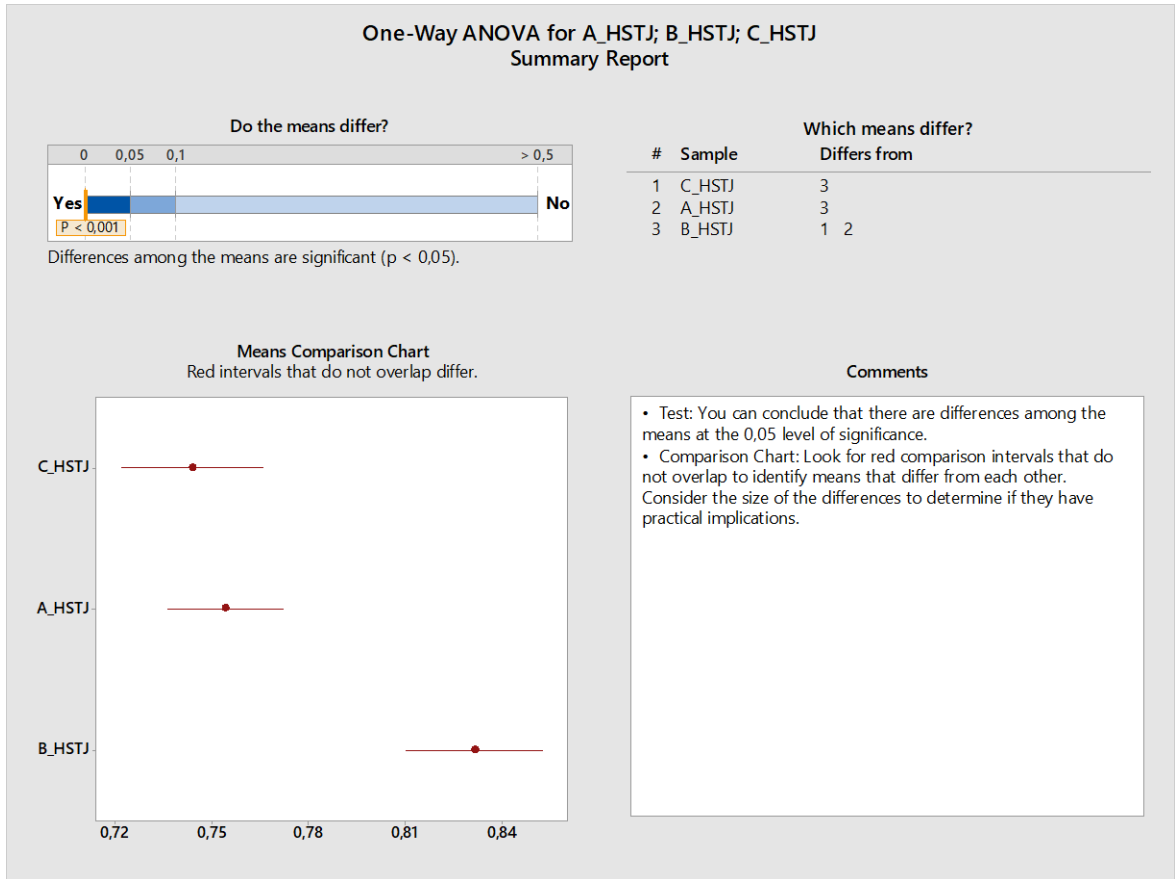
What difference can you detect with your sample sizes?

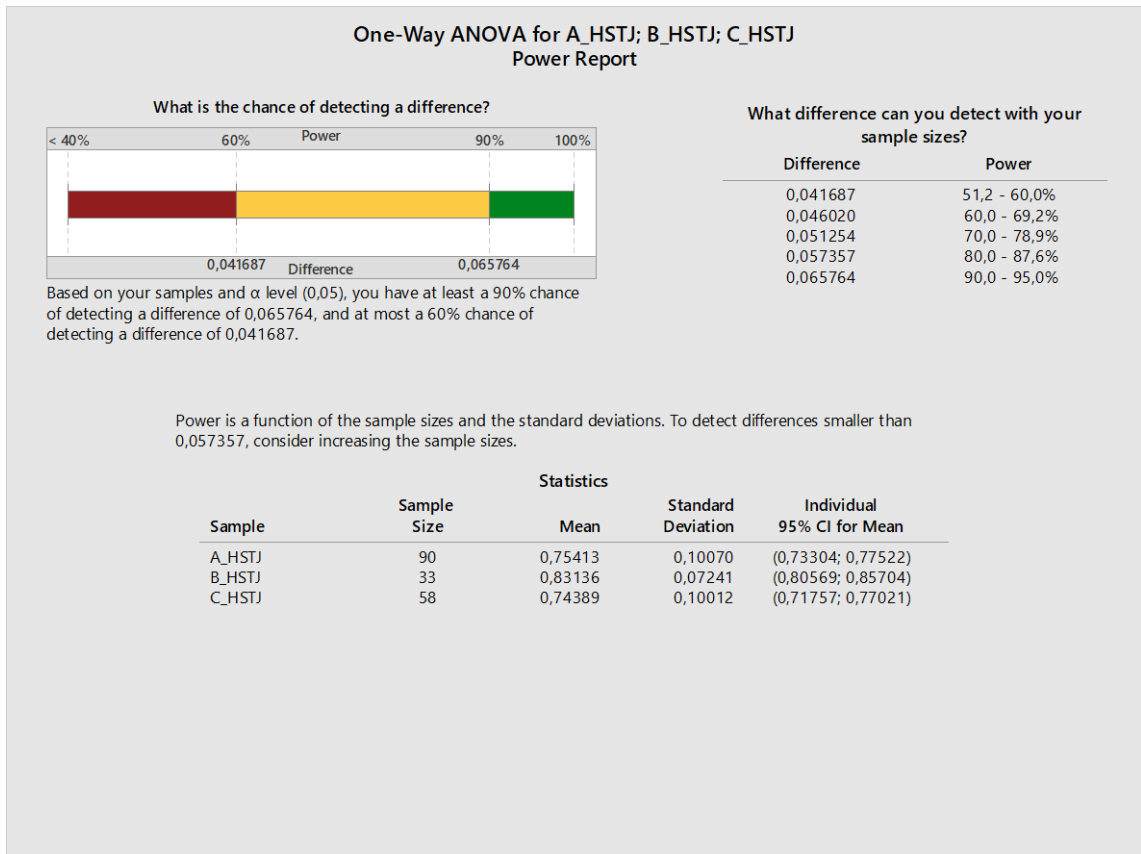
Difference	Power
0,054161	46,7 - 60,0%
0,063130	60,0 - 74,3%
0,070327	70,0 - 83,5%
0,078708	80,0 - 91,1%
0,090220	90,0 - 96,9%

Power is a function of the sample sizes and the standard deviations. To detect differences smaller than 0,078708, consider increasing the sample sizes.

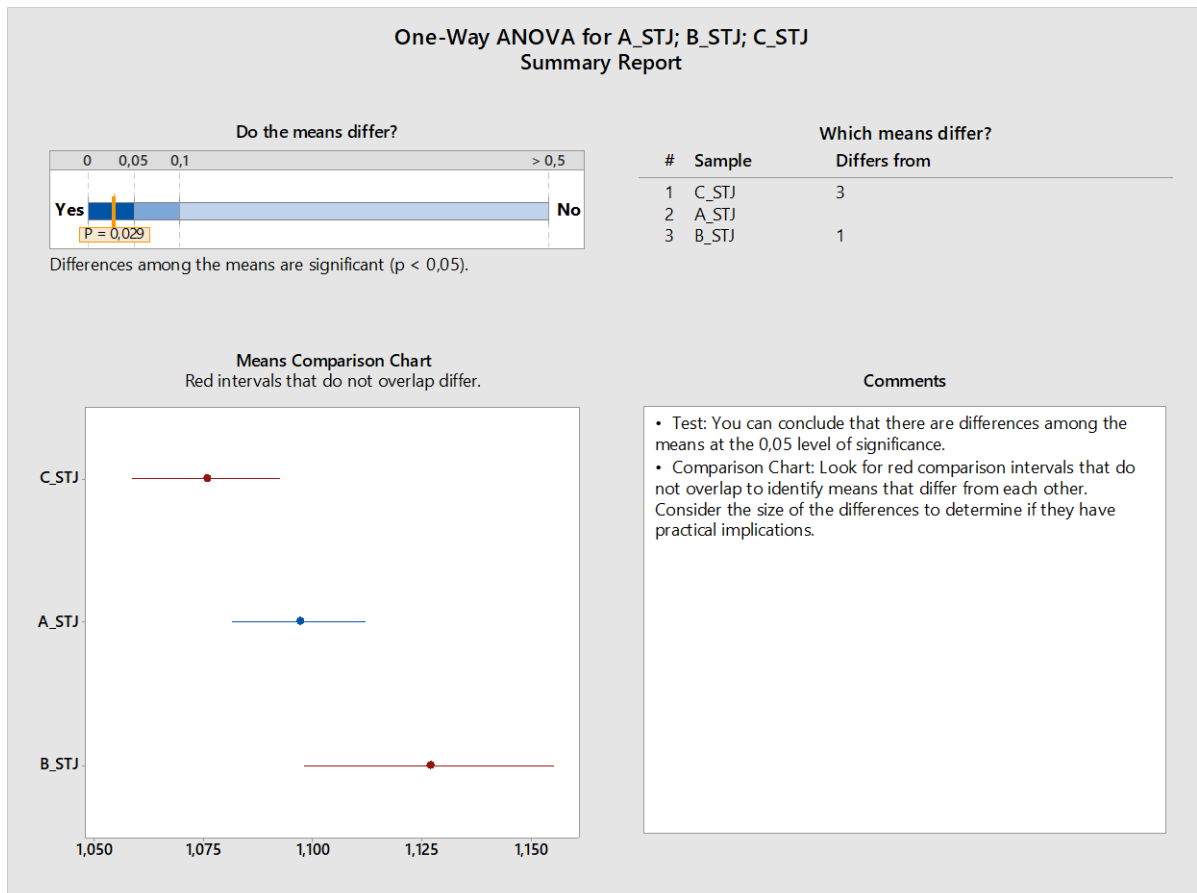
Sample	Sample Size	Statistics		
		Mean	Standard Deviation	Individual 95% CI for Mean
A_HRLC	90	1,2804	0,13859	(1,2514; 1,3094)
B_HRLC	33	1,3512	0,11163	(1,3116; 1,3908)
C_HRLC	58	1,2675	0,11918	(1,2362; 1,2989)

- HSTJ



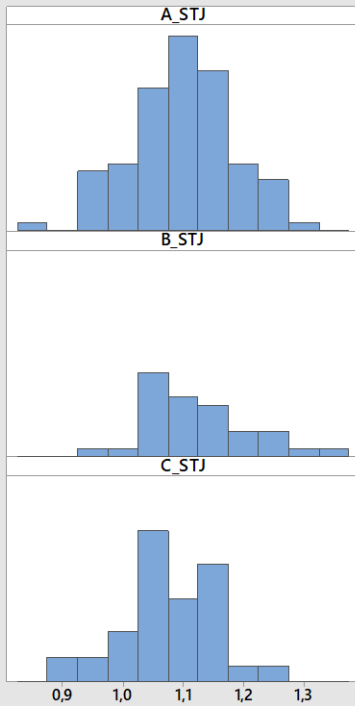


- STJ

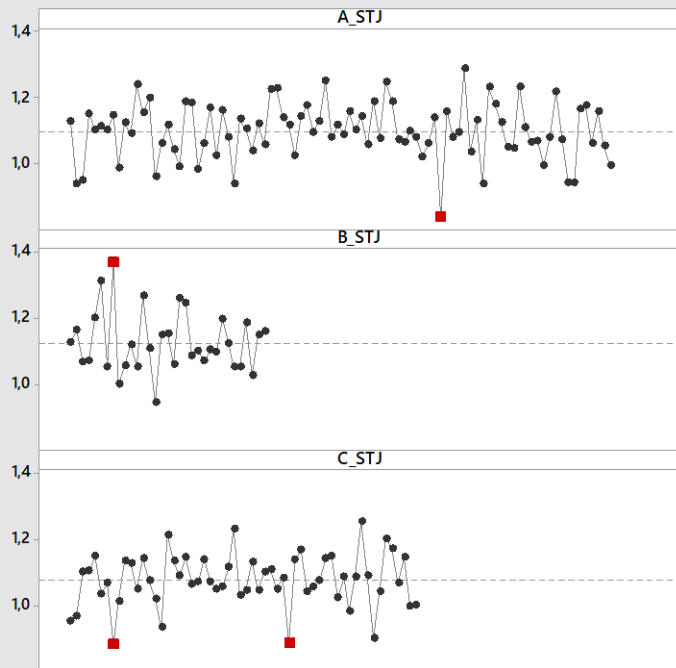


### One-Way ANOVA for A\_STJ; B\_STJ; C\_STJ Diagnostic Report

**Distribution of Data**  
Compare the location and spread.

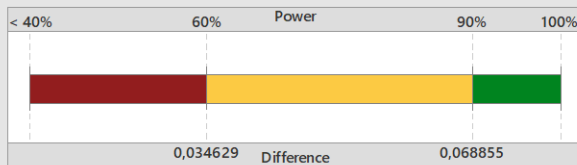


**Data in Worksheet Order**  
Investigate any outliers (marked in red).



### One-Way ANOVA for A\_STJ; B\_STJ; C\_STJ Power Report

What is the chance of detecting a difference?



Based on your samples and  $\alpha$  level (0,05), you have at least a 90% chance of detecting a difference of 0,068855, and at most a 60% chance of detecting a difference of 0,034629.

What difference can you detect with your sample sizes?

Difference	Power
0,034629	34,2 - 60,0%
0,048171	60,0 - 88,5%
0,053678	70,0 - 94,4%
0,060083	80,0 - 97,9%
0,068855	90,0 - 99,6%

Power is a function of the sample sizes and the standard deviations. To detect differences smaller than 0,060083, consider increasing the sample sizes.

Sample	Sample Size	Statistics		
		Mean	Standard Deviation	Individual 95% CI for Mean
A_STJ	90	1,0969	0,08446	(1,0792; 1,1145)
B_STJ	33	1,1266	0,09148	(1,0941; 1,1590)
C_STJ	58	1,0755	0,07888	(1,0548; 1,0963)

### 6.3 Normality test

Two types of comparisons can be carried out: parametric or non-parametric.

The first is when there are parameters: it is assumed, for example, to have a population distributed in a Gaussian way, then the parameters will be mean and standard deviation; if the two distributions are Gaussian and I compare the parameters, I get a parametric statistic.

In the case of a non-parametric analysis, the distributions are not parameterizable.

The best would be to have parametric and above all Gaussian distributions (if I have to deal with a patient population I have a random variability between one patient and the other, but they are common patients with a common pathology (aortic stenosis) but the variability should be casual).

So, the first step is understanding if distributions are normal, in this way, I can perform a parametric analysis. Another distinction can be made between continuous data and given attribute; the latter used for non-continuous variables. Our variables are continuous.

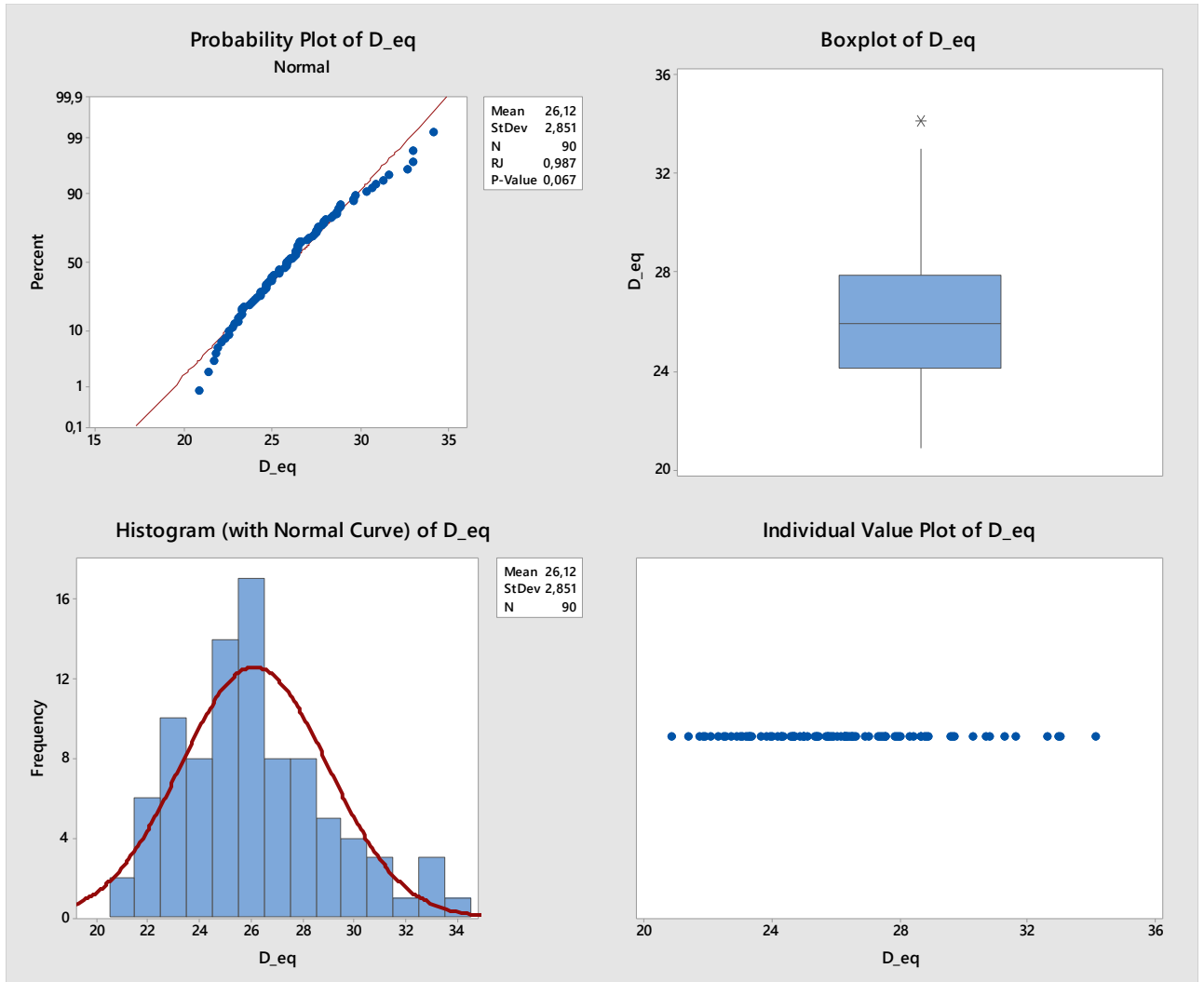
For each variable will be shown a:

- Probability plot of normality: returns mean and standard deviation; the Ryan - Joiner parameter tends to 1 in the case in which the distribution is perfectly normal (the straight line); the P – value is the probability for a given statistical model that, when the null hypothesis is true, the statistical summary would be the same as or of greater magnitude than the actual observed results. A P – value = 0.05 represents a CI = 95%:
  - o If P – value > 0.05, with CI = 95%, I can deem that the population is normally distributed;
  - o If P – value < 0.05, with CI = 95%, I can deem that the population is non-normally distributed.
- Boxplot;
- Histogram (with Gaussian curve).

- D equivalent ( $\text{Annulus perimeter}/\pi$ )

With a P – value = 0.067, with a significance level of 0.05, I can deem that the population is normally distributed, also, this hypothesis is validated by RJ = 0.987.

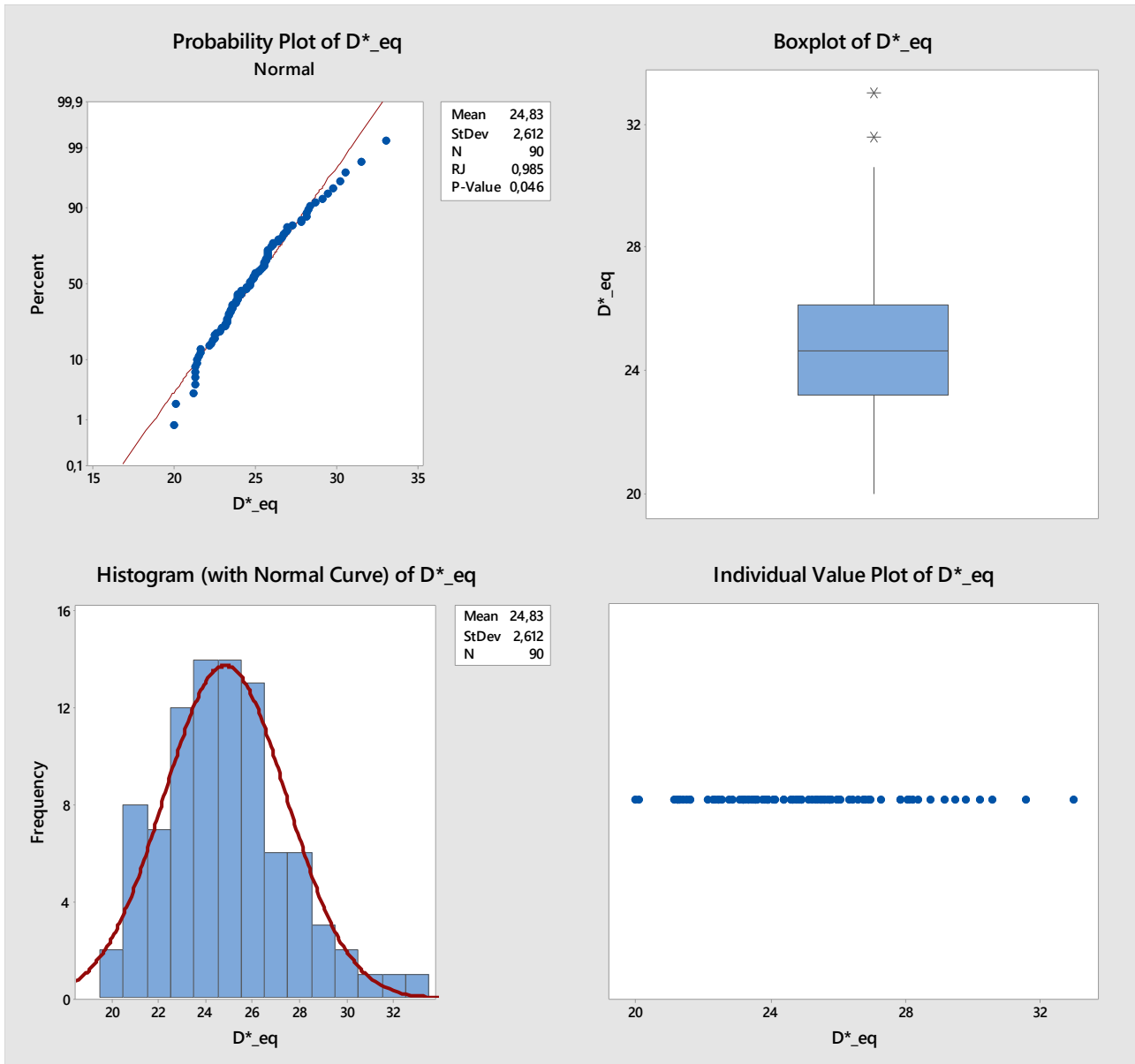
The boxplot shows the presence of an outlier.



- D equivalent  $[(4 \cdot \text{Annulus area} / \pi) \cdot 0.5]$

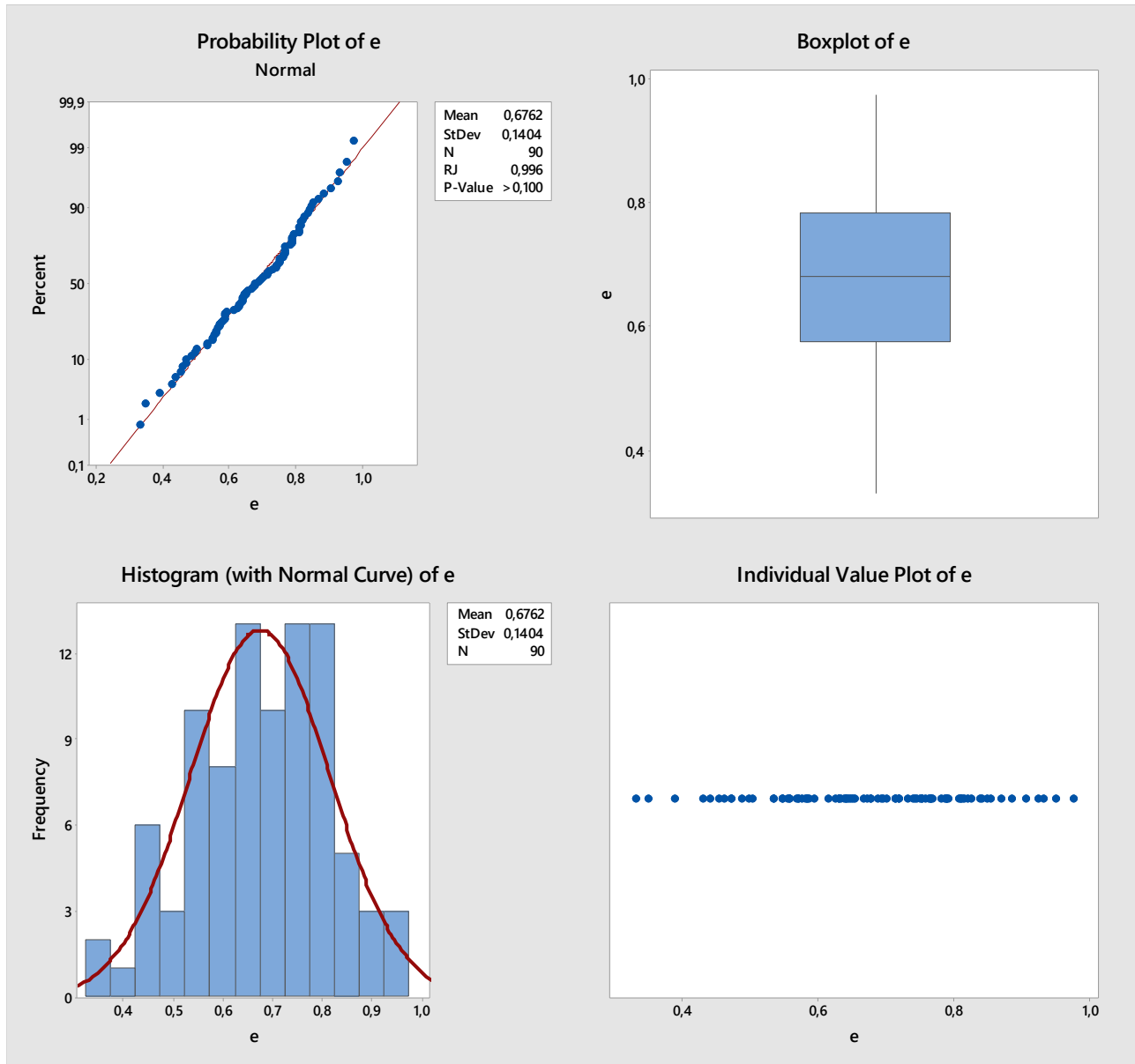
With a P – value = 0.046, with a significance level of 0.05, I can deem that the population is non-normally distributed, even if RJ = 0.987.

The boxplot shows the presence of two outliers.



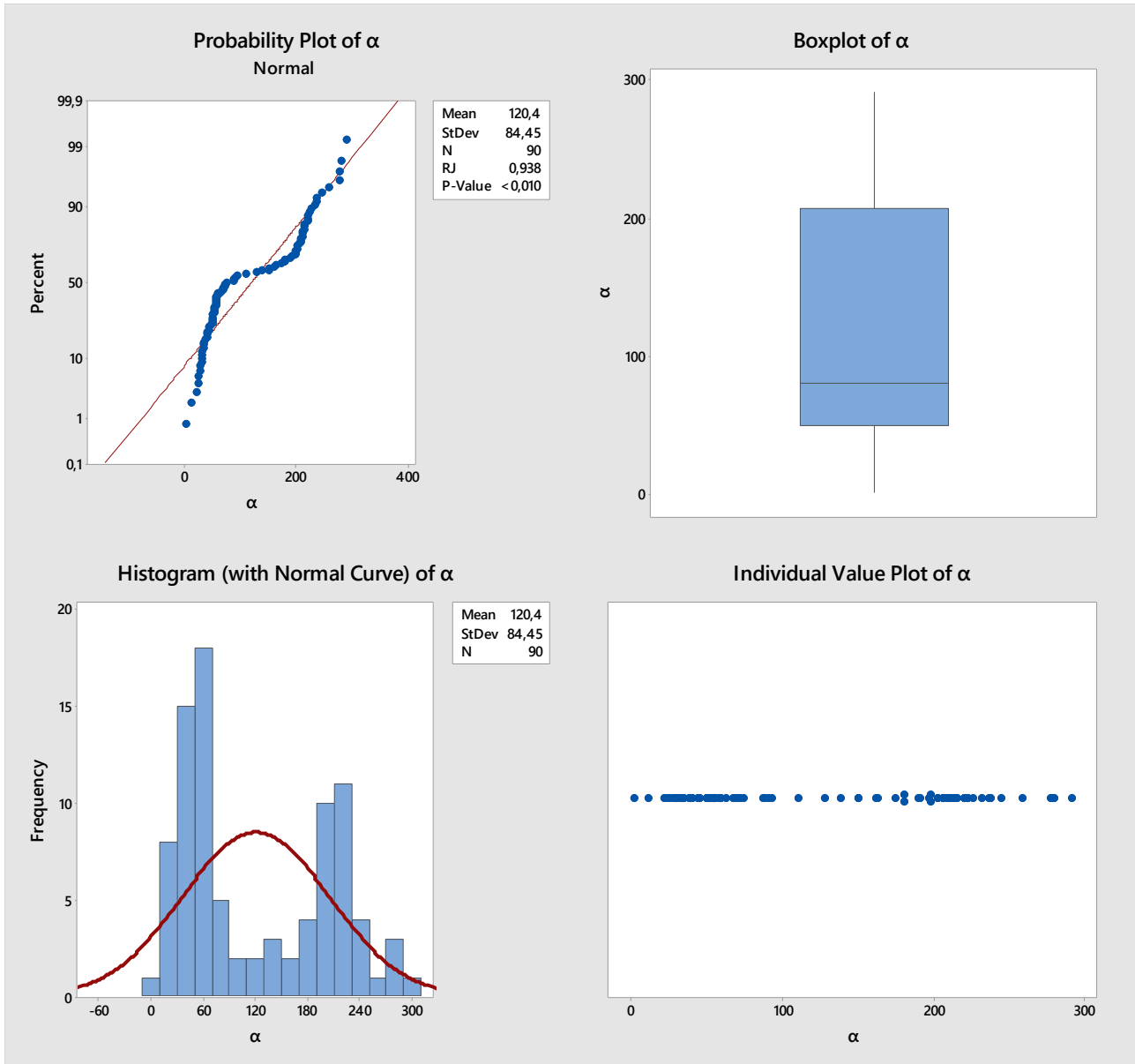
- $e (2 \cdot D_{\min} / D_{\max} - 1)$

With a P – value > 0.100, with a significance level of 0.05, I can deem that the population is normally distributed, also, this hypothesis is validated by RJ = 0.996.



- $\alpha$

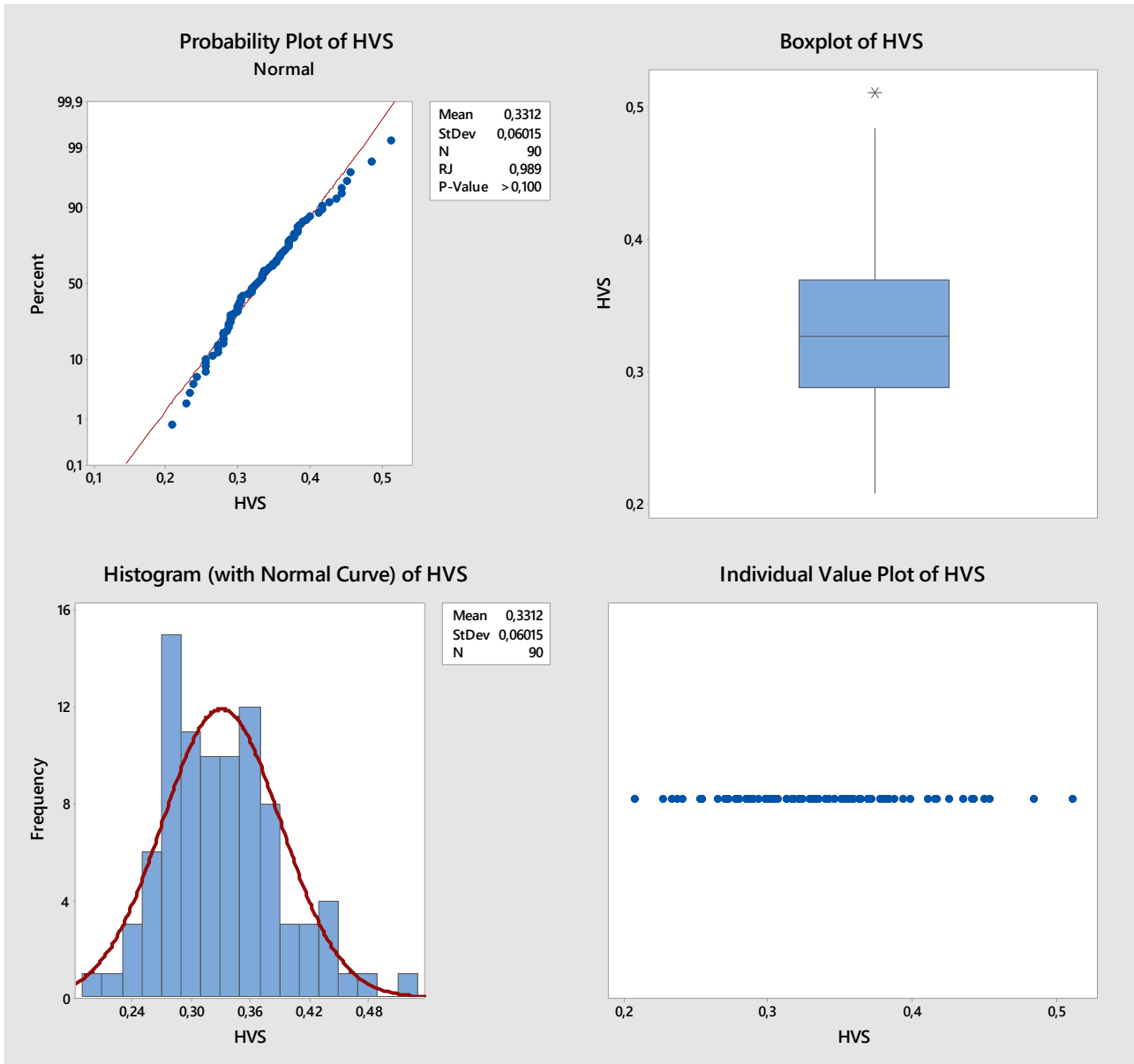
With a P – value < 0.010, with a significance level of 0.05, I can deem that the population is non-normally distributed, even if the RJ = 0.987.



- HVS

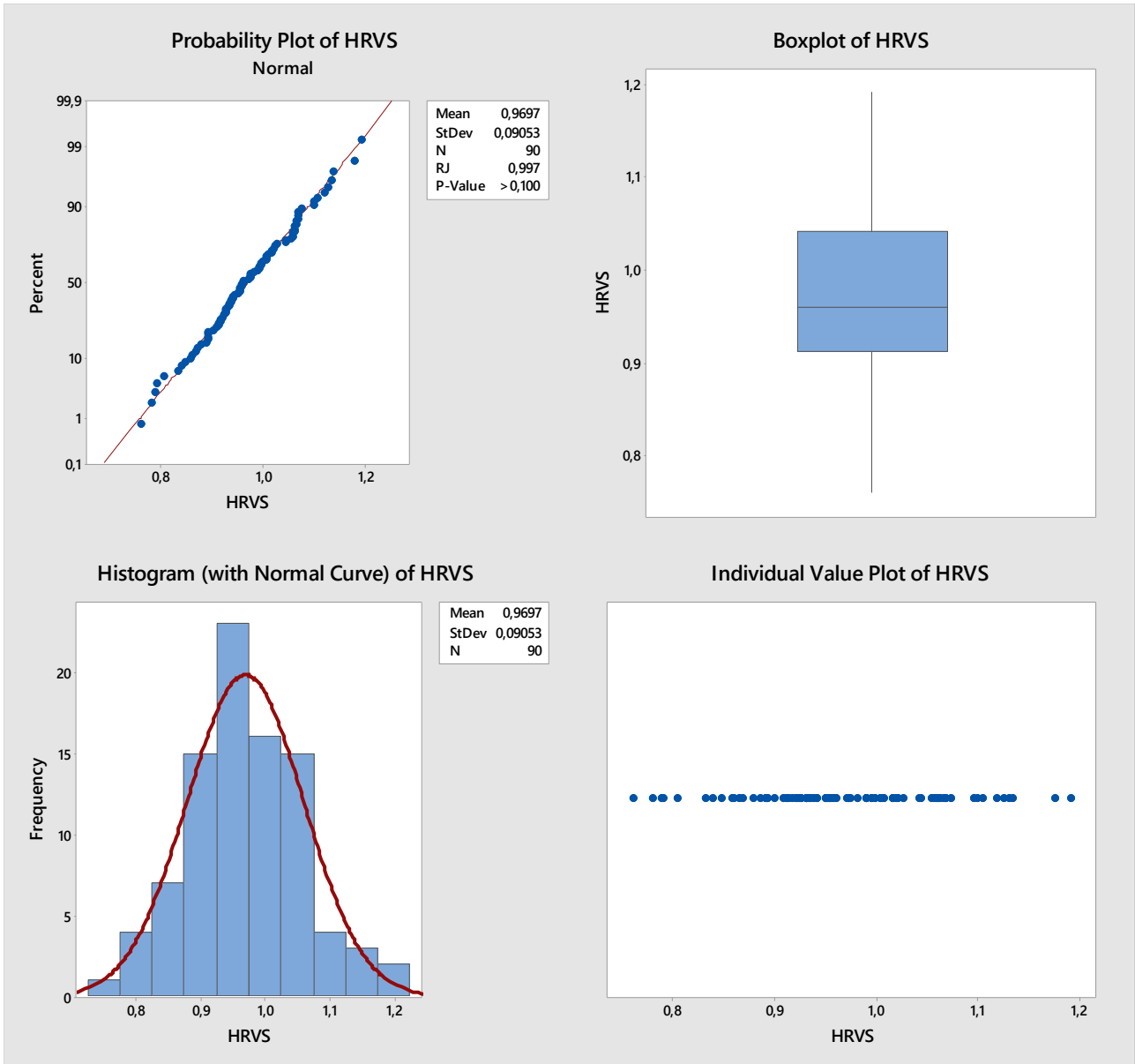
With a P – value  $> 0.100$ , with a significance level of 0.05, I can deem that the population is normally distributed, also, this hypothesis is validated by  $RJ = 0.989$ .

The boxplot shows the presence of an outlier.



- HRVS

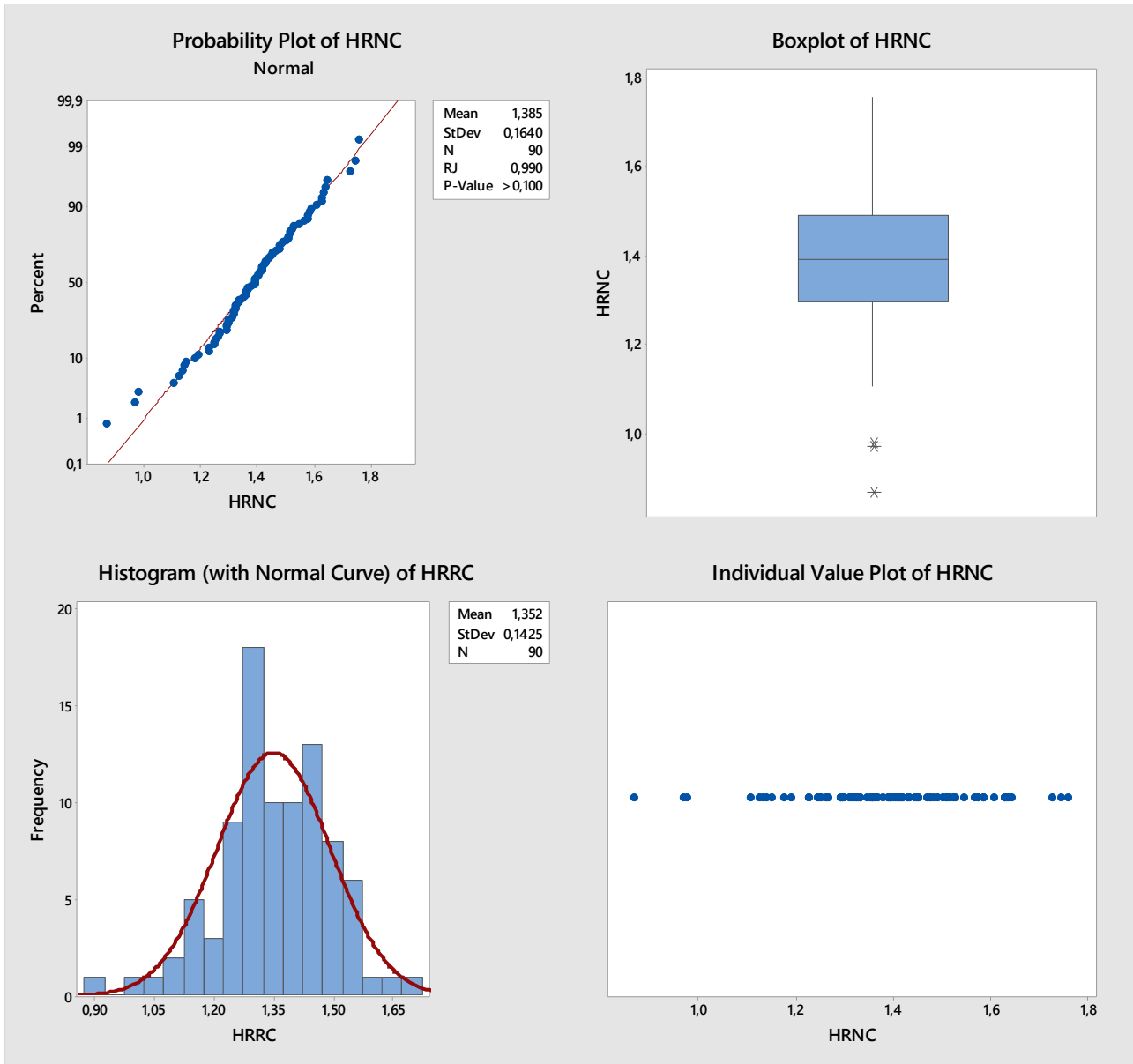
With a P – value  $> 0.100$ , with a significance level of 0.05, I can deem that the population is normally distributed, also, this hypothesis is validated by  $RJ = 0.997$ .



- HRNC

With a P – value  $> 0.100$ , with a significance level of 0.05, I can deem that the population is normally distributed, also, this hypothesis is validated by  $RJ = 0.990$ .

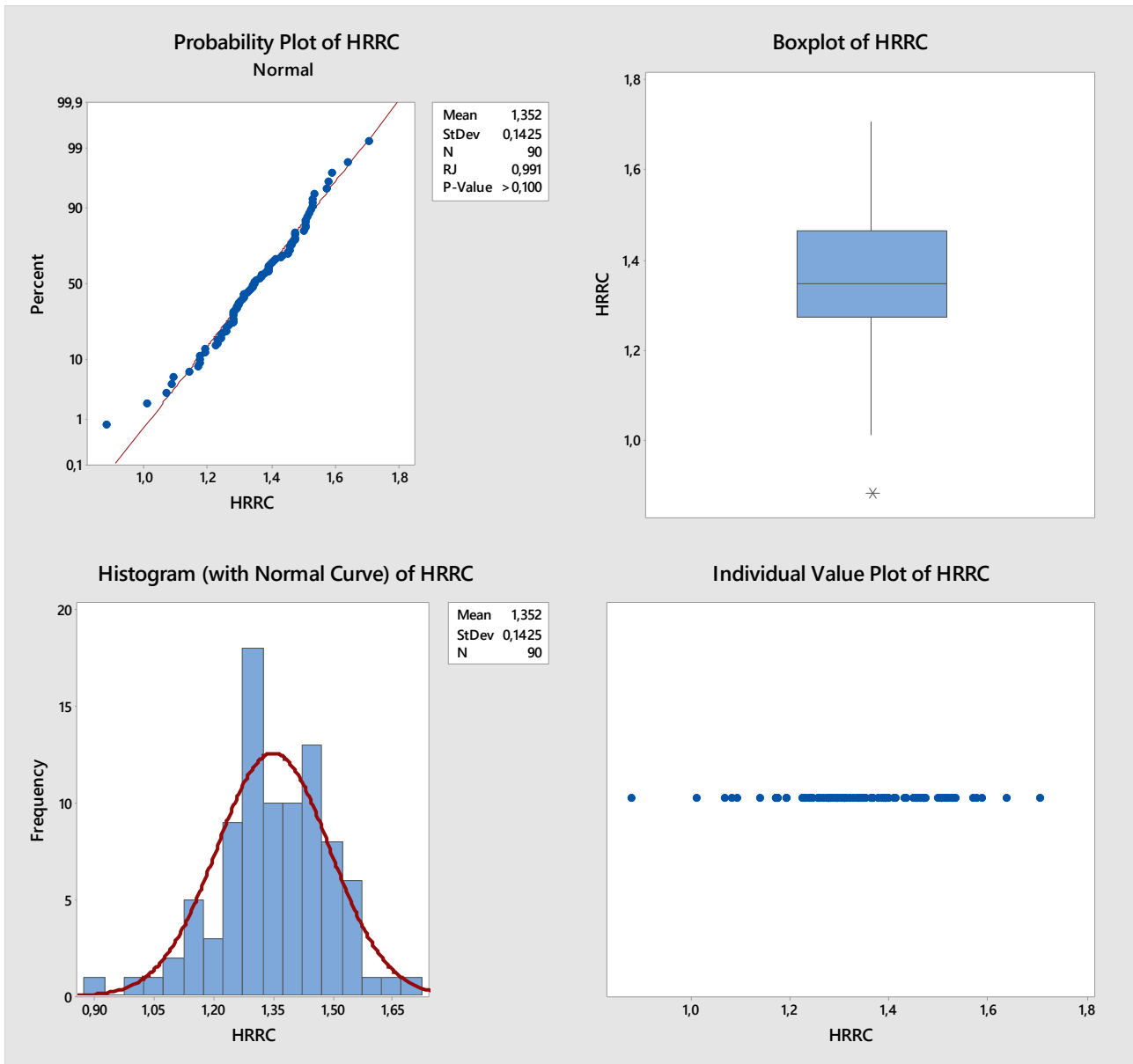
The boxplot shows the presence of two outliers.



- HRRC

With a P – value  $> 0.100$ , with a significance level of 0.05, I can deem that the population is normally distributed, also, this hypothesis is validated by  $RJ = 0.991$ .

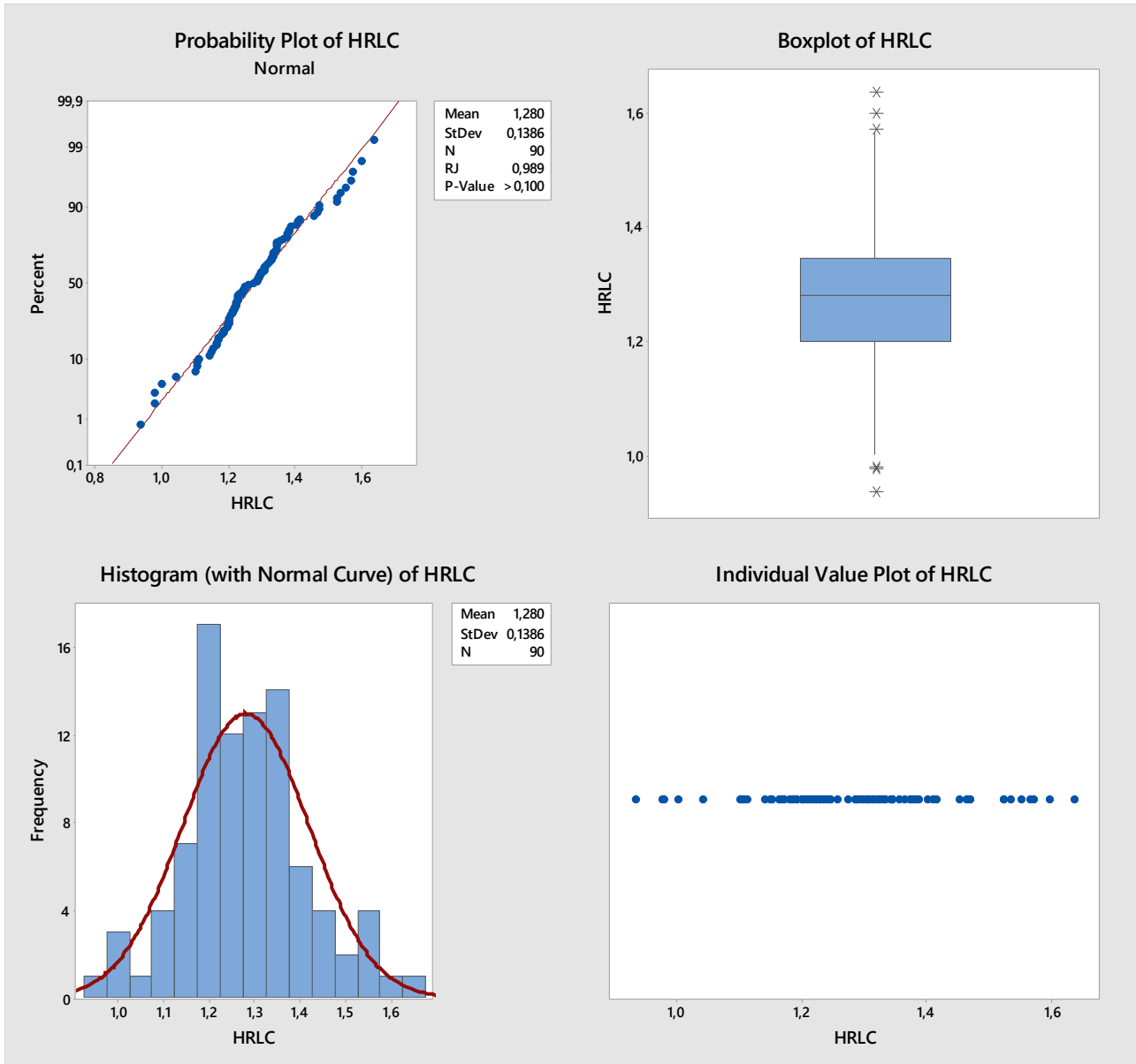
The boxplot shows the presence of an outlier.



- HRLC

With a P – value  $> 0.100$ , with a significance level of 0.05, I can deem that the population is normally distributed, also, this hypothesis is validated by  $RJ = 0.989$ .

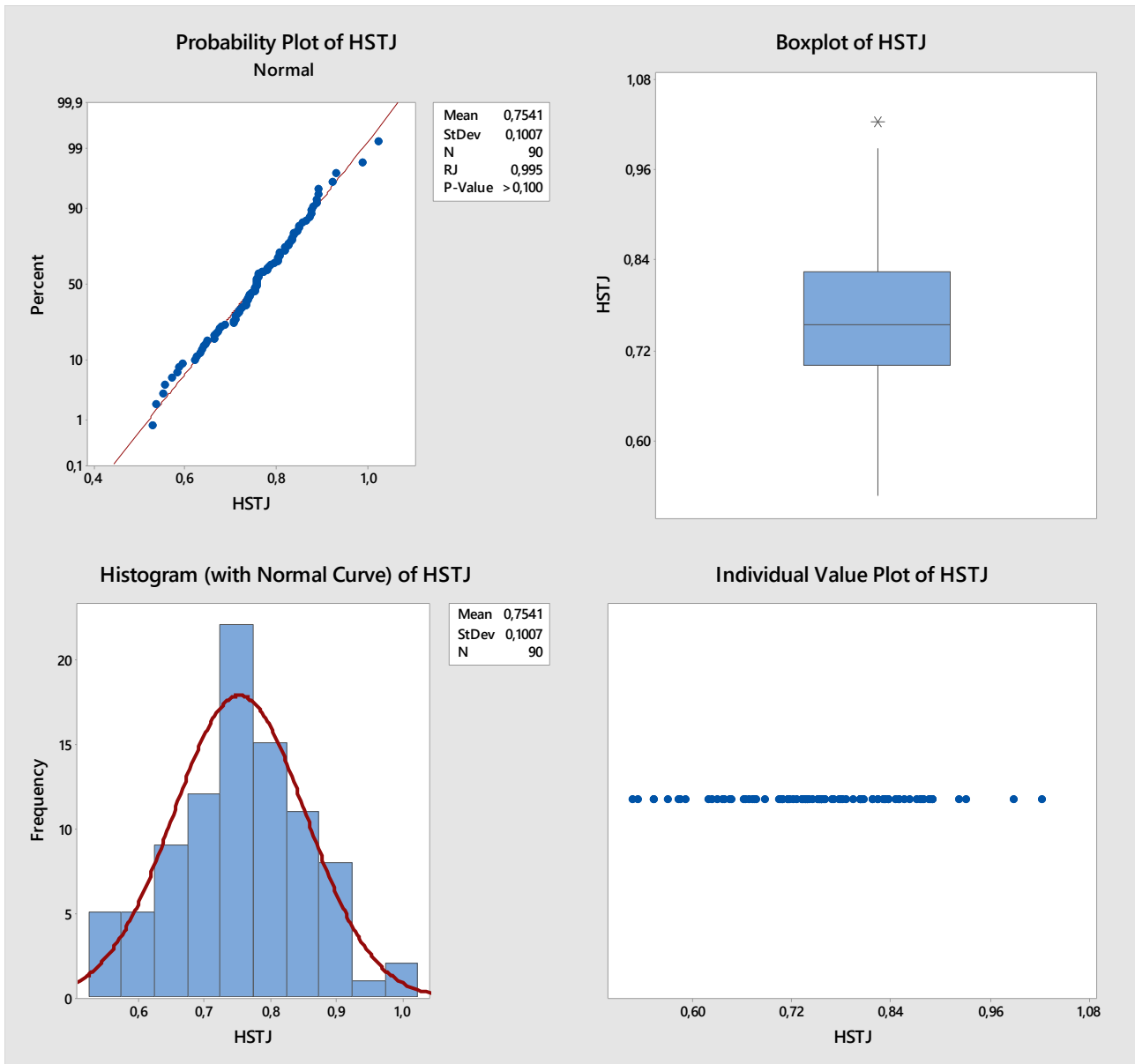
The boxplot shows the presence of some outliers.



- HSTJ

With a P – value > 0.100, with a significance level of 0.05, I can deem that the population is normally distributed, also, this hypothesis is validated by RJ = 0.995.

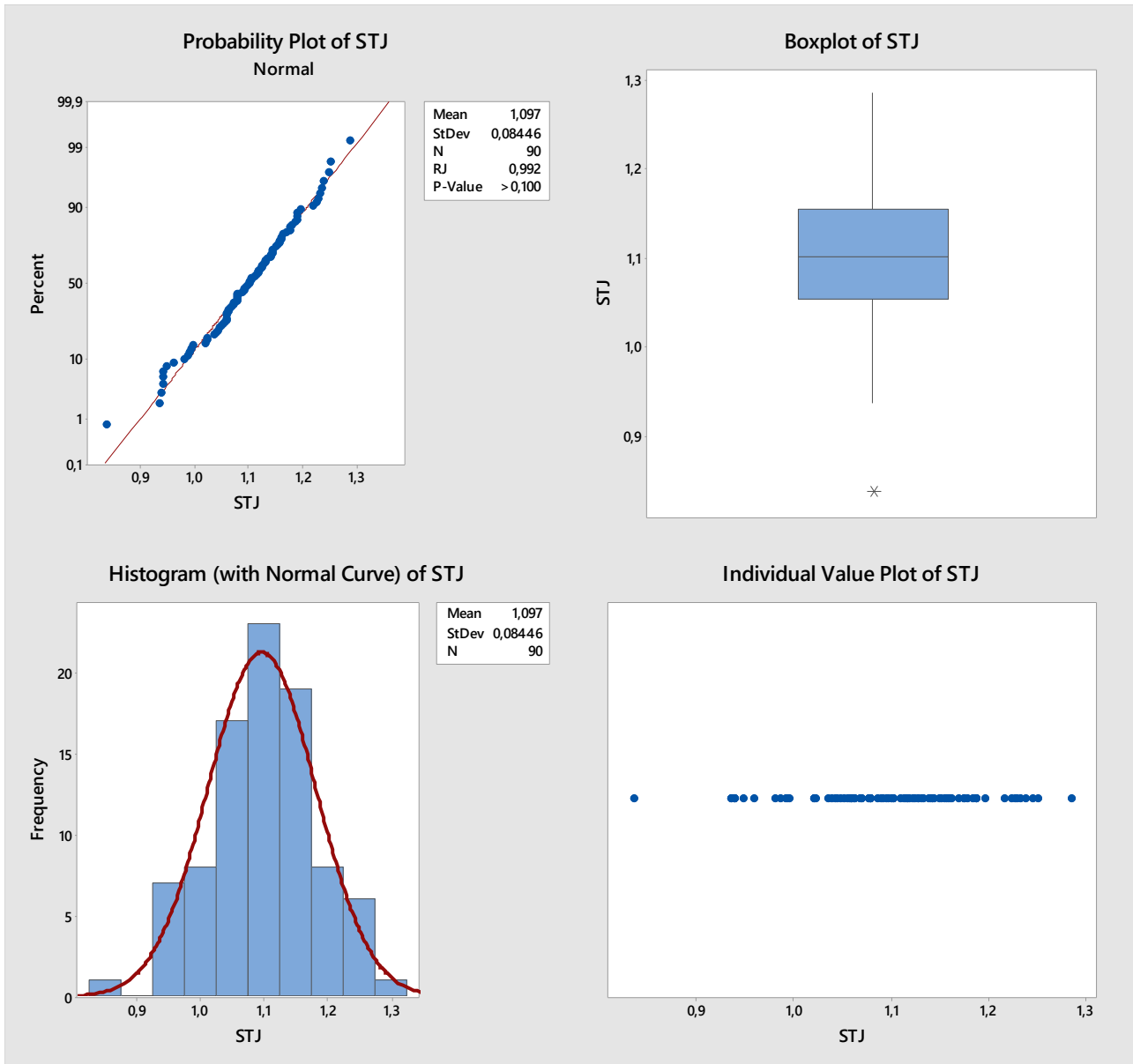
The boxplot shows the presence of an outlier.



- STJ

With a P – value  $> 0.100$ , with a significance level of 0.05, I can deem that the population is normally distributed, also, this hypothesis is validated by  $RJ = 0.992$ .

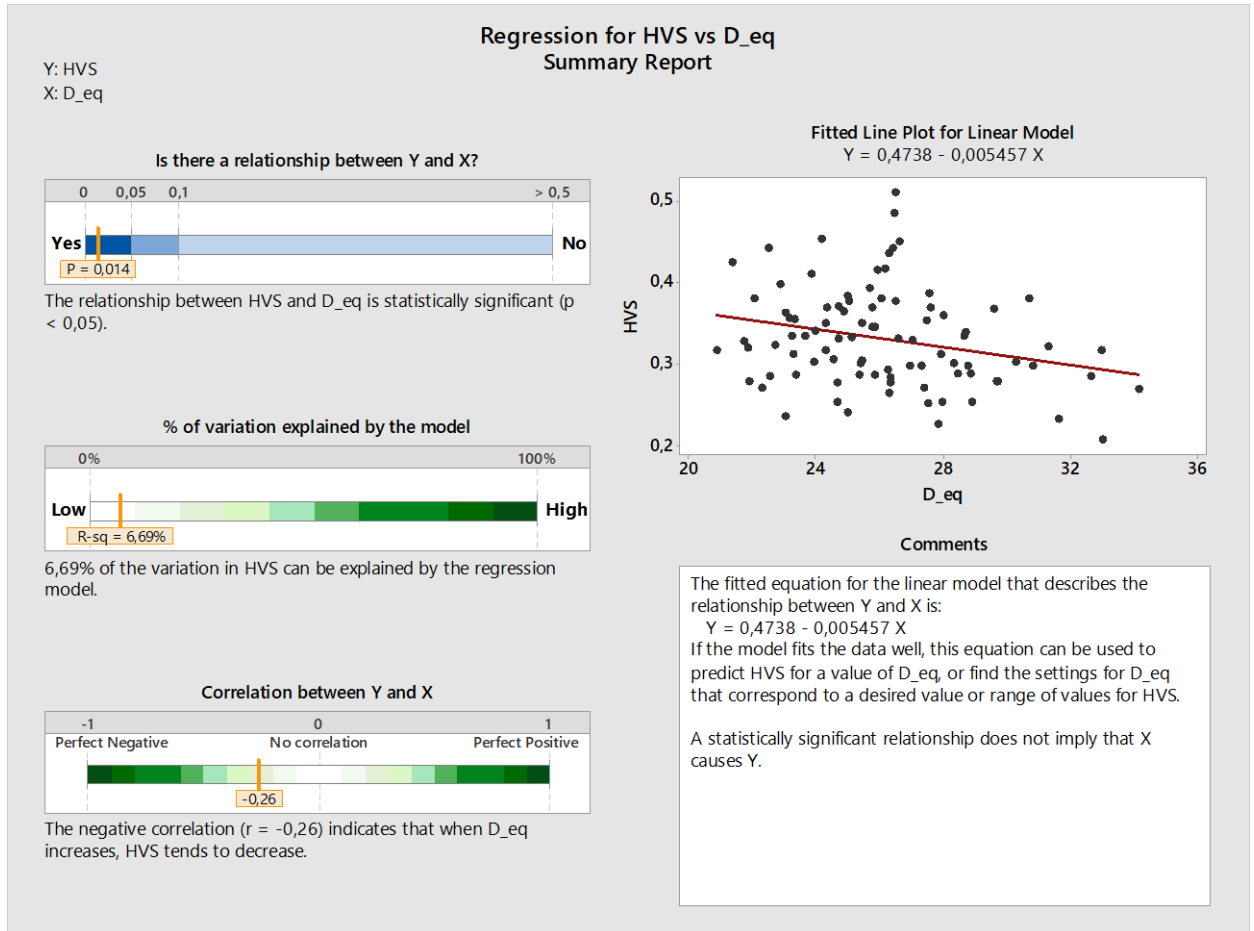
The boxplot shows the presence of an outlier.



## 6.4 Regressions

In this section we try to understand which parameters and how they influence each other.

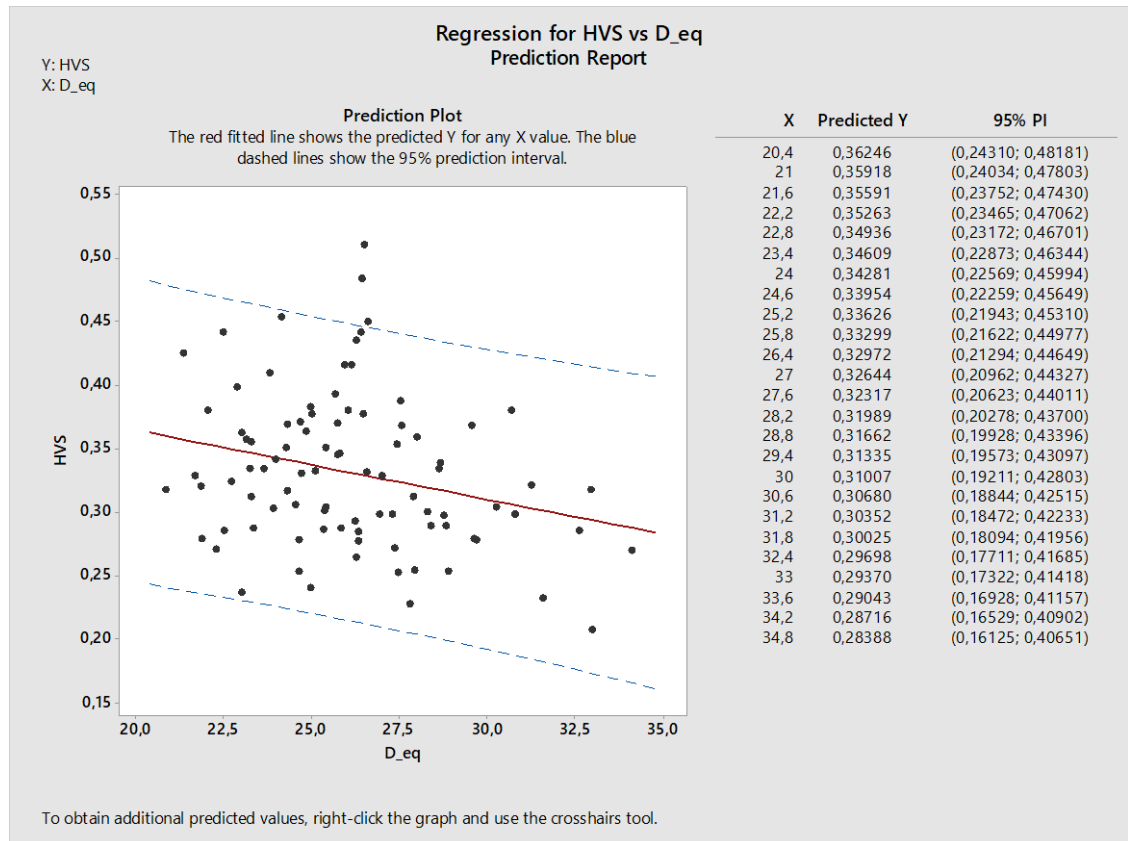
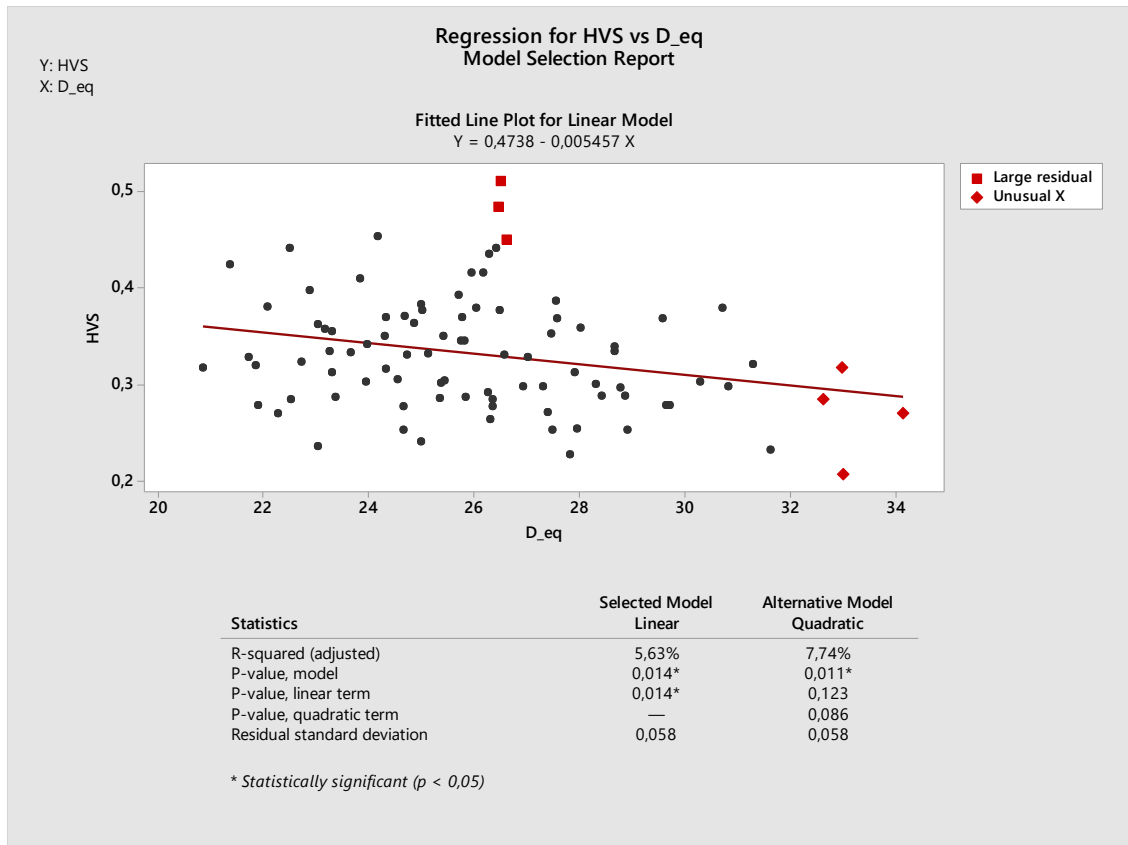
### ❖ D equivalent – HVS



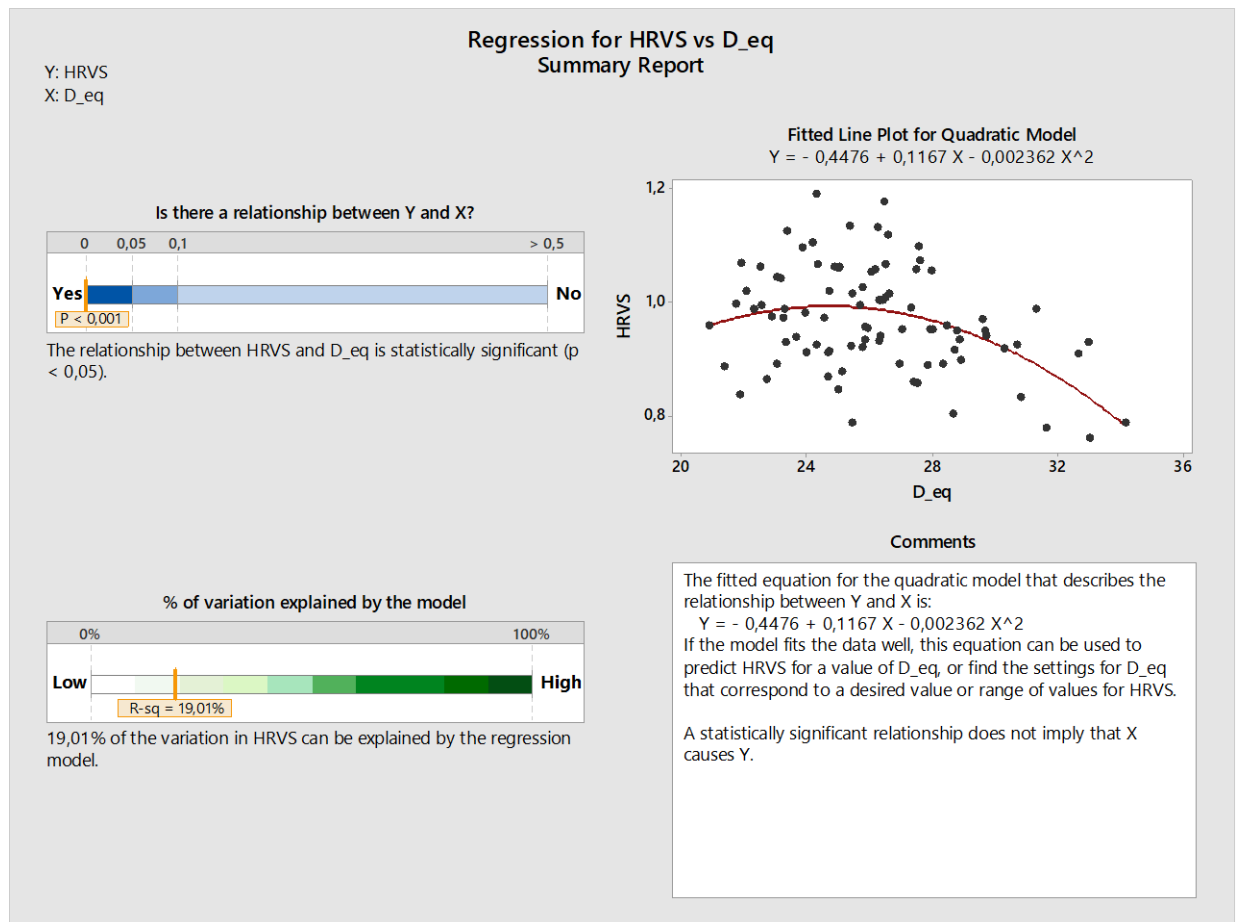
Report:

This sample is large enough ( $n = 90$ ) to obtain a precise estimate of the strength of the relationship.

- Large residuals: 3 data points have large residuals and are not well fit by the equation. These points are marked in red on the plots.
- Unusual X values: 4 data points have unusual X values, which can cause the fitted line to be pulled closer to the unusual points and away from other points. These points are marked in red on the Model Selection Report.



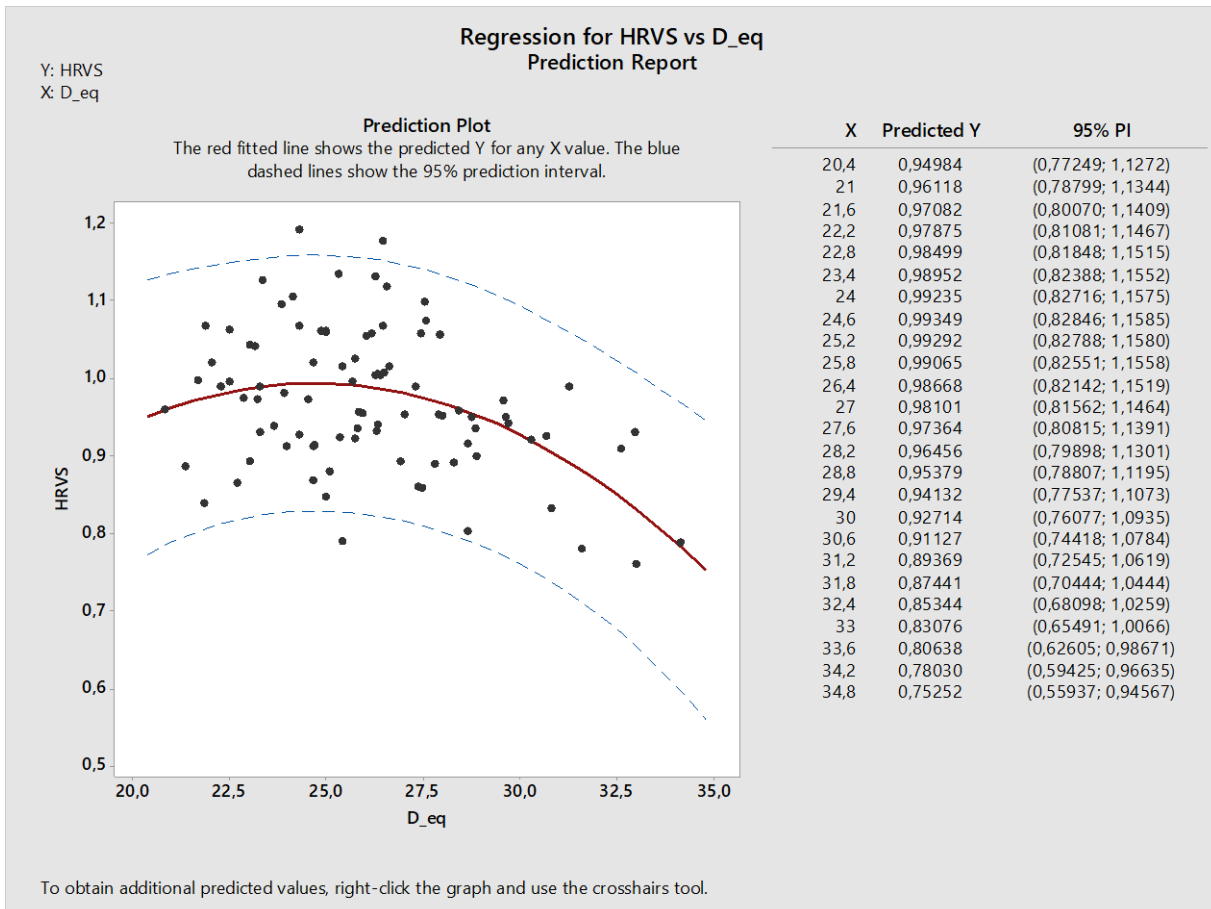
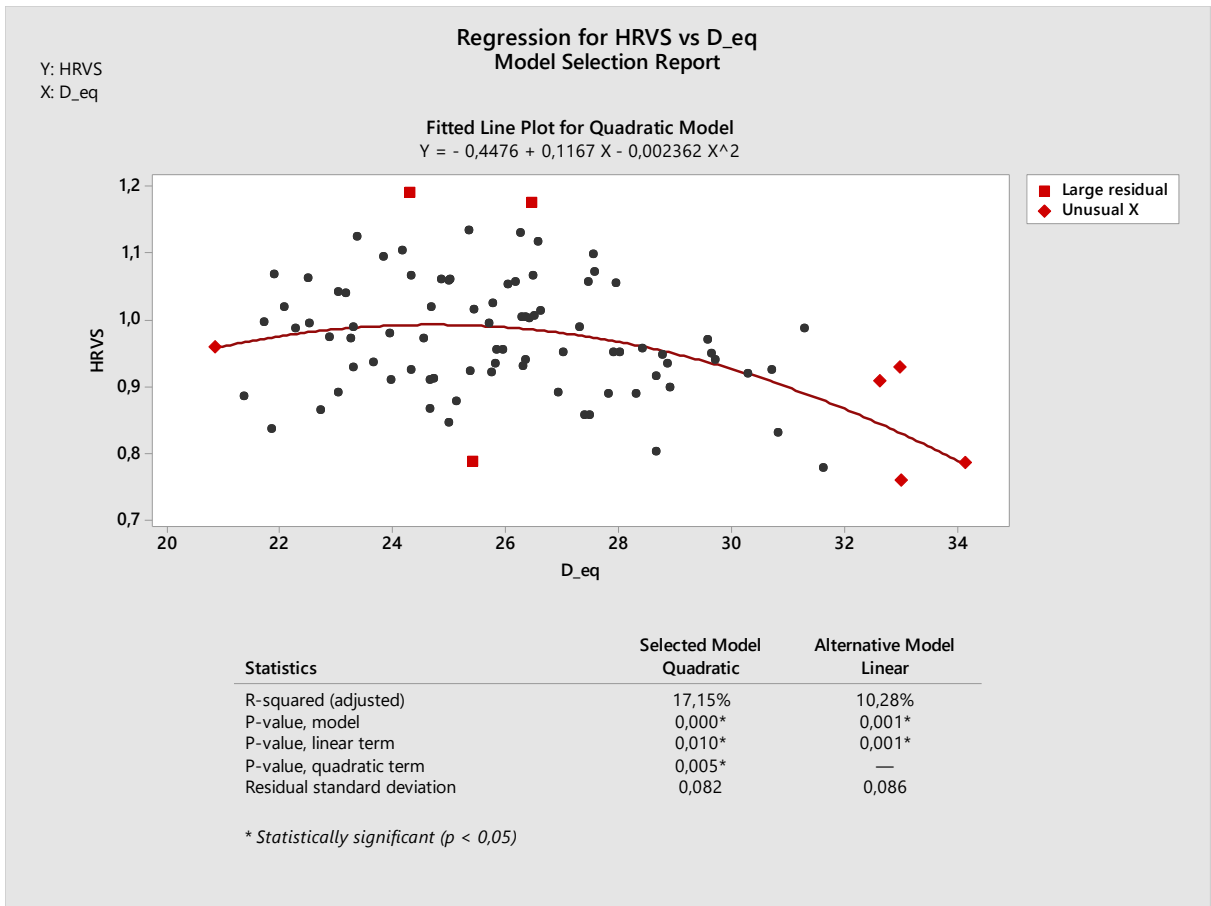
❖ D equivalent – HRVS



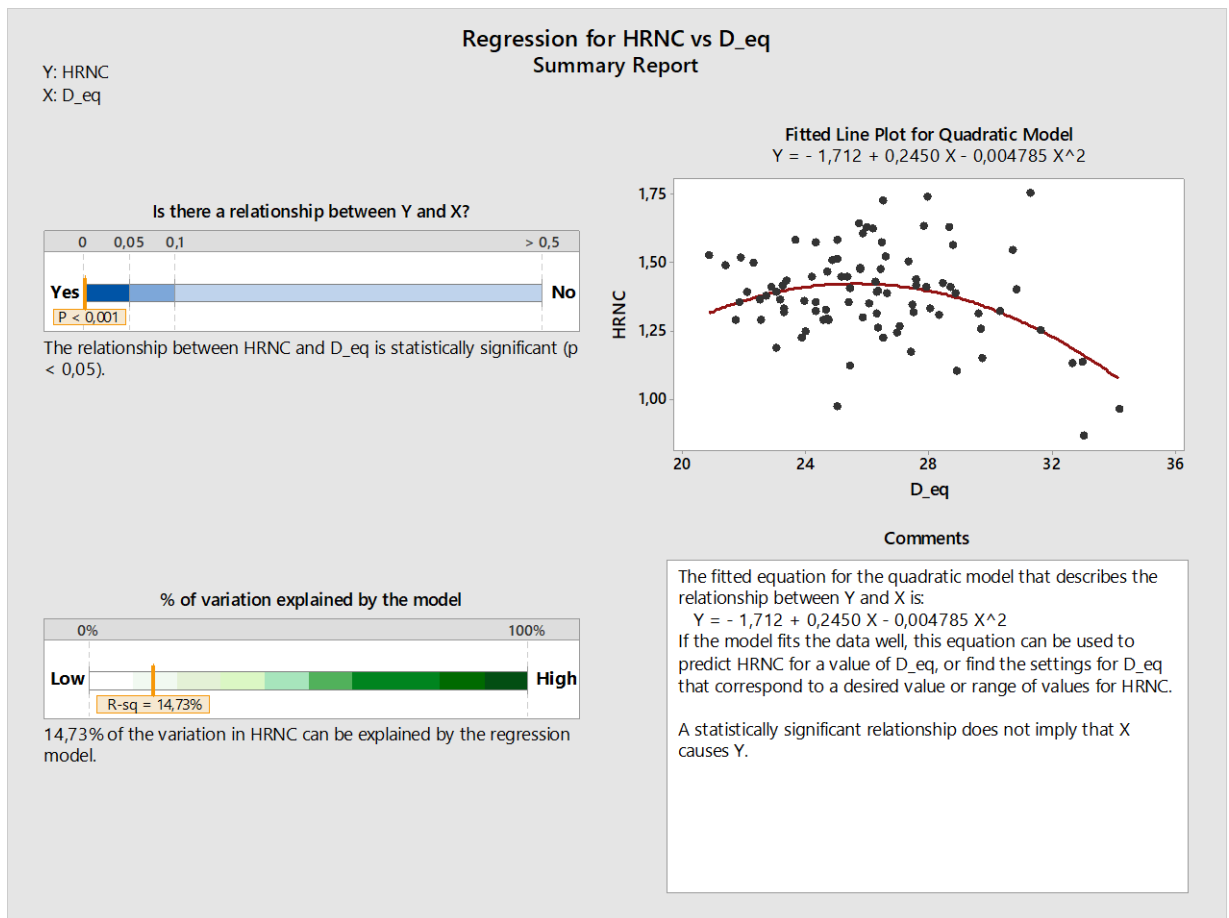
**Report:**

This sample is large enough ( $n = 90$ ) to obtain a precise estimate of the strength of the relationship.

- Large residuals: 3 data points have large residuals and are not well fit by the equation. These points are marked in red on the plots.
- Unusual X values: 5 data points have unusual X values, which can cause the fitted line to be pulled closer to the unusual points and away from other points. These points are marked in red on the Model Selection Report.



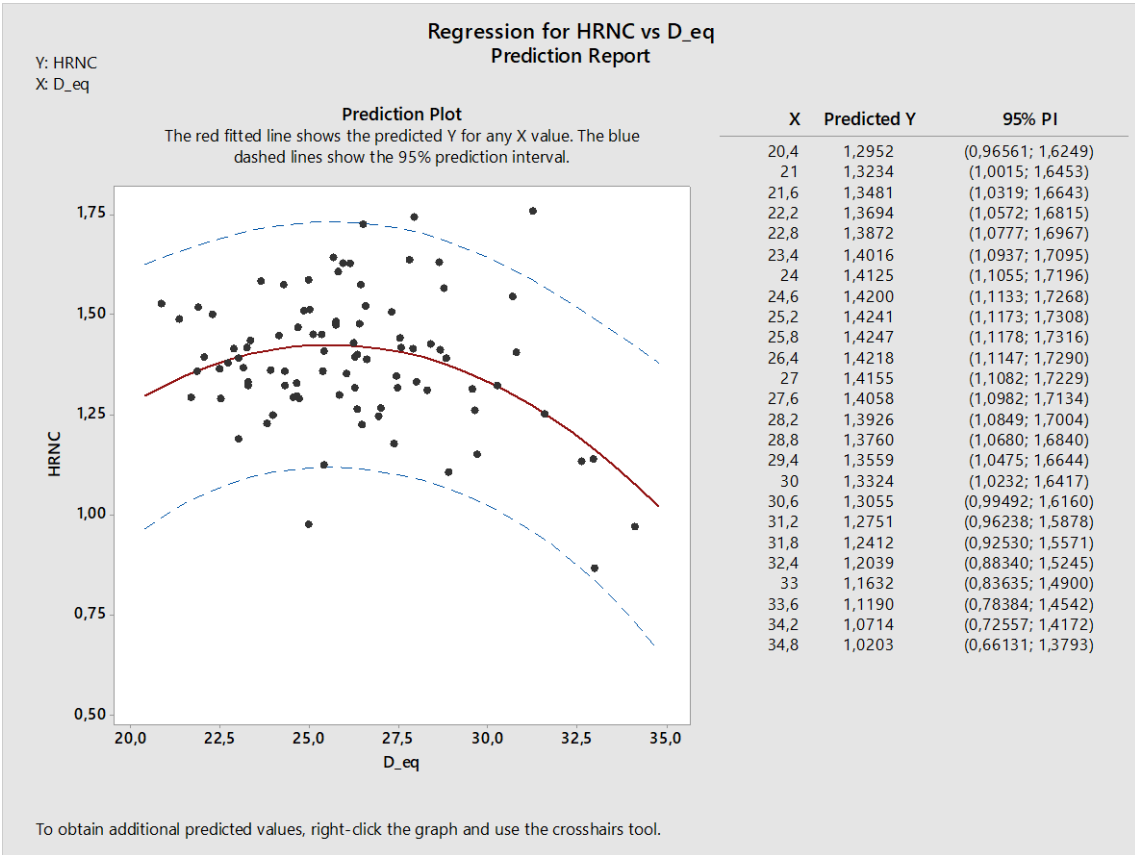
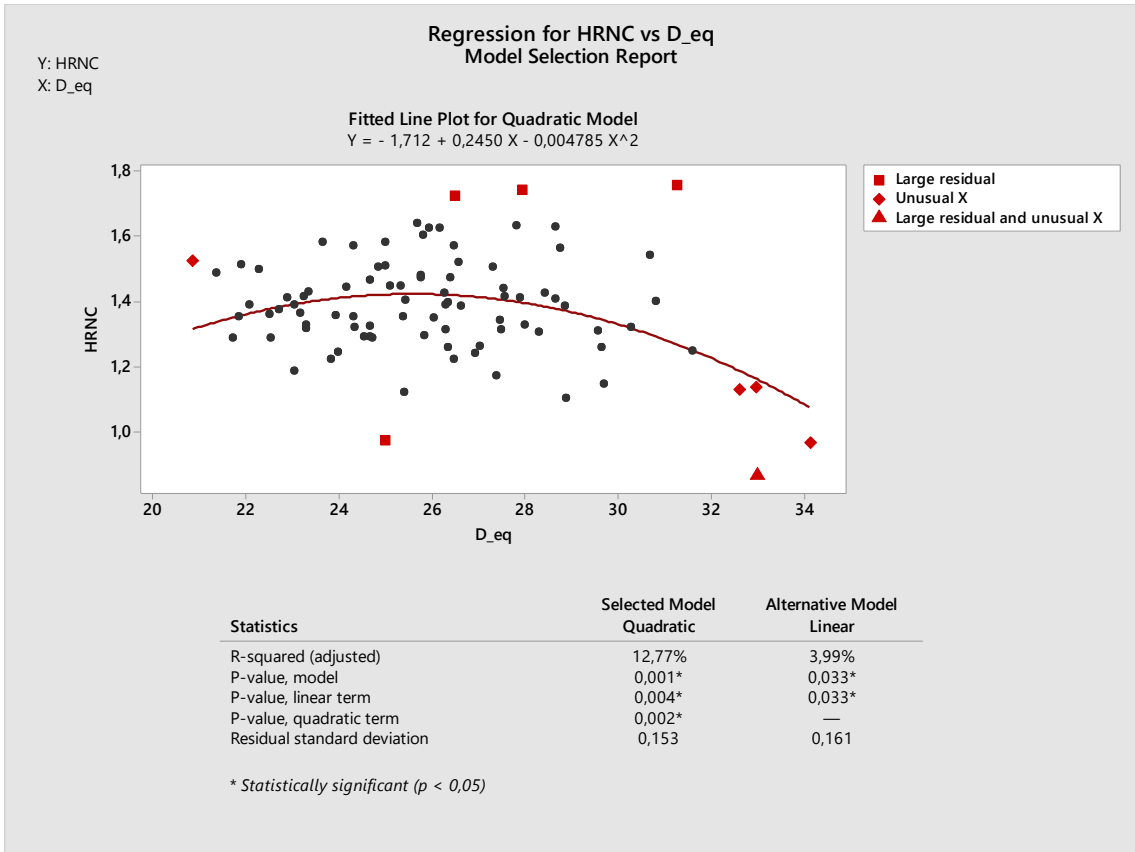
❖ D equivalent – HRNC



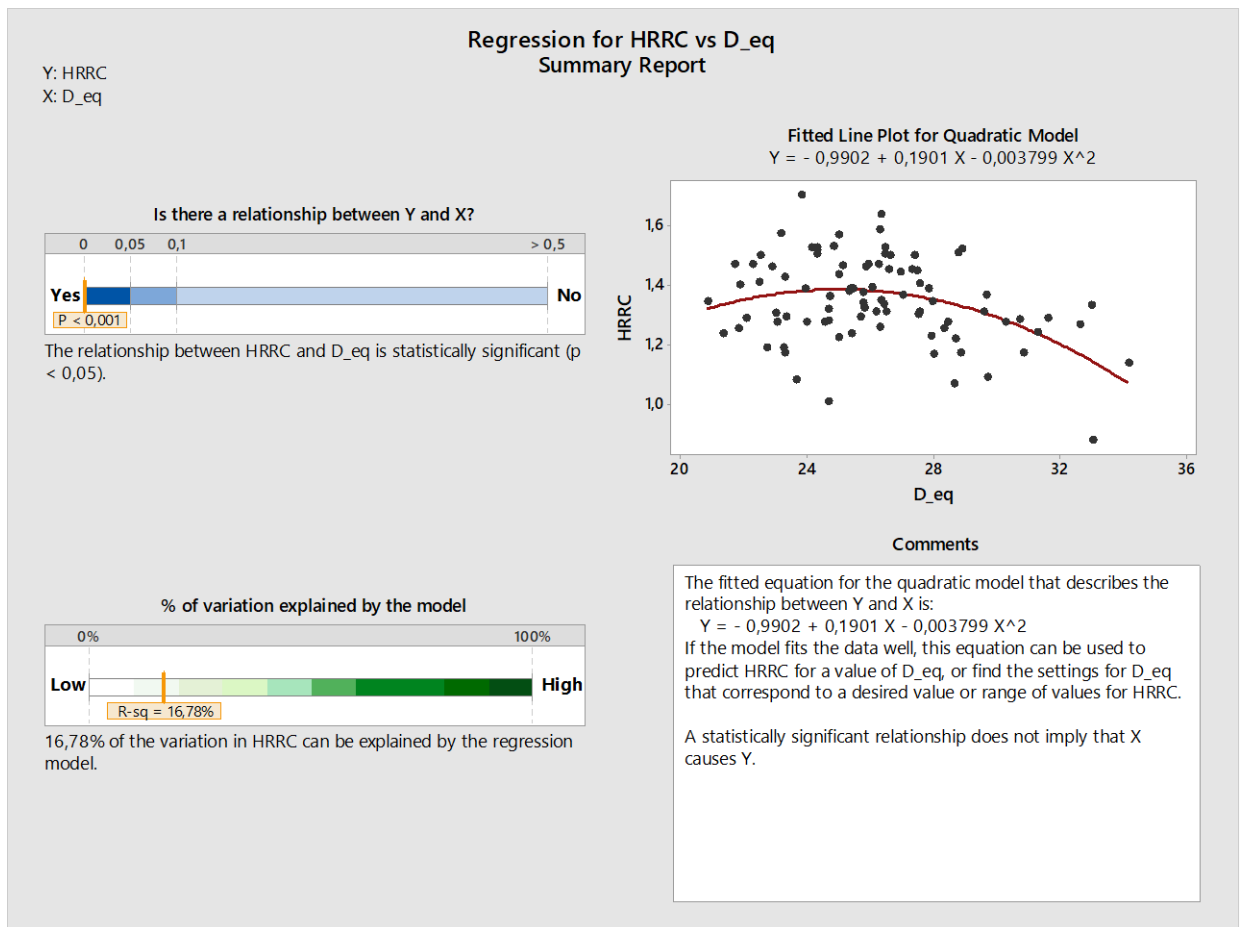
**Report:**

This sample is large enough ( $n = 90$ ) to obtain a precise estimate of the strength of the relationship.

- Large residuals: 5 data points have large residuals and are not well fit by the equation. These points are marked in red on the plots.
- Unusual X values: 5 data points have unusual X values, which can cause the fitted line to be pulled closer to the unusual points and away from other points. These points are marked in red on the Model Selection Report.



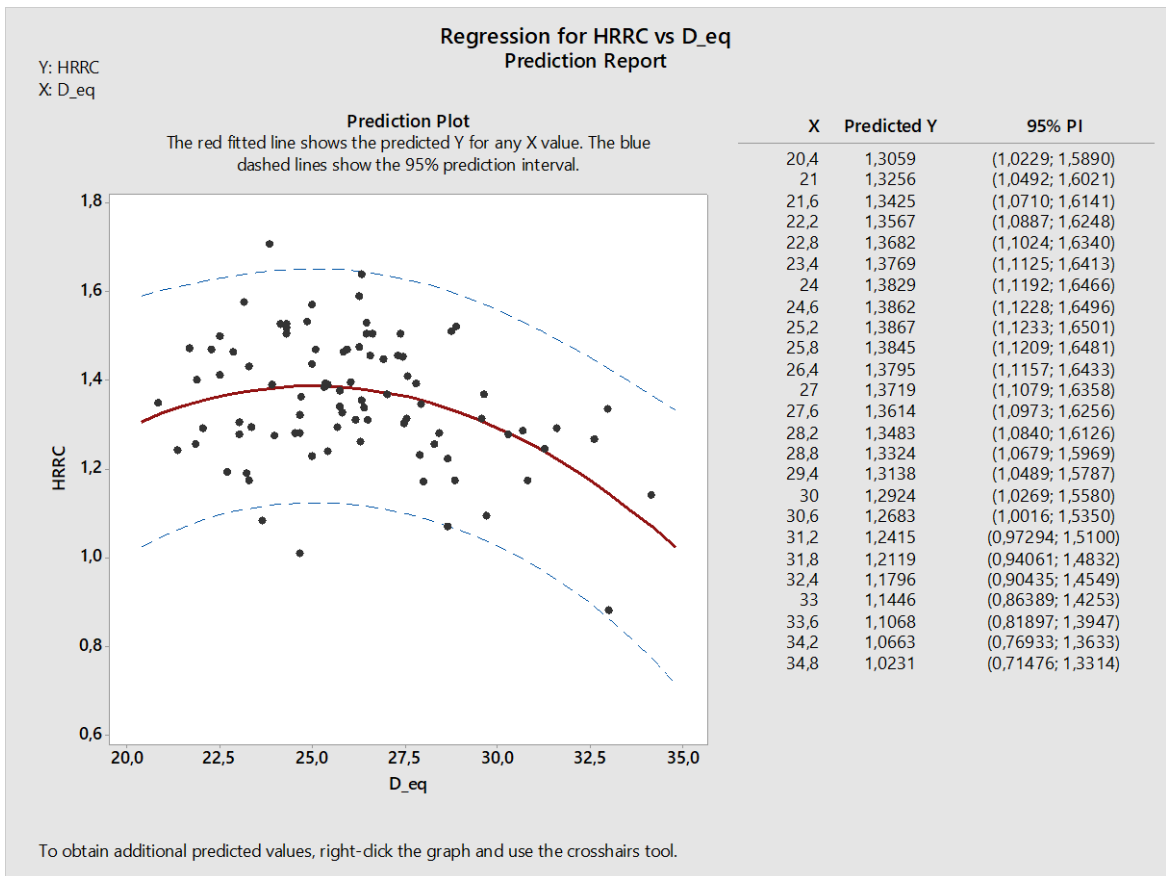
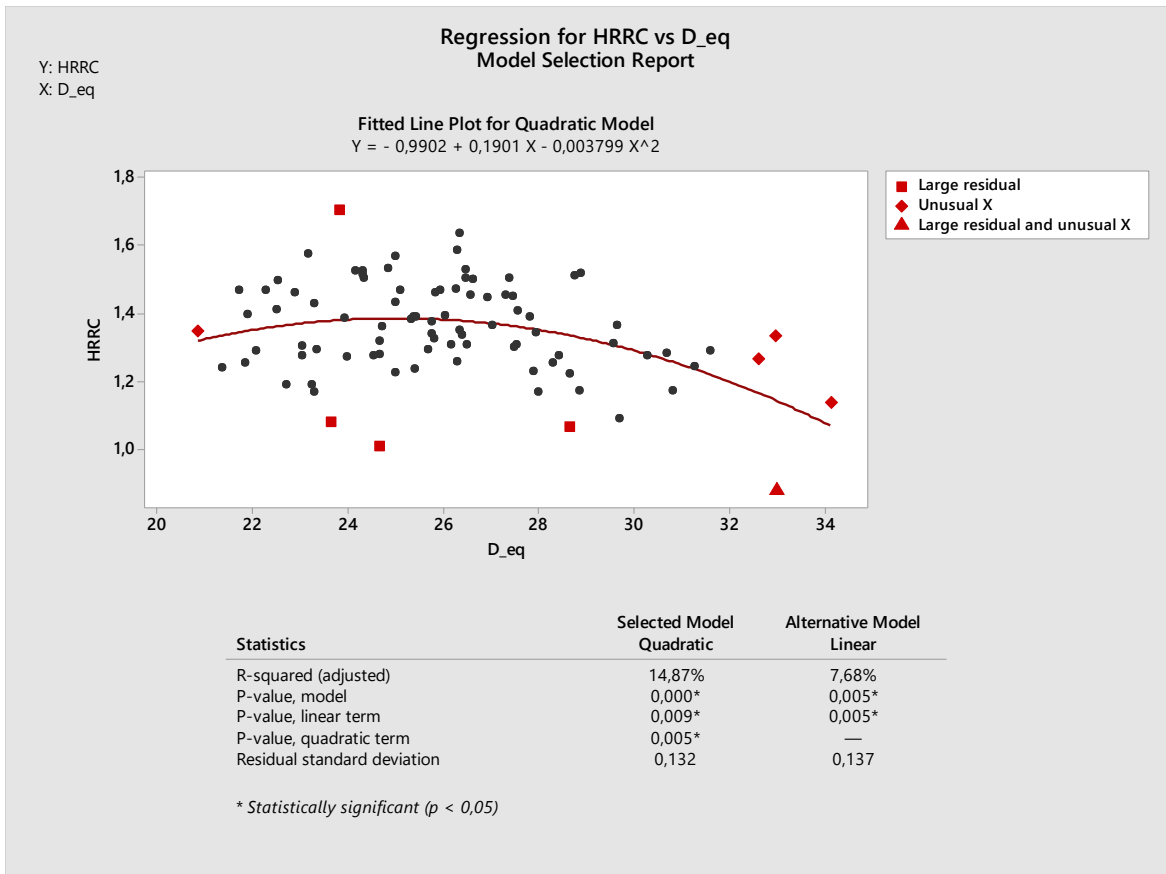
❖ D equivalent – HRRC



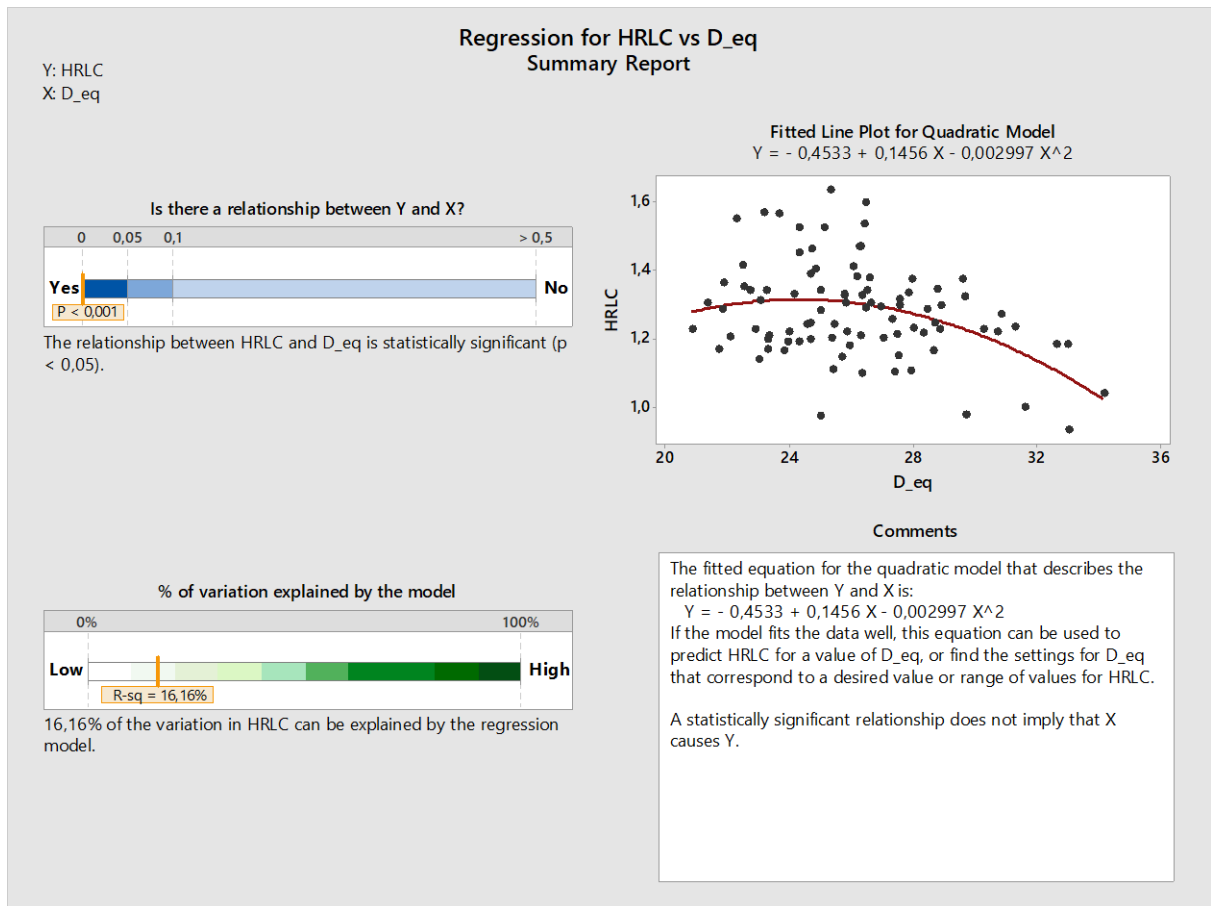
**Report:**

This sample is large enough ( $n = 90$ ) to obtain a precise estimate of the strength of the relationship.

- Large residuals: 5 data points have large residuals and are not well fit by the equation. These points are marked in red on the plots.
- Unusual X values: 5 data points have unusual X values, which can cause the fitted line to be pulled closer to the unusual points and away from other points. These points are marked in red on the Model Selection Report



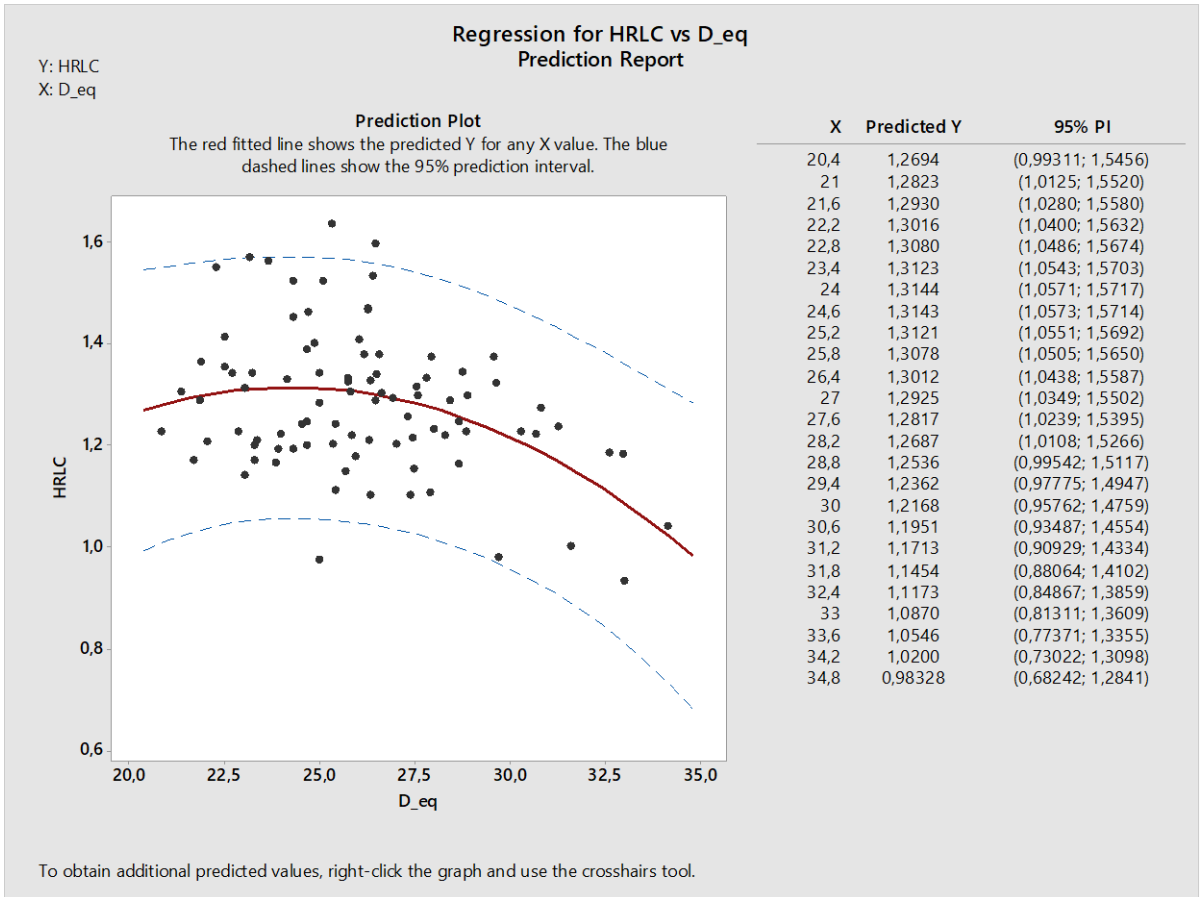
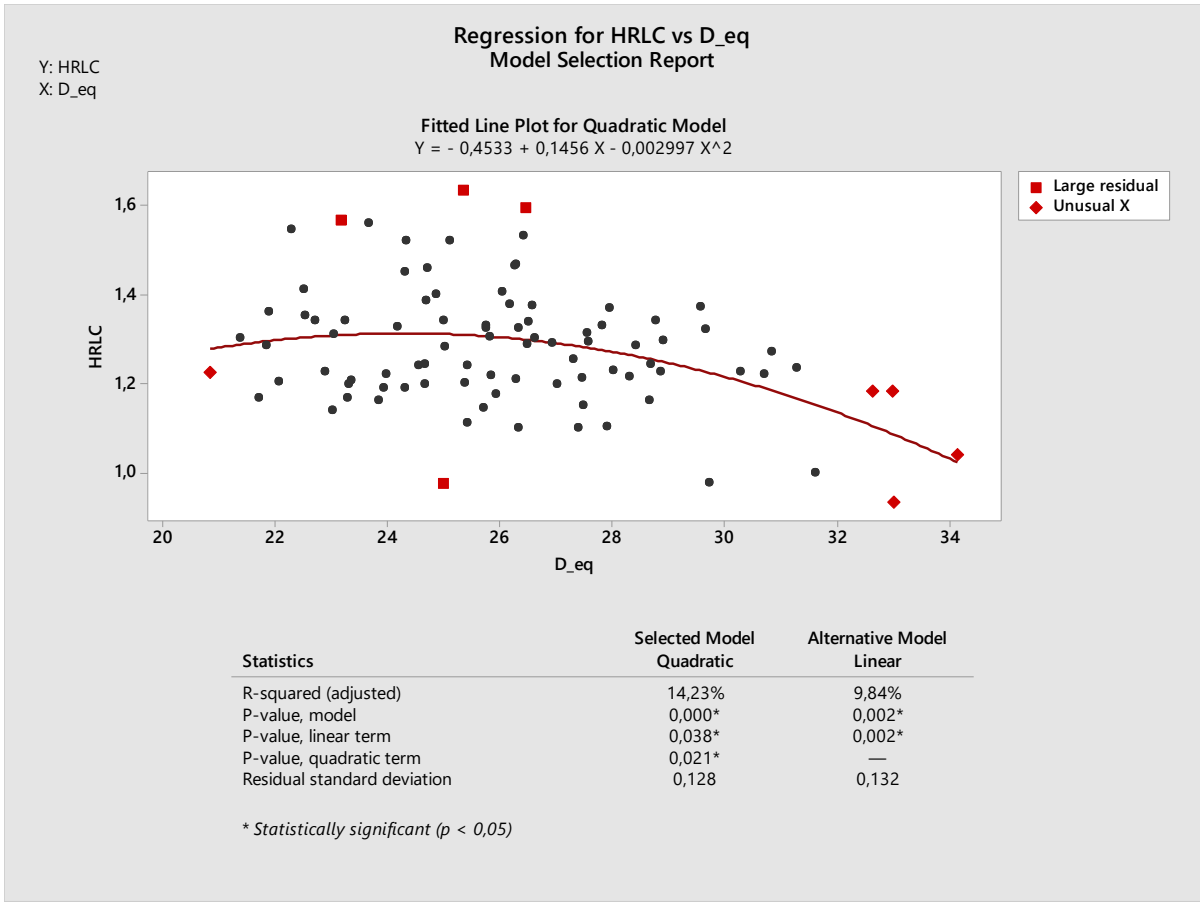
❖ D equivalent - HRLC



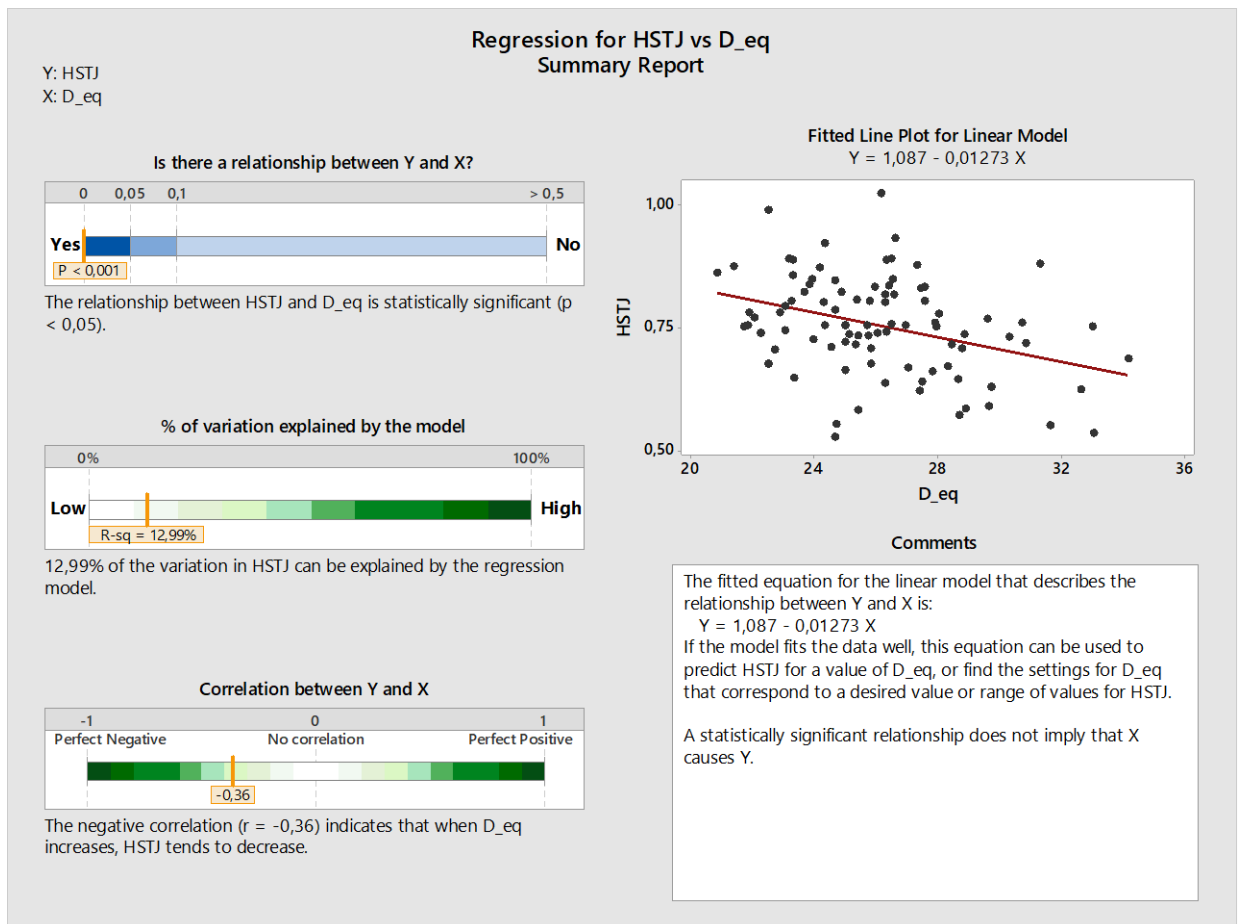
**Report:**

This sample is large enough (n = 90) to obtain a precise estimate of the strength of the relationship.

- Large residuals: 4 data points have large residuals and are not well fit by the equation. These point are marked in red on the plots.
- Unusual X values: 5 data points have unusual X values, which can cause the fitted line to be pulled closer to the unusual points and away from other points. These points are marked in red on the Model Selection Report.



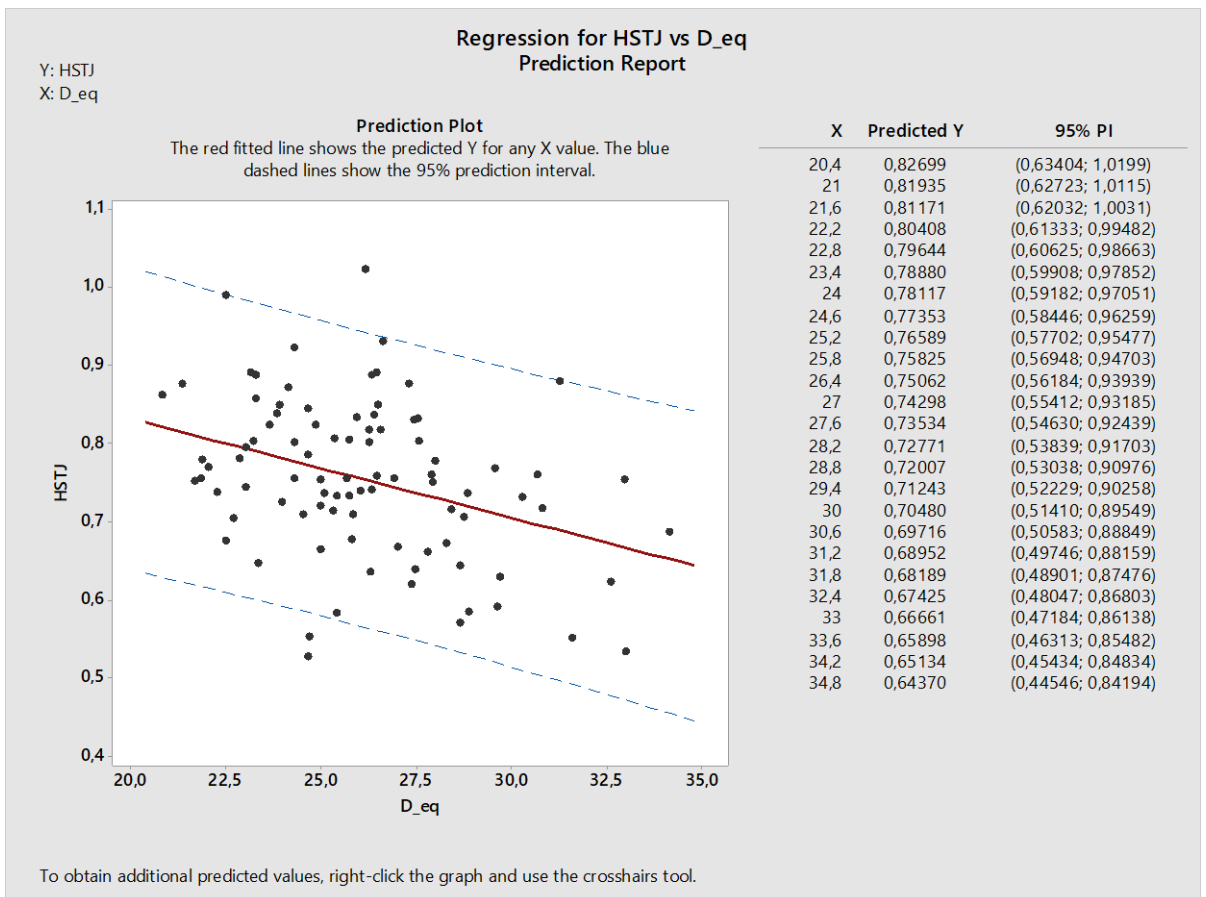
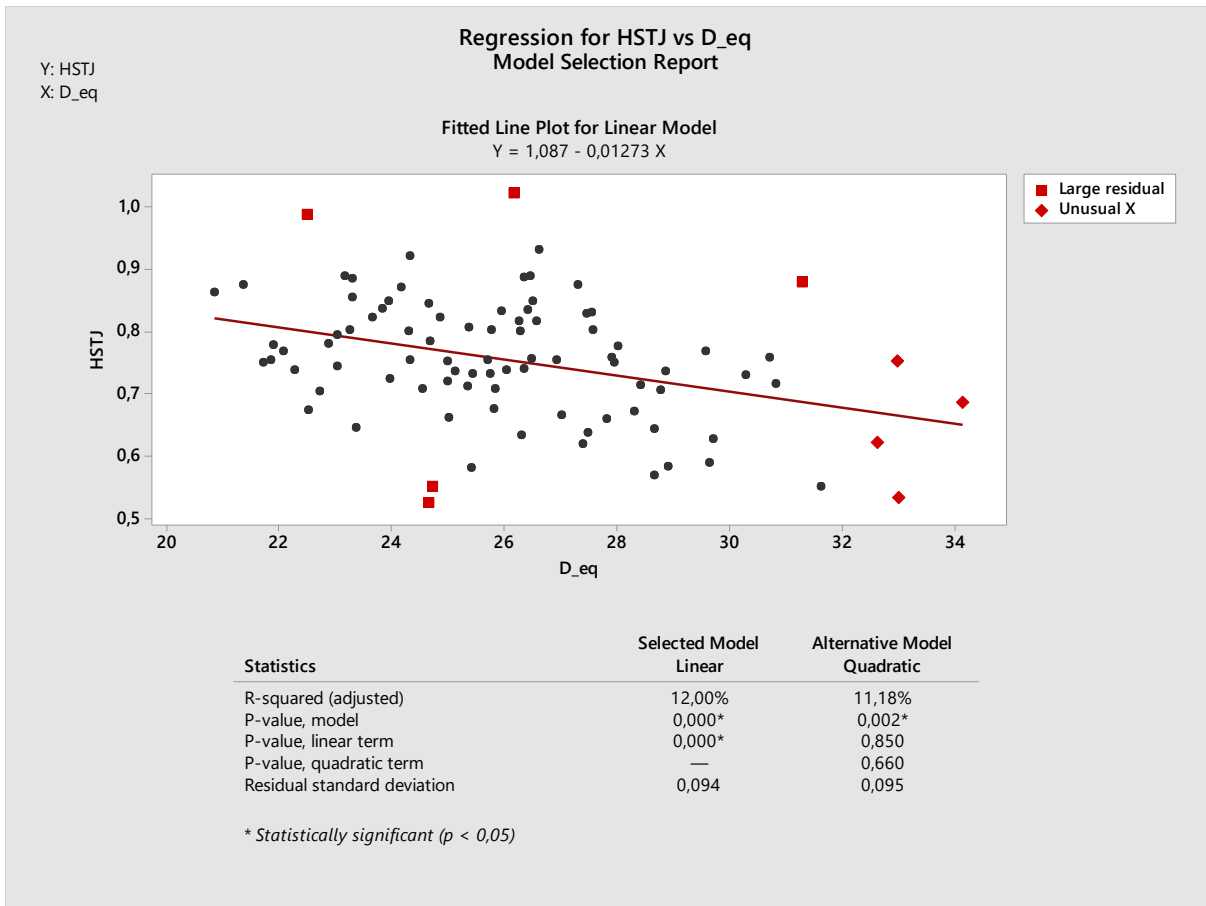
❖ D equivalent – HSTJ



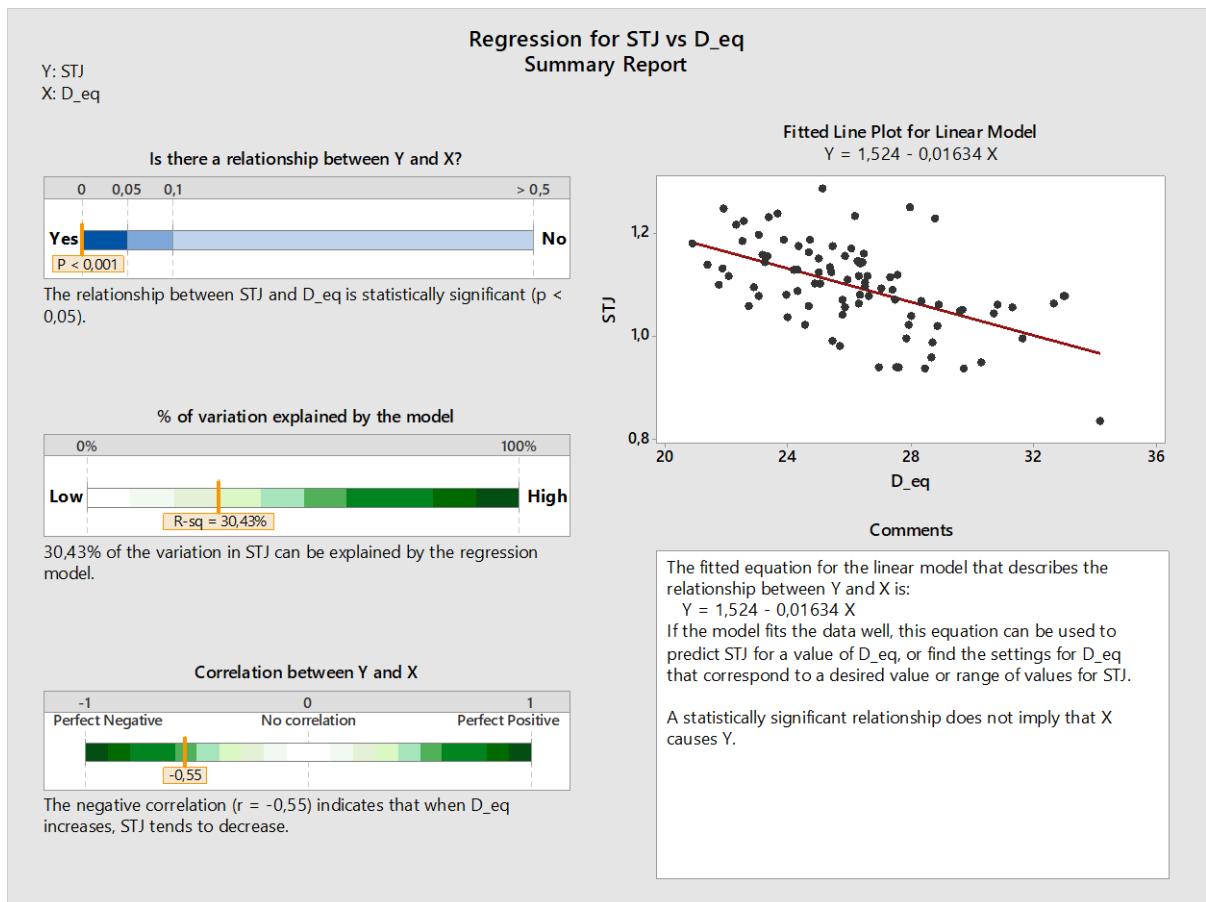
**Report:**

This sample is large enough ( $n = 90$ ) to obtain a precise estimate of the strength of the relationship.

- Large residuals: 5 data points have large residuals and are not well fit by the equation. These points are marked in red on the plots.
- Unusual X values: 4 data points have unusual X values, which can cause the fitted line to be pulled closer to the unusual points and away from other points. These points are marked in red on the Model Selection Report.



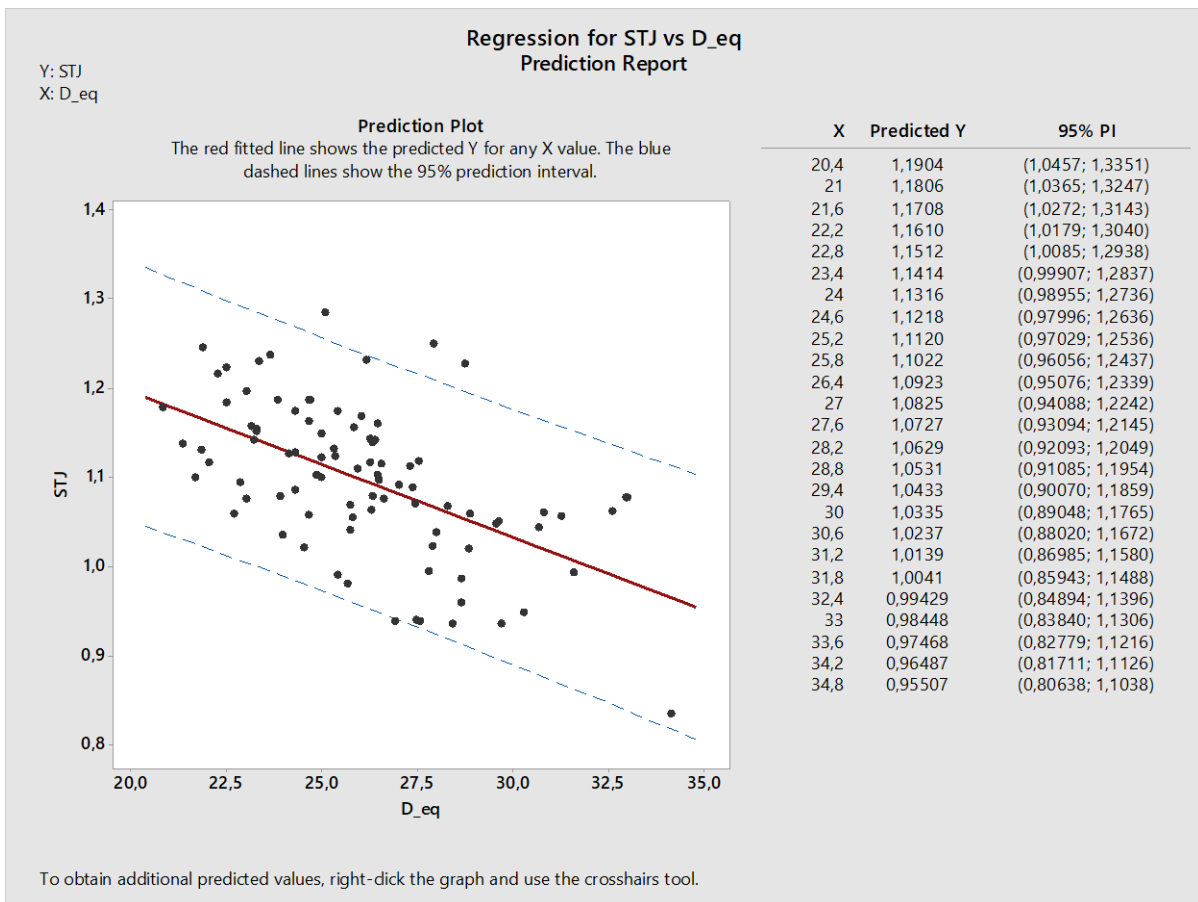
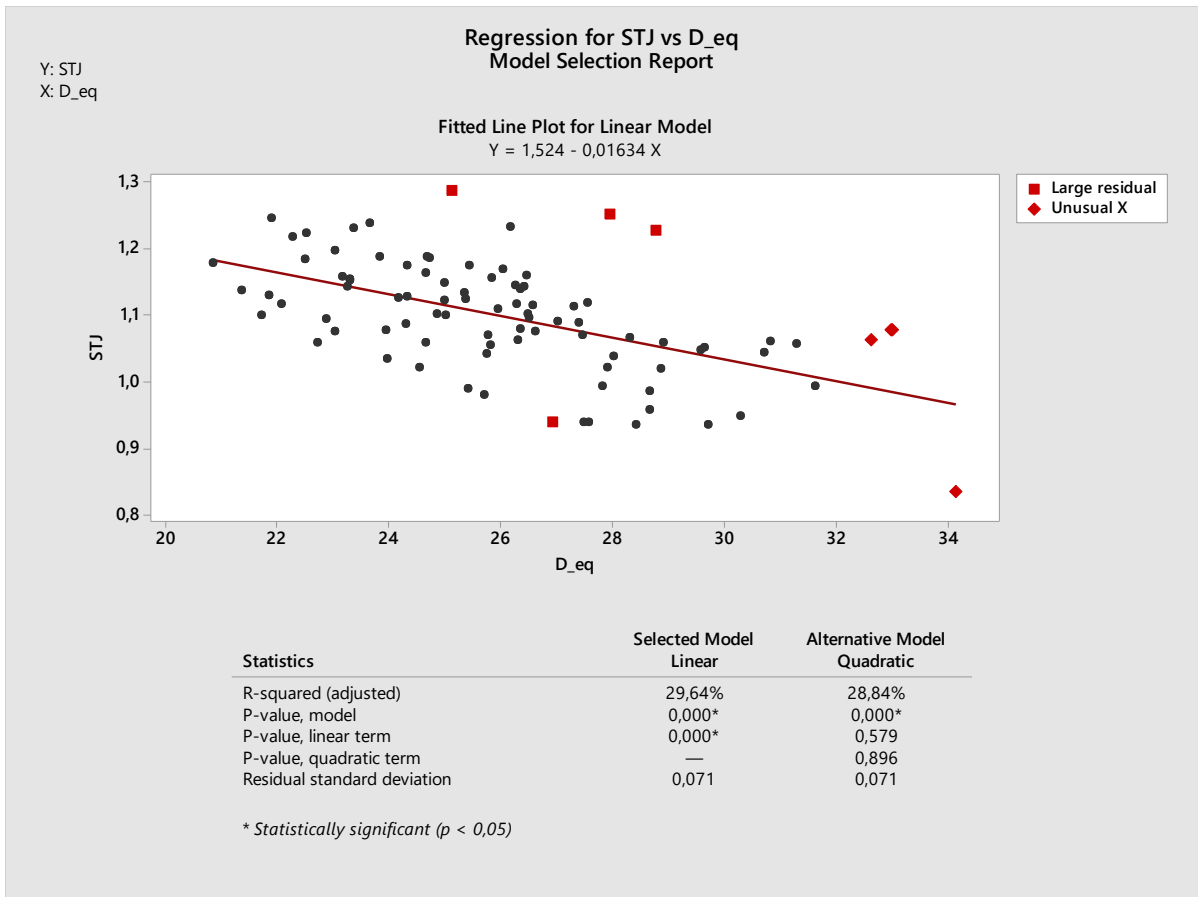
❖ D equivalent – STJ



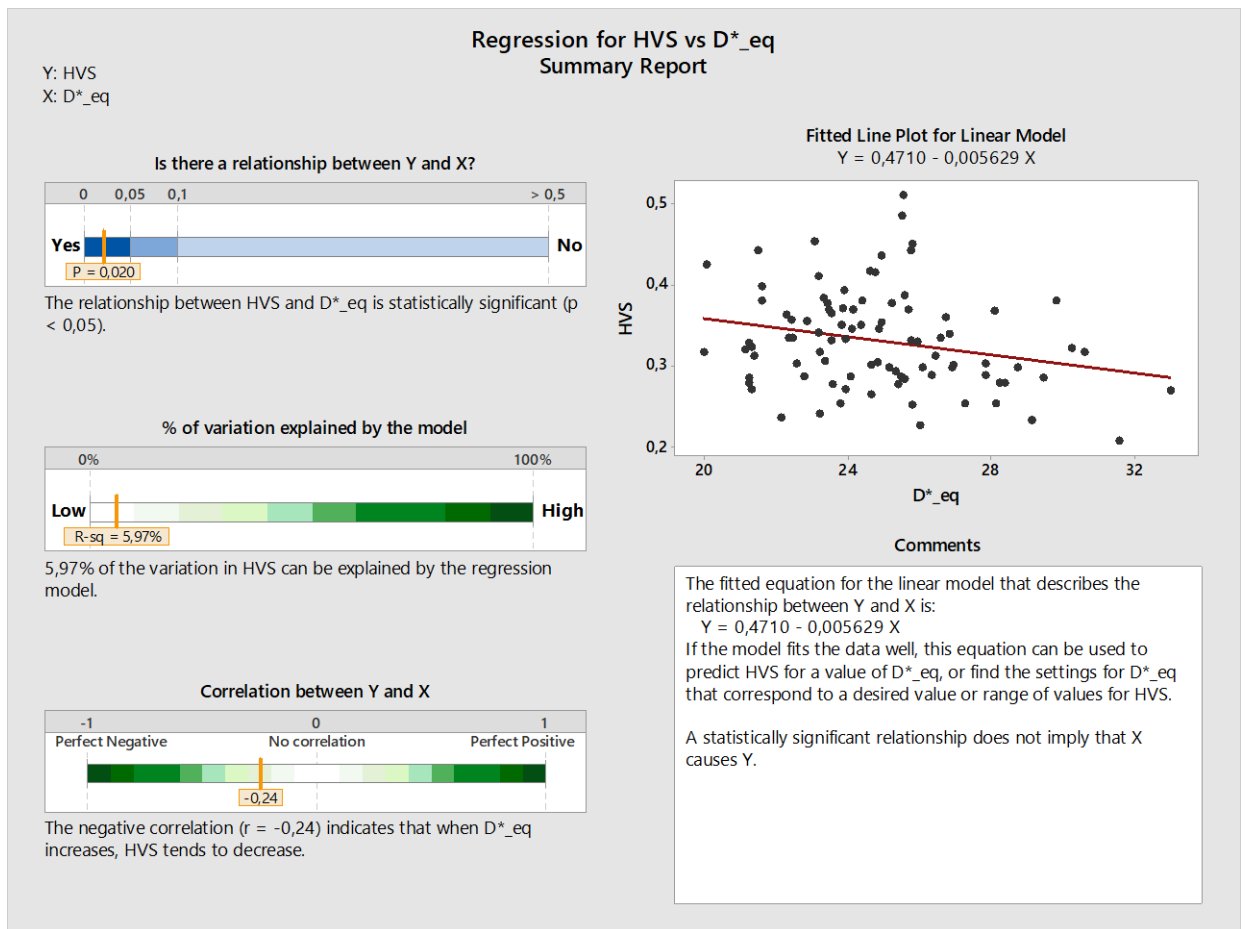
**Report:**

This sample is large enough ( $n = 90$ ) to obtain a precise estimate of the strength of the relationship.

- Large residuals: 4 data points have large residuals and are not well fit by the equation. These points are marked in red on the plots.
- Unusual X values: 4 data points have unusual X values, which can cause the fitted line to be pulled closer to the unusual points and away from other points. These points are marked in red on the Model Selection Report.



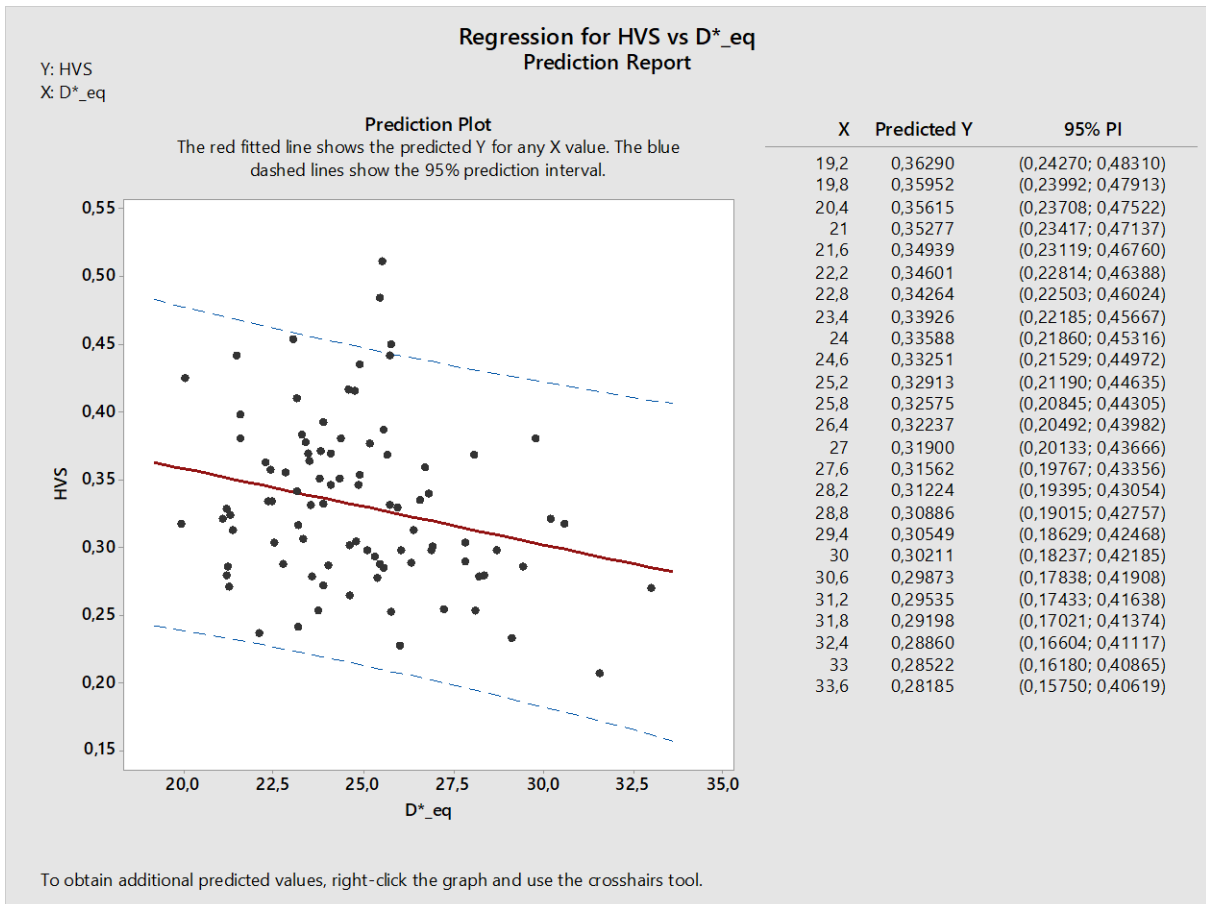
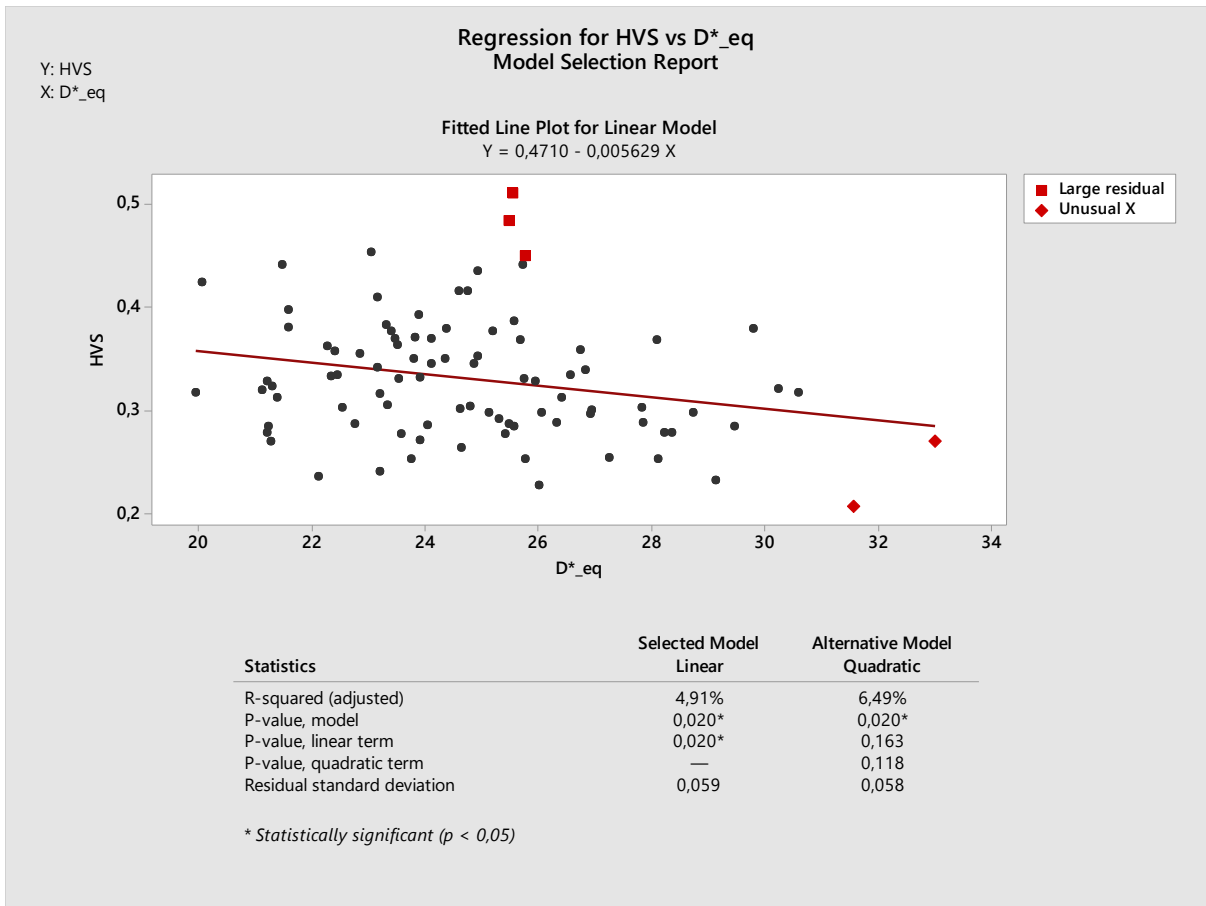
❖ D\*equivalent – HVS



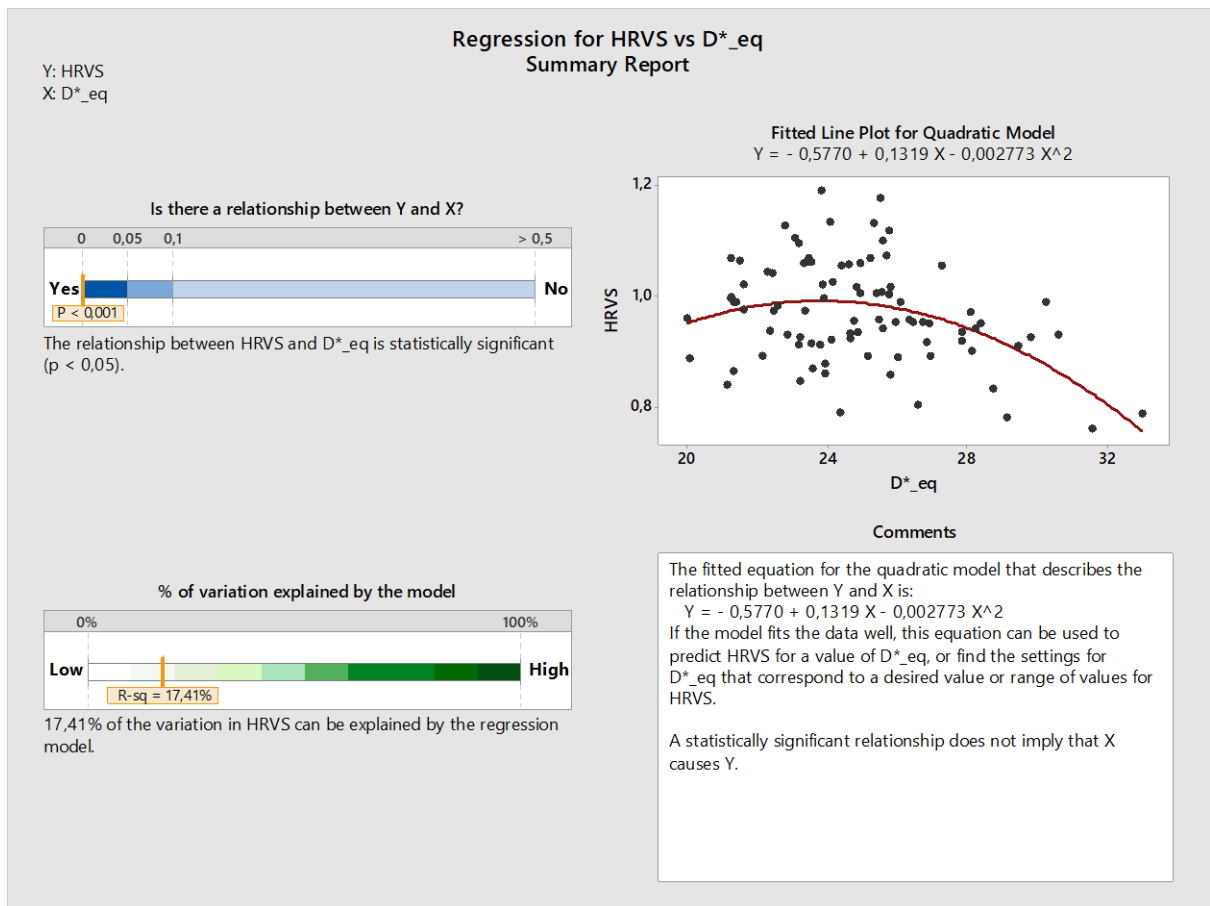
**Report:**

This sample is large enough (n = 90) to obtain a precise estimate of the strength of the relationship.

- Large residuals: 3 data points have large residuals and are not well fit by the equation. These points are marked in red on the plots.
- Unusual X values: 2 data points have unusual X values, which can cause the fitted line to be pulled closer to the unusual points and away from other points. These points are marked in red on the Model Selection Report.



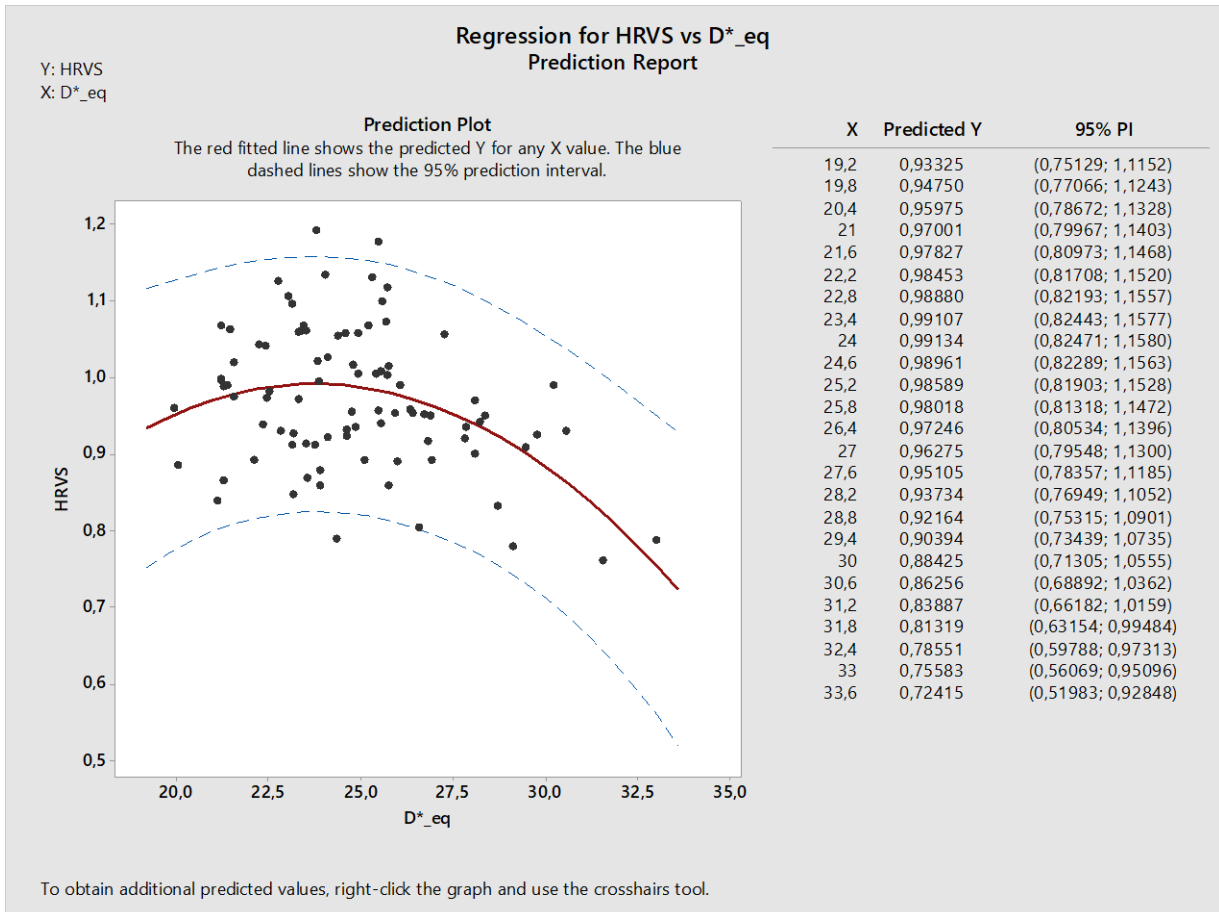
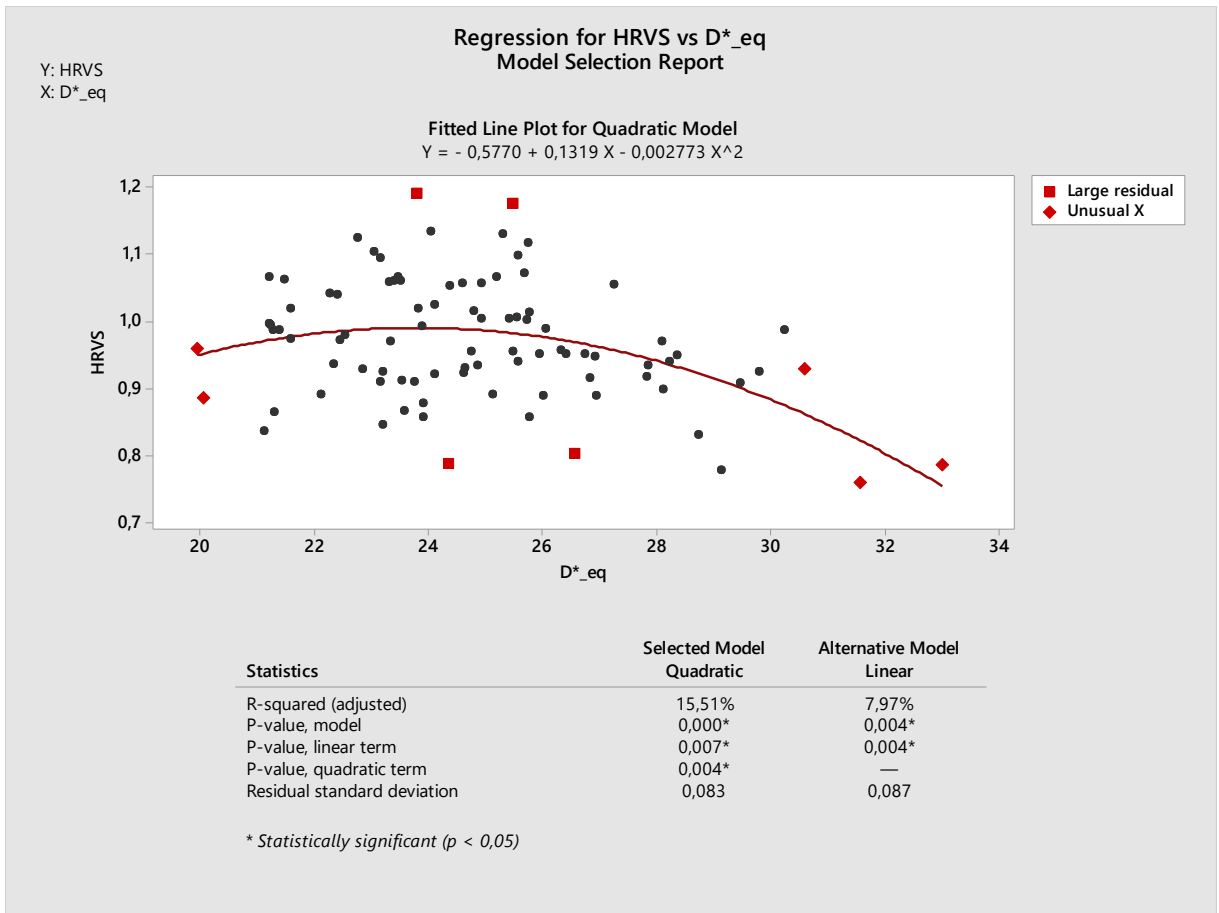
❖ D\*equivalent – HRVS



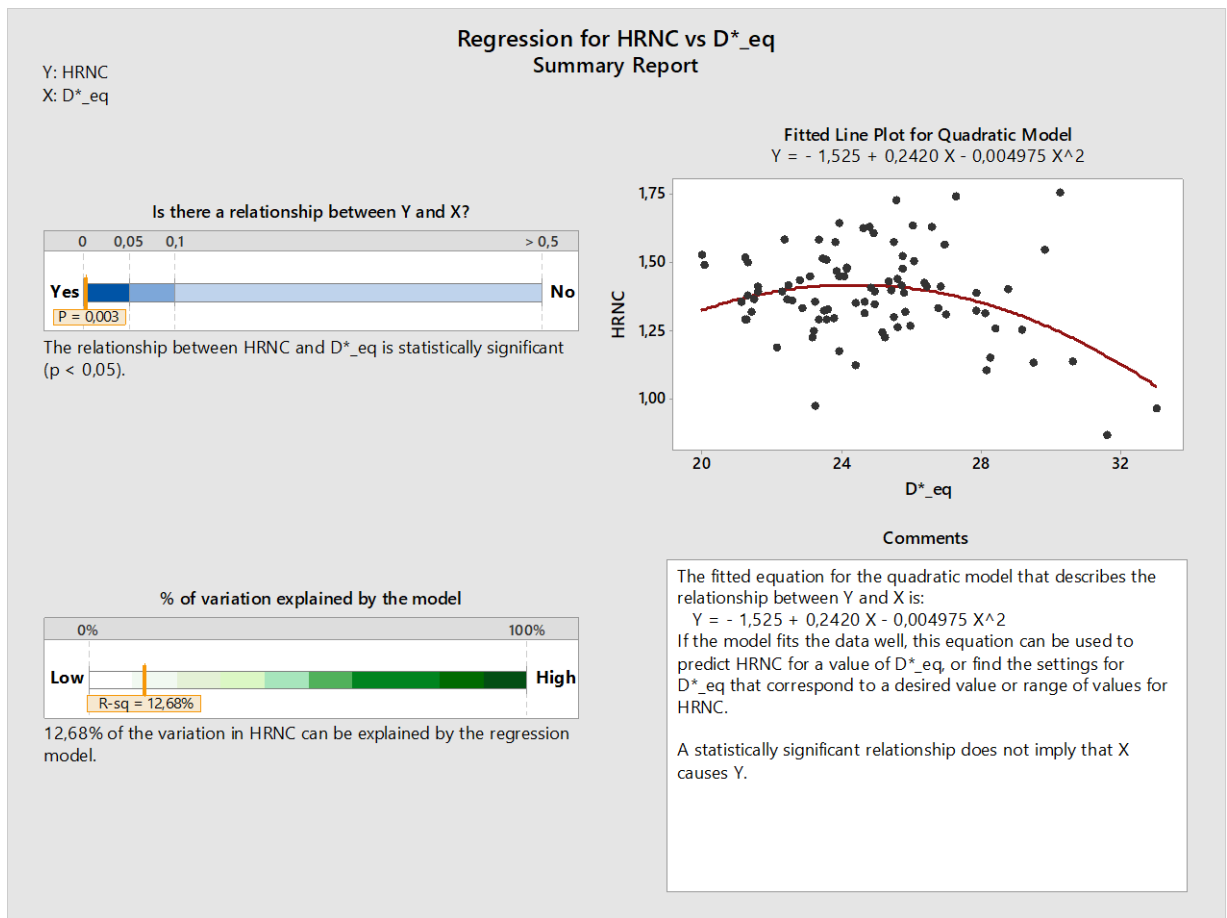
**Report:**

This sample is large enough ( $n = 90$ ) to obtain a precise estimate of the strength of the relationship.

- Large residuals: 4 data points have large residuals and are not well fit by the equation. These points are marked in red on the plots.
- Unusual X values: 5 data points have unusual X values, which can cause the fitted line to be pulled closer to the unusual points and away from other points. These points are marked in red on the Model Selection Report.



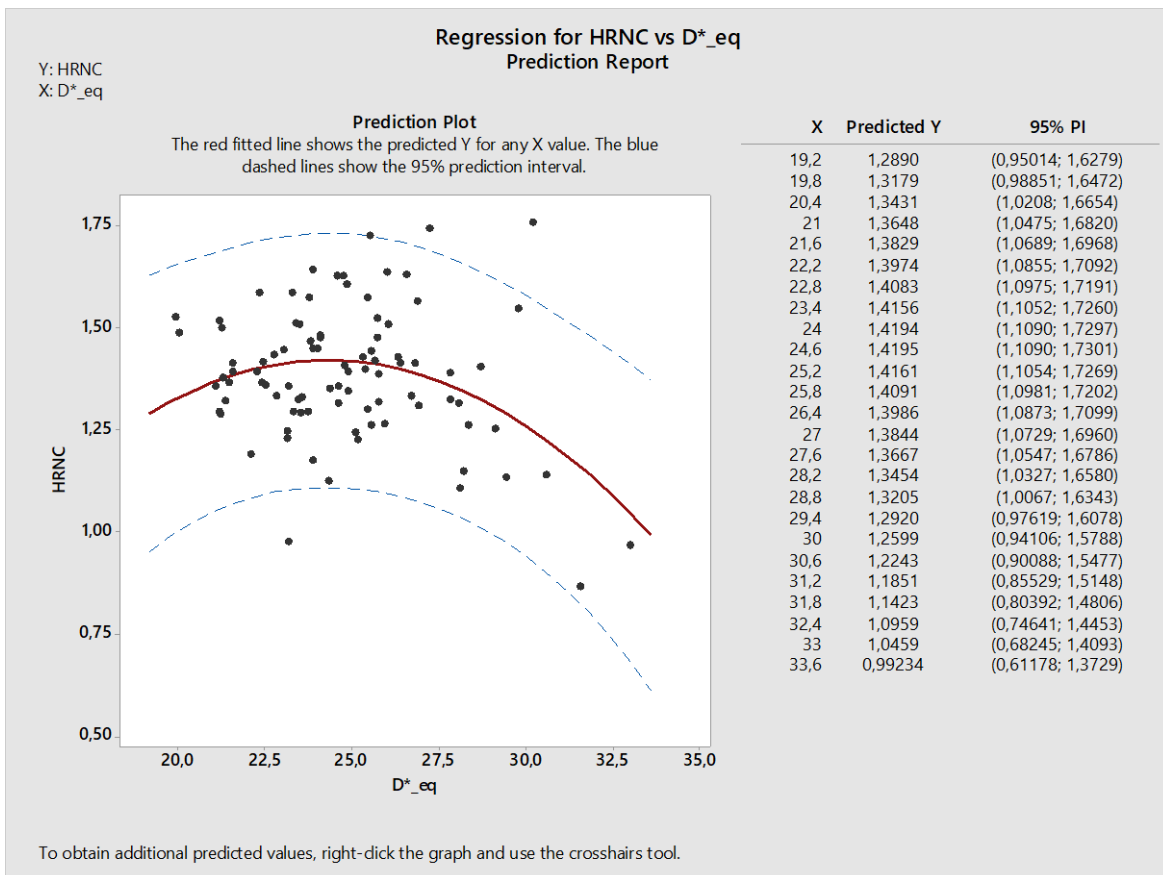
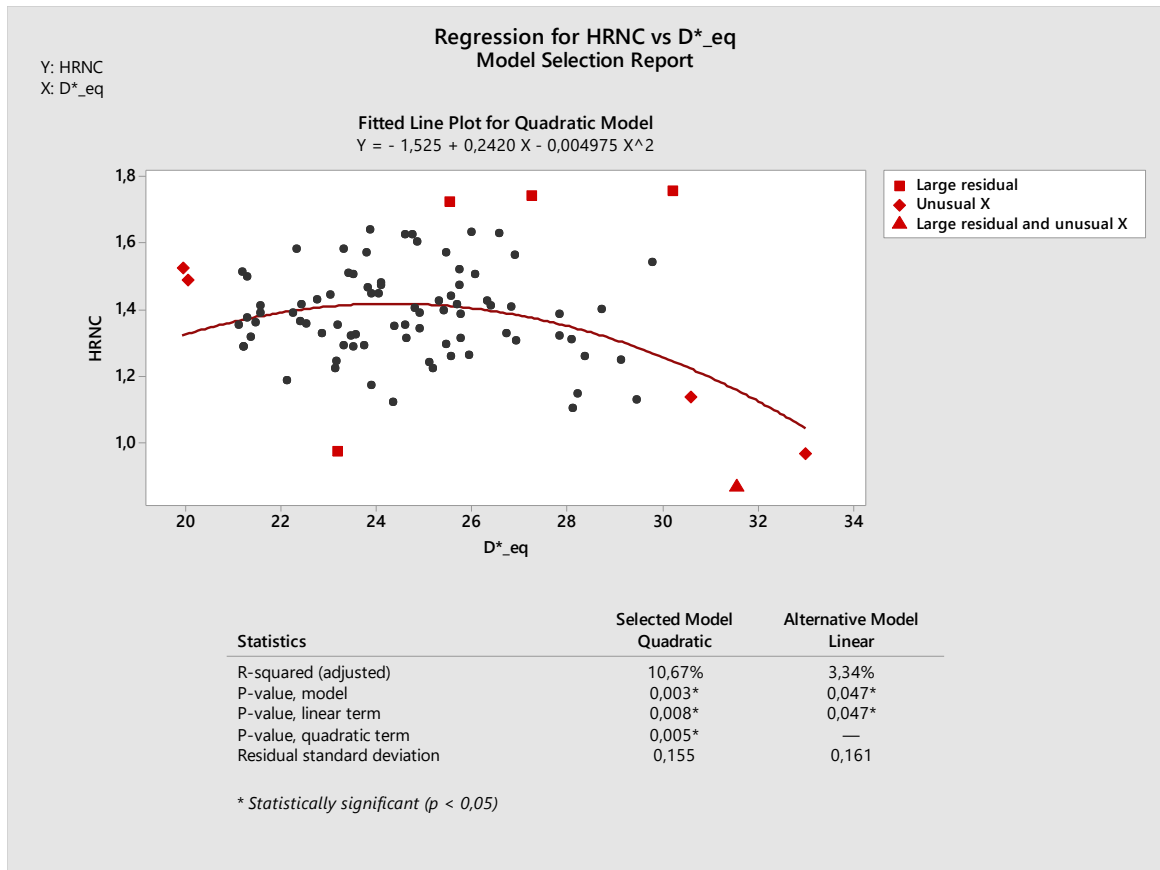
❖ D\*equivalent – HRNC



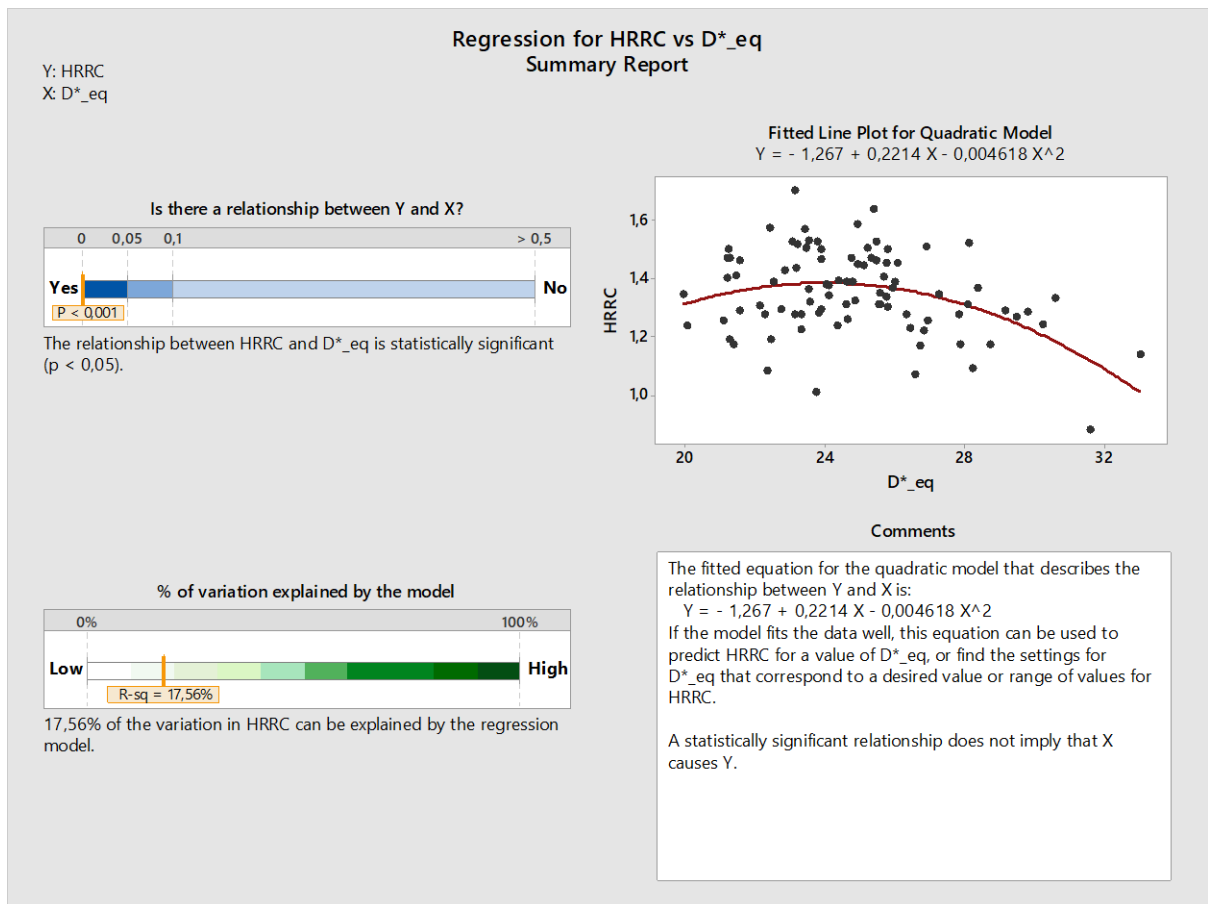
**Report:**

This sample is large enough (n = 90) to obtain a precise estimate of the strength of the relationship.

- Large residuals: 5 data points have large residuals and are not well fit by the equation. These points are marked in red on the plots.
- Unusual X values: 5 data points have unusual X values, which can cause the fitted line to be pulled closer to the unusual points and away from other points. These points are marked in red on the Model Selection Report.



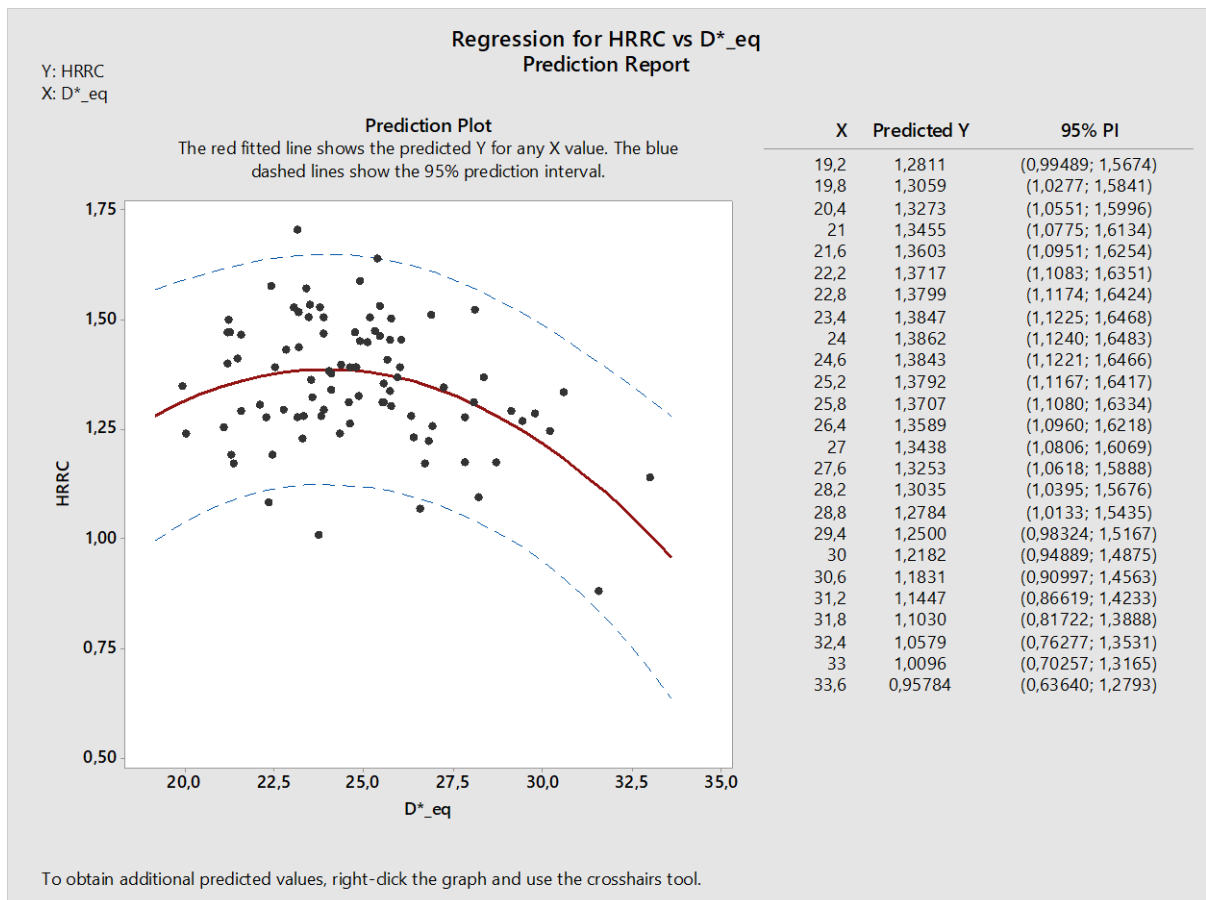
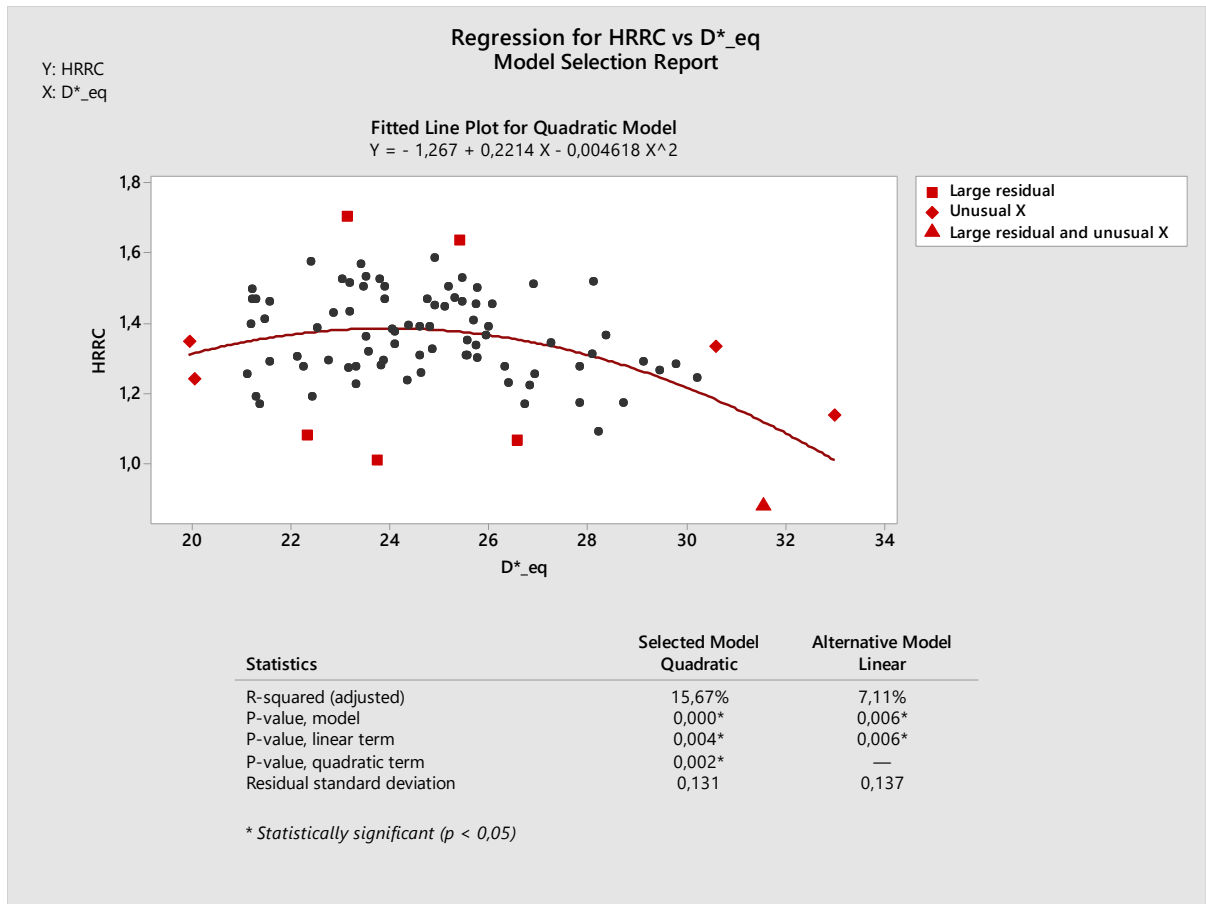
❖ D\*equivalent – HRRC



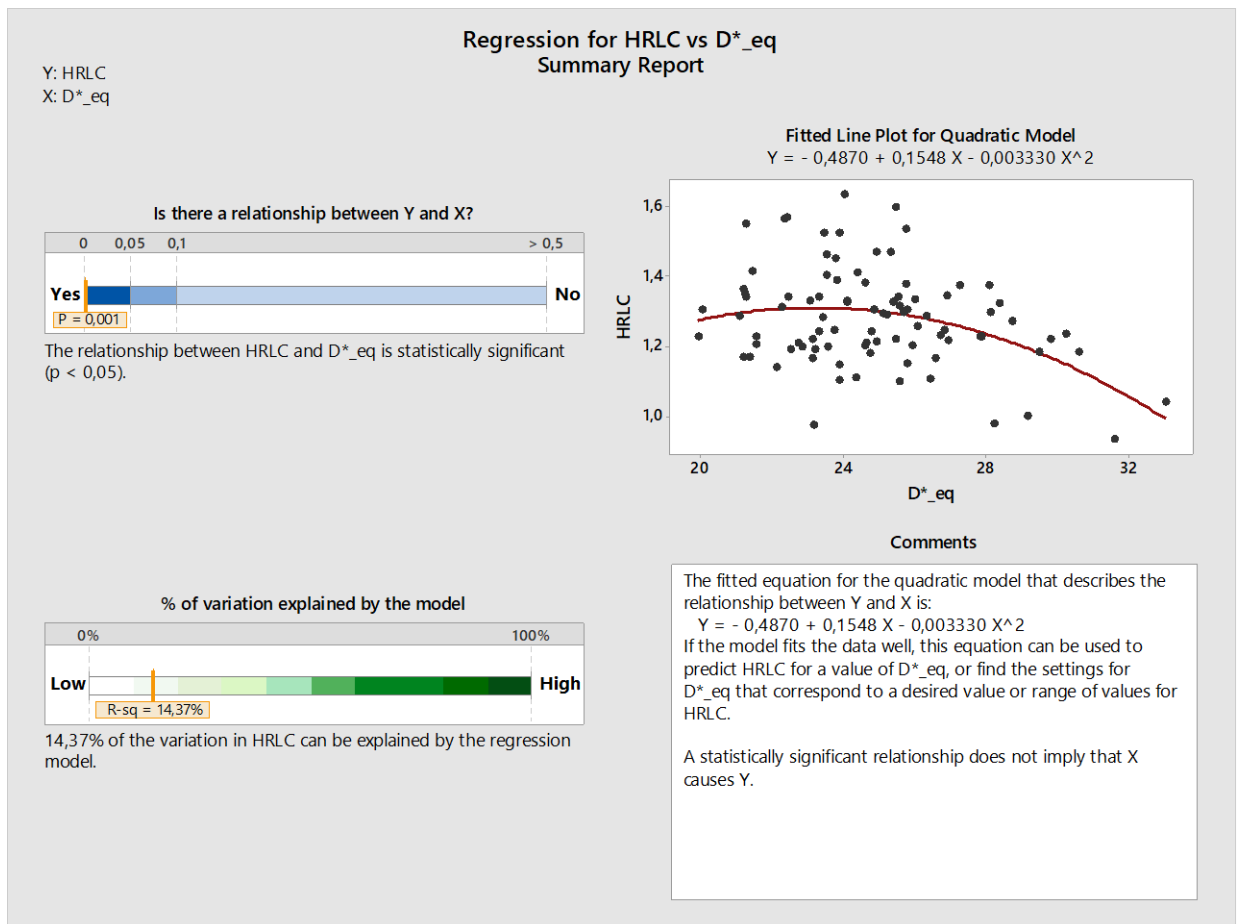
**Report:**

This sample is large enough (n = 90) to obtain a precise estimate of the strength of the relationship.

- Large residuals: 6 data points have large residuals and are not well fit by the equation. These points are marked in red on the plots.
- Unusual X values: 5 data points have unusual X values, which can cause the fitted line to be pulled closer to the unusual points and away from other points. These points are marked in red on the Model Selection Report.



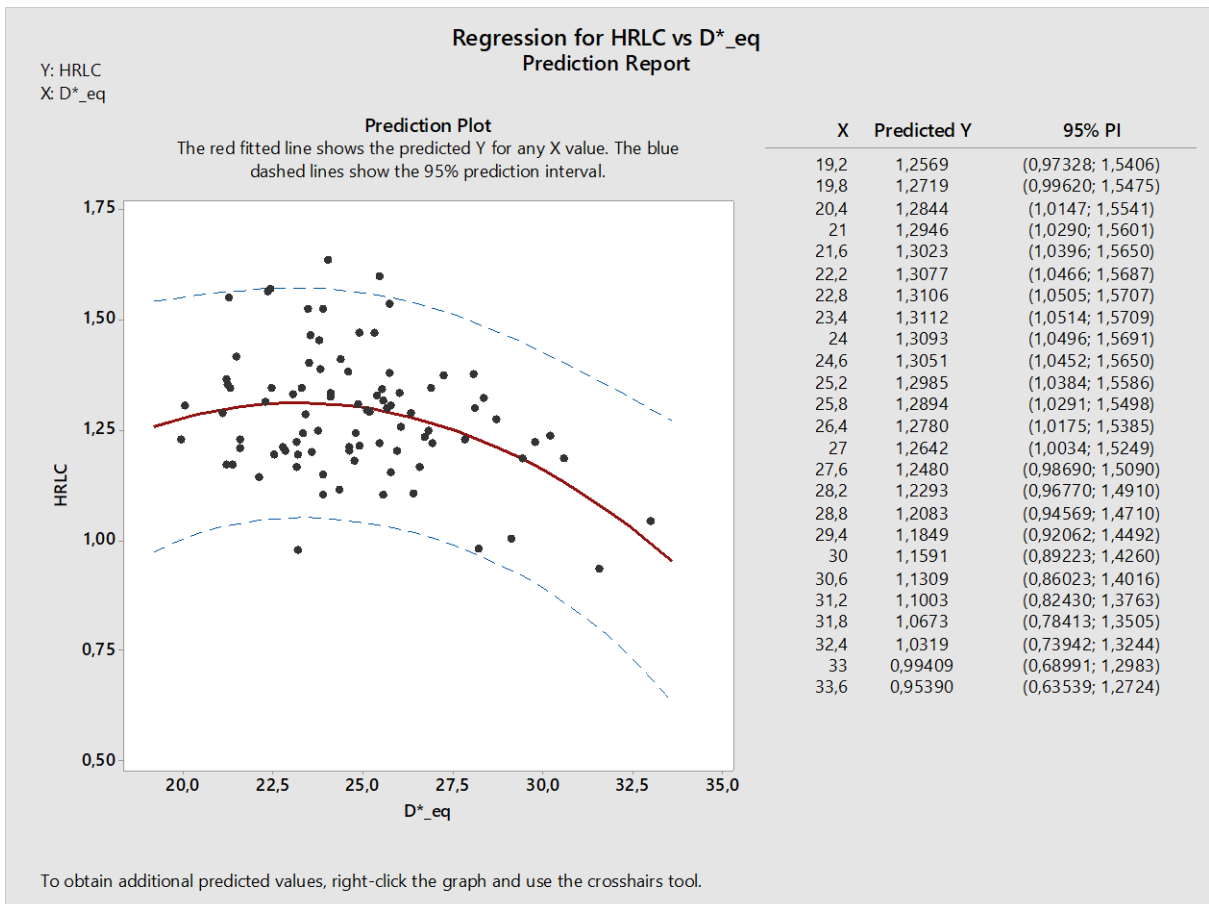
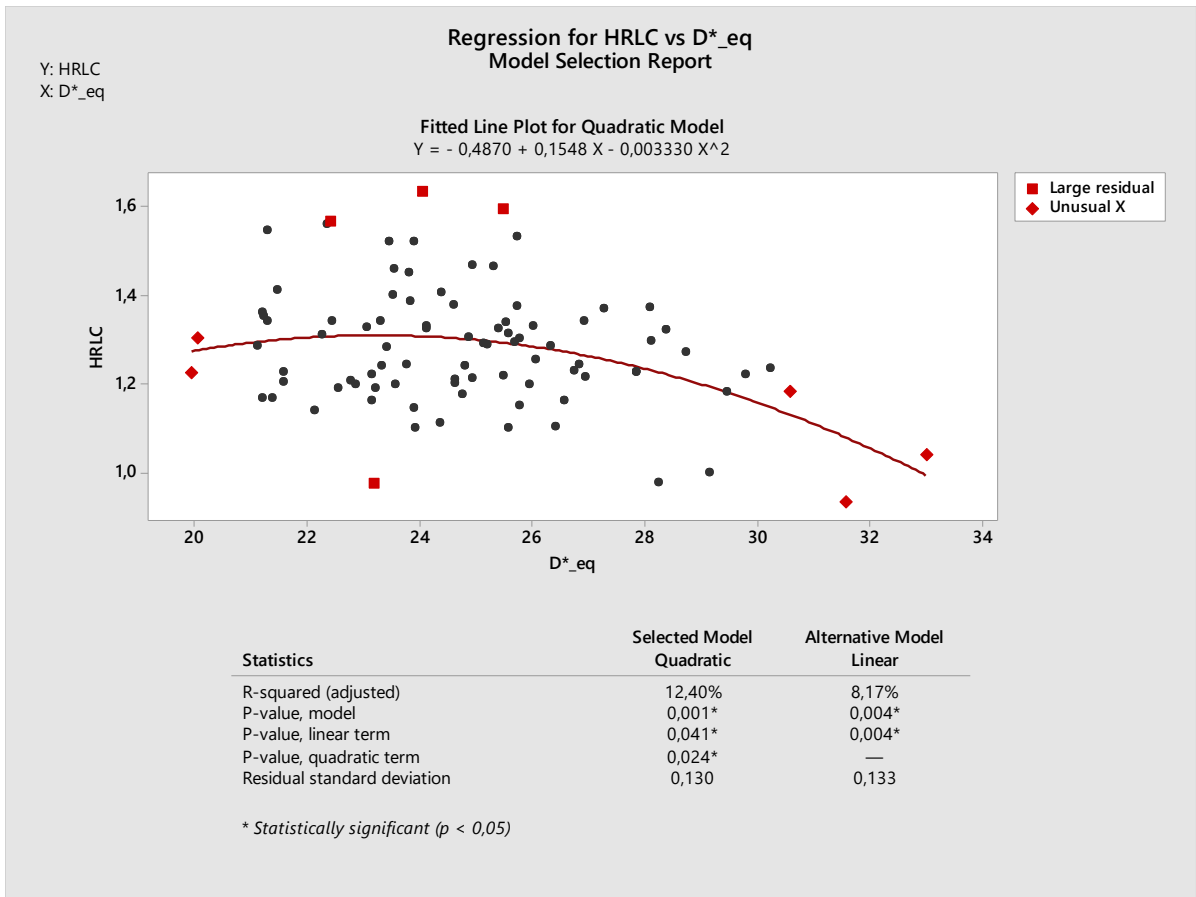
❖ D\*equivalent – HRLC



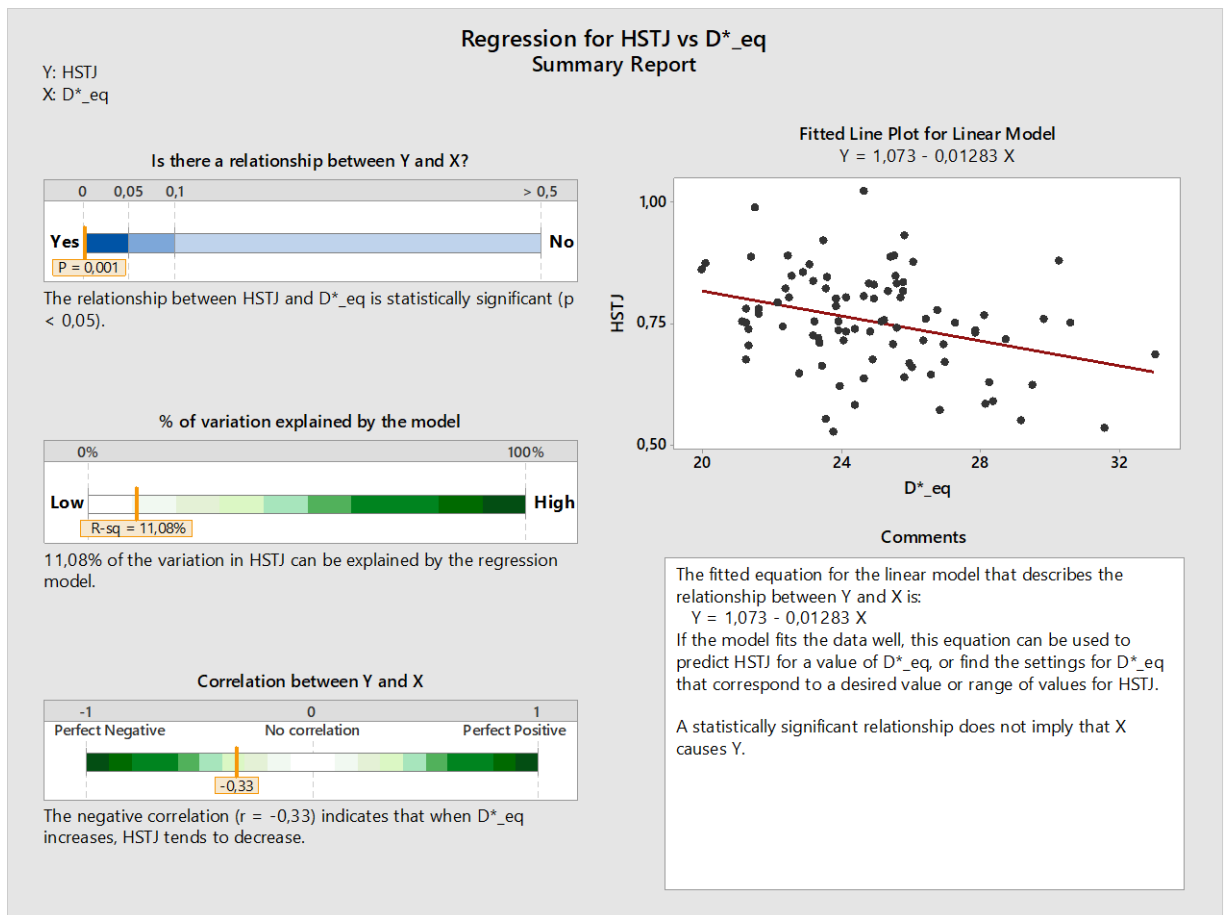
**Report:**

This sample is large enough (n = 90) to obtain a precise estimate of the strength of the relationship.

- Large residuals: 4 data points have large residuals and are not well fit by the equation. These points are marked in red on the plots.
- Unusual X values: 5 data points have unusual X values, which can cause the fitted line to be pulled closer to the unusual points and away from other points. These points are marked in red on the Model Selection Report.



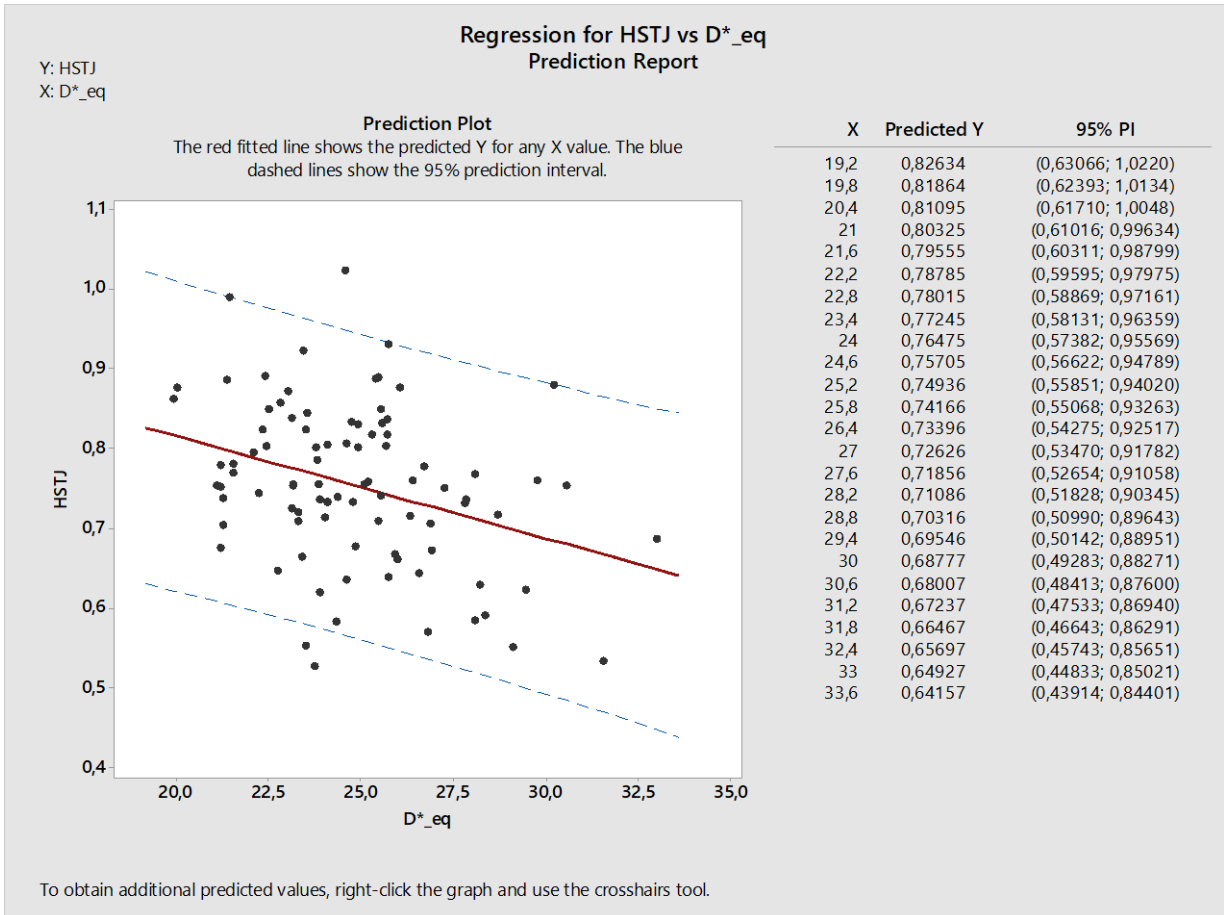
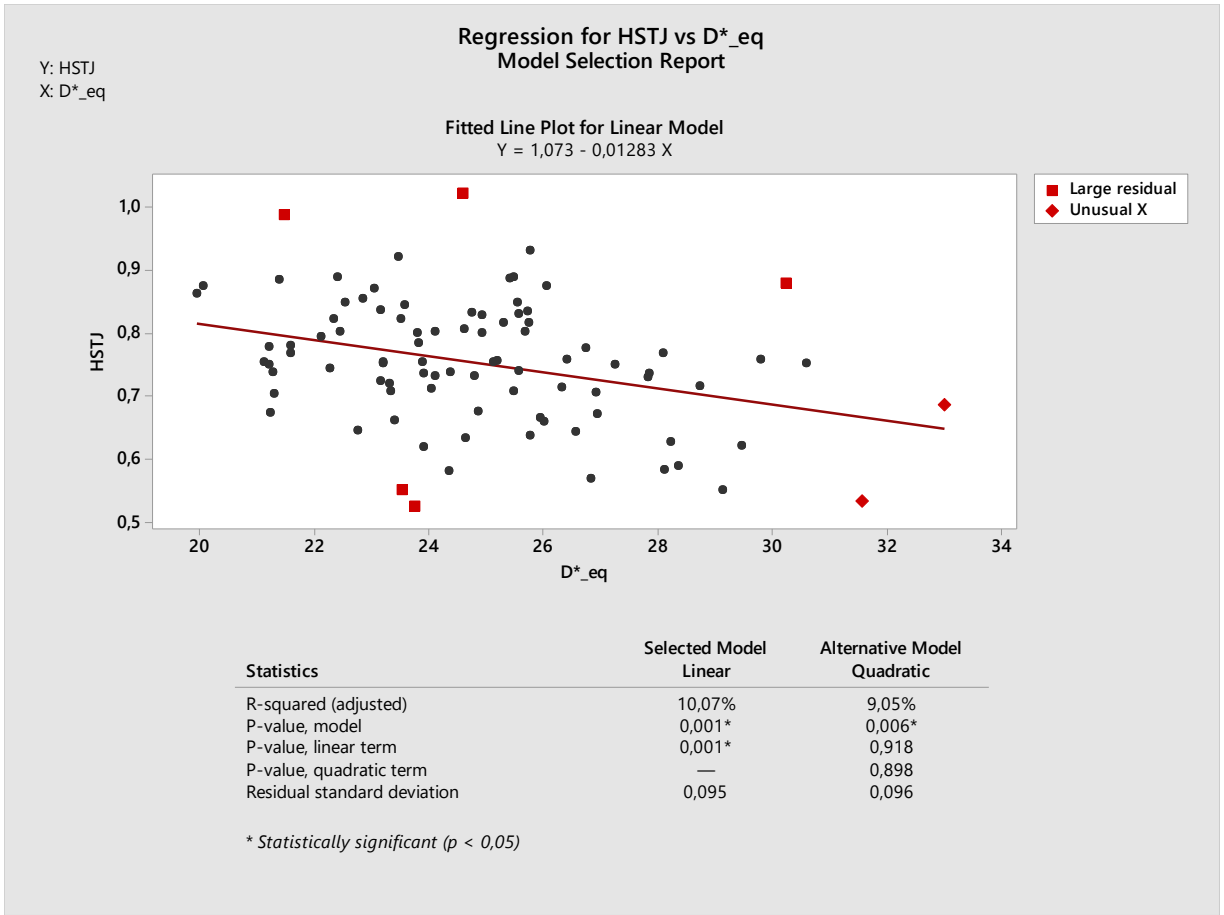
❖ D\*equivalent – HSTJ



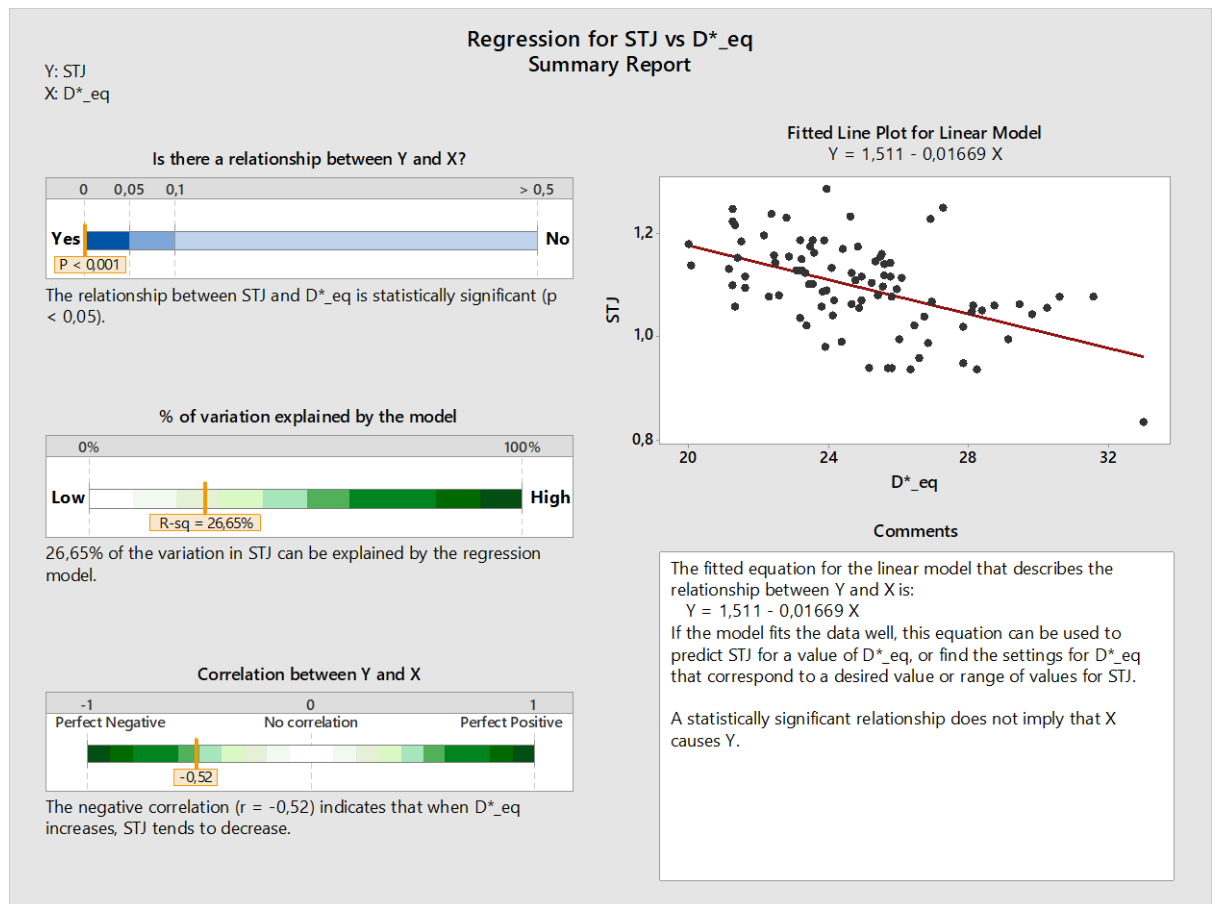
**Report:**

This sample is large enough ( $n = 90$ ) to obtain a precise estimate of the strength of the relationship.

- Large residuals: 5 data points have large residuals and are not well fit by the equation. These points are marked in red on the plots.
- Unusual X values: 2 data points have unusual X values, which can cause the fitted line to be pulled closer to the unusual points and away from other points. These points are marked in red on the Model Selection Report.



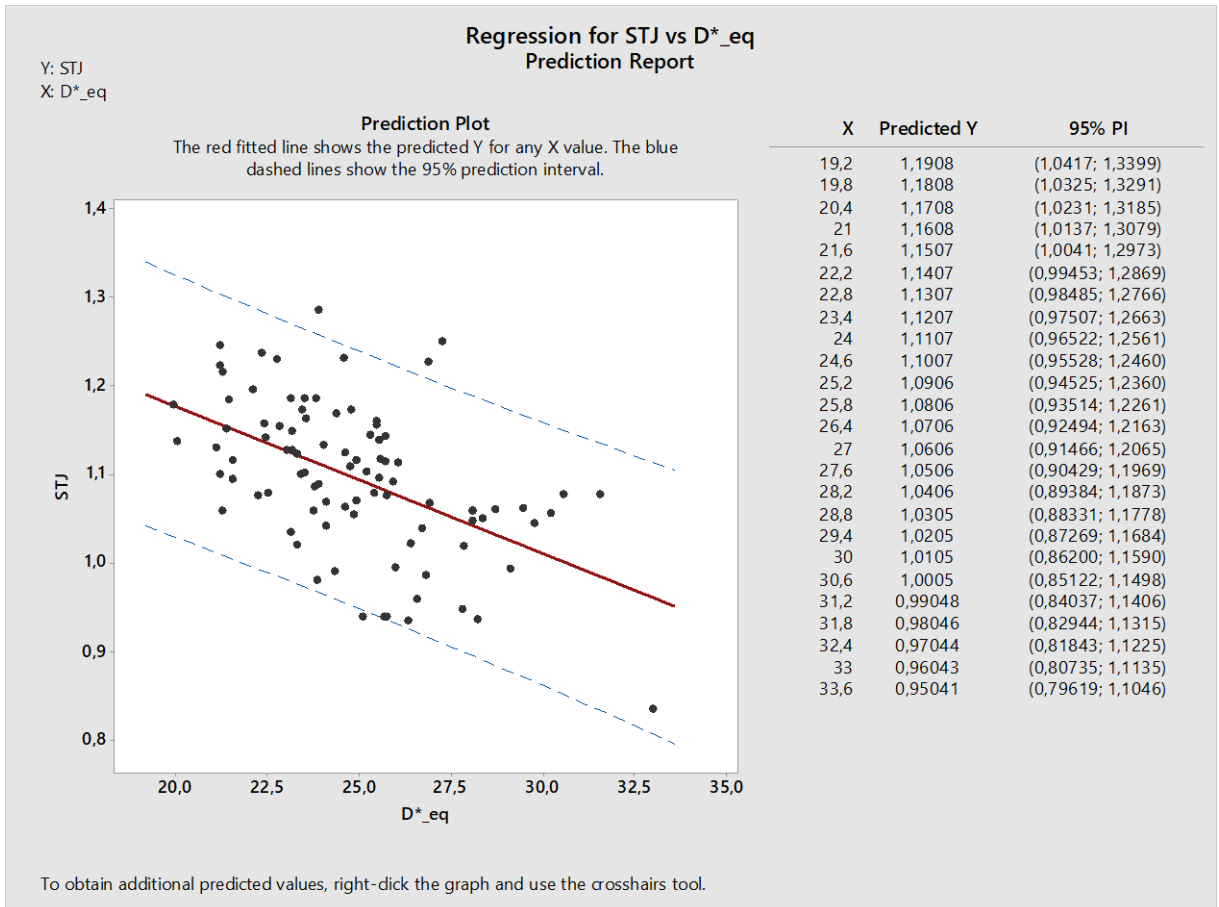
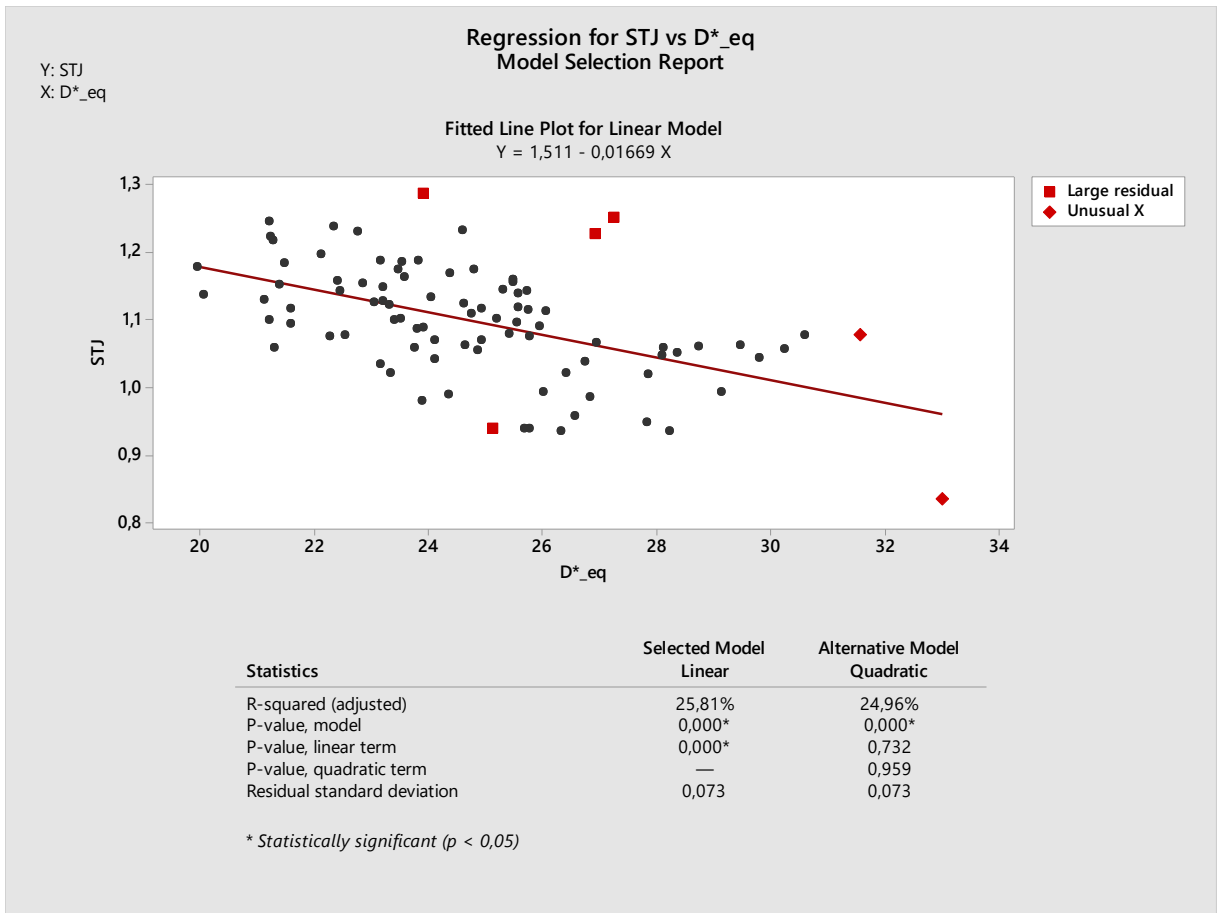
❖ D\*equivalent – STJ



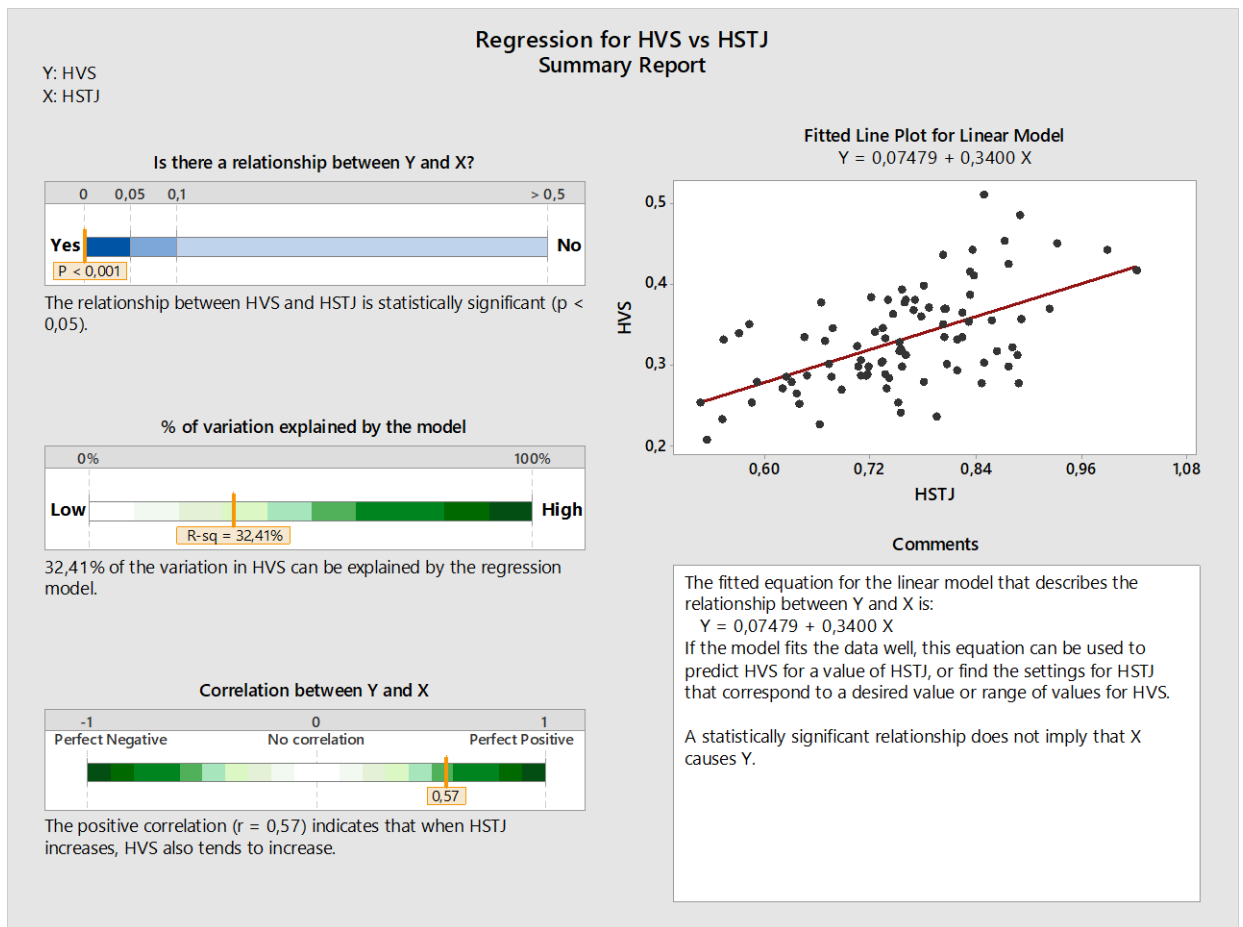
**Report:**

This sample is large enough (n = 90) to obtain a precise estimate of the strength of the relationship.

- Large residuals: 4 data points have large residuals and are not well fit by the equation. These points are marked in red on the plots.
- Unusual X values: 2 data points have unusual X values, which can cause the fitted line to be pulled closer to the unusual points and away from other points. These points are marked in red on the Model Selection Report.



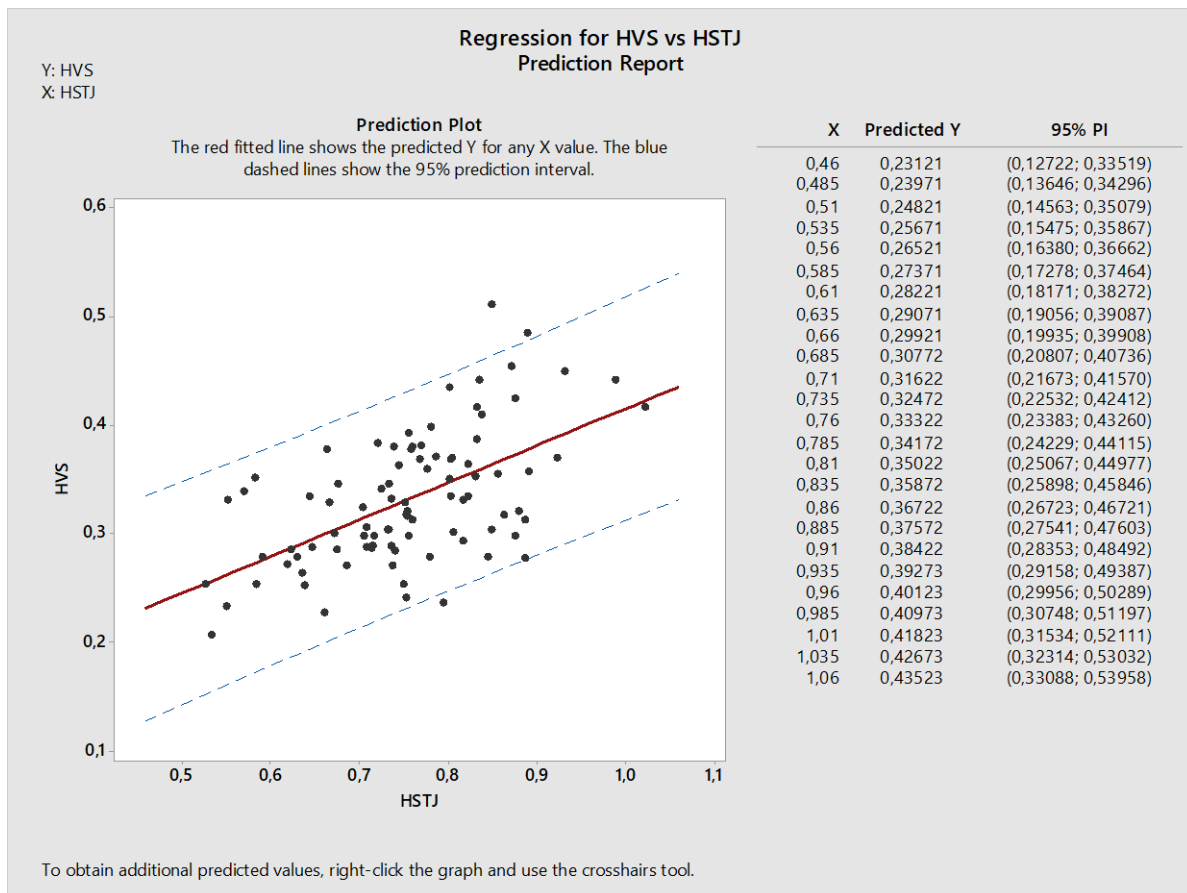
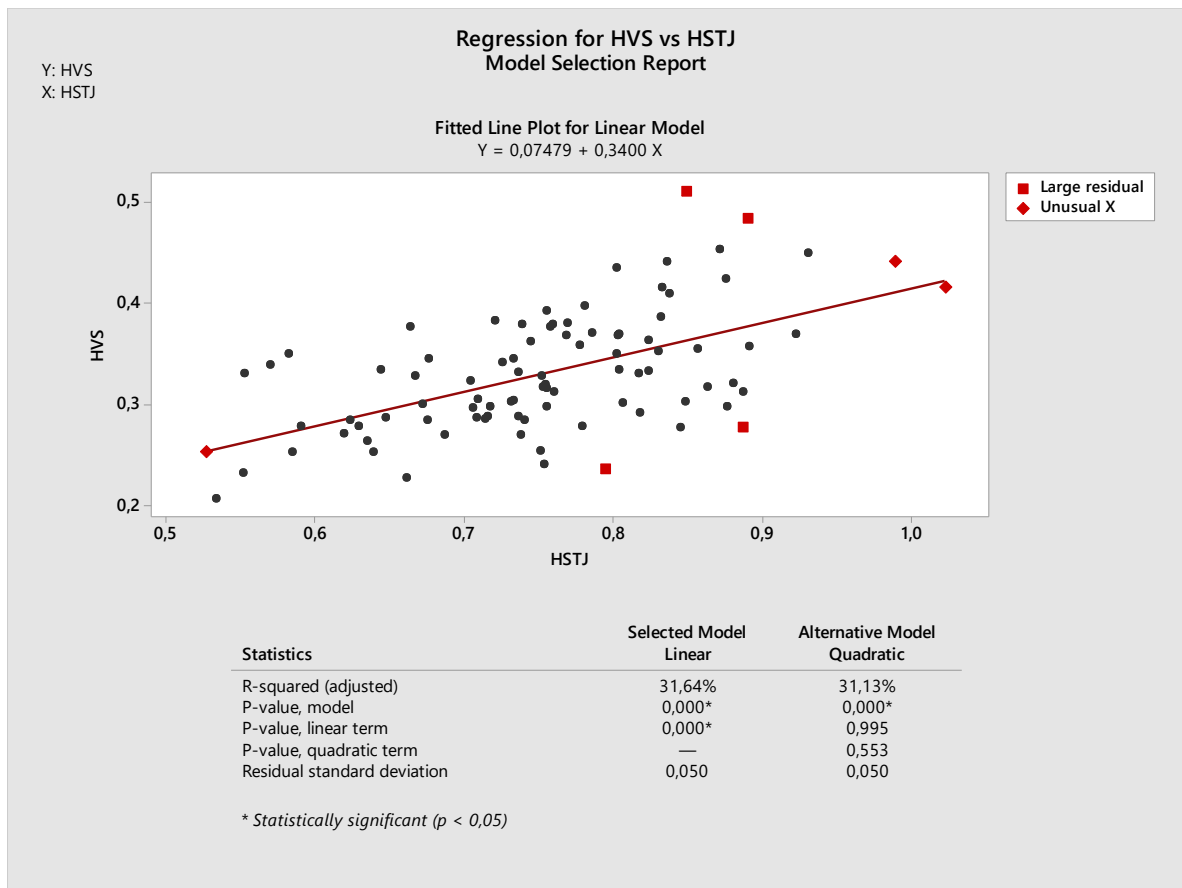
❖ HVS – HSTJ



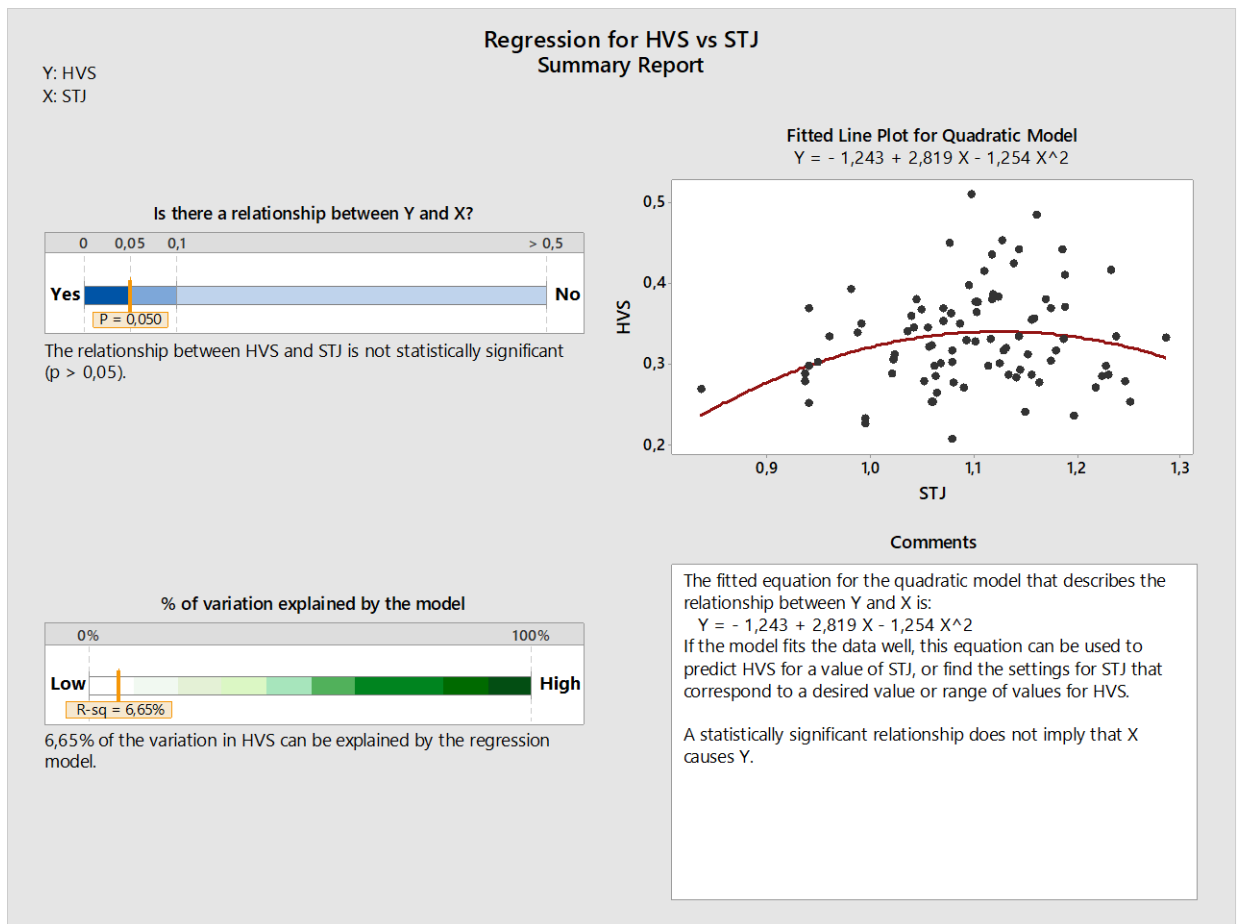
Report:

This sample is large enough ( $n = 90$ ) to obtain a precise estimate of the strength of the relationship.

- Large residuals: 4 data points have large residuals and are not well fit by the equation. These points are marked in red on the plots.
- Unusual X values: 3 data points have unusual X values, which can cause the fitted line to be pulled closer to the unusual points and away from other points. These points are marked in red on the Model Selection Report.



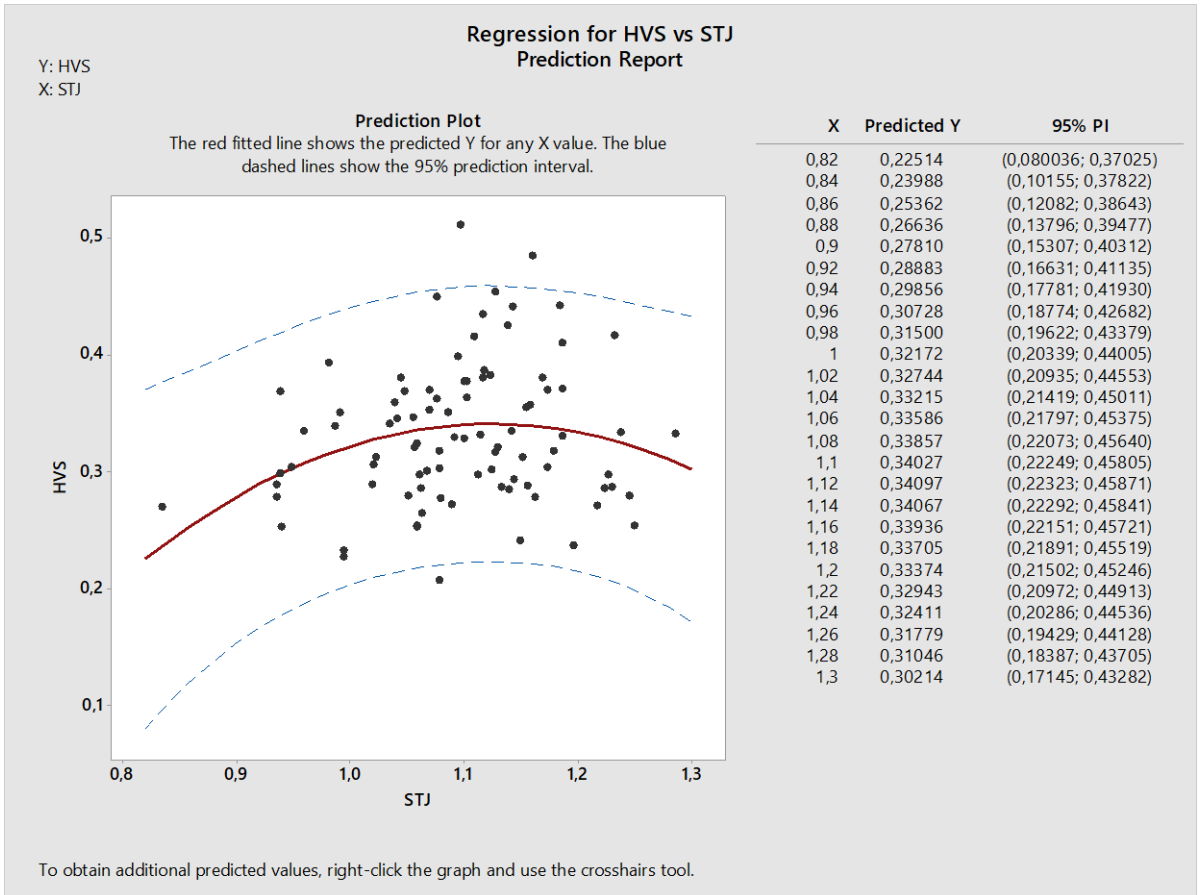
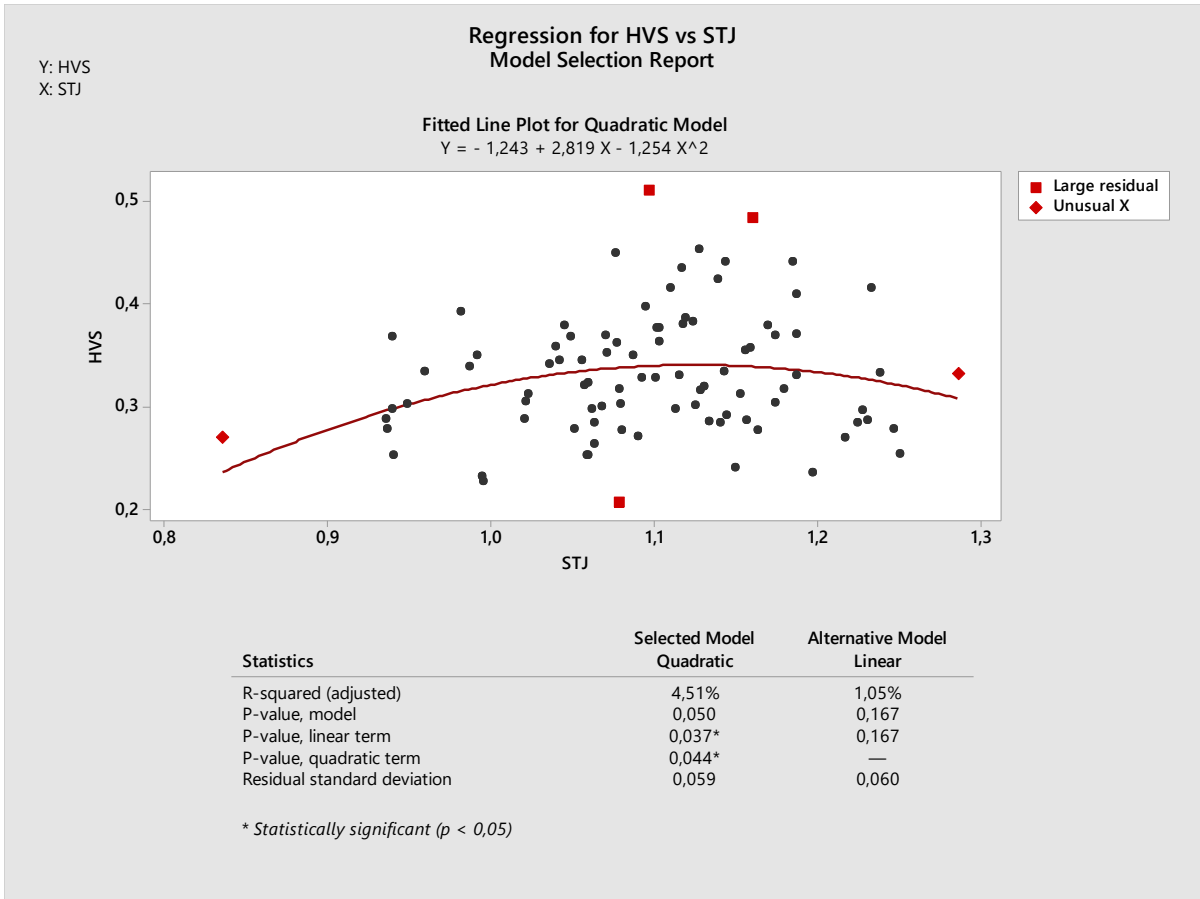
❖ HVS – STJ



**Report:**

This sample is large enough ( $n = 90$ ) to obtain a precise estimate of the strength of the relationship.

- Large residuals: 3 data points have large residuals and are not well fit by the equation. These points are marked in red on the plots.
- Unusual X values: 2 data points have unusual X values, which can cause the fitted line to be pulled closer to the unusual points and away from other points. These points are marked in red on the Model Selection Report.



## 6.5 Outliers

To detect any outliers, with Minitab, Grubbs' test has been performed.

Grubb's test is based on the assumption of normality. That is, one should first verify that the data can be reasonably approximated by a normal distribution before applying the Grubbs' test.

Grubbs' test detects one outlier at a time. This outlier is expunged from the dataset and the test is iterated until no outliers are detected. However, multiple iterations change the probabilities of detection, and the test should not be used for sample sizes of six or fewer since it frequently tags most of the points as outliers.

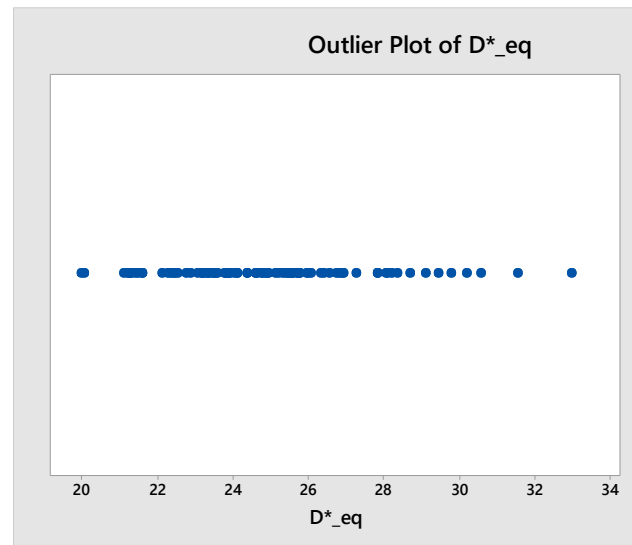
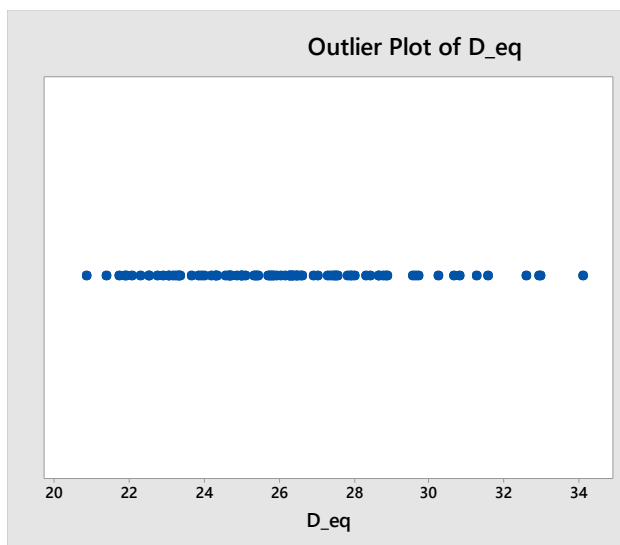
Results:

- Null hypothesis: all data values come from the same normal population
- Alternative hypothesis: smallest or largest data value is an outlier
- Significance level:  $\alpha = 0,05$

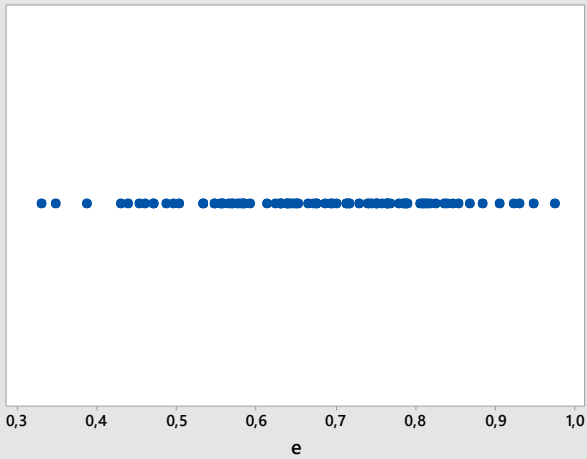
Grubbs' Test

Variable	N	Mean	StDev	Min	Max	G	P
D_eq	90	26,124	2,851	20,853	34,114	2,80	0,381
D*_eq	90	24,828	2,612	19,953	32,983	3,12	0,121
e	90	0,6762	0,1404	0,3299	0,9737	2,47	1,000
$\alpha$	90	120,39	84,45	1,28	290,78	2,02	1,000
HVS	90	0,33122	0,06015	0,20709	0,51033	2,98	0,207
HRVS	90	0,96973	0,09053	0,76013	1,19078	2,44	1,000
HRNC	90	1,3851	0,1640	0,8666	1,7559	3,16	0,104
HRRC	90	1,3516	0,1425	0,8793	1,7044	3,31	0,057
HRLC	90	1,2804	0,1386	0,9345	1,6345	2,56	0,846
HSTJ	90	0,7541	0,1007	0,5267	1,0220	2,66	0,609
STJ	90	1,0969	0,0845	0,8353	1,2848	3,10	0,134

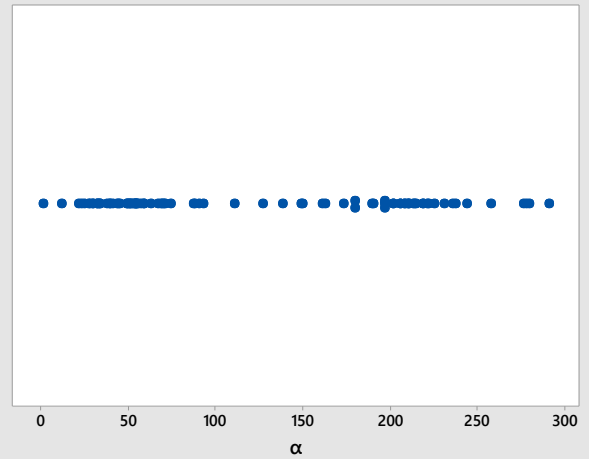
No outlier at the 5% level of significance



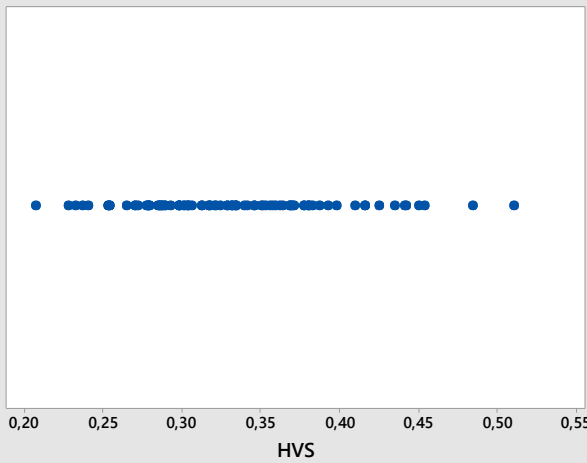
Outlier Plot of  $e$



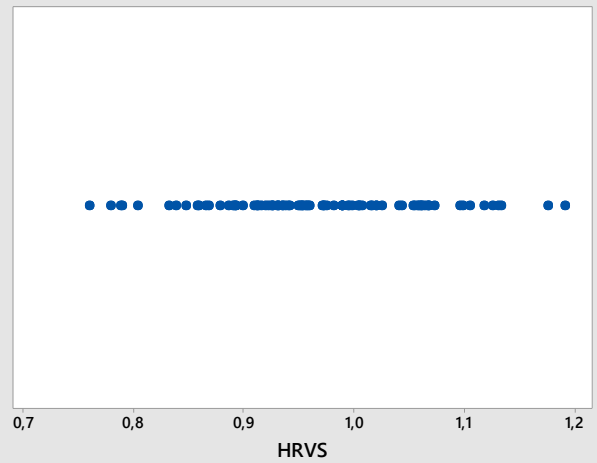
Outlier Plot of  $\alpha$



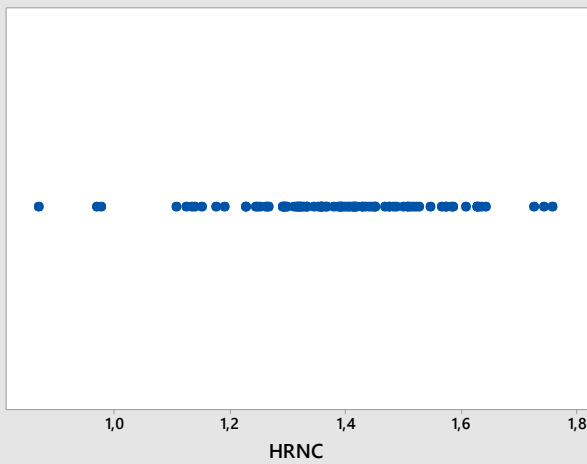
Outlier Plot of HVS



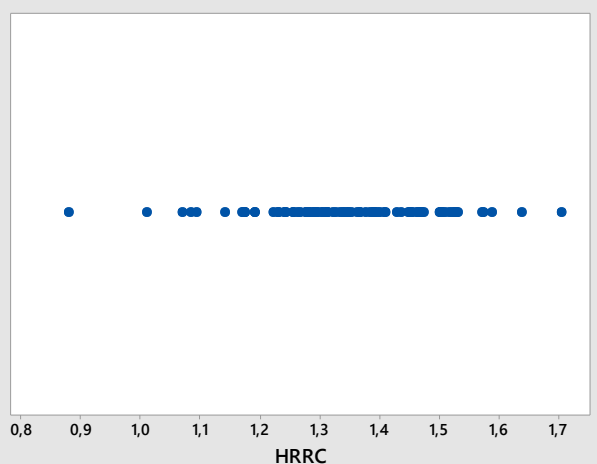
Outlier Plot of HRVS

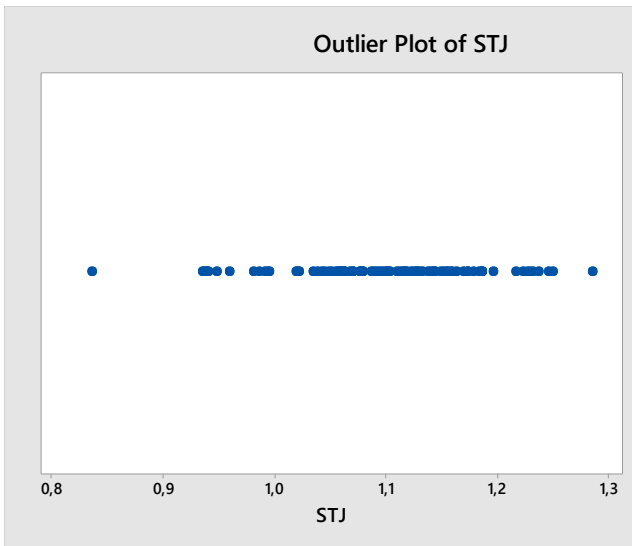
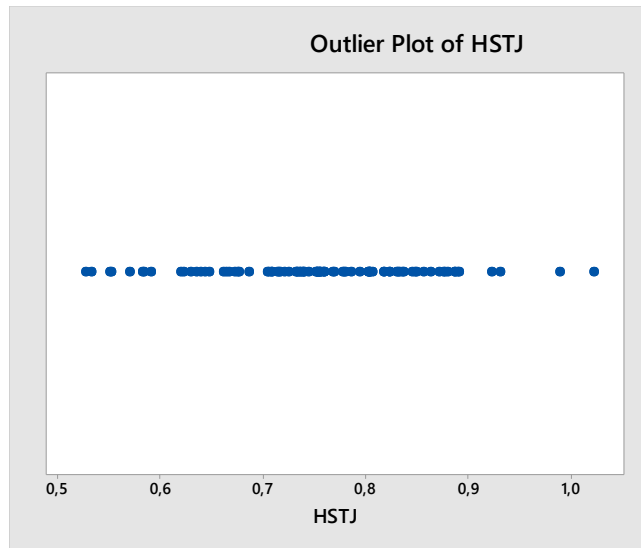
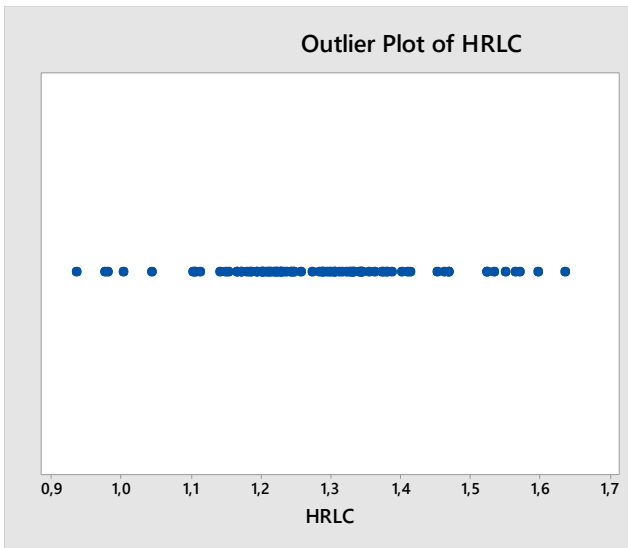


Outlier Plot of HRNC



Outlier Plot of HRRC





So, the data points marked in red on previously plot may be indicative of measurement values altered by poor quality in resolution of CT scans.

## 7 Conclusion

This work arises from the need to develop a model of aortic valve prosthesis as similar as possible compatible with the human anatomy, since today's prostheses, whose geometry is subject to strong simplifications, still impose their geometry on the aortic district.

Therefore, from the analysis of CT scan, the objective was to define a parametric geometry of the real aortic root.

Initially it was necessary to develop a procedure, using a dedicated software, which allowed the analysis of CT scans and the identification of the parameters useful to describe the geometry of the analyzed anatomical district. The method devised was applied to a database of 100 patients whose pre-operative CT scans were collected in different centers around Europe and with different methods.

The measures of interest were:

ANNULUS PLANE	VALSALVA SINUSES PLANE	SINOTUBULAR JUNCTION PLANE
Dequivalent (Annulus perimeter/ $\pi$ )	HVS VS plane distance ratio	HSTJ hSTJ(mean)/Deq
D'equivalent (4*Annulus Area/ $\pi$ ) <sup>0.5</sup>	HRVS 2*r0/Deq	STJ 2*rSTJ/Deq
e= 2*Dmin/Dmax-1"	HRNC 2*rNC/Deq	
$\alpha$ angle between Dmax and NC sinus (degrees)	HRRC 2*rRC/Deq	
	HRLC 2*rLC/Deq	

With:

- e = eccentricity;
- r0 = radius of the circumference defined by the nadirs of the semi-lunar leaflet attachments;
- rNC = radius of the non coronary cusp;
- rRC = radius of the right coronary cusp;
- rLC = radius of the left coronary cusp;
- hSTJ = distance between the annulus plane and the sinotubular junction plane;
- rSTJ = radius of the sinotubular junction.

These measures were statistically analyzed by carrying out normality tests, regressions and outliers test. With the measurements taken by two other operators, comparisons were made to validate the repeatability of the procedure.

**The normality test** stated that for all the parameters, except one, the populations are normally distributed.

**The regressions** stated that the relationships between:

- D equivalent and:
  - HVS
  - HRVS
  - HRNC
  - HRRC
  - HRLC
  - HSTJ
  - STJ
- D\*equivalent and:
  - HVS
  - HRVS
  - HRNC
  - HRRC
  - HRLC
  - HSTJ
  - STJ
- HVS and HSTJ

are statistically significant ( $P < 0.05$ ); while between:

- HVS and STJ

is not statistically significant ( $P > 0.05$ ).

**The outliers test** concluded there is no outliers at the 5% level of significance

**The comparison** between the databases calculated from the operators A and B, and A and C stated that there is not enough evidence to conclude that the means of the variables differ at the 0.05 level of significance, except for “e” in A/C comparison.

**The ANOVA** states that there are differences among the means at the 0.05 level of significance, except for e,  $\alpha$  and HRRC where there is not enough evidence to conclude that there are differences among the means at the same level of significance.

### ***Future developments***

Carrying out these studies, it will be possible to set a method useful for the design of new models of valve prosthesis and of an in vitro testing setups to be used for the verification of the structural and mechanical performance of the valve, in an anatomical “representative” environment.

The final aim is to optimize the valve design to obtain more representative results of the clinical reality.

## Index of figures

Figure 1.1 Sketch of a human heart.....	7
Figure 1.2 Scheme of the vessels that make up the circulatory system.....	8
Figure 1.3 Section of the heart wall showing the components of the outer pericardium (heart sac), muscle layer (myocardium), and inner lining (endocardium).....	10
Figure 1.4 In the human heart, blood flows from the right heart to the lungs, then to the left heart and then to the body. Atrioventricular valves prevent the reflux of blood into the atria when the ventricles contract. Pulmonary and aortic valves prevent reflux from the arteries to the ventricles when the ventricles relax. ....	11
Figure 1.5 With the atria and major vessels removed, all four valves are clearly visible. ....	12
Figure 1.6 Scheme of a sectioned heart.....	13
Figure 1.7 Echocardiogram showing the movements of the valvular flaps of the mitral (in particular the anterior flap), the variation of the diameter of the left ventricular cavity and of the thickness of the left ventricular wall, during a cardiac cycle of a normal subject. From D to C, ventricular diastole; from C to D, ventricular systole; from D to E, fast filling; from E to F, lendot filling (diastasis), from F to A, atrial contraction. The mitral valve closes in C and opens in D. Simultaneous recording of the ECG at the bottom. ....	16
Figure 1.8 Pressure pulses in the left atrium, aorta, and left ventricle, temporally correlated with aortic flow, ventricular volume, cardiac tones, venous pulse, and ECG, in a complete cardiac cycle of the dog. ....	17
Figure 1.9 The pressure-volume cycle of the left ventricle in a single cardiac cycle (from A to F). ....	19
Figure 1.10 Schematic representation of the heart conduction system. SN, sinus node; AVN, atrioventricular node; RBB, right branch; HB, His beam; LBB, left branch; PF, Purkinje fibers. ....	21
Figure 1.11 An obstruction of the outflow of the left ventricle can occur at four different levels. A. Valvular, often with loss of commissures and with a small central orifice; B. Spore valvular, most often due to hourglass narrowing of the ascending aorta; C. Under-valvular, due to the presence of congenital fibrous diaphragms below the valvular plane; D. Between the septum and the aortic limb of the mitral, as occurs in hypertrophic cardiomyopathy, where the septum is hypertrophic and the aortic limb of the mitral is moved forward during the systole. ....	23
Figure 1.12 Several valve morphologies in case of aortic stenosis. A. Normal tricuspid valve. B. Congenital stenosis with practically monocepatic valve and small eccentric orifice. C. Stenosis of rheumatic origin with vegetations and fusions of the flaps, which have thickened and retracted edges (coexistence insufficiency). D. Calcific aortic stenosis of a bicuspid valve. E. Senile aortic stenosis with calcification of cusps of an originally normal valve.....	24
Figure 1.13 In the diagram the pressure gradient is evident that is determined in systole between left ventricle and aorta. The ejection blow (below) reaches its maximum when the pressure gradient has the greatest amount. ....	25
Figure 1.14 The scheme indicates the focal points of maximum intensity of the ejection systolic murmur characteristic of aortic stenosis, with the typical irradiation towards the neck vessels. At the top, the carotid pulse track shows a slow ascent and a reduced performance (late and small pulse). ....	27
Figure 1.15 Chest diagram in antero - posterior projection of a man with severe aortic stenosis. The arrow indicates the poststenotic dilatation of the ascending aorta. In this case, a fair degree of left ventricular hypertrophy is also visible.....	29
Figure 2.1 Proposed nomenclature for the aortic root components.....	31
Figure 2.2 Schematic representation of the aortic root. AA = aortic annulus, ST = synotubular junction, H = commissural height.....	32
Figure 2.3 Normalized size of an un-pressurized human aortic root.....	32
Figure 2.4 Anatomic section of the aortic root.....	33
Figure 2.5 Appearance of opening an aortic valve in the presence (right) or absence (left) of the sinuses of Valsalva. ....	33
Figure 2.6 Aortic root vortices visualized using flow-sensitive time-resolved '4D' magnetic resonance imaging with flow sensitivity in all three directions. ....	34
Figure 2.7 Remodeling (a and b) and Reimplantation (c, d and e).....	36
Figure 2.8 Some examples of changes in surgical techniques and / or materials for the most anatomical aortic root reconstruction. Cochran (left), Robicsek (center) and Miller, 2004 (right). ....	36
Figure 2.9 Original drawing and realization of the dacron duct called "Valsalva" for the ability to rebuild, after implantation and pressurization, the shape of the sinuses of Valsalva.....	37

Figure 3.1 Currently clinically implemented transcatheter valves. (a) The balloon-expandable Sapien XT valve (Edwards Lifesciences) consists of a cobalt-chromium frame and bovine pericardial leaflets. (b) The CoreValve (Medtronic) has a self-expanding nitinol frame and porcine pericardial leaflets.....	41
Figure 3.2 Available transcatheter valve sizes from Edwards Lifesciences (a) and Medtronic (b) with their corresponding ranges of aortic annular diameters. The diameter of the aortic annulus must be between 18 and 29 mm, regardless of other parameters.....	42
Figure 3.3 Inadequate access route patency. (a) Maximum intensity projection CT angiographic image reveals a subocclusive stenosis in the right external iliac artery (arrow) inhibiting endovascular access through the right iliac arterial axis, with diffuse atherosclerotic calcifications in the other aortoiliac vessels. (b) Volume-rendered CT image obtained in a different patient shows general tortuosity of the aortoiliac arterial vessels, a finding that is most prominent in the left common iliac artery (arrow). .....	42
Figure 3.4 Entry site for transaortic access for TAVR. (a) Volume-rendered CT image shows the approximate target point ( <i>T</i> ) for transaortic access through a minimal right sternotomy or thoracotomy, typically located at the level of the second intercostal space. (b) For CoreValve devices (Medtronic), a minimum distance of 6 cm (double-headed arrow) between the entry point ( <i>T</i> ) and the aortic annular plane (dashed line) is recommended to accommodate the device length.....	45
Figure 3.5 Circulatory stasis in a large left atrial appendage producing a pseudothrombus during pre-TAVR evaluation. (a) Axial contrast-enhanced CT image demonstrates how slow flow can lead to incomplete filling of the left atrial appendage (*) during the arterial phase. When detected, an atrial appendage thrombus must be either confirmed or excluded. This is traditionally achieved with TEE, although delayed phase CT images can also be used. (b) Axial contrast-enhanced delayed venous phase CT image shows final complete filling of the appendage (*). The possibility of a left atrial appendage thrombus must always be reported immediately, since such a finding constitutes a procedural contraindication with a high risk of stroke.....	47
LEFT: Figure 3.6 Volume-rendered CT image shows the central position and oblique angulation of the aortic root and annular plane. ....	49
RIGHT: Figure 3.7 Coronal contrast-enhanced CT image shows the aortic root extending between the LVOT and the ascending aorta ( <i>Ao asc</i> ), with its borders formed by the sinotubular junction (dashed line) and the basal attachments of the aortic valve leaflets, which define the level of the annular plane (solid line). The aortic root contains the sinus of Valsalva (arrows) and aortic valve leaflets (*). .....	49
Figure 3.8 Double-oblique contrast-enhanced CT image of the aortic root at the level of the sinuses of Valsalva demonstrates the anatomy of the aortic valve, consisting of left coronary (green), right coronary (red), and noncoronary (yellow) cusps. Note the cloverleaf shape of the aortic root contour. <i>A</i> = anterior, <i>P</i> = posterior.....	49
Figure 3.9 a) Drawing illustrates the crownlike suspension of the aortic valve leaflets within the aortic root extending across the length of the aortic sinus. <i>AR</i> = virtual annular ring (green), formed by joining the basal attachments of the aortic valve leaflets; <i>STJ</i> = sinotubular junction (blue); <i>VAJ</i> = ventriculoarterial junction (yellow). Red = aortic leaflet insertion sites in the sinus of Valsalva forming a crownlike ring. (Reprinted, with permission, from reference 39.) (b) Coronal contrast-enhanced CT image demonstrates the levels of the sinotubular junction ( <i>STJ</i> ) (blue line), ventriculoarterial junction ( <i>VAJ</i> ) (yellow line), and annular ring ( <i>AR</i> ) (green line). Double-headed arrow = anatomic range of the sinuses of Valsalva. <i>CAU</i> = caudal, <i>CRA</i> = cranial. (c–f) Double-oblique reformatted images further clarify the changing shape of the aortic root contour. (c) The sinotubular junction forms the top of the crown, where the outlet of the aortic root in the ascending aorta ( <i>Ao</i> ) is a true circle. <i>A</i> = anterior, <i>P</i> = posterior. (d) The aortic root gradually becomes less circular, with a more cloverleaf shape at its midportion (ie, at the sinuses of Valsalva). At this level, the aortic valve leaflets are clearly seen. (e) The aortic valve leaflets (*) are just barely visible at the level of the ventriculoarterial junction, where the left ventricular structures give rise to the fibroelastic walls of the aortic valvar sinuses. Note that the aortic root contour is now becoming increasingly ellipsoid. (f) The bottom of the aortic root is formed by the virtual ring, or aortic annulus ( <i>Ao ann</i> ), which has an oval shape in most patients.....	50
Figure 3.10 Double-oblique reformatted CT images show the basal insertion sites of the right coronary cusp (orange dot), noncoronary cusp (yellow dot), and left coronary cusp (green dot). When these basal leaflet insertion sites are used as a reference for deriving a single 2D measurement of the annular plane (as in 2D echocardiography-derived measurements), the 3D anatomy is reduced to a 2D image. Furthermore, these images illustrate that none of the performed 2D measurements is along the true long or short axis of the aortic annulus, complicating simple comparisons between CT and echocardiographic measurements.....	51

Figure 3.11(a) On an echocardiographic image, the diameter of the aortic annulus (double-headed arrow) is measured by identifying two opposing points (orange dots) on the basal insertion sites of the aortic valve leaflets (\*). *Ao asc* = ascending aorta. (b) Corresponding double-oblique reformatted image through the aortic annulus reveals that the pathway (double-headed arrow) between these points (orange dots) does not correspond to the true long axis of the aortic annulus. Echocardiography-derived measurements often lead to underestimation of the true size of the annulus. Furthermore, because conventional echocardiography is a 2D imaging modality with a varying degree of operator dependency, it is almost impossible to compare single echocardiography-derived measurements with their CT counterparts, since both the measurement plane and the chosen oblique diameter will differ between these imaging modalities. *A* = anterior, *P* = posterior. .... 52

Figure 3.12 Possible measurements of the aortic annulus. Before taking any measurement, a correctly reformatted image along the annular plane must be obtained. This is achieved by interactively manipulating the reconstruction planes on a workstation so that the nadirs of all three cusps are identified on one transverse image. (a, b) Standard coronal (a) and sagittal (b) images are in themselves not suitable but can be used as a starting point, with the final double-oblique imaging plane (dashed line) containing the basal attachment points of the left coronary (green dot), right coronary (orange dot), and noncoronary (yellow dot) cusps. *A* = anterior, *Ao asc* = ascending aorta, *Cau* = caudal, *Cra* = cranial, *P* = posterior. (c–e) The resulting cross-sectional image can then be used to measure the true long- and short-axis annular diameters (arrows in c), the annular area (shaded oval in d), and the annular perimeter (dashed line in e). From each of these different types of measurements, the mean area diameter can be derived using the appropriate formula. *A* = anterior, *P* = posterior. .... 55

Figure 3.13 Double-oblique contrast-enhanced CT image through the aortic sinus reveals extensive leaflet calcifications, most prominently in the right coronary cusp. Prominent valve calcification may complicate device deployment and may be associated with an increased risk for postoperative paravalvular regurgitation. *A* = anterior, *P* = posterior. .... 57

Figure 3.14 Contrast-enhanced CT image at the level of the sinuses of Valsalva (a) and three-chamber view (b) show a CoreValve device in the aortic root. The obstructive effect of the extensive calcifications of the native aortic valve (\*) causes asymmetric deployment and positioning of the transcatheter valve. Despite a very convincing finding of severe paravalvular regurgitation at CT, echocardiography revealed only moderate regurgitation, underscoring the need to compare results from different imaging modalities to achieve the most complete assessment possible. .... 57

Figure 3.15 Slightly oblique coronal contrast-enhanced CT image at the level of the aortic root shows that an adequate distance (white double-headed arrow) between the annular plane and the nearest coronary ostium—in this case, the left main ostium (\*)—is necessary to avoid the rare but devastating complication of ostial occlusion due to displaced native valve leaflets during prosthesis deployment. As a rule of thumb, a minimum distance of 10 mm is recommended. It is also recommended that this distance be greater than the length of the aortic valve leaflets (black double-headed arrow). *Cau* = caudal, *Cra* = cranial. .... 58

Figure 3.16 For optimal device deployment, the inclination of the angiography tube must be such that, on the resulting fluoroscopic image (a), the basal insertion sites of all aortic valve leaflets are aligned in the same anatomic annular plane, corresponding with the correctly aligned double-oblique CT image (b). Green dot = left coronary cusp, orange dot = right coronary cusp, yellow dot = noncoronary cusp. On the basis of preprocedural CT-derived left anterior oblique–right anterior oblique and cranial-caudal angulation values, an accurate prediction of the best procedural fluoroscopic angulation for correct deployment of the transcatheter valve along an axis perpendicular to the aortic annular plane can be made. This approach obviates repeated angiographic test injections to determine the correct tube angulation, thereby reducing both the amount of contrast material used and the time required for the procedure. *A* = anterior, *P* = posterior.... 59

Figure 3.17 CT evaluation of the angulation between the ascending aorta, aortic root, and LVOT. A practically straight line between the ascending aorta and the LVOT (dashed line in a) indicates a much more favorable anatomic situation than does a steeper angulation (dashed line in b), since the latter can complicate stable deployment of the prosthesis. The technical difficulty of the procedure is further increased by the presence of a hypertrophic basal septum (\* in b), potentially creating increased resistance during device deployment. *A* = anterior, *Cau* = caudal, *Cra* = cranial, *P* = posterior. .... 59

Figure 3.18..... 61

Figure 3.19..... 62

Figure 3.20 *ATS 3f Enable*..... 63

Figure 4.1..... 67

Figure 4.2..... 67

Figure 4.3.....	68
Figure 4.4.....	68
Figure 4.5.....	69
Figure 4.6.....	69
Figure 4.7.....	70
Figure 4.8.....	70
Figure 4.9.....	71
Figure 4.10.....	71
Figure 4.11.....	72
Figure 4.12.....	72
Figure 4.13.....	73
Figure 4.14.....	73
Figure 4.15.....	74
Figure 4.16.....	74
Figure 4.17.....	75
Figure 4.18.....	76

## Index of the tables

Table 1 Overview of Sapien XT and CoreValve Transcatheter Valves and Their Respective Delivery Systems.....	41
Table 2 Recommended Minimum Vessel Diameter based on the Delivery Device.....	44
Table 3 Required Information from Preprocedural CT Examinations .....	47
Table 4 Overview of the Heterogeneity in Methods of Obtaining Annular Dimensions across Several Studies .....	54

## Bibliography

Berne, R. M. (s.d.). Il sistema cardiovascolare. Mattheew N. Levy.

Efstratios I. Charitos, H.-H. S. (2012). Anatomy of the aortic root: implications for valve-sparing surgery. *Annals of cardiothoracic surgery, Vol 2, No 1 January 2013.*

LaMorella, C. (2017). *Realizzazione di un modello fisico di radice aortica in silicone, basato su analisi statistica di CT scan, per test in vitro di protesi valvolari di tipo biologico.*

Marco Di Eusanio, K. P. (2015, Marzo). Sutureless aortic valve replacement. *Annals of cardiothoracic surgery.*

Paulis, R. D. (2007). LA CHIRURGIA DELLA RADICE AORTICA:.

Rodrigo A. Salgado, J. A. (2014). Preprocedural CT Evaluation of Transcatheter Aortic Valve Replacement: what the radiologist needs to know.

Rugarli, C. (2015). *Medicina interna sistematica.* Edra Masson.

Sergio Dalla Volta, L. D. (2005). *Malattie del cuore e dei vasi.* McGraw-Hill Education.

Sven Martens, A. P. (2009). Sutureless Aortic Valve Replacement With the 3f.

## Sitography

- <https://en.wikipedia.org/wiki/Heart>
- <http://ebook.scuola.zanichelli.it/sadavabiologiablu/il-corpo-umano/l-apparato-cardiovascolare-e-il-sangue>
- <https://www.edwards.com>
- <http://www.livanova.com>
- <https://en.wikipedia.org/wiki/OsiriX>
- <http://www.3mensio.com/>
- [https://en.wikipedia.org/wiki/Analysis\\_of\\_variance](https://en.wikipedia.org/wiki/Analysis_of_variance)
- [https://en.wikipedia.org/wiki/Grubbs%27\\_test\\_for\\_outliers](https://en.wikipedia.org/wiki/Grubbs%27_test_for_outliers)